CITY UNIVERSITY OF HONG KONG

香港城市大學

Nucleation and Growth of Cubic Boron Nitride Thin Films

立方氮化硼薄膜的形核與生長研究

Submitted to
Department of Physics and Materials Science
物理及材料學系
In Partial Fulfillment of the Requirements
For the Degree of Doctor of Philosophy
哲學博士學位

by
Chan Chit Yiu
陳喆垚

August 2005
二零零五年八月

Abstract

Cubic boron nitride (cBN) is a synthetic and an intrinsically super-hard material with the second highest hardness and thermal conductivity next to diamond. Cubic BN with its tetrahedral sp^3 structure is isostructural and isoelectronic to diamond. Diamond is far the most extreme material but cBN surpasses diamond in some properties. Unlike diamond, cBN is chemically inert to molten ferrous materials and resistant to oxidation up to 1200 °C at atmospheric conditions. These properties make cBN more attractive than diamond in many mechanical and tribological applications. Cubic BN has the widest bandgap (6.2 ± 0.2 eV) among III-V semiconductors, high electron mobility and hole mobility. In contrast to diamond it maintains high resistivity even at extreme temperatures. It can be doped for both p- and n-type conductivities and is piezoelectric. Therefore cBN is a potential candidate for construction of high-temperature, high power and high-speed electronic devices operating in harsh environment. Although cBN films are very attractive they have not been implemented into practical applications because of many accoutered problems like poor quality, low phase purity, high compressive stress (up to 20 GPa), poor adhesion to the substrates, small deposited area and limited film thickness (≤200 nm). These cBN properties suggest that the development of novel technologies for synthesis of high-quality, large-area and thick cBN films is very challenging.

This thesis presents a viable route towards the practical applications of cBN coatings through better understanding of the nucleation and growth behavior of the deposited cBN thin films. The aforementioned limitations have been overcome by the introduction of fluorine chemistry mediating by a complex He-Ar-N_2-BF_3-H_2 plasma induced in an electron cyclotron resonance (ECR) system. This deposition method enables the preparation of thick cBN films (>1 μm) with low internal stress and over large areas of silicon (Si) substrates. Fourier transform infrared (FTIR) spectroscopic examination shows that the films are composed of >80 % cBN phase. Detail analysis of

BN structures employing high resolution transmission electron microscopy (HRTEM) and transmission electron energy loss spectroscopy (EELS) revealed that a pure cBN layer is formed on top of an initial graphitic BN layer which accounts for the insignificant hexagonal BN (hBN) signal in FTIR spectra. The characteristic transverse optical (TO) and longitudinal optical (LO) phonons modes of cBN, generally appearing in the spectra of cBN crystals synthesized by high pressure high temperature (HPHT) methods, were found in our cBN films which are the indicatives of large cBN crystallites. It was found that the ion bombardment, gas composition, substrate temperature and growth time significantly affect the phase purity and crystallinity of cBN films.

However, the growth of cBN still follows the typical pattern with a graphitic precursor, amorphous/turbostratic BN (aBN/tBN) at the Si substrate interface. This work however illustrates that aBN/tBN are not necessary precursor layers for cBN growth. Using diamond substrates can eliminate aBN/tBN layer and cBN can directly be deposited on diamond at suitable deposition parameters. The distinctive features of cBN films grown on diamond in reference to those on Si substrates were also investigated. The critical experimental conditions inducing nucleation and maintaining the growth of cBN were revealed based on the detail HRTEM studies of interfacial cBN–diamond structures. The equivalent atomic configurations in cBN and diamond, and the alignment of their crystallographic planes suggest ‘perfect’ epitaxy in the HRTEM view-field. This work thus shows that diamond substrates play vital role at synthesis of high quality cBN films.

Regarding to the successful deposition of cBN using low energetic ion bombardment (–20 V) and fluorine chemistry, a surface chemical vapor deposition (CVD) growth process of cBN was developed. A new CVD surface growth mechanism, initiated by the introduction of fluorine chemistry, is also outlined herein. The proposed mechanism is based on the combination of HRTEM structural studies of the utmost layers of the cBN films, surface analysis of the film surface composition after exposure

to different plasma environments and an optical emission spectroscopic examination of plasma with variable composition particularly fluorinated species.

The surface roughness is another parameter controlling cBN nucleation and growth which was investigated at synthesis of cBN films employing a mass-selected ion beam deposition (MSIBD) which takes advantage in independent control of deposition parameters. Different surface roughness (0.2 to 170 nm) was obtained by scratching Si surface with proper grain sizes of diamond or alumina powders. The analysis of grown BN films show the interfacial tBN thickness increases, cBN nucleation threshold shift towards the higher ion energy with the increase in substrate roughness, and the orientation relationship of tBN with Si becomes more random. The differences in cBN volume fraction are however less obvious at higher ion energy (500 eV). The resulting featureless film morphology at high ion energy is probably associated with the preferred subsurface growth process. On the other hand, low ion energy leads to a surface-like growth process which predominantly yields granular morphology.

The fundamental understanding of the deposition parameters has led to the development of technology providing cBN films that are thick enough for reliable evaluation of mechanical properties. The measured hardness strongly depends on the crystallinity and crystal size/grain boundaries of the cBN films. The consistent and repeatable hardness of 70 GPa and elastic modulus of 800 GPa were measured on smoothed cBN films. The magnitudes of hardness and elastic modulus measured here are the highest ever obtained from the measurement of cBN films, and they are comparable to the values reported for cBN crystals synthesized by HPHT methods.

The works proves that the properties, adherence, film stability and overall thickness of cBN films are considerably affected by the chemical nature of substrates. Growing very thick cBN films (>3 μm) can easily be demonstrated on polycrystalline diamond by ECR-PECVD at very low bias voltage (–30 V) with assistance of fluorine chemistry. Cubic BN films also grow on polycrystalline diamond in epitaxial relationship which is important for development of device quality cBN and engineering

of novel electronic devices. The works indicates that growing large single crystal cBN films might be feasible at particle energies approaching the values of thermal energies using plasma enhanced chemical vapor deposition (PECVD). Evidently cBN still nucleates at effective bias of about –12 V.

The cBN films grown by PECVD do not show top thin non-cubic layers which contrast the films prepared by PVD. The surface free of non-cubic BN phases and absence of interfacial precursor aBN/tBN layers enables to grow extremely thin films, which allows constructing cBN-diamond (cBND) super-lattices. Absence of non-cubic phases on cBN surface also suggests that existing models cannot elucidate the cBN formation at PECVD since the particle energy is well below atomic displacement energy. Growing cBN by PECVD is more likely surface process.

Advantages of ECR-plasma coupled with fluorine chemistry are demonstrated to be capable of preparing high quality, low stress cBN films. The ECR technique in combination with a universal diamond buffer layer provides cBN–diamond bilayer composite with exciting mechanical properties particularly suitable for machining ferrous metals. Therefore cBND was deposited on cemented WC cutting inserts at 800 °C. The cutting test revealed that cBND adhesion and properties are already good enough for some industrial applications though cutting tools failed. The failure is however in the WC region whereas the separation of cBN and diamond from substrate is not observed. Thus the research work presented is important milestone towards the first industrial exploitation of cBN films.

Acknowledgements

I would like to thank my supervisor, Prof. Igor Bello for his continuous support and encouragement during my PhD studies. His friendly and helpful character let me leant a lot from him, especially the vacuum technology. I am grateful to work closely together with Dr. W.J Zhang who taught me a lot about the experimental and instrumental techniques concerning thin film deposition. I am fortunate to have a chance of staying in the Göttingen Univeristy under the supervision of Prof. H. Hofsäss, who provided me with invaluable working experience and knowledge in the studying field. Special thanks goes to Prof. S.T. Lee for providing an excellent research atmosphere and environment to me. This thesis would not have been possible without their support. Last but not the least, technical assistance from Felix Wong, V. Kremnican and X.M. Meng is highly appreciated. Finally, I would like to thank my loving wife, Rice Zeng for her spiritual support when I face difficulties.

Table of Contents

List of figures

List of tables

Chapter 1. Properties of boron nitride polymorphs

Boron nitride (BN) has been prepared in different modifications. It can form hexagonal BN (hBN), rhombohedral BN (rBN), wurtzitic BN (wBN) and cubic BN (cBN) lattice structures. Hexagonal BN and rBN are sp^2-bonded whereas wBN and cBN are sp^3-bonded structures. These allotropes are analogous to the structures formed by carbon. For example, cBN is similar to diamond and hBN structurally resembles graphite. Cubic BN films often confine hBN, amorphous BN (aBN) and turbostratic BN (tBN) structures. Turbostratic BN is disordered hexagonal phase with curled basal planes and distorted interplanar spacing. The most attractive BN allotrope is cBN. Its atomic density is higher by 54.7% than of hBN and smaller by only 4.3% than that of diamond. The high atomic density and strong chemical bonds of cBN provide the second highest hardness and properties similar to diamond. Some cBN properties surpass those of diamond. Cubic BN is the second most thermally conductive material. It is however more chemically and thermally stable than diamond. Unlike diamond, cBN is resistant to oxidation at high temperatures and does not react with molten ferrous materials. These properties and low friction coefficient make cBN the best material for machining ferrous materials including the tool steels and carbides. Cubic BN is a wide band gap semiconductor with a band gap of 6.2±0.2 eV. It can be doped for n- and p-type conductivity using Si and Be, which is still very difficult in diamond. These electronic properties along with the high thermal stability and thermal conductivity suggest using cBN for the construction of high power and high frequency electronic devices operated at high temperature. The band gap of cBN is also suitable for making ultraviolet (UV) detectors and UV light emitting diodes working in the deep UV range. But these electronic applications also involve high quality cBN with controlled defects and impurities. Therefore the effort for synthesis of device quality and single crystal cBN films is imperative. The highlighted properties of BN polymorphs as mentioned above are more discussed in the following sessions being concerned with their structural, vibrational, electronic and thermal properties

1.1. Structural properties of boron nitride

Boron nitride structures can be classified in four crystalline phases (Fig. 1-1). The most frequently encountered phase is hexagonal boron nitride (hBN), which has an sp^2-bonded layered structure with two-dimensional six-membered rings of alternating boron and nitrogen atoms stacking in a AA'AA'… fashion. The structure is slightly different as compared to graphite in which the hexagonal sheets are stacked directly above each other but with each successive layer rotated by 30°.

Boron nitride can also crystallize in rhombohedral modification. Rhombohedral BN (rBN) is basically similar to the graphite-like modification of hBN. The stacking sequence in rBN is threefold (ABCABC…) while twofold stacking is constructed in hBN. Such stacking difference can lead to the production of diamond-like tetrahedral structure via relatively simple cooperative lattice transformation by direct compression along the hexagonal axis (puckering mechanism). It consists of the splitting of the (0002) planes of the graphite-like phase into two sub-layers by means of B and N atoms displacements in opposite directions along the c-axis. The hBN or rBN lattice compression and splitting of basal planes leads to strong chemical bond formation between the (0002) planes, and finally a tetrahedral coordination of atoms can be induced and their stacking sequence will be preserved [4]. The tetrahedral atomic coordination of B and N atoms is the phase structure designated as cubic boron nitride (cBN). Cubic BN, the material of the interest in this work, can be obtained by direct physical transformation of rBN under high pressure and high temperature (HPHT). It is a hard, sp^3-bonded phase analogous to diamond. The structure of cBN can be considered as two interpenetrating face center cubic (FCC) sub-lattices, each containing only one type of atom, and shifted over 1/4 <111>. If all atoms are chemically identical, the lattice structure would be equivalent to that of diamond. The bonding of cBN is covalent, but slightly ionic in nature which is responsible for the presence of longitudinal optical and transverse optical phonon modes in the infrared absorption and Raman scattering spectra of BN under certain circumstances as being described in a

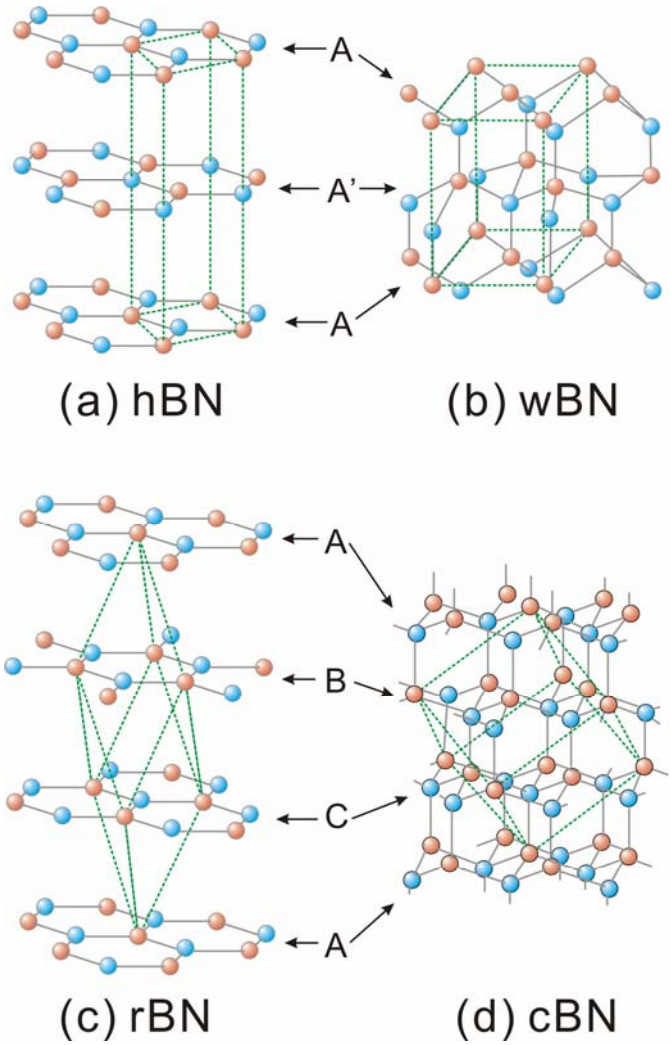

Fig. 1-1. Crystal structures of hBN, wBN, rBN and cBN. Boron atoms are designated by red color while nitrogen atoms are denoted by blue color. Unit shell showing the stacking sequence is indicated by green dotted lines.

later session. Finally, similar to lonsdaleite form of diamond, the meta-stable wurtzitic boron nitride (wBN) is also sp^3-bonded and hexagonal in structure.

In addition to the ideal hBN with the highest crystallinity showing long range order in-plane and along the c-axis of the BN sheets, other forms such as turbostratic boron nitride (tBN) and amorphous boron nitride (aBN) are also observed. The stacking of the hexagonal layer from tBN to aBN is increasing disturbed. Turbostratic BN is

characterized by an accidental stacking of the layers rotated randomly around the c-axis, and it has extensive lattice curvature. These tBN phases normally have a larger interplanar spacing by about 15% than the basal planes of ordered hBN [5]. The most disordered BN form is aBN having non-detectable order on microscopic scales.

1.2. Vibrational properties of crystalline BN structures

The structural properties of BN allotropes as discussed above somehow govern their vibrational properties which are different for dissimilar phases. These vibrational discrepancies are then very useful in identification of different phases which may exist in an unknown BN material. The frequencies of the normal modes of vibration (phonon modes) of BN crystals can generally be determined by Raman and infrared (IR) spectral analyses. The number, symmetry type and selection rules of phonon modes are dictated by the space groups of a crystal. Since the space group of the four common BN polymorphs (hBN (D_{6h}^4, $P6_3/mmc$), rBN, wBN (C_{6v}^4, $P6_3mc$) and cBN (T_d^2, $F\bar{4}3m$)) is different, they therefore have different symmetries for their phonon spectra. In case of hBN, the optical phonon at Γ point of the Brillouin zone is given by $\Gamma = 2E_{2g} + E_{1u} + A_{2u} + 2B_{1g}$. The first term $2E_{2g}$ mode is Raman active while the E_{1u} and A_{2u} modes are infrared active. The last term $2B_{1g}$ modes are optically inactive and can be treated as silent mode. Two peaks centered at 52 and 1366 cm^{-1} originate from $2E_{2g}$ symmetry. However, just one Raman scattering peak is present as depicted in Fig. 1-2 due to the cutting off the Raman-shift with wavenumber less than 100 cm^{-1} by the notch filter in our Renishaw visible Raman Spectrometer. The large anisotropy of inter- and intraplanar bonding is reflected in the large difference in the frequencies of these modes. Both modes are due to in-plane atomic displacements, but the low frequency mode is characterized by whole planes sliding against each other. This action is termed "rigid-layer shear mode". In contrast, the high-frequency mode is due to B and N atoms moving against each other in a plane [6]. In case of hBN with low crystallinity, additional peak feature centered at 750 cm^{-1} and peak-shift of 1366 cm^{-1} to lower

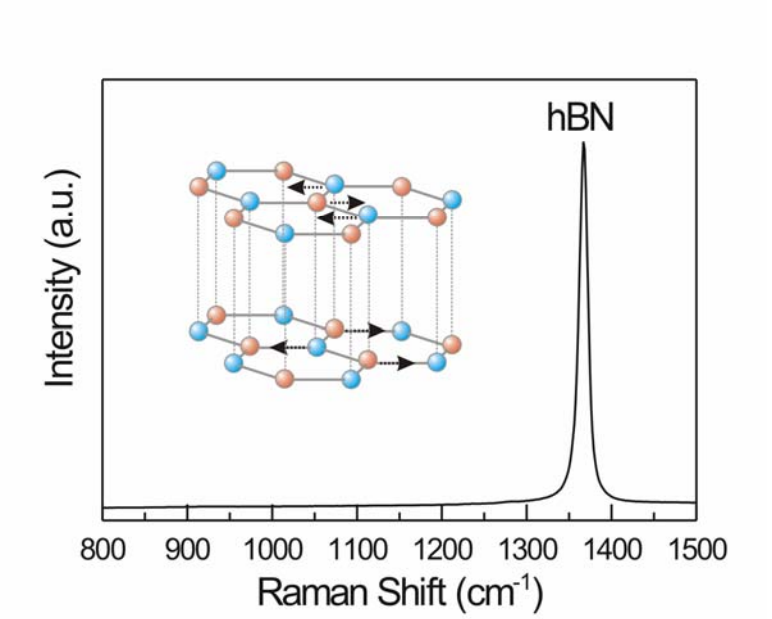

Fig. 1-2. Typical visible Raman scattering spectrum of hBN.

energies accompanying peak broadening are observed. This phenomenon can be explained by relaxation of selection rules in amorphous materials: most phonons become Raman active, so the Raman spectrum reflects mainly the density of states of phonons. In particular, the peak normally only infrared active could be developed in Raman spectrum [7]. Cubic BN has a zinc-blende structure with a tetrahedral symmetry. Since there is no inversion center in such a III-V cubic structure, the acquired Raman scattering spectra (Fig. 1-3) display two intensive lines corresponding to the Stokes' components of first-order Raman scattering with the emission of transverse and longitudinal optical (TO and LO) phonons in the center of Brillouin zone [8]. The absence of TO-LO phonons splitting in the Raman spectrum of diamond can be understood as the presence of an inversion center originated form involvement of single kind of atoms, i.e. carbon only. It is found that the orientation of the cBN crystal has a pronounce effect on the relative intensity between the TO and LO phonons. The cBN (111) crystal surface tends to give a very strong intensity of TO phonons (Fig. 1-3a) while the ones with (100) crystal surface exhibits a reverse trend (Fig. 1-3b). The presence of shoulder and tiny broad peaks at low energy side of TO and LO cBN phonons could be attributed to the presence of impurities.

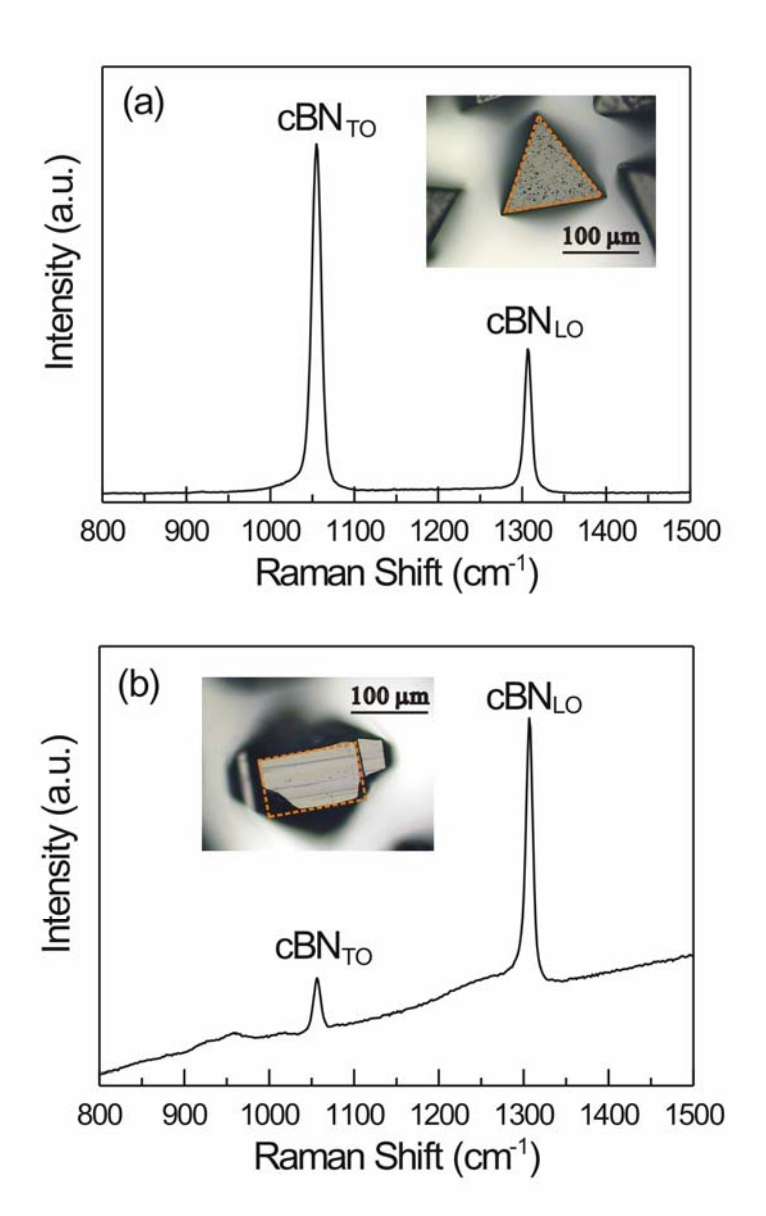

Fig. 1-3. Visible Raman scattering spectra of HPHT cBN crystal acquired under different crystallographic orientation, (a) cBN (111) and (b) cBN (100) oriented surface.

Regarding the IR active A_{2u} and E_{1u} normal modes of vibration (Fig. 1-4), the A_{2u} mode is an out-of-plane bending vibration excited by polarized light parallel to the principle c-axis. The corresponding ω_{TO} and ω_{LO} are 780 and 828 cm^{-1}, respectively. The E_{1u} mode corresponds to an in-plane stretching vibration and can be excited with polarized light perpendicular to three-fold axis. The corresponding ω_{TO} and ω_{LO} frequency are 1380 and 1610 cm^{-1}, respectively [9]. The origin of large energy

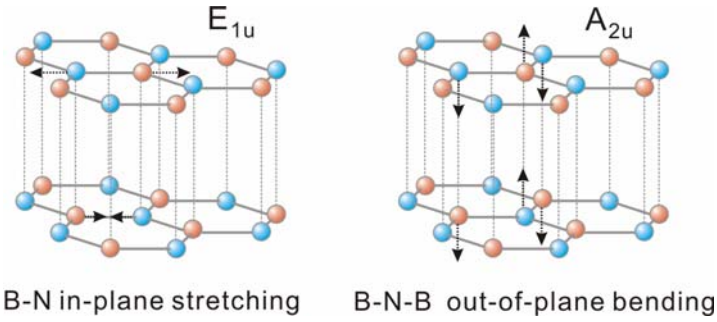

Fig. 1-4. Infrared active vibration modes of hBN.

difference between in-plane and out-of-plane vibration may be attributed to the more tightly bound of atoms in the plane than perpendicular to the plane.

By considering the sensitivity issue of hBN and cBN in IR and Raman, it is possible to determine the cubic fraction in the vapor deposited BN films. By using computer simulation employing the optical constants reported in the literature and experimental data, it is found that 1380 cm^{-1} (hBN) and 1070 cm^{-1} (cBN) roughly has the same sensitivity [10]. This provides a solid reason why the quantitative estimation of cBN is based on a simple mathematical calculation:

$$\text{Volume fraction of cBN} \approx \frac{I_{1070}}{I_{1070} + I_{1380}} \qquad (1\text{-}1)$$

where I_{1070} and I_{1380} are the transmitted intensity of the IR absorbance at approximately 1070 and 1380 cm^{-1}, respectively. However, substantial difference in sensitivity is presence in the visible and UV Raman scattering measurement of cBN and hBN. Peak intensity of hBN is two to three order of magnitudes stronger than that of cBN [11]. Raman spectral analysis of bulk cBN shows that the cBN TO mode exhibits a stress induced shift to higher energies. The pressure induced phonon shifts can be correlated to following equation as measured by Sanjurjo *et al.* [12]:

$$\omega_{TO}^{cBN} = (1054.7 \pm 0.6) + (3.39 \pm 0.8)\sigma \qquad (2)$$

which corresponds to $\Delta\omega_o \approx +3.4$ cm^{-1} per 1 GPa compressive stress. As a consequence, IR spectroscopy is frequently applied to determine the IR peak position of the cBN

reststrahlen band and to estimate the film stress. Particular attention has to pay to the high wavenumber (~1100 cm^{-1}) of cBN IR peak at the nucleation stage of cBN. This is attributed to the formation of small, separated cBN grain as proposed by Fahy *et al* [13]. The IR peak positions of various kind of polar bonding encountered during characterization of deposited BN films are tabulated in Table 1-1.

Table 1-1. Common IR peak positions encountered in BN film deposition.

	Bonding type	**Position [cm^{-1}]**	**References**	**Remarks**
1.	B-N-B (hBN)	780 (TO) 828 (LO)	[14]	Out-of-plane bending/deformation (A_{2u})
2.	B-N (hBN)	1380 (TO) 1610 (LO)	[14]	In-plane stretching, valence vibration (E_{1u})
3.	B-N (cBN)	1056 (TO) 1306 (LO)	[15]	T_2 symmetry
4.	B-N-B (wBN)	1200	[16,17]	Out-of-plane bending Tentative
5.	B-H	900-920 2500	[18,19] [20-22]	Bending Stretching
6.	$B-(OH)_3$	3000-3300	[20]	Tentative
7.	N-H	3250-3424	[9,18,20]	Stretching
8.	$N-H_2$	1540	[9]	Bending
9.	N-Si	900	[22,23]	Stretching, Si_3N_4:860cm^{-1}
10.	Si-Si	612	[16]	Bending

1.3. Electrical and electronic properties of cubic boron nitride

While phonon density of states governs the vibrational properties and thermal behavior of BN materials, electron density of states of BN dictates the electrical and electronic properties. Boron nitride, a compound isoelectronic to carbon, mainly differs from carbon in parametallic bonds and ionicity. Boron nitride does not have the parametallic π-bonds and is characteristic with crystal ionicity equal to 0.25 for cBN [24] As a consequence, all the allotropic phases of BN have a wide forbidden band in contrast to carbon system. The bandgaps of cBN and hBN is 6.2±0.2 and 5.8 eV, respectively [25]. The issue whether they are direct or indirect bandgaps is still not yet

clear because of some discrepancies between the theoretical and experimental results. The capacity in n- and p-type doping of cBN and electronic properties, but also extreme thermal and chemical stability are major cBN properties furnish the reasons for development and fabrication of high power and high temperature electronic devices operating in harsh environments and light emitting diodes capable of bandgap light emission. However, the electrical properties of cBN are not easy to characterize owing to small sizes of cBN crystals available. Most of the work is restricted to the HPHT synthesized cBN crystals with sizes on the order of 1 mm the best. Intrinsic or unintentionally-doped cBN crystal can exhibit n-type [26,27] or p-type [28-30] semiconducting character which may depend on the preparation methods. The origin of conductivity is not identified yet; carbon (B_C), oxygen (N_O) [31] and nitrogen vacancy (V_N) may work like donors in the cBN crystal [32]. Since ion-deposited cBN films intrinsically exhibit p-type conductivity, ion bombardment induced defects may play a crucial role in the type of cBN conductivity. Both beryllium (Be) and magnesium (Mg) were demonstrated to be a p-type dopant, while silicon (Si) and sulphur (S) produce donor levels in cBN. Be atom acts like the B atom in the lattice by reproducing the sp^3-like tetrahedral bonds. As a consequence, the induced acceptor state in the gap is just a perturbation of the p-like states at the top of the valence band. It was calculated that Be atoms can substitute B in cBN lattice with low formation energy making a shallow acceptor level close to the valence band minimum. The possibility of substituting of nitrogen in BN lattice by Be atoms has to lead to the formation of deep mid-gap levels [33], which is not favorable. Mg induced impurity states are considered to be less effective for p-type doping than Be induced states [34]. Beryllium and Mg impurities are substituted only to boron substitution sites. The Si behavior is slightly more complicated. Since Si is a group IV element it is amphoteric in nature, i.e. depending on the doping concentration, substrate orientation and growth conditions it might incorporate on both the B and N sites similarly like in GaAs. The incorporation might be dependent on crystal orientation. For example, Si is non-amphoteric on (001) GaAs when doping concentration is bellow 10^{18} cm^{-3}. It favors the Ga sites. In cBN, Si was found to be an ineffective n-type dopant in cBN thin films [35]. This may be

associated with the nanocrystalline nature of cBN films confining large amount of grain boundaries which may prevent the effective doping of Si into the cBN nano-grains. However, increase in concentration of Si during deposition may easily lead to the destabilization of sp^3-bonding in cBN, and result in the formation of hBN. In case of S-doped cBN, properties are not as good as those of Si-doped cBN [26]. The highest electron mobility achieved so far is 1 $cm^2/V{\cdot}s$ in contrast to 825 $cm^2/V{\cdot}s$ in Si-doped cBN [36], while the highest reported hole mobility of semiconducting cBN is 215 $cm^2/V{\cdot}s$. Though the electron and hole mobilities are not promising, when compared to the values of diamond, high temperature high-speed devices were successfully fabricated. Mishima *et al* [37] demonstrated that the cBN p-n junction diode is functional from room temperature up to 650 °C which is comparable to the highest operation temperature of SiC transistor. A summary of the electrical and electronic properties of cBN is tabulated in Table 1-2.

Table 1-2. Electrical and electronic properties of cBN.

	Dopant	**Carrier density [cm^{-3}]**	**Activation energy [meV]**	**Mobilities [$cm^2/V{\cdot}s$]**	**Resistivity [Ω·cm]**	**Ref**	**Remarks**
p-type	Be	5×10^{17}	220	2		[38]	Single crystal
			260			[39]	Polycrystalline
			230		$1\text{-}10^2$	[37]	Single crystal
		5×10^{16}	240			[40]	Single crystal
		4×10^{18}		215		[41]	CVD cBN film
	Mg	5×10^{18}	300	27	5×10^{-2}	[28]	PVD mixed BN
	None	5×10^{18}	60	500		[29]	PVD cBN Film
		5×10^{16}		177	8×10^{-2}	[28]	PVD mixed BN
n-type	S	$10^{12}\text{-}10^{14}$	320-470	1	2×10^4	[26]	Single crystal
			50			[31]	Single crystal
	Si		240		$10\text{-}10^3$	[37]	Single crystal
		1.5×10^{17}		825	10^{-1}	[36]	Single crystal
	None	10^{12}	470	20	5×10^5	[26]	Single crystal

1.4. Thermal properties of cubic boron nitride

The unique and attractive thermal properties of cBN, i.e. high thermal oxidation temperature and high thermal conductivity, can be combined with other promising physiochemical properties of BN to give a superior performance in optical, electronic and mechanical applications. While the thermal conductivity is highly related to the electrical conductivity in metal at a given temperature, the thermal conduction in electrically insulating materials such as diamond and cBN entirely refers to the lattice vibrations, i.e. the phonons. The lattice thermal conductivity is limited by phonon-phonon scattering and phonon-defect scattering. At high temperatures, the thermal resistivity is due to phonon-phonon scattering while the thermal conductivity is limited by scattering of the phonon by static lattice defects at low temperatures [42,43]. This immediately provides a reason why the reported room-temperature thermal conductivity of cBN thin film (950 W/m·K) [44] in the literature is comparatively lower than that of the bulk HPHT cBN crystals (1300 W/m·K). Cubic BN with small grain sizes may introduce another source of phonon scattering at the grain boundary, which accounts for the reduction of the thermal conductivity [43]. In an extreme case, the existence of different isotopes in a crystal may also disturb its periodicity and causes additional phonon scattering. Thus, solids which are isotopic pure (100%) should give an enhancement of phonon mobility and therefore the thermal conductivity [45].

There is a number of studies on BN oxidation, but they mostly are related to hBN. It was generally indicated that weight gain kinetics were observed for BN oxidation in dry air and oxygen, and weight loss kinetics were observed in water vapor. It was also reported that the oxidation of BN was sensitive to water vapor due to the formation of volatile product, HBO_2 [46]. The thermal oxidation stability of hBN is expected to be poor in wet atmospheres as the activation energy of hBN oxidation in dry oxygen is around 320 kJ/mol, which is about two-times larger than in water vapor environment [47]. It seems that the BN grains after oxidation are smaller along a-axis which implies that c-axis is much less reactive than a-axis. Fig. 1-5 demonstrates the thermal oxidation

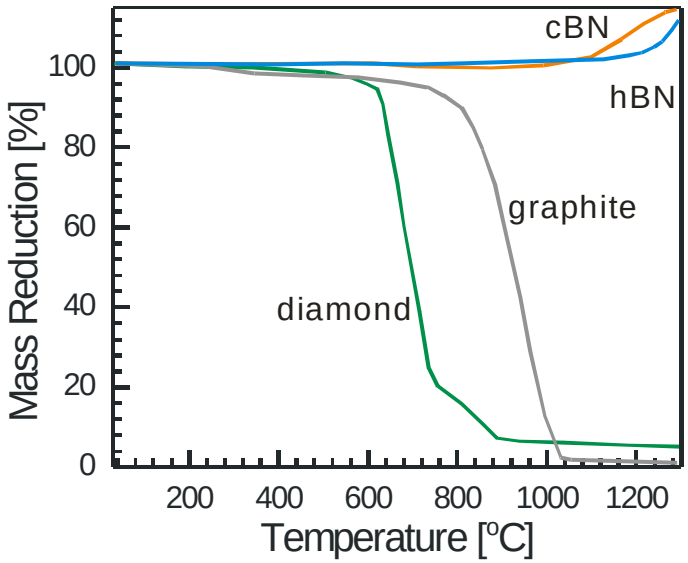

Fig. 1-5. Thermal oxidation of diamond, graphite, cBN and hBN conducted in an air stream using thermogravitic analysis.

stability of diamond, graphite, cBN and hBN conducted in a stream of air using thermogravitic measurements [48]. It is believed that the complete pyrolysis of diamond and graphite is caused by oxidative cleavage of the carbon-carbon bonds, irrespective of bonding properties. The high heat resistance of cBN and hBN is due to the high oxidation resistance of the constituent atoms, although pyrolysis to B_2O_3 and NO_2 occurs above 1100 °C [49].

Chapter 2. High pressure high temperature synthesis of cubic boron nitride

High pressure high temperature (HPHT) synthesis represents a technique which is the only method used in the mass production of bulk cBN crystals for industrial applications. Understanding this method, thermodynamic behind the conversion processes and mechanism of cBN formation may guide the experimental effort towards reducing the pressure and temperature thresholds. Therefore it is useful to give a brief summary on the direct conversion of graphitic BN into diamond-like BN phases being often assisted with catalysts. Thermodynamics says that the crystallinity and morphology of the starting materials as well as the catalysts and nature of pressure play crucial roles in the cBN formation.

2.1. Milestones in cubic boron nitride synthesis

Just two years after the first successful HPHT synthesis of diamond by Liander (ASEA group) and Bundy (GE research group), Wentorf synthesized the cubic form of boron nitride (cBN) under HPHT conditions with a zincblende (zBN) structure in 1957. This form is also called zBN in Japan or βBN in the former USSR [50]. In 1962, Wentorf [31] first demonstrated the potential of using cBN as a semiconductor. Therefore various impurities (such as Be, Si, S and KCN) were incorporated and studied under HPHT conditions. Later on, Bundy *et al* [51] (1963) proposed for the first time a phase diagram with cBN being the stable phase at ambient conditions. In 1975, this was however reconsidered by Corrigan and Bundy [1] who showed a cBN/hBN transition line parallel to that of diamond/graphite suggesting cBN as a thermodynamically metastable phase at normal condition. Though the synthesis and doping of cBN were reported in early 1960s, a substantial progress was achieved only two decades later. In late 1980s, Mishima *et al* [37,52] reported the electrical properties and UV emission of the cBN junctions. Nearly the same period, in 1988, Solozhenko *et al* [53] proposed

cBN is the thermodynamically stable BN polymorph up 1600 K at ambient pressure, which contrasts the early phase diagram proposed by Wentorf. Later on Solozhenko *et al* [54] refined their proposed phase diagram to a more precise one based on the new experimental and theoretical data.

2.2. Direct transformation at static pressure [8,55]

Regardless of exact position of the thermodynamic equilibrium line, a significant barrier hinders the direct transformation from sp^2 to sp^3 under ambient conditions. The threshold pressures of the direct transformation are affected by crystallinity/grain size and morphology of the starting hBN materials. The hBN to wBN transformation is highly pressure sensitive but insensitive to temperature because this transformation (≥12.5 GPa) was realized even at room temperature [1,51]. wBN seems to be prepared from well-crystallized hBN while poor crystallized hBN is converted to cBN at 6.0 GPa and 1200 °C but never into wBN even at pressures as high as 13.5 GPa [56]. If the applied hydrostatic pressure is high enough, cBN could also be realized under room temperature. Ueno *et al* [57] found that the rBN-to-cBN transition at room temperature is reversible at 15 GPa and becomes irreversible, at least above 55 GPa. The nature of the pressure also plays an important role for the diffusionless mechanism. A uniaxial compression (≥ 5.6 GPa at RT) of a highly textured rhombohedral structure in [0001] direction would be the most efficient for rBN→cBN martensitic transformation. The application of a shear essentially reduces the free activation energy and leads to various mechanism of structural deformation, whose occurrence is impossible under hydrostatic compression [58].

In general, the threshold pressure of cBN formation decreases with increasing amount of disordered structure in sp^2-bonded BN material. Since the direct transformation of cBN from hBN occurs via a destructive-reconstructive diffusion-like process, the activation barrier of transformation could be reduced by using the hBN material starting with highly defective structures and smaller grain sizes. The largest

reduction of the synthesis temperature is obtained by using aBN as a starting precursor material. Increasing three-dimensional order shifts the threshold temperature to high values for a constant pressure [59]. Sumiya *et al* [60] observed that aBN as starting material can directly be transformed to cBN using lower pressure and temperature (P-T) conditions. A small amount of cBN could be obtained at pressure higher than 6 GPa and temperature greater than 800 °C. Petrusha *et al* [61] suggested that in the imperfect initial structures, the heterogeneous mechanism was activated. It can decrease the value of Gibbs free energy of heterogeneous nucleation (ΔG^*) due to preferable nucleation in sites of various defects: vacant positions in the structure, dislocations, grain boundaries (triple joints) and structure of deformations (planes of twin junctions) were characterized by high energy and could be consumed for nucleation of new phase. The imperfection can also contribute to the activation of diffusion processes. Recently, Huang *et al* [62] demonstrated that the cBN phase nucleated directly from the sp^3-hybridized amorphous matrix, which was originally induced by ball-milling and is therefore responsible for the reduced HPHT conditions (7.7 GPa, 900 °C). The cBN grains, as revealed by HRTEM, were less than 3 nm in size and they are nucleated directly from the amorphous matrix. This cBN nucleation mechanism is completely different from the so-called diffusionless "puckering" mechanism. The cBN grains nucleated directly from the amorphous matrix via a diffusion process.

2.3. Boron nitride conversion at static pressure with catalytic assistance [8,55]

In contrast to the direct transformation process which is very sensitive to the nature of starting hBN material, the nature of catalysts is vital in determining the threshold pressure and temperature for nucleation and growth of cBN. Specifically, such a catalytic process can be summarized as follows. The catalyst/solvent is added into hBN in order to decrease the high activation energy barrier, act as a flux precursor and

form a eutectic compound containing hBN which is partially dissolved into this eutectic. The driving force for cBN formation is the solubility difference between hBN and cBN in the eutectic flux, under fixed HPHT conditions.

The commonly employed catalysts/solvents are alkaline (Li_3BN_2), alkaline earth metal nitrides (Mg_3N_2, Mg_3BN_3, $Mg_3B_2N_4$, $Ca_3B_2N_4$, Ca_3N_2 and $Sr_3B_2N_4$), ammonium salts and water. NH_3-based substance such as ammonium borate resulted from the reaction of the starting hBN with water may act as flux and thus facilitate the cBN synthesis [63].

Generally, the threshold temperature of cBN formation agrees with the eutectic temperature of the system and the maximum temperature at constant pressure coincides with the equilibrium temperature between cBN and hBN. Fukunaga *et al* [64] studied the nucleation and growth cBN using $Ca_3B_2N_4$ solvent and found that cBN was precipitated even at 3.6 GPa. The minimal temperature for cBN growth was governed by liquid forming temperature line. Most recently, by using supercritical N-H fluid, the threshold pressure of BN crystallization at HPHT has been reduced down to 1.9±0.2 GPa [65]. The main features of the cBN crystallization from the solution in this fluid are the large number of small cBN nuclei and the high cBN growth rate. The grown cBN crystals are characterized by small sizes and imperfect morphology.

The cBN crystals prepared by catalytic conversion process have predominant tetrahedral or octahedral shapes (usually truncated). The colour of cBN crystals which varies generally from black to brown is due to the boron content. Crystal surface is smooth in case of low oxygen content in hBN starting sample but irregular and pitted in other case. The colour of the cBN crystal is attributed to the imperfection of the crystal due to some defects, faults and impurities. While nitrogen is well-known to be major impurity in HPHT diamond, oxygen may be the candidate, which plays a major role in quality of cBN crystal. Taniguchi *et al* [32] suggested that barium element itself has potential as an oxygen getter in the HPHT growth of cBN, in which colourless crystal

could be obtained using $Ba_3B_2N_4$ (tens ppm of oxygen) while using Li_3BN_2 resulted in amber crystal (thousand of ppm oxygen).

2.4. Boron nitride conversion at dynamic pressure [8,55,66]

Shock wave induced dynamic pressure is used to transform the initial graphite-like soft phases into final diamond-like hard phases of BN. This method is similar to martensitic phase transformation of hBN to wBN under static compression at room temperature condition as described in previous session. The basic product of the polymorphous transformation of the graphitic BN under shock compression is the wurtzitic modification [66]. This is attributed to fact that the formation of the cubic modification of BN in the purely deformative way needs a mutual torsion of the layers. This form of the deformation is highly inconvenient, because it cannot be realized by the motion of dislocations. Therefore, cBN can arise from hBN only in the way of a diffusive transformation. Similar to static compression, the perfection of the hBN structure is a very important factor determining the final composition of the transformed product. Borimchuk *et al* [67] investigated the influence of the index of the three dimensional order (p_3) of the graphitic BN on the phase composition of the transformed product. In the material with an initially almost perfect lattice (p_3=0.95) as identified. With a decreasing index p_3 the content of cBN was increasing. In the fully turbostratic material ($p_3 = 0$) only cBN was identified.

2.5. Summary to high pressure high temperature boron nitride conversion

High pressure high temperature synthesis with assistance of metal catalysts can produce bulk quantities of small cBN crystallites. Only these techniques have been commercial so far. However cBN synthesis employing amorphous BN as starting material as well as catalyst/solvent process under HPHT could be the best way for further commercial exploitation of cBN.

Chapter 3. Low pressure synthesis of cubic boron nitride

High pressure high temperature (HPHT) synthesis of cubic boron nitride and relevant parameters governing the formation of cubic phase are discussed in previous chapter. In following we extend the discussion further towards the cBN formation by low pressure methods. The high kinetic barrier encountered in this cBN synthesis is overcome by employing energetic ions or neutrals induced by the different plasma systems. Regardless the methods used the energetic particles are vital in low pressure synthesis. However, their kinetic energies have been continuously lowered closer to the values of thermal energies via involvement of chemically reactive species and mediating chemical reactions. Two groups of competitive methods are then employed for cBN growth, i.e. physical vapor deposition and plasma enhanced chemical vapor deposition. They differ in kinetic energy of particles and chemical environment employed. The methods of synthesis applied to the development of cBN thin film technology and learning on fundamental phenomena using experimental and modeling approaches has however been extrapolated to interfacial studies and synthesis of viable thick cBN for industrial exploitations.

3.1. Foundations on technology of thin cBN films

Cubic BN films have been prepared by physical vapor deposition (PVD) and plasma enhanced chemical vapor deposition (PECVD). PVD is a group of deposition techniques based on physical removal of solid material, which is then transported and deposited on the substrate. PVD also refers to all ion beam and sputtering techniques including those aided with reactive environments. The energy of sputtered particles (~1–2 eV) is insufficient and substrate biasing is required to promote cBN growth by energetic ion impact. Energetic impact is also needed for the growth of cBN films using electron beam evaporation of boron and simultaneous bombardment by ion beams containing nitrogen reactants. All ion based PVD methods employed for cBN

deposition [68] including mass separated ion beams deposition (MSIBD) [69] and sputter deposition [70] with direct current (DC), radio-frequency (RF) and pulsed bias are similar in their physical principles.

The elucidated abbreviation PECVD above designates the depositions at which non-condensable molecular gases supplied into reactors are converted to condensable radicals in electrical discharge, plasma, mostly via electron-molecular collisional processes. In the plasma, the gas phase activation and chemical reactions are usually at relatively low pressures. The condensable radicals then form solid products on the substrates via gas–surface reactions, which may proceed with evolution of gases. These processes can be illustrated by the following chemical pathway reactions

$$(XY)_{Gas} + (ZW)_{Gas} \rightarrow (XZ)_{Gas} + (YW)_{Comd.\ Rad.} \rightarrow \text{Solid Product} + \text{Gas}_{Exch.\,\text{Reac}}.$$

This generalized reaction also satisfies the processes in conventional CVD driven solely by thermal energy. Although high temperatures are employed for the activation of molecular gases, cBN synthesis using conventional CVD methods has not been successful. Energetic ions generated by a sufficiently high bias potential are needed to obtain cBN films [71,72]. However, the effective bias differs by plasma potential varying with the deposition parameters (pressure, power supplied into plasma and gas composition). The value of plasma potential is difficult to determine during the deposition and its magnitude is relatively small in most cases, so that only the bias voltage is usually reported.

3.2. Low pressure synthesis by plasma enhanced chemical vapor deposition

The plasma enhanced chemical vapor deposition (PECVD) of boron nitride materials is usually carried out with assistance of toxic and explosive diborane or corrosive borotrihalides. Due to potential hazardous nature of the gases, some attempts in BN synthesis have been made using less reactive boron precursors with a low toxicity.

Table 3-1 gives a summary of common boron precursors employed in either CVD or PECVD synthesis of BN. It is worthy noting, successful depositions of solid BN films inevitably require hydrogen to be involved in the chemical reactions regardless the form of its supply. Hydrogen might be confined in molecules of boron precursor or additional hydrogen gas should be fed into CVD mixtures of borotrihalides to fulfill the thermodynamic chemical reactions. Otherwise no solid BN can be obtained. Owing to structural and physical similarity between BN and diamond polymorphs, one may logically deduce that cBN synthesis could be established on hydrogen chemistry. In deed a number of works published prove the presumption of cBN synthesis based on the hydrogen [73]. The referenced work postulates that cBN could be prepared without using any substrate bias since atomic hydrogen acts as a selective etching agent and assists the stabilization of sp^3-bonding similar to the deposition of diamond films. However, their results are mostly based on infrared data and need further substantiation by other characterization techniques. Konyahshin *et al* [74] extended the study of the surface of the tBN and aBN after hydrogen plasma treatment by using high-resolution Auger electron spectroscopy and found that special features of Auger spectra that are typical for sp^2 BN, are found to be much weaker or even disappear when the aBN and tBN surface is hydrogen plasma treated. Though the hydrogen has showed etching ability to BN phases, there was no difference in etching rates between well-crystallized cBN and hBN under hydrogen plasma etching as observed by Bartl *et al* [75]. It is considered that if the sp^2-bonded hexagonal phase could be preferentially etched as in the case of the diamond film, the cubic phase content would increase with increasing hydrogen flow rate. However, Kim *et al* [76] found that hydrogen etched hexagonal and cubic phases simultaneously and the amount of cubic phase in BN:C film was decreased with increasing hydrogen as revealed by their FTIR absorption spectra (cBN phase content reduced from 75% to 50% for hydrogen flow rate increased from 1 to 6 sccm). This result implies that the incorporation of hydrogen into the cBN film synthesized by a CVD process could play a role in delaying the nucleation of the cBN phase [77-79]. A compilation of experimental results using diborane diluted in hydrogen and helium in the literature showed that only high cubic BN phase was obtained using the helium

based plasma, which may give additional hint on the role of hydrogen in deposition of BN films. Borotrifluoride seems to be suitable precursor gas for boron and fluorine in cBN synthesis by low pressure PECVD since boron incorporate to solid BN films and fluorine plays a similar role like hydrogen in the CVD diamond where atomic hydrogen is effective etchant of non-diamond phases and stabilizing agent of diamond surfaces. The fluorine role is discussed in Chapter 6, 7 and 8.

Table 3-1 Typical boron precursors used for BN synthesis

Boron precursor	**Chemical formula**	**Remarks**	**Ref.**
Borotrichloride	BCl_3	Corrosive gas	[80]
Borotrifluoride	BF_3	Corrosive gas	[81]
Trimethyborazine (TMB)	$CH_3{\cdot}B_3N_3H_3$	Non-corrosive and non-explosive liquid with a low toxicity	[16]
Diborane	B_2H_6	Explosive and toxic gas	[82]
Borane-ammonia	$BH_3{\cdot}NH_3$	Non-toxic, white crystalline solid	[83]
Borazine	$B_3N_3H_6$	Non corrosive liquid, less toxic than other precursors such as diborane and borotrichloride	[84]
Borane-dimethylamine (BDMA)	$BH_3{\cdot}NH(CH_3)_2$	Solid at room temperature. To obtain vapors, the precursor is heated up to 37 °C. The resulting vapor is carried to the reaction chamber via an inert gas.	[85]

3.3. Low pressure synthesis of cubic boron nitride by physical vapor deposition

While in cBN synthesis by PECVD, the attention has particularly been paid to the species providing surface stabilization and selective etching, PVD techniques have been dealing with nucleation and growth as functions of the deposition parameters (threshold substrate temperature, threshold bias voltage, ion flux, deposition flux, ratio of ions to deposited atoms, etc.) It is believed that both the nucleation and growth of cBN are associated with a number of elementary processes involving subplantation, densification,

peening processes, thermal and pressure spikes, but involving also chemical reactions. These factors are the driving forces behind the cBN formation. During the course of cBN film development, several growth models have been proposed to explain the nucleation and growth mechanism. The models are based on general structural patterns of BN films observed on different substrates. The cBN is confined in a sandwich structure, i.e. between the aBN/ tBN precursor layers and a very thin non-cubic surface layers. Cubic BN films are however nanocrystalline in nature and therefore cannot provide cBN Raman peaks like nanodiamond cannot. The structural pattern described led to several speculative models (stress, subplantation, thermospike, sputtering, momentum models) all based on the phase transformation or enrichment effects induced by energetic particles. Since the PECVD deposited cBN films can also be prepared with assistance of energetic ion bombardment only, it is widely recognized that the whole cBN formation process are governed by physical processes rather than chemical processes. Although several growth models exist, they cannot give a complete picture on the cBN formation. According to the stress model proposed by Mckenzie *et al* [86], the stress induced by the energetic ion impact can reach values corresponding to HPHT synthesis of cBN. The origin of compressive stress may be attributed to the creation of interstitial sites by atomic peening effect. The incorporation of Ar (possibly at interstitial) in the cBN films could be as high as 1.5% as revealed by RBS. The stress model explains the cBN growth as a result of internal biaxial compressive stress in the BN film due to the ion bombardment. The formation of graphitic BN interlayer before cBN growth can easily be explained by accumulation of stress reaching the critical threshold values in the HPHT. The anisotropic compressibility of hBN under biaxial compressive stress will lead to the texture formation of tBN interlayer with its c-axis parallel the substrate. However, this model cannot explain the inability of growth cBN at room temperature. The model also cannot elucidate the cubic phase formation in BN films prepared by PECVD where internal stress is far below that required for hBN to cBN conversion (<1 GPa). Similarly, the ion deposition of cBN can also be treated as a cylindrical thermal spike [87], and the complete rearrangement of the spike volume can be regarded as result of the formation of dense modification of boron nitride. Base on

the difference of sputtering yield between cBN and hBN, Reinke *et al* [88] suggested that the hBN characteristic with higher sputtering yield will be resputtered more efficiently by the energetic ion bombardments and the cBN with low sputtering will survive during the film growth. In case of subplantation model [89], the energetic ions can be implanted within the top several layers of substrate surface. As the number of implanted ions increases, the local density of the bombarded region increases corresponding. Consequently, the stress will build up accordingly. All these will drive the transformation of sp^2-bonded BN to sp^3-bonded BN. Since the subplantation model describes the energetic ion deposition process of cBN as a sub-surface implantation process and includes the typical ion atom interaction processes, it might satisfactory explain some cases of cBN synthesis at which ion energies are considerable, i.e. above atomic displacement energies.

Chapter 4. Thermodynamics and kinetics of BN

Thermodynamics and kinetics of BN is means leading to understanding of the phase stability of different polymorphic BN modifications and perspective view on the controversial issue of the thermodynamic stability of cBN at standard temperature and pressure (STP) conditions. Basically, according to the early established data and the assumed similarities to diamond system, one may adopt the BN phase diagram proposed by Corrigan and Bundy [1] and treat cBN as the metastable phase at STP conditions. This prediction is based on the existence of a common threshold pressure of about 4-5 GPa for the cBN growth. The extrapolated hBN-cBN solid line towards lower temperature intersects at the pressure axis, which is evidence of graphitic modification being the stable phase as indicated by the dotted-line in Fig. 4-1. However, in accord with the recent experimental and theoretical studies, Solozhenko proposed that cBN should be the thermodynamically stable phase at STP conditions. In particular, the calculated equilibrium line for hBN and cBN modifications does not intersect the pressure axis as suggested by the Corrigan-Bundy [1], but intersects the temperature axis at 1570 K [53] as illustrated in Fig. 4-1 by the solid line. By using supercritical fluid, Solozhenko was able to prepared bulk cBN crystal at pressure as low as 2 GPa (shaded area in Fig. 4-1) [3]. Demazeau *et al* [90] observed that a considerable reduction of the thermodynamic conditions may result from the use of non-conventional catalysts such as voltatile hydrazine (NH_2NH_2) under supercritical conditions. Employing seed single crystals of diamond, it was shown that the cBN crystal growth had been possible on the seed surfaces in the systems (hBN-Mg_3N_2-NH_3) at 0.5-2.0 GPa and 1300K [91]. Based on numerous in-situ diffraction experiments using synchrotron radiation including kinetic measurements, Will *et al* [92] verified the theoretical results calculated by Solozhenko and thus suggested that cBN is definitely the stable phase at STP conditions in contrast to metastable diamond. Also, calorimetric measurements of the combustion enthalpy of cBN with fluorine seem to provide evidence that the cubic and not the hexagonal phase is stable under STP conditions in contrast to the

diamond-graphite system [75]. Besides, Kern *et al* [93] studied the lattice dynamics and phase stability of cBN using *ab initio* and found that at low temperature cBN is the stable modification; the cBN/hBN coexistence line intersects the temperature axis at 1440 K. It seems that cBN is the thermodynamically stable phase at STP conditions, and that hBN becomes stable at temperatures of about 1200-1800 K. The onset temperature of the phase transition from cBN to hBN depends significantly on the grain size and impurities, and the formation of hBN starts preferably at the surface [94]. Furthermore, Albe *et al* [95] reported the theoretical study of BN modifications at hydrostatic pressures using density functional theory (DFT) within local density approximation (LDA) and predicted cBN as a stable modification at STP condition.

Although cBN is considered to be the stable phase at STP conditions, cBN has not been prepared by conventional (thermally activated) CVD, and cBN is difficult to prepare by both PECVD and PVD. The syntheses employing the two later techniques require ion assistance.

A qualitative explanation on cBN phase stability can be given by the two empirical chemical rules of Ostwald and Ostwald-Volmer. The Oswald's rule states that a system will not reach the stable ground state directly, but instead passes through all less stable states (hBN in this case). According to the Ostwald-Volmer's rule, the less dense phase (again hBN) will nucleate first, which is a general thumb rule for kinetic reaction behavior [96]. Therefore, hBN is usually the end product of conventional chemical reactions leading to the formation of boron nitride. [97].

In general, the phase diagram just provides the information about a reaction whether it is feasible to occur thermodynamically or not. The rate, at which the reaction proceeds, depends on the nucleation of a new phase and the activation energy of the transformation (if intermediate state is involved). There is nothing about the kinetics that can be extracted from the phase diagram. While applying pressure can modify the thermodynamic reactivity of BN, a large activation barrier often limits the reaction rate

at high pressure. From the standpoint of kinetics, the driving force of transformation (a difference in free energy between the initial and the final phases), the activation energy barrier and the possibility of alternative behavior (leading to the metastable phase formation) are the three most important factors in a solid-phase transformation. Reliable data on the kinetics of cBN crystallization can be obtained only in-situ using X-ray diffraction. However, studies of compounds of low-Z elements, specifically BN, at HPHT in real time are only possible with the using of high intensity synchrotron X-ray radiation. The incorporation of BN clusters that approach surface of a growing cBN crystal is hampered by the necessity to form only the B-N bonds with the formation of B-B and N-N bonds being inadmissible, which can result in increase of activation energy [98]. High activation energy can also be realized as reported by Yoo *et al* [99] who studied the direct elementary reactions of B and N at HPHT. Despite the thermodynamic stability of BN at high pressures, boron and nitrogen do not react at ambient temperature at 50 GPa (the highest pressure of this experiment). This observation implies that there is a large kinetic barrier to reaction, especially in the dissociation of N_2.

Up till now, there is still no consensus of opinions about which BN modification is the thermodynamic stable phase at ambient conditions. It has been pointed out in a study that theoretical study using DFT within the LDA and the generalized gradient approximation (GGA) on structural properties of BN result in different conclusions. Janotti *et al* [100] found that LDA calculations predict dense cubic structures as ground state structures, while the GGA calculations predict less dense hexagonal layer structure as ground states. In case of thin film BN deposition, advocates of cBN being the metastable phase argued [101] that effect of surface tension induced by the nanometer-size curvature of critical nuclei could drive the metastable phase region of cBN nucleation into stable phase region of the BN phase diagram; consequently cBN nucleation would occur prior to hBN nucleation in competing growth of cBN and hBN upon CVD. The additional pressure notably increases with the decrease of crystal particle size. In the size range below 3 nm, the additional pressure rises to above 3.0

GPa, which is above the Corrigan-Bundy line. The effect of surface tension, so-called the nanosize-induced additional pressure on Gibbs free energy of critical nuclei should be reasonably taken into account. The nucleation of cBN synthesis upon HPHT supercritical fluid system would be limited in nanometer scale.

For rBN and wBN, Solozhenko *et al* measured the compressibility of wBN at room temperature up to 66 GPa and found that there is no thermodynamic stability region for wBN [102] on the equilibrium phase P-T of boron nitride. Similary, rBN also has no thermodynamic stability region. At low temperatures far from the phase equilibrium, the rBN has a higher Gibbs free energy than the graphite-like hBN and both the diamond-like wBN and cBN forms of this compound [58].

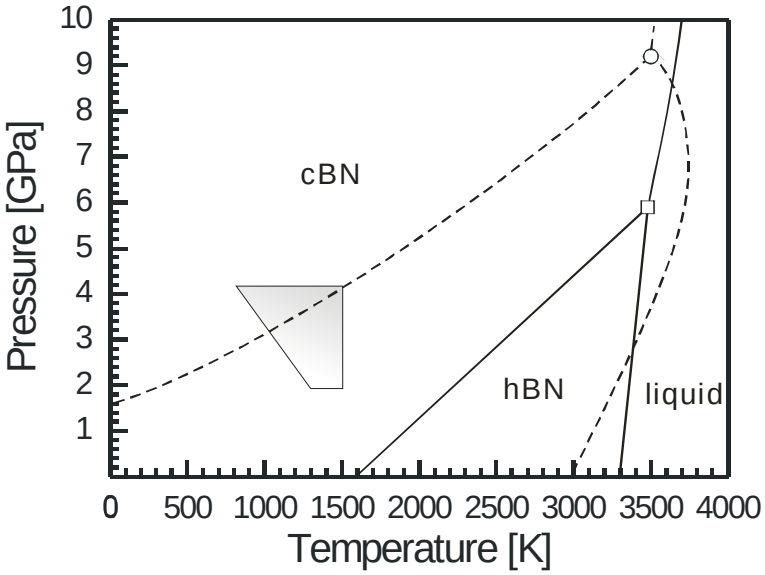

Fig. 4-1 Equilibrium phase diagram of boron nitride. Dotted line – proposed by Corrigan and Bundy [1]; Solid line – proposed by Solozhenko [2] and shaded region – cBN obtained under supercritical fluid [3].

Chapter 5. Experimental methods and characterization techniques

This chapter describes methodology of synthesis and characterization of boron nitride films used in this work. Plasma enhanced CVD and PVD techniques, specifically ECR-PECVD, RF-MS and MSIBD were employed to investigate the parameters affecting the cBN nucleation and growth. Employing different techniques can provide better understanding of cBN nucleation and synthesis which in return may also contribute to further technological development of cBN films and their industrial applications.

5.1. Deposition systems used in BN synthesis

5.1.1. Electron cyclotron resonance plasma enhanced chemical vapor deposition

An electron cyclotron resonance plasma enhanced chemical vapor deposition (ECR-PECVD) exploiting a He-Ar-N_2-BF_3-H_2 gas mixture was used to deposit cBN films. A schematic diagram of the experimental setup is in Fig. 2-1. The plasma was generated with an ASTeX 1.5-kW microwave source. A magnetic field of ~875 G was applied to the central region of the reaction chamber. Mirror-polished Si (100) wafers (50×50 mm^2 with thickness of 0.5 mm) were used as substrates. Prior to the deposition, the substrates were pre-scratched with a diamond powder (grain size ~3 μm) and then cleaned in ultrasonic baths of acetone and ethanol in sequence. In the reaction chamber, the substrates were mounted on a DC-biased tantalum plate, which was set on a resistively heated hexagonal BN (hBN) holder. After evacuating the chamber to a pressure of 10^{-6} Torr, the samples were cleaned in situ using a He/Ar/N_2 plasma and negative substrate bias to remove residual impurities and oxides from the substrate surfaces. The cleaning procedure was followed by introducing H_2 and BF_3 into the chamber for the successive nucleation and deposition of BN films. Additional

experiment details are summarized in Table 5-1. Both the substrate bias and deposition duration were varied over wide ranges to investigate their effects on the phase purity and crystallinity of cBN films. The substrate temperature was measured with an optical pyrometer.

The same deposition system was also used for preparation of cBN on diamond-coated Si substrate (cBND/Si) for studying the cBN nucleation and growth. Diamond films were first deposited on Si (100) substrates using a commercial 1.5 kW ASTeX microwave plasma CVD reactor. A bias-enhanced nucleation (BEN) was performed using a 5%CH_4/95%H_2 gas mixture at a total gas flow rate of 300 sccm, pressure 20 Torr, microwave power 800 W, substrate temperature of 850 °C and bias voltage of –150 V. The BEN took 15 minutes. During the growth, a 1%CH_4/99%H_2 mixture was used at a dynamic pressure of 40 Torr maintained by a total gas flow rate of 300 sccm. The deposition temperature was varied from 750 to 850 °C to control the film morphology. The microwave power was maintained at 1400 W. The diamond film thickness ranged from 40 nm to 10 μm.

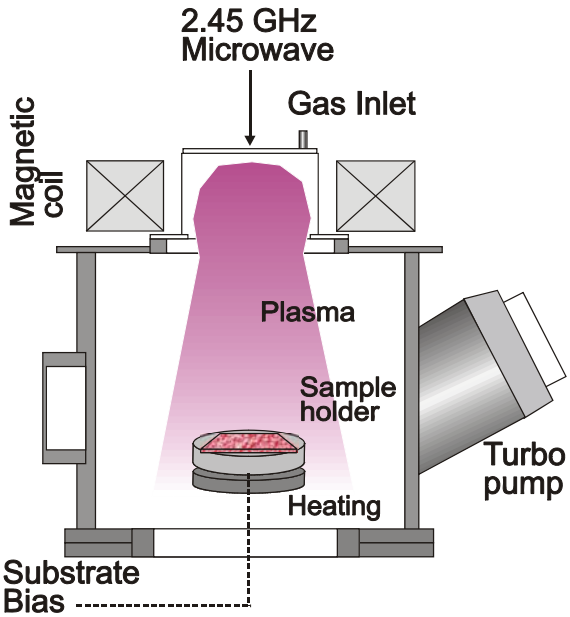

Fig. 5-1. A schematic diagram of ECR-PECVD system for the deposition of cBN films.

Table 5-1. Process parameters for the deposition of cBN films by ECR-PECVD. Cleaning of Dia/Si substrates could be at positive biasing with the introduction of BF_3.

		Cleaning	Deposition
Ar	sccm	10	10
He	sccm	140	140
N_2	sccm	50	50
BF_3	sccm	---	1
H_2	sccm	---	1 – 10
MW power	W	1400	1400
Pressure	mTorr	1.5	1.6
Substrate temperature	°C	900	600 – 900
Bias voltage	V	– 150	0 ~ – 60
Duration	h	0.5	1 ~ 6

5.1.2. Mass-selected ion beam deposition of boron nitride films

BN films were also prepared on Si (100) substrates with different surface roughness employing mass selected ion beam deposition (MSIBD). Two series of substrates were differently pretreated. The first series of substrates was scratched by diamond powders with grit sizes of 0.25, 1 and 3 μm. The second series of substrates was scratched by proper sizes of alumina powders in order to generate equivalent surface roughness. The typical size of the substrates was about 0.5×0.5 cm^2. Prior to loading the samples into the deposition chamber, all the pre-scratched Si substrates were cleaned by ultrasonic agitation in acetone and ethanol baths. In each BN deposition, four Si substrates were simultaneously heated to 250 °C and sputter-cleaned by 1 keV Ar^+ ion beam. The BN growth was carried out at 10^{-8} mbar by sequential deposition of mass-selected $^{11}B^+$ and $^{14}N^+$ ion beams in cycles. The ion energies varied from 75 to 500 eV. The boron and nitrogen ion beams with current densities of 25 μA/cm^2 and dose of 10^{15} ions/cm^2 were scanned to ensure the thickness homogeneity and stoichiometry of the films (with hardly measurable systematic deviations) over an area of 0.8 cm^2. The corresponding deposition system and the simplified ion-beam trajectory are shown in Figs. 5-2 and 5-3.

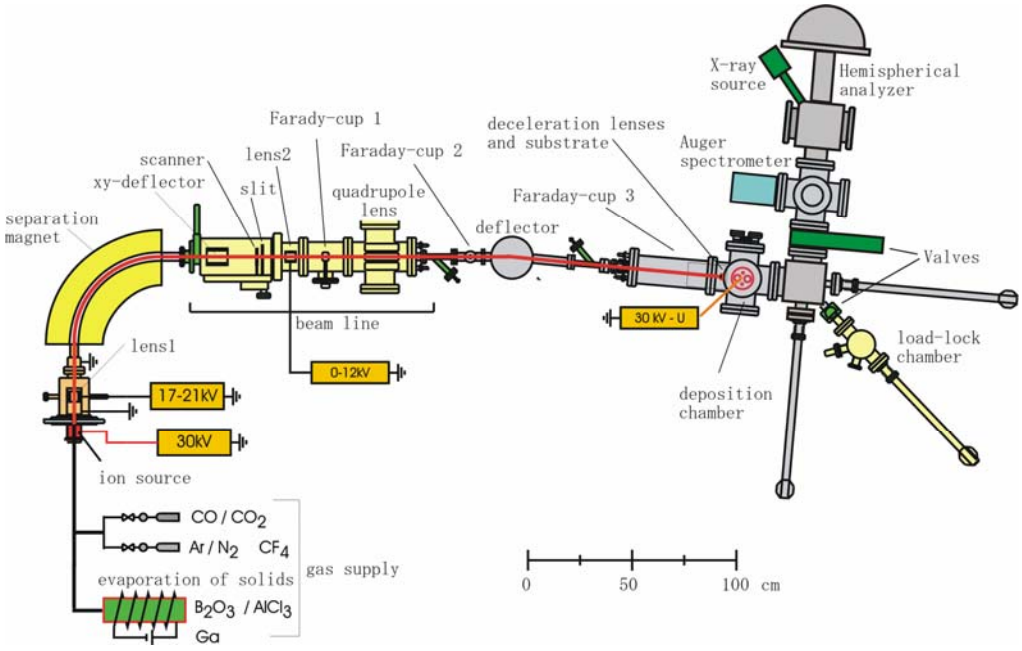

Fig. 5-2. Mass selected ion beam deposition system used for deposition of cBN films (With courtesy of Hans C. Hofsäss, the George August University, Göttingen, Germany)

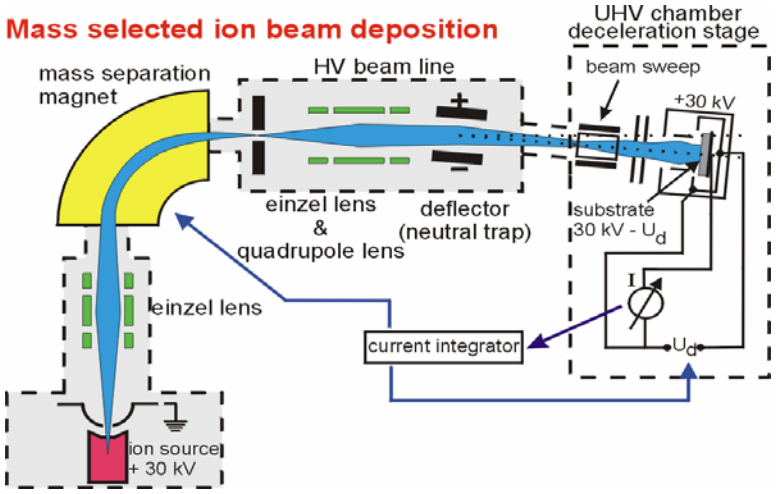

Fig. 5-3. Schematic drawing elucidating the path of B^+ and N^+ ion beams supplied by a Sidenius hollow cathode ion source. The ion beams are transported at ~30 keV and then slowed down to impact the sample at energy on the order of hundreds eV. (With courtesy of Hans C. Hofsäss, the George August University, Göttingen, Germany)

5.1.3. Radio-frequency magnetron sputtering (RF-MS)

Radio-frequency magnetron sputtering (RF-MS) is another PVD deposition to investigate nucleation and growth processes of cBN films. Unlike MSIBD suitable only for studying the deposition processes, the magnetron sputter deposition is scaleable for mass production. The schematic shown in Fig. 5-4 is a modified Kurt J. Lesker vacuum deposition system. It comprises a planar magnetron with an hBN sputtering target, three inches in diameter, coupled to a 13.56 MHz RF generator (Advanced Energy, RFX500) through an auto-tuning matching box unit. Typical RF power of 150 W was imposed on high purity pyrolytic BN target (3N), which is equivalent to a target power density of 3.3 W/cm^2. The substrate is independently biased by a 333.3 kHz pulse generator (ENI) in order to control ion energy of the species impinging the substrate. The substrate was resistively heated by a 1.0 kW baroelectric ceramic heater (Advanced Ceramics). The substrate temperature was monitored by a K-type thermocouple. Typical deposition parameters are summarized in Table 5-2.

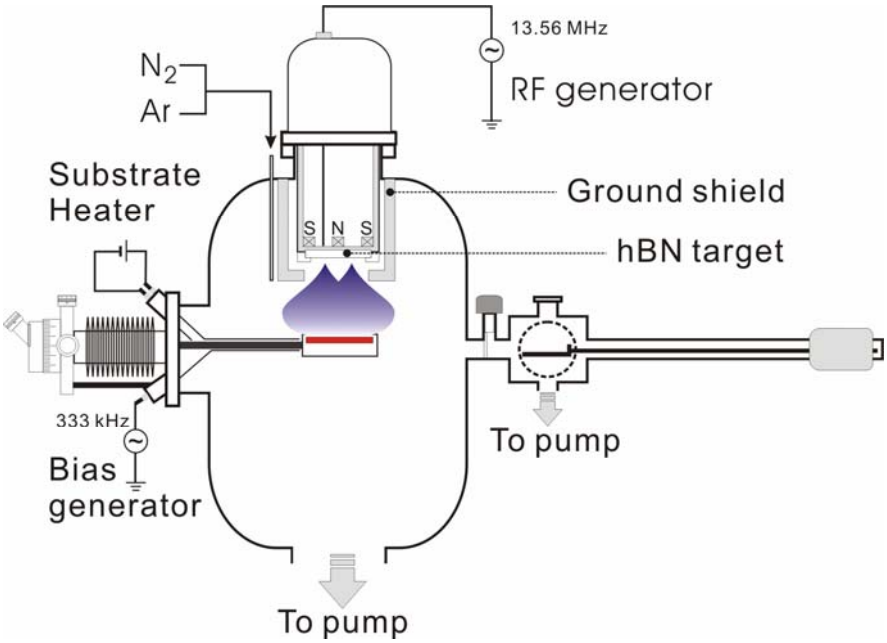

Fig. 5-4. Schematic of an ultra-high vacuum sputter deposition system for cBN synthesis equipped with a radio-frequency magnetron using an hBN target, three inches in diameter.

Table 5-2. Deposition parameters of cBN films by RF-MS.

		Cleaning	Deposition
Ar	(sccm)	90	20
N_2	(sccm)	---	10
RF target power	(W)	---	150
Pressure	(mTorr)	---	16
Substrate	(°C)	900	800-900
Bias voltage	(V)	–120	–90
Duration	(min)	5	180

5.2. Characterization techniques in analysis of cubic boron nitride films

A number of characterization techniques was employed in analysis of boron nitride films synthesized within this work. The analytical techniques were selected upon their effectiveness to resolved different boron nitride phases, availability, desired properties being measured and cross-checking the data obtained. Table 5-3 summarizes the characterization techniques used herein. The most common technique and important was Fourier transform infrared (FTIR) absorption spectroscopy used for the routine identification and quantitative estimation of cBN and hBN phases. FTIR provides information on local BN bonding very quickly, and it is considered to be insensitive to the ordering of the phases inside the films. The primary advantage of FTIR is that it resolve cBN phase with relatively short range of crystallinity on the order of tens nanometers. The longer range of ordering (crystallinity) of BN crystallites, signified as high crystallinity, can be evaluated either by micro-Raman or X-ray diffraction spectroscopy. The extracted spectral data particularly full width at half maximum and

Table 5-3. Characterization techniques used in this study.

Technique	Model	Remarks
FTIR	Perkin Elmer PC 1600	
Raman	Renishaw Raman 2000	514.5 nm
XRD	Rigaku X-ray diffractometer	Glacing angle, 40 kV
TEM	Philips CM200 (FEG)	Equipped with EELS
SEM	Philips XL30 (FEG)	
AFM	Digital Inst. Nanoscope IIIa	Si Tip, Tapping mode
XPS	VG ESCA-Lab 220i X	Al K_α , hν=1486.6eV
XANES	Canadian Synchrotron Radiation Facility (CSRF) at the Synchrotron Radiation Center, University of Wisconsin-Madison	beam size: 1×5 mm^2, energy resolution near B K-edge: 0.1 eV, 1800 lines/mm grating
Indentation	MTS Nanoindenter XP	Berkovich diamond tip

relative intensities of the peaks characteristic to cBN and hBN phases can be used to determine the crystal size and preferred orientation of the crystals, respectively. While these two techniques provide macroscopic information on the BN films, high resolution transmission electron microscopy equipped with electron energy loss spectrometer is used to reveal the local lattice arrangement and elemental distribution, which is prominent means to study interfaces, structural and atomic arrangement of various phases emerging at cBN nucleation and growth. On the other hand surface properties of the BN films were investigated by scanning electron microscopy (SEM), atomic force microscopy (AFM) and X-ray photoelectron spectroscopy (XPS). SEM and AFM reveals morphological information while XPS provides us with chemical analysis and bonding information on materials to the probing depth of several tens angstroms. The probing depth can varies upon the photoemission take off angle (angle resolved XPS). XPS can use either achromatic X-ray sources Mg K_α ($h\upsilon$ = 1253.6 eV) and Al K_α ($h\upsilon$ = 1486.6 eV) or monochromatic Al K_α for high spectral resolution. Unlike XPS which uses the preset energy of photons, X-ray absorption near edge spectroscopy (XANES) varies the energy of X-ray photons extracted from synchrotron radiation source over

wide range of energies. The XANES can be used to determine the local bonding and orientation of hBN on the surface and in depth depending on probing signals. The samples used for XANES study are given in Table 5-4.

Fig. 5-5. Snapshot of milling head with cBND coated WC and uncoated WC cutting inserts under ball milling test.

The mechanical properties of thick CVD prepared cBN films were evaluated by nano-indentation measurement to determine their hardness and elastic modulus. Coatings of cBND (cBN with diamond as buffer layer) on cutting inserts were tested by milling of mold steel M238 (Hardness Brinell ~250 HB). In severe milling operation (Fig. 5-5) the cBND coated and uncoated reference inserts were mounted on a machining head with a diameter of 5 cm. During machining, the inserts periodically impacted on the 30 mm thick plate with length of 30 cm at a peripheral speed of 10.2 m/s. The cutting depth was 0.3 mm.

Table 5-4. Preparation, substrate and thickness of cBN thin film samples, and the phase concentration and preferable orientation of the tBN in the films.

Sample name		A					B			C	
		A_1	A_2	A_3	A_4	A_5	B_1	B_2	B_3	C_1	C_2
Substrate		Mirror-polished Si	0.25μm-Dia scratched	1μm-Dia scratched	3μm-Dia scratched	3μm-Dia scratched	Mirror-polished Si	Dia-coated (1μm) Si	Dia -coated (6μm) Si	Mirror-polished Si	Dia-coated (40μm) Si
Preparation technique		MSIBD					MS			ECR-PECVD	
BN film thickness	(nm)	80					80		70	1000	200
Substrate bias	(V)	150				500	75			30	
Substrate temperature	(°C)	250					800			900	
Deposition pressure	Torr	10^{-8}					10^{-2}			10^{-3}	
Ions		$^{11}B^{+}$, $^{14}N^{+}$					Complex			Complex	
cBN from FTIR	(%)	90	74	66	60	85	40	90	85	80	90
Surface roughness	(nm)	0.2	10	50	128	143	6	15	135	22	10

Chapter 6. Deposition of cubic boron nitride on silicon – a parametric study towards high quality film

Energetic ion bombardment in N_2 and Ar plasmas conventionally applied to cBN deposition restricts the size of cBN crystallites and induces high internal stress levels limiting the obtainable non-delaminating film thickness (to ~200 nm). This chapter describes the introduction of fluorine chemistry mediating by a complex He-Ar-N_2-BF_3-H_2 plasma produced in an ECR (electron cyclotron resonance) system that overcomes the indicated limitations and enables to prepare thick cBN films (>1 μm) with low stress. The films were deposited using a low substrate bias (–30 V) and high substrate temperature (900 °C). FTIR spectroscopic examination shows that the films are composed of > 80% cBN phase. Detailed analysis of BN film structures employing HRTEM and transmission EELS reveals that a pure cBN layer is formed on top of an initial tBN layer which accounts for the insignificant hBN signal in FTIR spectra. The appearance of characteristic TO and LO phonon modes of cBN in visible Raman spectra demonstrates the larger crystalline size (~100 nm – also confirmed by HRTEM) in contrast to the films reported previously. The ion bombardment, gas composition, substrate temperature and growth time significantly affect the phase purity and crystallinity of the cBN films formed are further elucidated in this chapter.

6.1. Methods of cubic boron nitride synthesis

Since ion kinetic energy, associated with microstructure and physical properties of the films, depends on the method of synthesis. This is one of the reasons for presentation of some results on synthesis of cBN films prepared by two fundamental methods being successfully used, i.e. physical vapor deposition (PVD) and plasma enhanced chemical vapor deposition methods (PECVD) as classified in Ref. [103]. The PVD techniques comprises for example ion beam assisted deposition (IBAD) [104], laser ablation [5,105], magnetron sputtering (MS) [106], ion beam sputtering [107,108]

and mass selected ion beam deposition [69]. In these techniques, ion bombardment with high kinetic energy was demonstrated to be a key factor for cBN formation. The advantages of PVD techniques account for the deposition of nearly pure cBN phase and the cBN growth at room temperature after nucleation at elevated temperature [109]. Corresponding to the growth mechanism (ion-bombardment induced physical transformation from sp^2- to sp^3-hybridized BN), however, cBN films deposited by these methods also have serious drawbacks. Among them high internal stress, poor adhesion to the substrate, limitation in film thickness (typically ~200 nm) and poor crystallinity (nanocrystalline nature and highly defective crystallites) are foremost shortcomings limiting electronic and mechanical applications. Therefore, much effort has been made to overcome these problems using novel approaches.

Cubic BN films have been synthesized via chemical routes employing CVD similar to those used in diamond deposition. In conventional CVD, chemical reactions are solely driven by thermal energy maintaining high temperatures. In contrast, PECVD uses molecular non-condensable gases which are converted to reactive condensable radicals in interaction with electrical power supplied. The induced radicals are highly reactive, and gas phase and radicals-substrate reactions are effective at much lower temperature than in conventional CVD. The cBN growth employing this method is very unique, because particularly cBN deposition still has to be maintained at relatively high temperatures (normally >600 °C) and ion bombardment. Using very low kinetic energy does not provide cubic BN phase. All PECVDs are ion assisted techniques and they require a suitable boron gas precursor in order to provide a high-quality cBN structure. Therefore, intensive studies on cBN formation using different boron-containing gases, such as diborane (B_2H_2) [110], trimethyl borozine (TMB) [77] and boron trichloride (BCl_3) [80,111], together with nitrogen and inert gases (Ar, He), have been carried out. Very recently, by introducing fluorine into the gas phase, thick and adherent cBN films were synthesized by bias-assisted direct current (DC) jet plasma CVD using a gas mixture of Ar-N_2-BF_3-H_2 [112] and microwave plasma (MP) CVD employing a mixture of He-N_2-BF_3-H_2 [113]. The plasma processes in such gas mixtures enable continuous

preferential etching of non-cubic phase by fluorine species [114], and therefore open the way to synthesize cBN films via new chemical pathways, while the ion energy is substantially reduced. However, the area of films deposited so far by DC jet is limited to approximately 1 cm in diameter and the films are contaminated with the electrode materials. In addition, this particular growth process is not cost-effective because it consumes large amount of gases at flow rates of several ten thousands sccm. On the other hand, films prepared by MPCVD can barely be prepared with cubic phase purity of 70%. The lower cBN content is believed to be caused by low plasma density, and thus a low ion/deposited atom ratio in microwave plasmas. Unlike standard MPCVD, higher degrees of ionization, dissociation and excitation can be obtained in an electron cyclotron resonance (ECR) operational mode [115]. The ECR plasma activated species undergo fewer collisions along their paths to the substrate due to the longer mean free path at low pressure used in this mode. Therefore, the ion/deposited atom ratio is greatly increased. The collective effect of low energetic chemistry, enhanced ion/deposited atom ratio, plasma uniformity and ease of controlling the deposition conditions and capacity in scaling the deposition offer some advantages over the DC jet and MPCVD processes. There are just several studies [110,116] reporting the growth of cBN using ECR PECVD. Shapoval *et al* [116] reported the formation of cBN films (~100 nm) using BF_3 and NH_3 at ~700 °C without applying any external substrate bias. They however presented only IR absorption spectrum. The absorption peak position at 1110 cm^{-1} in their spectrum is believed to be associated with Si sub-oxide rather than cBN. In addition to boron-based halogen gas precursors successfully used previously, Ye *et al* [110] succeeded in synthesis of cBN films at a substrate bias of –100 V using a B_2H_6-Ar-N_2 gas system, but the cBN content was just 55%. In this chapter, the deposition of cBN films employing ECR PECVD assisted by fluorine chemistry was systematically studied. The effects of ion bombardment, BF_3/H_2 gas flow ratio, substrate temperature and deposition time on the phase purity and crystallinity are investigated.

6.2. Effect of helium additives in plasma on cubic boron nitride deposition

In DC jet plasma, cBN films were deposited in a gas mixture of Ar-N_2-BF_3-H_2 [112]. These authors substituted argon by helium in this fluorinated gas mixture and used microwave plasma to deposit cBN [113]. However, no explanatory reasons were provided. In this study, BN films were also deposited from Ar-N_2-BF_3-H_2 gas mixture but employing ECR PECVD. Using this gas mixture, many experiments with variable growth parameters over wide ranges led to synthesis of fairly poor-quality BN films. Substitution of argon by helium in the gas mixtures however sharply increased the bias current by one order of magnitude. The considerably higher plasma density and ion/atom ratio in helium based plasma then yielded high-quality cBN films after optimizing the deposition parameters. The used experimental procedure further elucidates the importance of ion flux density impinging the growing surface of cBN films. Similarly, Kim *et al* [84] found that the threshold voltage for cBN nucleation could be reduced from −300 to −200 V by increasing the plasma density by an order of magnitude in their helicon plasma deposition system. The increase in bias current in our helium-based ECR plasma has to be induced through additional ionization reactions which differ from electron impact ionization because paradoxically ionization increases with adding the element (He) with highest ionization potential. These unique ionization reactions are based on interaction of excited He atoms in highly energetic states and other plasma constituents. Such ionization reactions are highly probable if energy accumulated in excited metastable states is higher than the ionization potential of the interacting neutral particles. This phenomenon is known as Penning ionization. Since helium has highly energetic metastable states, it can enhance the plasma density in interaction with gases of lower ionization potential via the described phenomenon. Penning ionization can become the prevalent mechanism of ionization whenever noble gases such as helium or neon are used as one of the gas components [117]. Experimentally, a small addition of Ar into gas mixture, as elucidated from Fig. 6-1, can

also lead to an increase in bias current. Argon can be ionized more easily than helium due to its lower ionization potential. However, in the case of mixtures, the mechanism of ionization can be much different because of a variety of ionization reactions. The flow rates for Ar and He were optimized at 10 and 140 sccm, respectively, in order to obtain the highest bias current at a given substrate bias voltage.

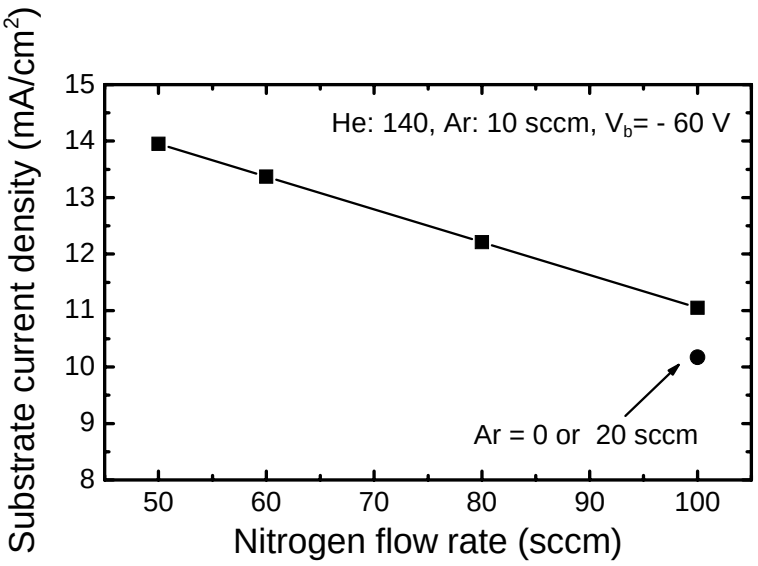

Fig. 6-1. Variation of substrate current density as a function of nitrogen flow rate at –60 V.

The flow rate of nitrogen was also found to affect the bias current, which is illustrated in Fig. 6-1. The substrate current density (J_b) decreased with an increase in nitrogen flow rate from 50 to 100 sccm, while the total gas pressure correspondingly increased from 1.5 to 2 mTorr, at a constant bias voltage of –60 V. Reducing the nitrogen flow rate by a factor of two (from 100 to 50 sccm), the substrate current density increased by nearly 30%, which is more favorable for cBN formation, as discussed above. This difference in current density is also associated with the change in mean free path and thus energetic gain of electrons participating on ionization collisions and collision number. Further decreasing the nitrogen flow rate led to the formation of BN films enriched in boron and black in appearance indicating that the stoichiometry and phase purity of the films deteriorated. Following the experimental evidence, a

nitrogen flow rate of 50 sccm was preset as the optimum value satisfying both the high bias current and nitrogen abundance.

6.3. Effect of the substrate bias and role of the ion bombardment

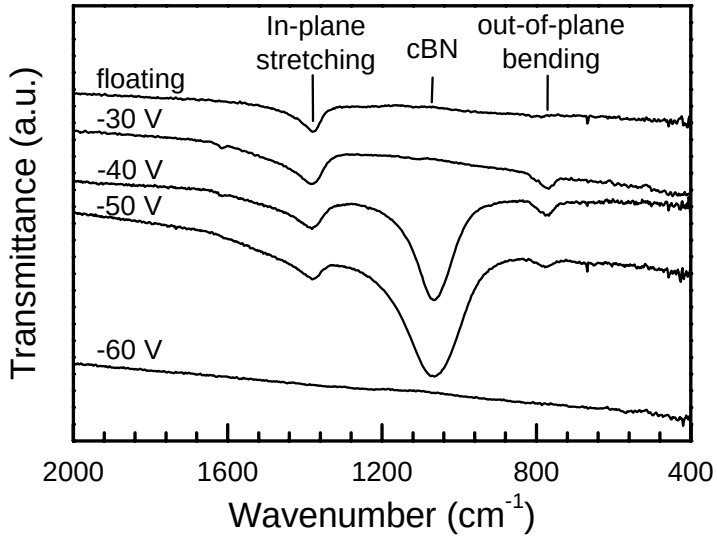

Fig. 6-2. FTIR spectra of boron nitride films prepared on silicon at different substrate biases.

Fig. 6-2 shows IR absorption spectra collected from BN films deposited on Si substrates prescratched with 1-μm diamond powder at different values of substrate bias. The deposition time was kept constant (one hour). When the substrate bias was greater than –60 V considerable etching of the substrates was observed. However reducing the bias voltage to values of –50 and –40 V resulted in cBN films formations. In both the cases, the FTIR spectra show strong absorption peaks centered at approximately 1070 cm^{-1}, indicating the presence of cBN phase. Two weaker absorption peaks centered at 1380 and 780 cm^{-1} are assigned to the in-plane stretching and out-of-plane bending vibrational modes of hBN, respectively. The cBN content was estimated to be higher than 80% using the equation $I_{1070}/(I_{1070}+I_{1380})$ for calculating the phase fraction, where I_{1070} and I_{1380} are the IR absorbance intensities of the peaks at 1070 and 1380 cm^{-1}, respectively. The up-shift of the cBN peak from the reference value of 1065 cm^{-1},

characteristic to cBN crystals synthesized by HPHT methods, is associated with the compressive internal stress caused by ion bombardment induced during the film deposition. The higher internal stress causes a greater up-shift of the cBN absorption peak. The position of absorption peaks reported for cBN films prepared by PVD methods is usually shifted to higher wavenumbers, typically to 1080-1100 cm^{-1}. In contrast, the up-shift of cBN absorption measured on the films presented here decreased significantly implying lower internal stress. In the search for films with extremely low stress, the bias voltage was reduced to –30 V and below. However, the deposition on silicon at a bias lower than –30 V for one hour yielded only hBN. The FTIR spectrum measured for the film prepared at a floating potential shows that the out-of-plane deformation mode of hBN diminished, suggesting that under restricted ion bombardment, the basal hBN planes are aligned in parallel direction with the substrate surface.

6.4. Evolution of cubic phase of boron nitride

In the deposition of cBN films by either PVD or CVD using fluorine chemistry [118-120], an amorphous/turbostratic BN intermediate layer is formed prior to the nucleation and growth of the cBN layer. The nucleation mechanism has not been clearly understood, but the formation of such an interface requires a certain incubation time to form cBN nucleation sites. Thus growing interfacial layer and nucleation incubation time only indicate that nucleation sites for cBN cannot directly be activated on Si probably because of significant differences in cBN and Si physical properties. In Fig. 6-2, it has been shown that for the bias voltage of –40 and –50 V, cBN phase already formed after one-hour deposition while only sp^2-hybridized BN was obtained for the bias voltage of –30 V. However, even at –30 V, cBN is obtained when the deposition time is prolonged to two hours. This suggests that the incubation time for the cBN nucleation at –30 V is considerably longer than that at –40 and –50 V. Representative FTIR spectra collected from BN films prepared at –30 V for 1, 2, 4 and 6 hours are shown in Fig. 6-3a. The film prepared for two hours already contains nearly 50% cBN.

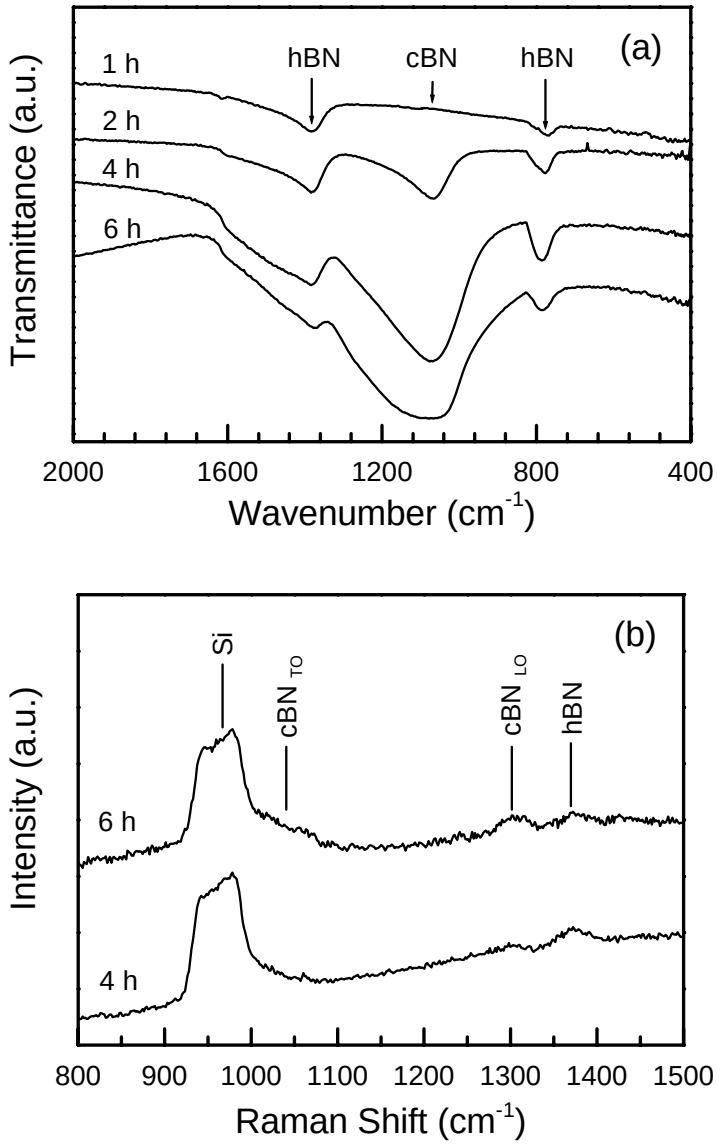

Fig. 6-3. (a) FTIR and (b) Raman spectra showing the time evolution of cBN films at the –30 V bias.

The cubic phase expanded proportionally with the deposition time as indicated by simultaneous increase in intensity of FTIR absorption peaks characteristic to cBN with respect to the intensities of absorption peaks corresponding to hBN. This observation suggests that the interfacial hBN does not expand after the cBN formation. Correspondingly, the film thickness increased with deposition time elapsed, for example, from 0.2 μm to 0.5 μm in case of films prepared for 2 and 4 hours, respectively, as demonstrated by the SEM cross-sectional images in Fig. 6-4. The cBN film deposited

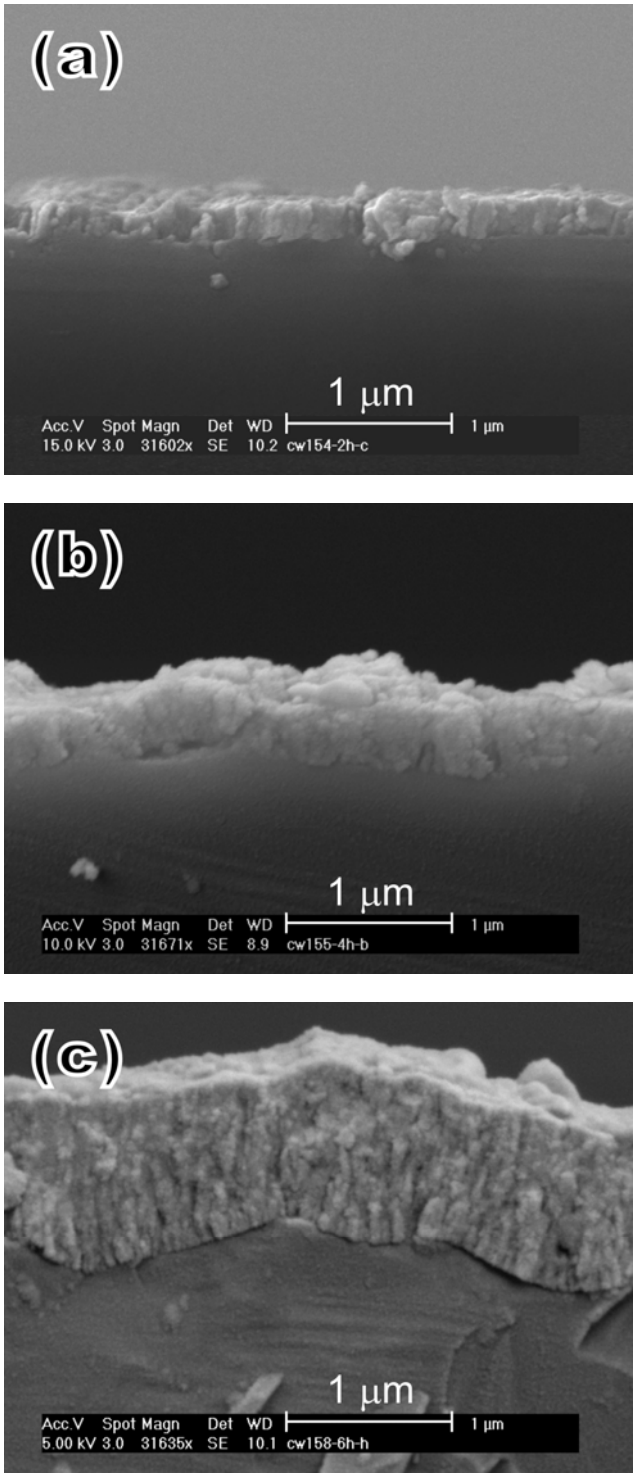

Fig. 6-4. SEM micrographs showing the cBN films deposited at –30 V for (a) 2 h, (b) 4 h and (c) 6 h. Their thicknesses are 0.2 μm, 0.5 μm and 0.9 μm, respectively.

for 6 hours is about 1 μm thick showing clearly a columnar structure. Evidently, sp^2-hybridized BN layers grew on the silicon substrates prior to cBN formation at investigated operation conditions. Once cBN is nucleated, the growth of cBN phase is preferable. The preferential phase growth is probably maintained via simultaneous deposition of different BN phases on established cBN crystallites and selective etching of non-cubic phases by thermally and plasma activated fluorine species [114].

The energy of ions impinging the substrate is proportional to the effective bias which is given by the difference of plasma potential and bias applied to the substrate ($V_{eff} = V_p - V_b$). Plasma potential can however change from units to tens volts and some cases even more depending on the discharge conditions. In this particular case, plasma potential was only ~2 V as measured by a probe against earth just above the grounded substrate. The plasma potential is thus insignificant when compared to the substrate bias applied from an external power supply. Therefore we use bias applied to the substrate as a deposition parameter keeping in mind that the effective bias in some conditions can be much higher. When the substrates were at floating potential or at earth potential no cBN was deposited even for 10 hours. The effective bias at grounded substrate and given deposition condition is just about 2 V and ion energy has to be smaller than 2 eV. This energy is inadequate to induce cubic phase. The threshold bias voltage for cBN nucleation and growth are higher as experimentally proved herein. Ion bombardment in PECVD is still indispensable like in PVD techniques. In both PVD and CVD, completely reliable model for cBN nucleation is still disputed though different nucleation sites and conditions have been revealed experimentally. Some environments were recently found beneficial to the nucleation of cBN: i) the re-orientation of interfacial hBN plane (perpendicular to the substrate surface) in order to provide the reactive BN sites and lattice match (3:2) between hexagonal and cubic BN [109]; the accumulation of internal stress which gradually increases with the increase in film thickness [121]. Both factors, ion energy and time dependence should be helpful for the understanding of the experiments presented here.

Raman spectra taken from thin films are usually unavailable. They cannot be obtained because cBN normally have poor crystallinity and highly defective crystallites. In general, Raman peak intensity decreases and the peaks of cBN substantially broaden as the crystal size decreases and defect states increase. Therefore, it is difficult to obtain well-defined Raman spectrum from cBN films composed of small and highly defective crystallites. No Raman spectra have been collected from cBN films prepared under ECR PECVD conditions, so far. In this work, the bias voltage was greatly reduced by introducing fluorine chemistry. This approach resulted in larger crystal size and simultaneous reduction of crystal defects. Such cBN structures formed at –30 V bias for 4 and 6 hours deposition then allowed collecting Raman spectra as illustrated in Fig. 6-3b. Both the relatively small film thickness and probing depth of a Raman instrument enable to induce the intense silicon second order peak of substrate centered at 950 cm^{-1}. The weak and broad peak located at about 1360 cm^{-1} is assigned to the E_{2g} optical vibration mode of hBN. There is a clear peak at about 1300 cm^{-1} and a peak forming a shoulder of the silicon 2^{nd} order signal at about 1050 cm^{-1}. With reference to the Raman spectra collected from HPHT cBN crystals, these two peaks should be assigned to the transverse optical (TO) and longitudinal optical (LO) phonon modes of cBN [12]. Both the peak shift and broadening were caused by the combined effects of small crystal size, presence of defects and internal stress, as reported previously [122]. Smaller crystallites can lead to the down-shift and asymmetric broadening of the peaks. Conversely, high internal compressive stress inside the film can result in the up-shift of the peaks.

6.5. Hydrogen/boron trifluoride ratio as the deposition parameter

Hydrogen is another plasma component whose concentration may greatly affect the cBN quality. The experiments summarized in Fig. 6-5 show the influence of hydrogen flow rate on the formation of cBN films grown at a substrate bias of –40 V and temperature of 850 °C for 4 h. When the H_2 flow rate was as low as 2 sccm with reference to the 1 sccm for BF_3 gas, only thin hBN film was grown or substrate etching was observed. The increase in flow rate to 4 sccm resulted in formation of BN films

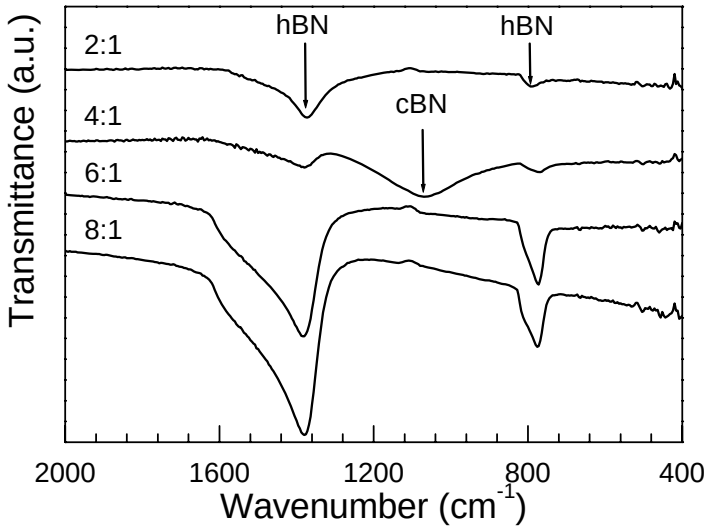

Fig. 6-5. Influence of the H_2/BF_3 ratio on the formation of cBN films prepared at a constant substrate bias voltage of –40 V and temperature of 850 °C for 4 h.

with high cBN content. On the other hand, abundant hydrogen in the plasma, for example, supplied at a flow rate of 6 sccm, led to the growth of thick BN films with hexagonal phase. A number of studies [81,114] revealed that variation of the amount of hydrogen in gas mixture can control the production rate of solid BN from gas phase and manipulate the equilibrium between etching and the formation of BN film. This can be visualized, to some degree, by the observation of a slight drop in pressure when hydrogen is introduced into the H_2-Ar-N_2-BF_3 plasma due to the formation of solid BN. The origin of the increase in deposition rate with increasing H_2 flow rate using fluorine chemistry in this study may be attributed to the saturation of reactive fluorine ions/atoms by the atomic hydrogen and the formation of less reactive HF species.

6.6. Synergetic effect of temperature and fluorine chemistry at cubic boron nitride growth

The effect of substrate temperature on the nucleation and growth of cBN has been systematically studied in PVD deposition techniques. These deposition methods rely

solely on the phase transformation driven by energetic ion bombardment to obtain films with pure cBN phase, and therefore are insensitive to the deposition temperature. The advantage of using these techniques for cBN nucleation and growth is the very low threshold temperature, which can be as low as 150 °C for nucleation and room temperature for growth [109,123]. However, high ion energies used at PVD hamper the evolution of larger crystallites, and structure is typically nanocrystalline, similar to nanodiamond prepared at bias enhanced nucleation and ion assisted growth. As previously said these structures do not reveal cBN Raman peaks due to the cBN nature just described. A different situation, however, is in the case of the cBN film prepared by ECR-plasma employing fluorine chemistry. The cBN films prepared by the ECR PECVD method and fluorine chemistry require a higher substrate temperature, as obviously illustrated by the effect of substrate temperature on the formation of cBN at 600, 750 and 900 °C as shown in Fig. 6-6. All the films were deposited for 2 hours. Evidently, the cBN content dramatically increased from 600 to 900 °C. The corresponding intensity for hBN from deformation and stretching vibration modes also substantially decreased. It is believed that the increase in cBN phase to the detriment of hBN phase at high temperature is caused by improved preferential etching of hexagonal over the cubic phase via thermal activation of fluorinated species. Correspondingly, the deposition rate at high substrate temperature was found to be lower than that at low substrate temperature.

The BN films deposited at low substrate temperature have higher compressive stress than those prepared at 900 °C (peeling off occurs more easily) due to the higher defect density. Unlike the low-temperature deposition, the defects formed by ion bombardment at high temperatures may migrate more effectively and be annealed out to a certain extent, perhaps in addition to their etching off in the surface regions by the plasma-activated reactive environment. One of the PVD models for cBN formation is based on the film stress [86]. In this model, the stress is presumed to be a driving force for the conversion of BN phases into cBN. However, the BN films prepared at 600 and 900 °C in this experiment show properties that contradict the stress model. For example,

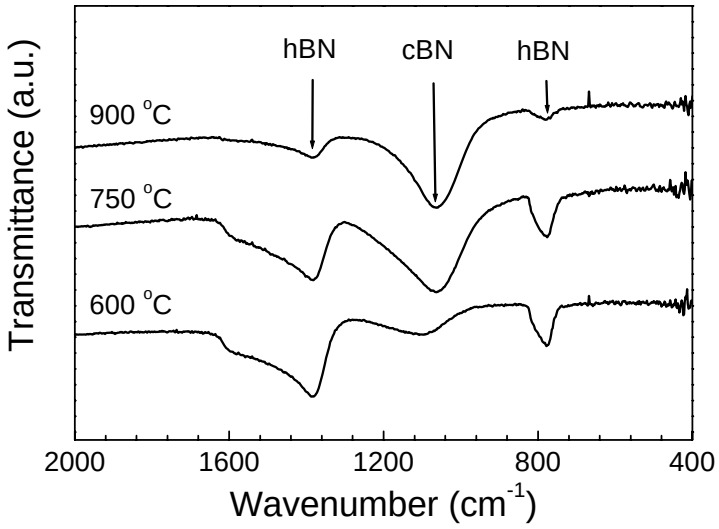

Fig. 6-6. FTIR spectra showing the effect of substrate temperature on the formation of cBN. The deposition time is 2 h for all the samples.

the films prepared at 600 °C with higher intrinsic stress (greater blue-shift of cBN peak in FTIR according to equation 1-2) contain only 23% cBN, which is considerably less than the content of films produced at 900 °C with presumably lower internal stress. Thus, the stress model can hardly explain the phase transformation in our case.

6.7. Uniformity of cubic boron nitride films

Although the deposition can be carried out on substrate of three inches in diameter only substrates with a size of 45 mm by 35 mm were used in these experiments. The deposited cBN films covered the whole area of these substrates, showing great uniformity. FTIR absorption spectra acquired in different regions, particularly in the central and edge regions, show phase structural discrepancy smaller than 5%. The purity of the cubic phase is a little higher at the central region than at the edge of the substrate. This slight difference is caused by the temperature distribution across the substrate. Higher temperature favors the selective etching of non-cubic phase, so the film thickness reduces somewhat from the edge towards the center of the substrate. Film thickness variation is typically less than several percentages, as determined by SEM

observations.

6.8. Phase structure of boron nitride films

Fig. 6-7 shows cross-sectional TEM (XTEM) images collected from the 1.1-μm-thick cBN film at (a) lower magnification and (b) higher magnification with an enlarged top region of the cBN film. The XTEM analysis indicates columnar growth of the cBN films, with lateral column sizes ranging up to 0.1 μm. More detailed analysis of the cBN columnar structure using TED provides further insight into the film properties.

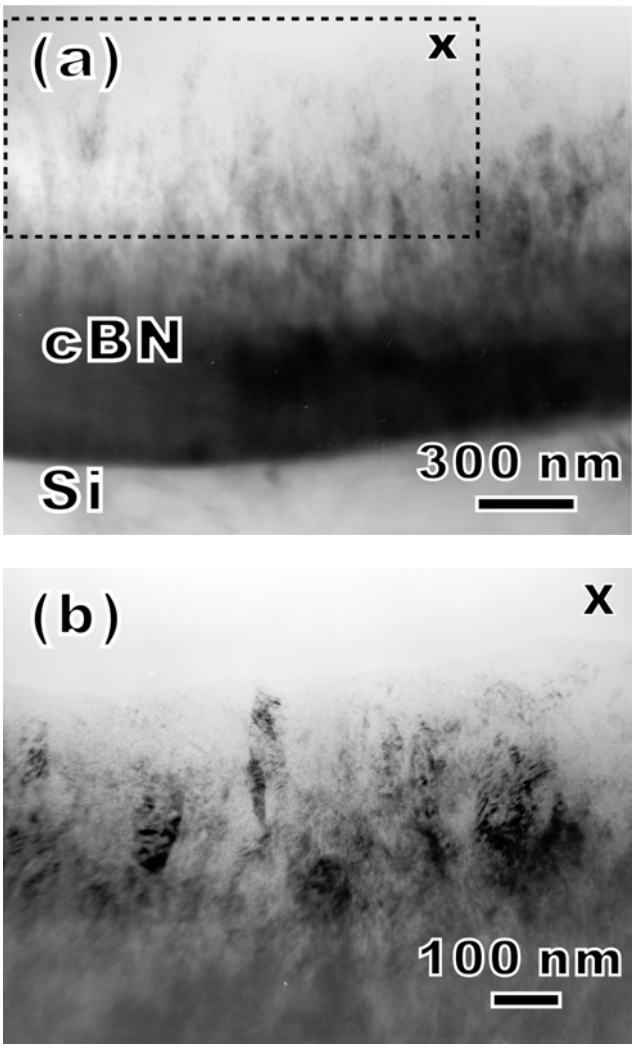

Fig. 6-7. Cross-sectional bright-field TEM image (a) in low magnification revealing the total thickness of 1.1 μm, and (b) of corresponding enlargement of the columnar cBN grains.

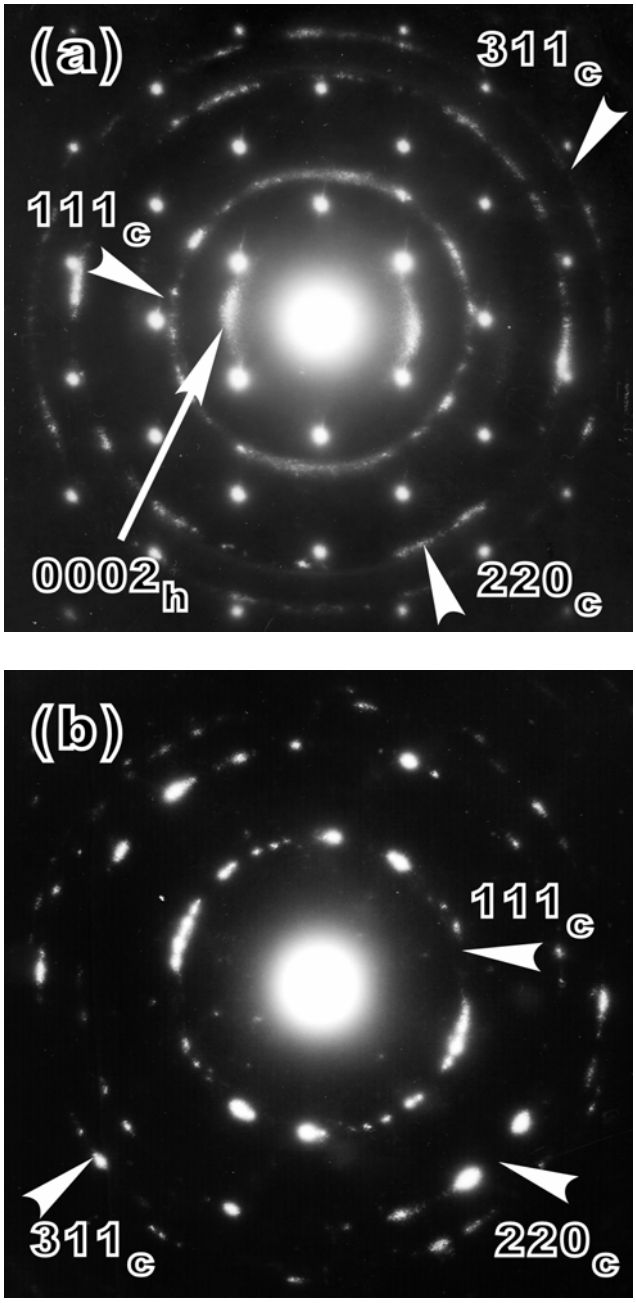

Fig. 6-8. Selective area diffraction patterns of BN films taken from (a) an interfacial region of silicon, tBN and cBN, and (b) a region inside a columnar grain.

The TED pattern in Fig. 6-8a was collected from the interfacial transition region of the BN film. Discontinuous diffraction rings are designated as cBN (111), (200) and (311), in figure, The inner elongated intensive and little diffused diffraction spots indicate the preferential orientation of tBN (0002) crystallographic planes while the sharp electron diffraction reveal the single crystalline Si substrate. The electron diffraction forming elongated diffraction spots indicates textural growth of tBN phase with the (0002) planes perpendicular to the substrate in the transition region of the BN film. In the second diffraction pattern collected from an upper film region, as shown in Fig. 6-8b, only cBN (111), (200) and (311) diffraction rings are observed. These cBN rings are discontinuous with some elongated diffraction spots. This appearance of the TED pattern implies that larger crystallites with preferential orientation exist in the columnar cBN structure. Further information on the BN film presented here is obtained by transmission EELS. Fig. 6-9 shows both the B and N K-edges, the fingerprints of the structure. In general, such spectra reflect unoccupied sates, which may reveal π* and/or σ* states characteristic to hexagonal and cubic phases, respectively. For sp^2-bonded BN, the boron K-edge at 188 eV consists of two components: a sharp peak at the edge onset due to the excitation of K-shell electrons to the unoccupied π* antibonding states, and a

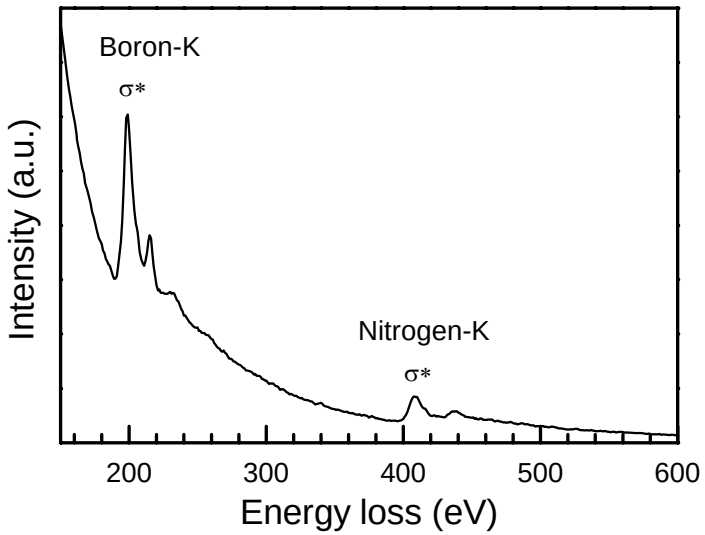

Fig. 6-9. Transmission EELS spectrum showing B and N K- edges acquired from a cBN columnar grain.

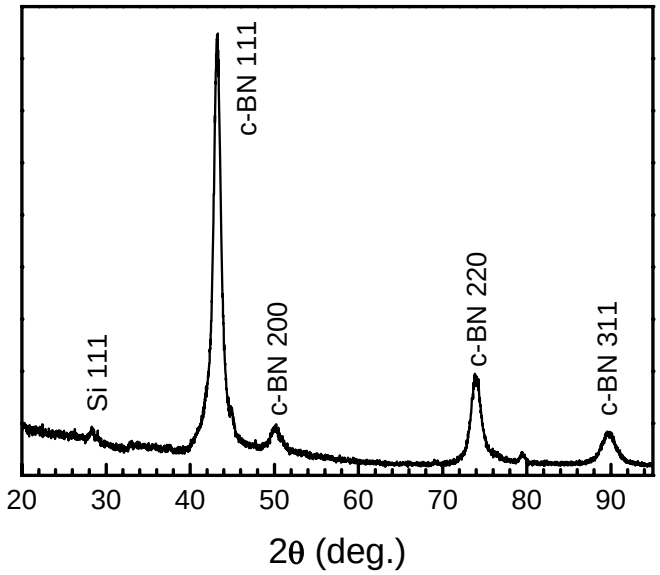

Fig. 6.10 Glancing-angle X-ray diffraction pattern of the cBN film prepared at –30 V and 900 °C for 6 h.

broader peak due to excitations to the σ* antibonding states. In sp^3-bonded material, only the σ* states exist and the π* peak is absent. The appearance of only σ* peaks in Fig. 6-9 provides powerful evidence that BN layer above the interfacial transition region is dominated by sp^3-bonded cBN phase. Fig. 6-10 illustrates the glancing angle X-ray diffraction spectrum collected from the cBN film corresponding to the sample whose SEM image is presented in Fig. 6-4c. The incident angle of X-ray was set at 0.05° and the X-ray diffraction was measured in a 2θ continuous mode with a step of 0.02°. The diffraction peaks of cBN 111, 220, 311, 200 are identified in figure. Si 111 diffraction also appears at 28.4°. The average size of cBN crystallites can be estimated from the diffraction pattern using Sherrer formula

$$L_{hkl} = \frac{K\lambda}{\sqrt{B^2 - b^2}\cos\theta}$$

where $K = 0.9$, $\lambda = 1.5418$ Å, and B and b are the full width at half maximum (FWHM) of the diffraction peak and the intrinsic instrument broadening in radian, respectively. The calculated mean crystal size of cBN is about 100 Å as found from the most intense

cBN 111 peak. Zhang *et al* [120] reported that the crystal size, determined from the X-ray diffraction peaks, may be under-evaluated when defects such as stacking faults and twins, and internal stress in the cBN crystallites are present. The peak shifts in FTIR and Raman spectra being indicatives of stress and undoubtedly presence of defects are reasons to believe that the real crystal size should be much larger than that calculated using Sherrer equation.

6.9. Summary to the parametric study of cBN growth on silicon

Energetic ion bombardment in N_2 and Ar plasmas conventionally applied to cBN deposition restricts the size of cBN crystallites and induces high internal stress levels limiting the obtainable non-delaminating film thickness (to ~200 nm). This chapter presents the preparation of thick cBN film (>1 μm) with low stress through the introduction of fluorine chemistry employing a complex He-Ar-N_2-BF_3-H_2 plasma produced in an ECR system to overcome the limitations observed in PVD deposited cBN films. Our cBN films were deposited using a low substrate bias (–30 V) and high substrate temperature (900 °C). Fourier-transform infrared spectroscopy shows that the films are composed of >80% cBN. Detailed analysis of BN film structures employing high resolution transmission electron microscopy and transmission electron energy loss spectroscopy shows that a pure cBN layer is formed on top of an initial turbostratic BN layer which accounts for the small hBN signal in FTIR spectra. The appearance of characteristic TO and LO phonon modes of cBN in visible Raman spectra demonstrates the larger crystalline size (~100 nm – also confirmed by HRTEM) in contrast to the films reported previously. The ion bombardment, gas composition, substrate temperature and growth time significantly affect the phase purity and crystallinity of the cBN films formed were discussed.

Chpater 7. Deposition of cubic boron nitride on diamond – the route to elimination of interfacial graphitic boron nitride layer

In Chapter 6, we have discussed controlling principal deposition parameters leading to high quality cBN films prepared on Si substrates employing PECVD assisted with fluorine chemistry. The growth of cBN follows typical pattern with a graphitic precursor aBN/tBN layers at the Si substrate interface. It can however be demonstrated that aBN/tBN are not necessarily the precursor layers for cBN growth. Using diamond substrates can eliminate aBN/tBN layer and cBN can directly be deposited on diamond at suitable deposition parameters. The distinctive features of cBN films grown on diamond in reference to those on Si substrates have systematically been investigated as illustrated below. The critical experimental conditions inducing the nucleation and maintaining the growth of cBN are revealed based on detailed HRTEM studies of the interfacial cBN–diamond structures. The interfacial studies show orientation relationship between cBN and underlying polycrystalline diamond. The equivalent atomic configurations in cBN and diamond, and the alignment of their crystallographic planes suggest perfect epitaxy in the HRTEM view-field.

7.1. Experience in diamond and cubic boron nitride coatings

Diamond films synthesized by CVD methods have been exploited in various industrial areas for more than two decades though the diamond coating is not trivial and is affected by the substrate nature. Nevertheless diamond-coated cutting tools are commercially available. They provide reliable high-performance machining of various materials (excluding ferrous materials) from wood to hard aluminum alloys used in car and aerospeace industries. The diamond coated tools also last longer than conventional traditional WC or high-speed steel tools. The substrates however have to endure high deposition temperatures, which precludes coating plastics and low melting metals like

aluminium. Apart from temperature, another crucial requirement is diamond adhesion to substrate which depends very much on the substrate properties. Good diamond adhesion is usually obtained on the substrates forming carbides, i.e. substrates which are chemically active to carbon. The formation diamond on substrates with very high chemical reactivty and high mutual solubility including transition metals, iron and cobalt is however difficult and diamond adhesion to these substrate is poor which is highly contraversial. Hence materials like Si, Mo and W with limited diffusion carbide layer are suitable for growing polycrystalline diamond films. Because of chemical nature, high temperature requirements, and mismatching physical parameters the diamond coatings often require pretreatment of substrates and buffer or/and gradient layers to provide good performance of polycrystalline and nanocrystalline diamond films. Highly oriented diamond films can be obtained on hetero-substrates like Si, SiC, Ir [124] via precise controlling alpha parameter [125] associated with deposition temperature and methane concentration in hydrogen CVD growth enviroment. Single crystal diamond over large area is possible only by hommoepitaxial growth, i.e. CVD synthesis on diamond surfaces because significant mismatch of non-diamond materials and diamond in lattice parameters and surface energy.

Chemical and physical vapor depositions of cBN films at low pressure started almost the same time as diamond film synthesis, but accomplishment in cBN synthesis lags behind the achievements in diamond growth. The deposition of cBN is based on ion-assisted methods which is partly responsible for nanacrystalline nature of cBN and associated with sequential growth of amorphous material, turbostratic BN, and finally cBN. The interfacial aBN/tBN layers serve as incubation media vital for the nucleation of cBN. The ion bombardment with the energy ranging from tens to hundreds eV was found to be essential for the formation of cubic phase of BN, but which also hampers growing larger crystallites and induces a significant compressive stress (5-20 GPa) leading to the delamination of the films and limiting the maximal thickness to ~200 nm [126]. The recent CVD progress utilizing fluorine chemistry allows the deposition of thick (>20 μm), nearly stress free (<1 GPa) cBN films on Si substrates under a reduced

bias voltage [127]. However, the films still show a layered-structure associated with an aBN/tBN interface [120]. These interfacial soft layers make the BN films sensitive to the humid environment because of high diffusion rate of oxidizing air constituents in sp^2 bonded BN structure and reactive boron dangling bonds at the substrate interface. Formation of new chemical substance at substrate via oxidizing reaction and inherent film stress may then lead to the film delamination. The formation of interfacial precursor aBN/tBN and high energetic ion bombardment inhibit epitaxial growth and are a part of reasons for poor cBN behavior. The precursor BN layers are also major obstacles for further advances of cBN films and their mechanical and electronic applications.

7.2. Significance of substrate in the deposition of cubic boron nitride

Most of the cBN film depositions have been carried out on Si substrates. Silicon is used because it is a cheap, common, single crystalline wafer easily available in electronic grade quality. Silicon may not be the best substrate for growing high quality cBN films. The experience in heteroepitaxial growth shows that the epitaxial quality of diamond grown on Si is inferior to that grown on other substrates (e.g., iridium). The lattice parameters (Si–5.43Å , diamond–3.567Å) and surface energies (Si–1.24 J/m^2, diamond–3.7 J/m^2) of Si and diamond differ considerably [128]. The mismatch introduces strain at the substrate interface, and the higher surface energy of diamond leads to minimization of the diamond–silicon contact areas so that three-dimensional islands and thus polycrystalline diamond grows on silicon. The lattice parameter of cBN (3.615Å) [50] is slightly larger than that of diamond and its surface energy is expected to be very similar to that of diamond. The cBN growing conditions are however more complex than for diamond because ion assistance is needed. More compatible substrates than Si imply lower bias voltage and consequently lower damaging effect induced by ions during the first stage of BN growth referring to substrate–film interface. The best

compatibility of diamond and cBN makes diamond the obvious choice for substrates favoring the cBN growth. This does not exclude the choice of other substrates for heteroepitaxial cBN growth. One example is cBN growth on AlN single crystalline films at 200 °C using N^+ and B^+ mass-selected ion-beams with energies of 500 eV [129]. The N^+ and B^+ beams were periodically switched after the accumulation of one monolayer of each ion type to maintain stoichiometry. The resulting cBN films were analyzed by HRTEM. This analysis reveals the absence of interfacial aBN and alignment of AlN $(10\bar{1}0)$//tBN (0002) // cBN (111) planes in small confined areas. A significant finding in this work is a localized growth of cBN and wBN directly on AlN implying that the aBN and tBN interlayers observed on Si prior to cBN nucleation are not indispensable precursors for the cBN nucleation and they might be eliminated with a proper substrate selection.

7.3. Effect of diamond interfacial layer on nucleation and growth of cubic boron nitride

The effect of the diamond interfacial layer on the cBN formation was investigated in experiment involving the BN deposition on both diamond-coated Si and referenced Si substrates simultaneously. As discussed in Chapter 6, during the growth of cBN films fluorine works as a selective etchant preferentially removing the sp^2-bonded aBN and tBN constituents. Hydrogen can balance the etching ability of fluorine, and the H/F ratio is associated with the phase purity and deposition rate of the films (a high H/F ratio results in increase of the hBN content, while a low ratio may rather induce etching of the substrate than deposition). The critical value of H_2/BF_3 ratio for the nucleation and growth of cBN films has to be investigated. In the experiments presented herein, the H_2/BF_3 ratio varied in a wide range for each bias voltage to obtain films with high cBN content. The low bias deposition of films with high cBN content required low H_2/BF_3 ratio. When the substrate was at earth potential only etching of the substrates or very thin hBN films were observed on both Si and Dia/Si though the H_2/BF_3 ratio varies over

a large range.

The significance of interfacial layer is demonstrated on a series of cBN films prepared on polycrystalline diamond/silicon (Dia/Si) substrates with reference to the films grown on silicon at extremely low substrate bias. The H_2/BF_3 ratio was optimized, above the point at which only etching occurs, and maintained at values of 1.3:1, 2:1, 3:1, and 3.5:1 for the bias voltage of –10, –20, –30, and –40 V, respectively. At –10 V, only a very thin hBN film is deposited on Si while the film grown on Dia/Si confines both cBN and hBN as FTIR spectra indicated in Fig. 7-1. Three absorption peaks at about 1380, 1078 and 780 cm^{-1}, in Fig. 7-1, correspond to the hBN in-plane, cBN and hBN out-of-plane phonon modes, respectively. For the bias voltage of –10 V, only a very thin hBN film was deposited on the Si substrate while a film composed of both cBN and hBN was deposited on the Dia/Si substrate. Since the –10 V bias is the lowest value inducing the cBN nucleation on diamond at given deposition parameters it is denoted as the threshold value providing the cBN nucleation and subsequent growth. The increased

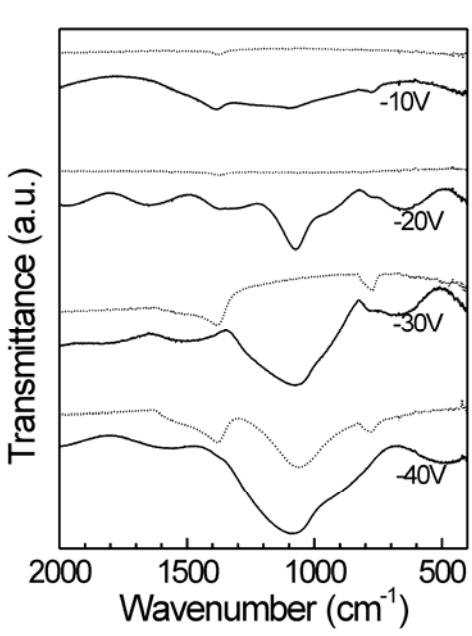

Fig. 7-1. FTIR spectra of cBN films deposited at different substrate bias voltage. The solid lines correspond to the films deposited on polycrystalline diamond, and the dotted lines designate the films grown on silicon.

bias to –20 and –30 V also provides only hBN films on Si substrates. The film thickness however increases with the increase in bias voltage due to the enhanced adsorption and promotion of surface reactions at higher energies. The same bias (–20 and –30 V) applied to poly-Dia substrates yields nearly pure cBN phase. Further increase of the bias to –40 V also leads to the cBN growth on the Si substrate, but the cBN absorption peak becomes broader and shifted to the higher wavenumber. The change of this FTIR signature indicates increase of defects and residual stress as a result of more intense ion bombardment at higher bias voltage.

A nucleation stage is required at cBN deposition on Si substrates as demonstrated by the cross-sectional HRTEM image in Fig. 7-2. The image was obtained from a cBN sample which was at the initial growth stage. Obviously, prior to the cBN formation, layers of aBN and tBN grow in sequential order. The tBN (0002) basal planes are almost perpendicular to the substrate surface. The edges of tBN (0002) planes then serve as cBN nucleation sites. The aBN/tBN interfacial layers are then needed to incubate cBN nuclei. The minimal bias of –30 V, needed for the deposition of cBN films on Si substrates, can thus be taken as the critical bias voltage for the cBN nucleation on Si substrates. The analysis above reveals that a bias voltage of –20 V is the optimal value for the deposition of low-stressed cBN films with high phase purity and high crystallinity.

Cubic BN films prepared on mirror-polished Si substrates by PVD usually are smooth and often featureless which contrast the films grown by PECVD at low substrate bias. PVD process is characteristic with subsurface growth and morphology dominated by surface roughness of initial substrates. Different film morphology (Fig. 8-2) is however evolves at PECVD growth. Fig. 8-2 represents SEM micrographs showing the growth surface of CVD prepared cBN on (a), (b) Si and (c), (d) Dia/Si substrates. The cubic phase content of BN films prepared by ECR PECVD with assistance fluorine chemistry strongly depends on the substrate temperature (described in Chapter 6). The SEM images, in Figs. 8-2a and b, of the films grown on Si at –40 V

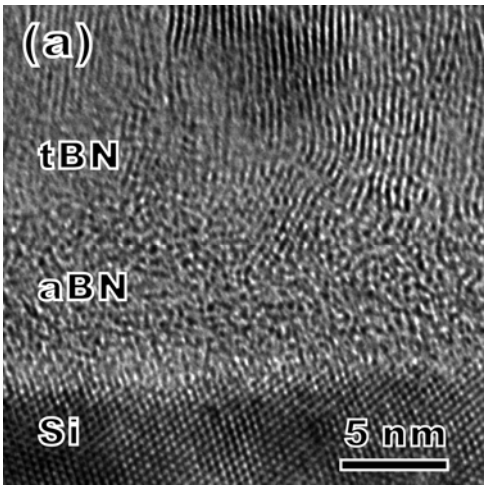

Fig. 7-2. Cross-sectional HRTEM image of the interfacial regions between the cBN film and Si substrate. The sample was prepared with a substrate of –40 V. Note the tBN is textured with its (0002) basal planes perpendicular to the substrate surface.

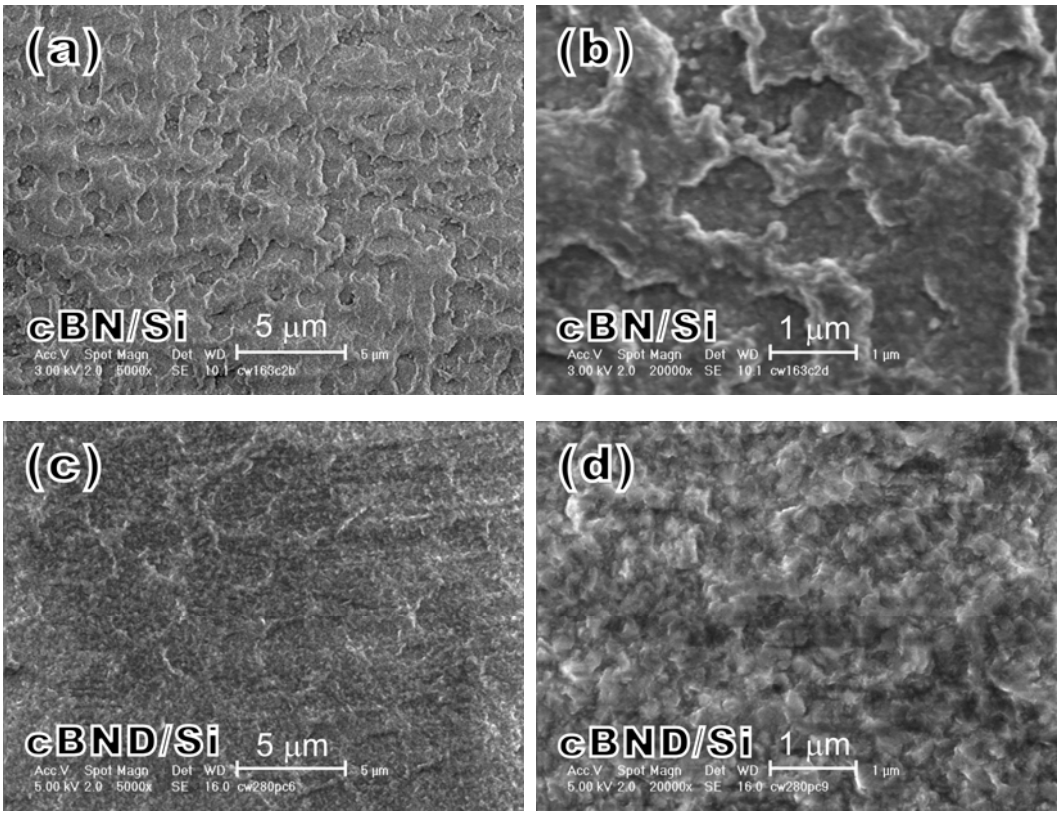

Fig. 7-3. SEM micrograph illustrating the growth surface of (a), (b) cBN and (c), (d) cBND coated Si.

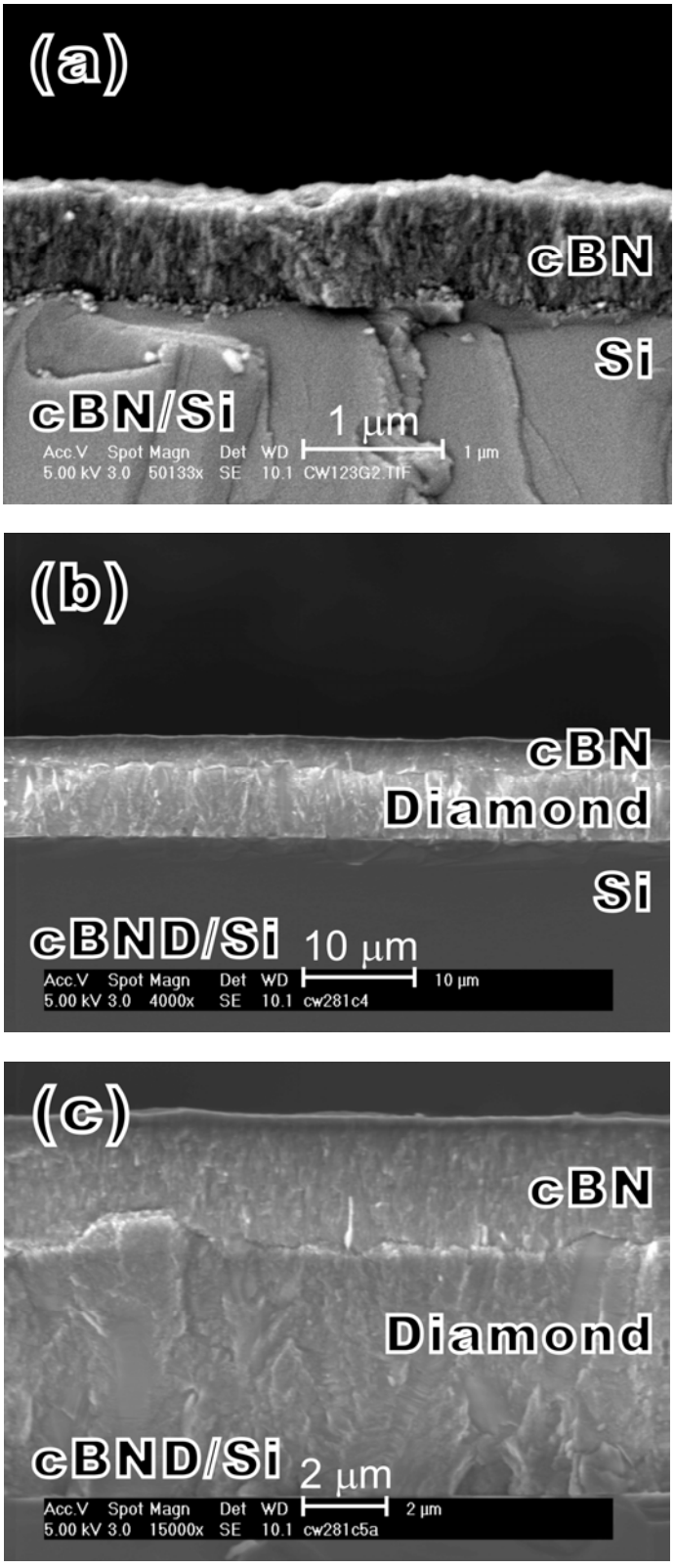

Fig. 7-4. Cross-sectional SEM micrographs elucidating (a) 1-μm-thick and (b) 3-μm-thick cBN synthesized on Si and Dia/Si substrates, respectively.

and 900 °C, reveal rugged surface morphology which is evidence of strong etching effect by fluorinated species generated inside the ECR plasma. The grain size cannot directly be identified in the given images. In the case of cBN deposited on the Dia/Si substrates (Figs. 7-2c and 7-2d), faceted surfaces emerge. The grain sizes are considerably larger than those prepared on Si. Some of them are bigger than 200 nm across. These films have high adherence to the substrates, and they are stable in humid environment. They do not show any delamination sign after more than a year exposure to humid environment even at cBN thickness larger than a micrometer.

Cubic BN films grown on diamond particularly exhibits outstanding adhesion properties. For example, the SEM cross-sectional image, in Fig. 7-4, shows a cBN film with thickness about 3 μm synthesized on diamond (Dia/Si). No signs of delamination are observed, whereas the thickness of cBN grown on Si is often limited to a value just

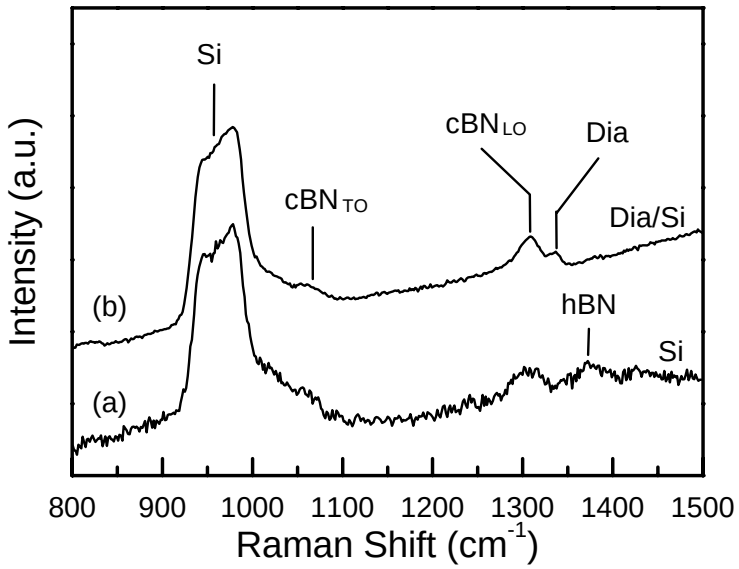

Fig. 7-5. Raman spectra of a 900 nm cBN film deposited with a bias voltage of –40 V on Si (lower trace) and on diamond using fluorine chemistry CVD (upper trace). Note the relatively strong hBN line in the film deposited on silicon, which is missing in the spectrum of the film deposited on diamond.

above 1 μm. While discrepancy in film thickness exists columnar growth can be obtained for both kinds of the substrates at proper tuned conditions. The faceted surface structure is obtained at lower deposition rates (0.2 μm/h), i.e. using higher deposition temperatures (950 °C). The growth rate can be increase up to 0.8 μm/h by reducing the temperature (800 °C) and increasing H_2:BF_3 ratio without affecting the content of cubic phase, but sacrificing the crystallinity. The inherent compressive stress is also increased due to the enhanced secondary nucleation of cBN crystallites.

Further examination of the representative samples discussed above was carried out by Raman analysis (Fig. 7-5). The spot size of the laser beam (514.5 nm) used in micro-Raman analysis was about 1 μm. The Raman spectrum accumulated from the sample with the cBN films reveals two additional peaks located at about 1048 and 1296

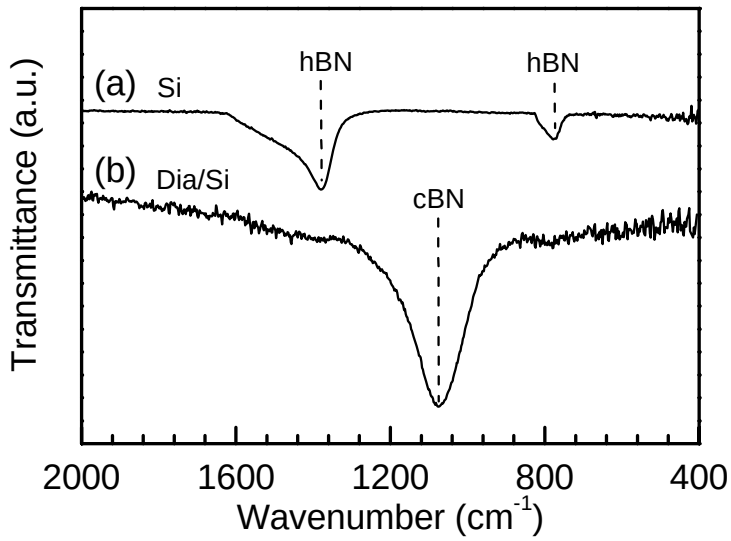

Fig. 7-6. FTIR spectra acquired from the BN film grown at a bias of −30 V on a Si substrate partially coated with polycrystalline CVD diamond; a) The spectrum obtained from a region free of CVD diamond after 1 h deposition shows only an hBN phase; b) The spectrum collected from a region precoated with CVD diamond after 1 h deposition indicates a nearly pure cBN phase.

cm^{-1}. These two peaks are assigned to scattering by the transverse and longitudinal optical (TO and LO) phonon modes of cBN. The peak positions of the TO and LO phonon modes are downshifted with respect to the values of 1056 and 1304 cm^{-1} , respectively, known for single cBN crystals synthesized by HPHT methods. The scattering downshift in wavenumber and peak broadening are caused by small sizes of crystallites and/or still high defect density as previously discussed in Chapter 6. Because of overlaping the diamond peak with cBN LO peak, the measurement of the FWHM of the cBN LO peak is inaccurate. The rough estimate, however, gives the FWHM of LO and TO phonons modes to be about 30 and 50 cm^{-1}, respectively. The values are consistent with the crystal size of about 200 nm as shown in Fig. 7-3d.

The role of the diamond substrate at cBN growth can be elucidated by an experiment using a Si (100) substrate partially coated by polycrystalline CVD diamond. BN deposition was carried out by ECR PECVD (bias voltage:–30 V; feeding gas composition: H_2:BF_3:N_2:Ar:He=3.5:1:50:10:140; temperature: ~900 °C) aided with fluorine chemistry and mediated by helium ionization reactions for an hour. The film grown on the diamond coating (Fig. 7-6b) is mainly cBN (content ≥ 98%) while no cBN could be detected on the diamond free Si surface (Fig. 7-6a). Nevertheless, cBN emerges even on bare Si after 6 h of deposition. The experiment demonstrates that cBN can grow directly on diamond (at –30 V) without precursor layers while a very long incubation time and thick hBN interlayer is needed for cBN nucleation on Si at identical deposition conditions. In addition, the cBN film grown on the diamond-coated substrate is characteristic with a smaller compressive stress when compared to the cBN film synthesized on the Si substrate at equivalent deposition conditions. Okamoto *et al* [130] observed a red-shift of 10 cm^{-1} in IR absorption spectra for the cBN films deposited on diamond substrate with reference to those of cBN grown on Si substrates. This suggests that the internal stress in the cBN film prepared on diamond is smaller than that on Si, which obviously is given by better compatibility of physical properties of cBN and diamond.

7.4. Growth mechanism of cubic boron nitride – role of diamond

Epitaxial growth of cBN film on diamond film represents so far the most striking development in this field. The advantage of a diamond substrate for cBN deposition stems from the remarkable similarity between the structural and physical properties of cBN and diamond (The lattice constant of cBN is larger by only 1.3% than that of diamond). Cubic BN film was grown on as-deposited polycrystalline CVD diamond employing ECR PECVD. The epitaxial growth was studied at the bias variable from –10 to –40 V. The data presented below were obtained from cBN films deposited using a bias of –20 V and a deposition temperature of 950 °C on a thin diamond film synthesized on a Si (100) substrate. The cBN thickness under these conditions can be larger than 3 μm. Thin films (200 nm thick cBN on 30 nm thick diamond) were however used to study the epitaxial growth by cross-sectional HRTEM with an atomic resolution. Low resolution TEM shows that the diamond columnar grains are seamlessly extended with cBN from the diamond interface up to top of the cBN film and laterally expanded from the diamond interface to the cBN surface. The cross-sectional HRTEM image (Fig. 7-7a) shows epitaxial cBN growth on diamond evidenced from the alignment of $(111)_{Diamond}//(111)_{cBN}$ planes. The contrast in the interfacial regions (Fig. 7-7a) is induced by stress probably due to the lattice parameter mismatch. However the seamless boundary between the two different cBN and diamond lattices could not be traced by HRTEM imaging. Therefore elemental mapping employing EELS was necessary to observe this interface. Fig. 7-7b shows an elemental compositional mapping of the interface region depicted in Fig. 7-7a. The scattered electrons have characteristic energy losses corresponding to the different elements (B, C, and N) in our films. The elemental mappings (Fig. 7-7b) show a sharp interface between the C and the BN layer and prove definitively, together with the HRTEM image (Fig. 7-7a), that cBN grows epitaxially on diamond. Transmission electron energy-loss spectroscopy (EELS) shows (insets in Fig. 7-7b) the B and N signals with the characteristic sp^3-bonding and fine structure of cBN in the upper (BN) region with no sign of C. The typical C signal of cubic diamond is observed (inset in Fig. 7-7b) only in the lower (diamond) region, in

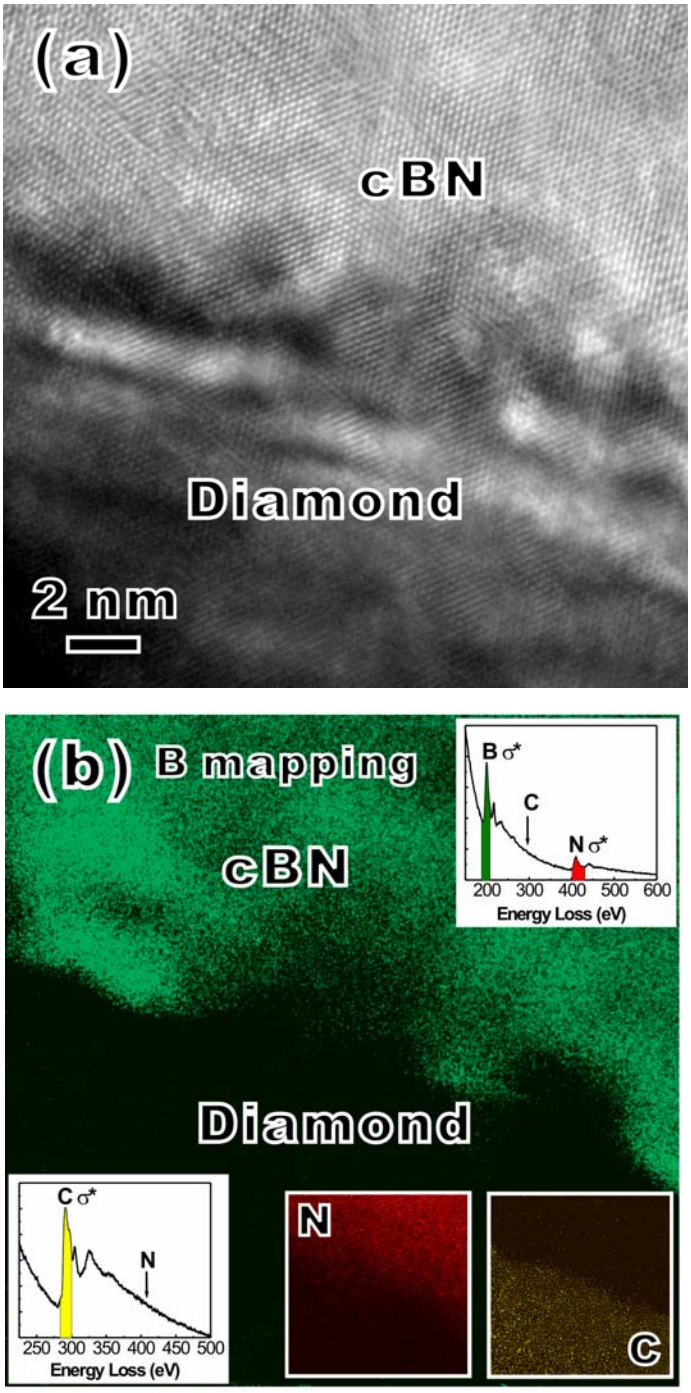

Fig. 7-7. Epitaxial growth of cBN on diamond: (a) HRTEM imaging indicates a seamless boundary between the cBN film and the diamond interlayer; (b) The interface between the diamond and cBN is revealed by elemental mapping of boron, carbon and nitrogen using EELS.

accord with the mapping data. The epitaxial relationship of cBN and diamond can also be substantiated by XRD at a glancing angle [131].

To further investigate the crystal relationship of the cBN crystals with the underlying diamond substrates, HRTEM was also performed to study the interface structure between cBN and diamond. It is found that cBN are directly grown on the underlying diamond crystals at most of the interface regions. However, the small-angle grain boundaries and twining crystal orientation relations between cBN and the underlying diamond were observed, as shown in Figs. 7-8a and 7-8b, respectively. In Fig. 7-8a, a clear and clean interface between cBN and diamond is observed. The corresponding Fourier-transformed image, as inserted in Fig. 7-8a, indicates undistinguishable patterns from cBN and diamond. Close examine of the HRTEM image, however, shows a small-angle grain boundary of about 6°. The appearance of the small-angle grain boundaries here is believed to be due to the lattice mismatch between cBN and diamond. The twinning relation of cBN with the underlying diamond is also clearly demonstrated by the HRTEM and Fourier transformed images in Fig. 7-8b. Comparing to Fig. 7-8a, the cBN is contacted with diamond at a smaller region, and aBN is formed around this contact region. When the cBN layer follows the diamond in a seamless way the cBN grows directly and epitaxially on the diamond layer with their (111) planes completely parallel to each other, then stress is built in the interfacial region, as indicated by the contrast change at the interface region in the HRTEM image (Fig. 7-8). The building up of the stress in the epitaxial region is also considered to be due to the 1.3% lattice mismatch between diamond and cBN. The observation of the stress in the epitaxial region suggests that a higher bias voltage (ion bombardment with high kinetic energy) may be intentionally applied at the initial growth stage of cBN on diamond so that the bombardment induced stress can eliminate the small-angle grain boundaries caused by the lattice mismatch. Then the bias voltage should be switched to the minimal available value to maintain the cBN growth with the lowest bombardment-induced defects.

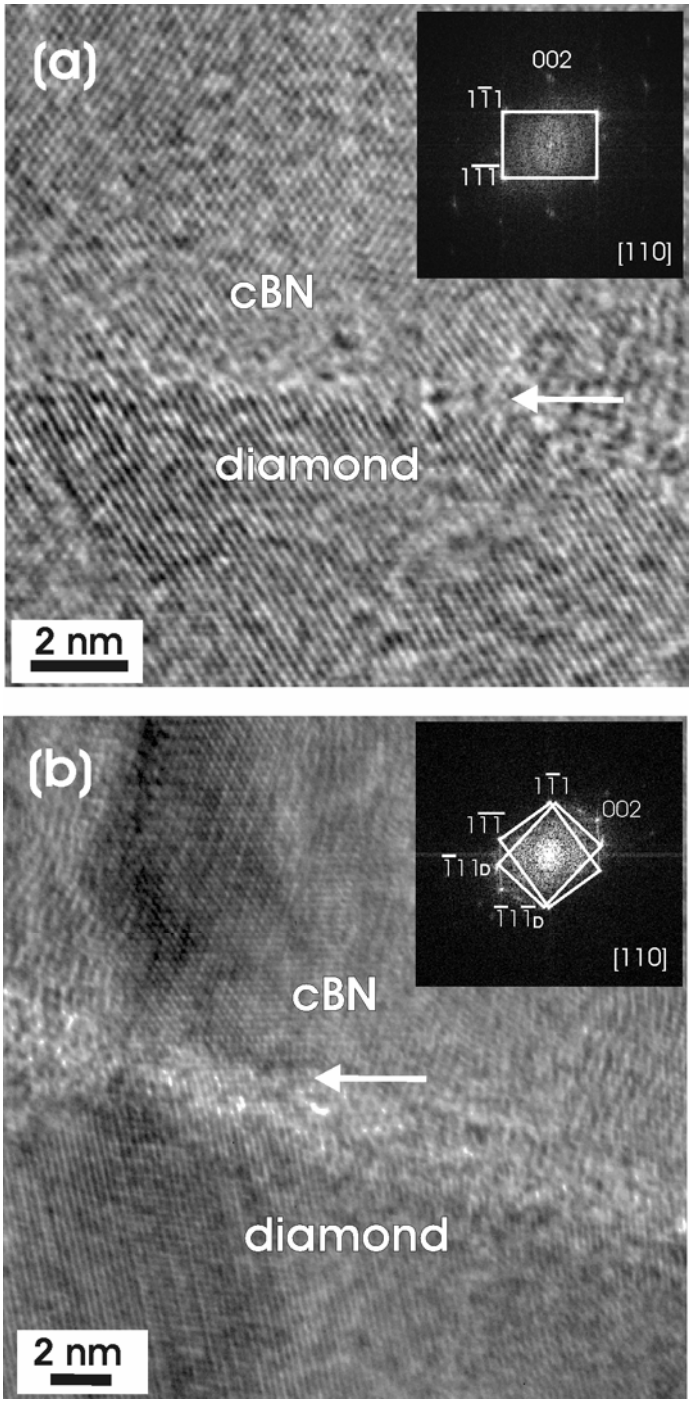

Fig. 7-8. The cBN grows directly on the diamond with no aBN or tBN layer. Cross-sectional HRTEM images of the diamond/cBN interface, showing (a) a small-angle grain boundary of about 6°, and (b) a twinning orientation relation between cBN and diamond crystallites. The inserts are the Fourier transformed patterns of the corresponding HRTEM images.

While direct contact is formed between cBN and diamond, there also exists a few aBN/tBN at some local interfacial regions, as shown by the HRTEM image in Fig. 7-9. It is interesting to note here that the basal planes of the tBN here are not perpendicular but parallel to the substrate surface, which contradicts the observation in the initial deposition stage of cBN films on Si substrates by both PVD and PECVD methods. On Si substrates, nucleation and growth of cBN films are two distinct processes. The nucleation, which is equivalent to the biased-enhanced nucleation of diamond [124], necessitates the formation of a precursor material: a dense, stressed matrix (a textured tBN layer with its basal planes normal to the substrate surface, as shown in Fig. 7-9) generated by ion impact. Small cBN nuclei (containing say tens of atoms) precipitate in this matrix after achieving the necessary density, structure and composition (nucleation stage). The edges of the tBN (0002) basal planes have been demonstrated to be the preferential nucleation sites for cBN, hence the observation of the interfacial tBN with its basal plane parallel to the substrate surface further demonstrates that the nucleation stage is not resolved at the deposition of cBN on diamond substrates. The minimal kinetic energy (bias) required for growth is typically lower than that necessary for structuring the precursor matrix and starting nucleation.

Most of the previous attempts utilized ion-assisted PVD methods; the energetic species bombardment was essential to both cBN nucleation and growth. It is generally accepted that nucleation and growth are two distinct processes that may require different optimal conditions to achieve the highest film quality. The critical bias voltage for the growth was indeed found to be lower than for nucleation. However, both the nucleation and growth in PVD were governed by the physical phase transformation from aBN/tBN to cBN due to energetic species impact, equivalent to the biased-enhanced nucleation of diamond as recently elucidated. [132] This process is a subsurface process; hence a thin aBN/tBN surface layer on top of the cBN film is inevitable, and the cBN is essentially nanocrystalline since it grows by coalescence of nanocrystallites and re-nucleation of cBN in the aBN/tBN phase. The high-energy particle impact involves many atomic displacements, yielding a high concentration of defects, which cannot be completely

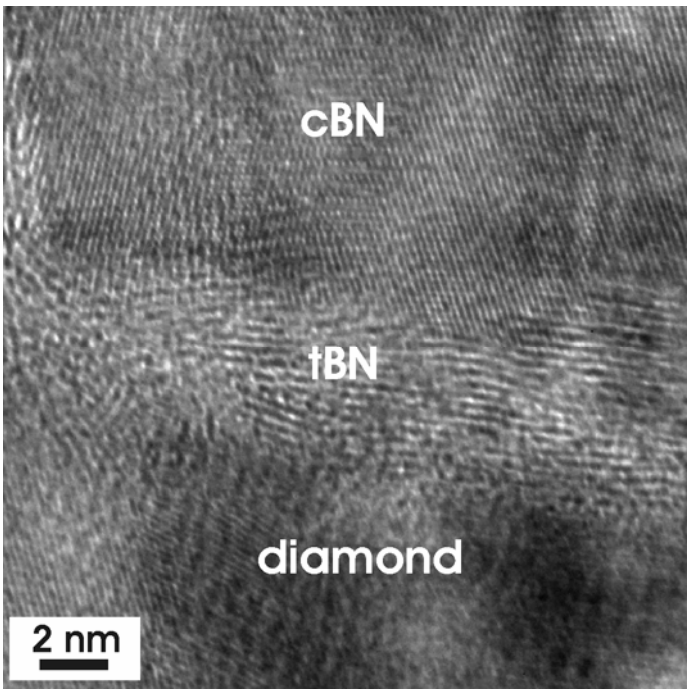

Fig. 7-9. Cross-sectional HRTEM image showing the appearance of tBN interface between cBN and diamond crystallites. Note here that the interfacial tBN has its basal planes parallel to the substrate surface.

annealed out. The first attempt using a PVD method to grow cBN directly on diamond failed [133]. Deposition on CVD polycrystalline (faceted and rough) diamond films resulted in a higher fraction of non-cubic BN, due to the geometrical effects associated with energetic bombardment of a rough surface. Planarization and special polishing of the diamond was essential to improve the cBN content of the film with respect to that deposited on silicon. The aBN/tBN inter-layer, the nanocrystalline nature, and the stress were, however, not improved. A recent publication, on work utilizing planarized and highly polished textured (001) diamond films, reported the growth of oriented cBN layers on diamond without the tBN interlayer [134]. Yet the high ion energy (280 eV) used for bombardment resulted in a highly defective cBN layer, for which no Raman cBN signal could be obtained. Many years of experience of studying epitaxial growth of a variety of different materials has established that energetic species cannot produce

high-quality epitaxial, single-crystal films with low defect density [135].

Growth of cBN using fluorine-assisted CVD is essentially different from the ion-assisted growth of cBN previously described. The CVD growth is a surface, not a subsurface, process, analogous to the CVD growth of diamond. It involves surface deposition of B and N layers and preferential etching of tBN constituents by fluorine. The small energy required in the process (–20 V bias) serves to break the B-F bond and facilitate the further N bonding necessary for the growth of the next layer. The crystalline size resulting from the CVD process is much larger and the crystalline quality much better than for cBN grown by ion-assisted PVD methods [126]. The surface nature of the CVD growth process is manifested by the faceted cBN surface free of the top aBN/tBN layer, which is inevitably present on cBN grown by PVD [136]. Remarkably, the same conditions (20 V bias) that produce the epitaxial cBN on diamond invariably lead to tBN growth on those parts of the Si substrate not covered with a diamond interlayer (a nucleation treatment with a minimum bias voltage of 30 V is needed to grow cBN on bare Si). Therefore, the fluorine-assisted CVD is capable of growing cBN directly on diamond, with hardly notable conventional nucleation stage. The way the columnar diamond structure is followed immediately by the successive cBN further substantiates this conclusion.

7.5. Summary to cubic boron nitride growth

This chapter shows that the discussed PECVD method aided by fluorine chemistry is capable of growing cBN directly on diamond with hardly notable conventional nucleation stage. The cBN nucleation on diamond is supported by the bias voltage –10 V whereas the bias voltage of –30 V is necessary to induce cBN nuclei employing fluorine chemistry. The direct growth of cBN on diamond is driven by the similarity in the diamond and cBN lattices as well as other physical properties. Epitaxial and twinning crystal orientation relations are observed between cBN and diamond. The small-angle grain boundaries are formed at the regions of the interface due the slight

lattice mismatch. A high bias voltage (ion bombardment with higher kinetic energy) is suggested to be applied at the initial growth stage to build up a little stress to eliminate small-angle grain boundaries and obtain “seamless” epitaxy.

Chapter 8. Growth mechanism of cubic boron nitride films by plasma enhanced chemical vapor deposition

The cBN growth on Si and Dia/Si substrates are discussed in previous chapters. This chapter outlines the deposition mechanism of cBN films prepared by PECVD with assistance of fluorine chemistry. The interpretation of mechanism is based on HRTEM examination of all interfaces across the substrate–film systems. The absence of continuous graphitic surface layers is revealed on the cBN films synthesized by PECVD aided with fluorine chemistry contradicting the observation on cBN films grown by PVD. In conjunction with the studies of the elemental surface composition by angular-resolved XPS and the plasma species involved in the growth process using OES (Optical emission spectroscopy), there is proposed a growth mechanism which is different from that known for cBN films synthesized by PVD employing highly energetic ion bombardment.

8.1. Briefing on diamond and cubic boron nitride nucleation and growth

Cubic BN growth by PVD takes advantage of the bombardment of the growth surface by highly energetic species, and involves two distinct stages, i.e. nucleation and growth. The nucleation is preceded by growing soft incubation interlayers of aBN and tBN in sequence. The cBN nucleates on the edges of tBN (0002) basal planes. The energetic particle bombardment is crucial not only to the cBN nucleation, but also is responsible for the growth of highly stressed, nanocrystalline cBN films with poor adhesion. As a result, the limited available thickness hinders the practical use of these films for both mechanical and electronic applications. Since PVD growth of cBN employs relatively high kinetic energies of ions, typically 80 eV and more, the energetic particles are introduced below the growth surface to the depth of several atomic layers. This process is denoted as shallow implantation or also subplantation process [89].

Growing cBN films by PVD is then phenomenological process characteristic with some reactions leading to cBN nucleation and growth several atomic layers below the surface [137]. The cBN nucleation and growth rather in the bulk than on the film surface are therefore thought to be the origin of the top sp^2-bonded aBN/tBN layers covering the cBN crystallites of PVD grown cBN films.

Chemical vapor deposition of diamond employs high chemical reactivity of atomic hydrogen to mediate surface growth reactions of methane radicals and selectively etch sp^2-bonded (graphitic) carbon with respect to diamond. Hydrogen enables growing polycrystalline diamond including highly oriented films on non-diamond substrates but also homoepitaxial single crystal diamond films. However, hydrogen is ineffective in selective etching of sp^2-bonded BN. This partially explains failure of many attempts to grow cBN by hydrogen based CVD methods [71]. Introducing fluorine chemistry in PECVD process however makes remarkable difference in cBN growth. Several fluorine-based PECVD methods have led to synthesis very thick cBN films, with thickness of up to ~20 μm [120,127]. Alike in CVD diamond, the nucleation stage of cBN is required, even with aid of fluorine chemistry. Diamond nucleation can be induced by either ion bombardment – bias enhanced nucleation (BEN) or mechanical scratching. The growth can be then maintained at thermal energies of particles. On the other hand the cBN nucleation and growth is far more complex. The cubic BN nucleation can be induced only with assistance of kinetic energies of ions, whereas the cBN growth has not been demonstrated without the assistance of kinetic energies of ions yet. The cBN growth can however be maintained at lower ion energies than those used in nucleation process. Unlike in diamond growing directly on substrates, cBN nucleation take place via incubation layer typically confining aBN and tBN sublayers [120] described earlier. The introduction of fluorine chemistry for the growth process which follows the nucleation enables the drastic reduction of the bias voltage and thus ion kinetic energies. Lowering the kinetic ion energy down to <20 eV and coupled with PECVD using fluorine chemistry might allow growing cBN films truly via surface processes which could be

extended to layer-by-layer growth and large area epitaxial single crystal cBN films on proper substrates.

8.2. Examination of the substrate – amorphous and turbostratic boron nitride interface

Reviewing earlier works on cBN films prepared on Si substrates show that the incubation layer (for cBN nucleation) is composed of an amorphous intermixed layer followed by a graphitic BN layer with an in-plane texture. The amorphous is probably formed because of amorphization of the Si substrate at its sputter-cleaning of deposition as well as intermixing in early stage of deposition induced at inherently strong ion bombardment causing introduction of growth species below the surface and atomic displacement. The reconstruction of the amorphized structure does not take place until building up internal forces (originated e.g. from accumulated stress and densification) driving structural transformation. The transformation is certainly affected by temperature because migration/diffusion of deposited species is temperature dependent phenomenon. The formed amorphous layer is visualized in the cross-sectional HRTEM image (Fig. 8-1a) of a cBN film prepared on Si substrate. The thickness of the amorphous layer is 5 nm. Reducing the energy of growth species and employing strong etchant as in our ECR plasma process, may however lead to elimination of the amorphous B-N-Si mixed layer during the BN film deposition as depicted in Fig. 8-2b. Since the intermixed layer is highly defective structure with many non-terminated bonds, it is more reactive than their crystalline counterparts. Thus, this amorphous layer may be etched off easily.

Direct growth of tBN on Si substrate had been reported by Iwamoto *et al* though it was found only on a very localized region [138]. Their study reports the substitution of argon sputtering process induced at negative substrate bias by hydrogen plasma process employing positive substrate bias. The etching process is then rather dominated

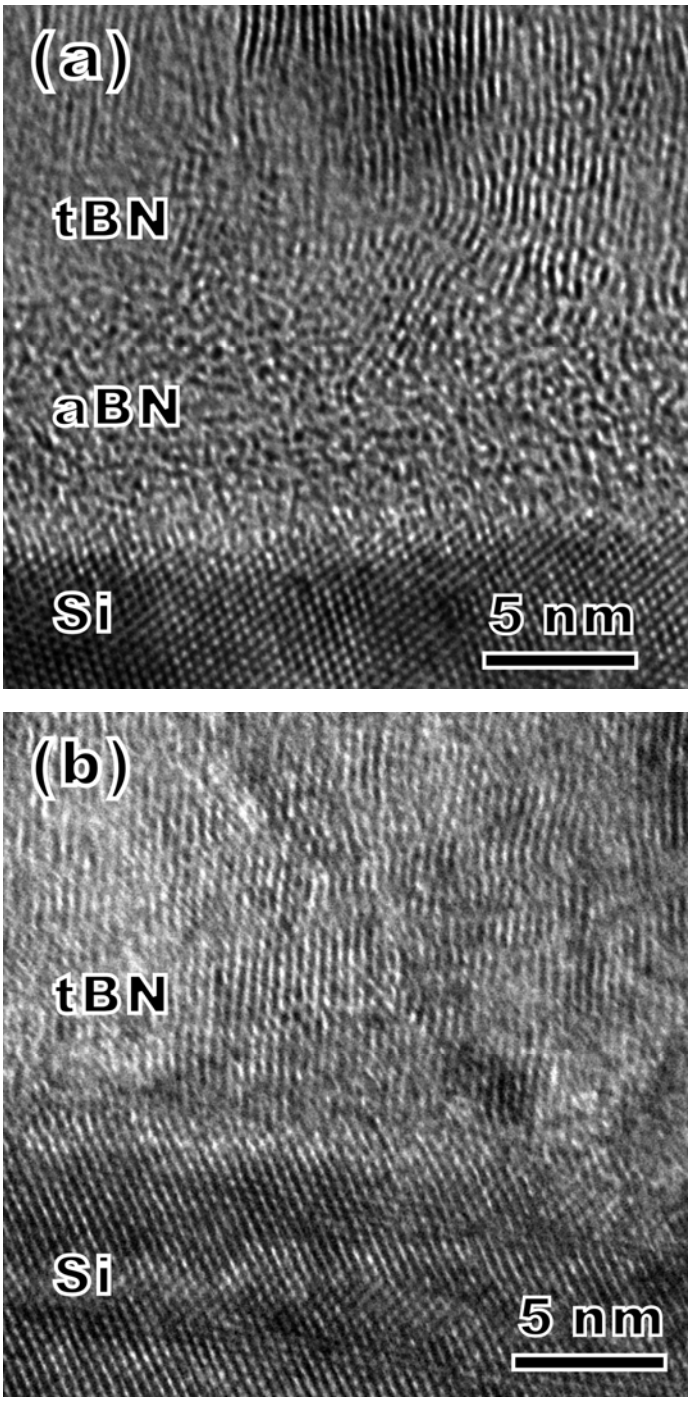

Fig. 8-1. Growth sequence of cBN – BN-Si interface: (a) conventional growth sequence via aBN/tBN interlayer; (b) direct growth of tBN on Si by eliminating the aBN layer.

by chemical etching via atomic hydrogen reaction than physical sputtering effect. In ion-assisted PVD techniques, the viable solution to preserve the underlying substrate lattice information is to choose a substrate which is not easily amorphized. The ionic materials like AlN were proved to be a good candidate for cBN growth. It was

demonstrated that cBN grew on AlN without any amorphous precursor layer and even directly on AlN without any incubation layer. Tendency of epitaxial growth in very localized regions was also observed [129]. Metallic materials such as gold (Au) can always preserve their crystal structures under ion bombardment. Therefore it may be presumed that Au is suitable to evaluate the underlying crystal structure at the BN nucleation though each substrate material also introduces other growth characteristics specific to the chemical nature of the substrate. Fig. 8-2 illustrates cross-sectional TEM of the PVD deposited cBN on a thin gold layer prepared on a Si substrate. The proof of the Au layer was checked by in-situ XPS measurement right after its deposition and prior to cBN growth process. The dark contrast in TEM images (Fig. 8-2) denotes gold layer. The contrast originates from the large difference in atomic number. As evident from Fig. 8-2b, the tBN layer is grown directly on the Au interfacial layer without any obvious amorphous structure. The cBN nucleates on the edges of tBN once its thickness reached 7 nm. The detail of the cBN-tBN orientation relationship is discussed below.

The thickness of the nucleation/incubation layer varies with deposition techniques and parameters. It is typically in the range of 5-30 nm for PVD and on the order of 50-100 nm for PECVD methods. Kuhr *et al* [79] speculated the thick nucleation layer was related to the inevitable presence of hydrogen in their PECVD deposition processes. The hydrogen incorporation could be as high as 25% and 15% in the nucleation and cubic layer, respectively. The interfacial tBN with a relatively open structure is considered as a trapping source where the hydrogen and other gaseous contaminants could incorporate. The incorporated constituents then alter the tBN texture. Since PECVD uses less energetic species than PVD, the PECVD technique requires a thicker nucleation layer to establish the conversion of randomly oriented tBN to structures normal of the substrate planes which only occurs if the biaxial stress in the film exceeds a threshold value as suggested by Mckenzie [86]. However, there exists an apparent minimum in substrate temperature for the nucleation of pure cBN on Si substrate which indicates that the intrinsic stress itself is insufficient for all the B and N atoms to surmount the activation energy barrier between the layer hBN and the three dimensional cBN structures.

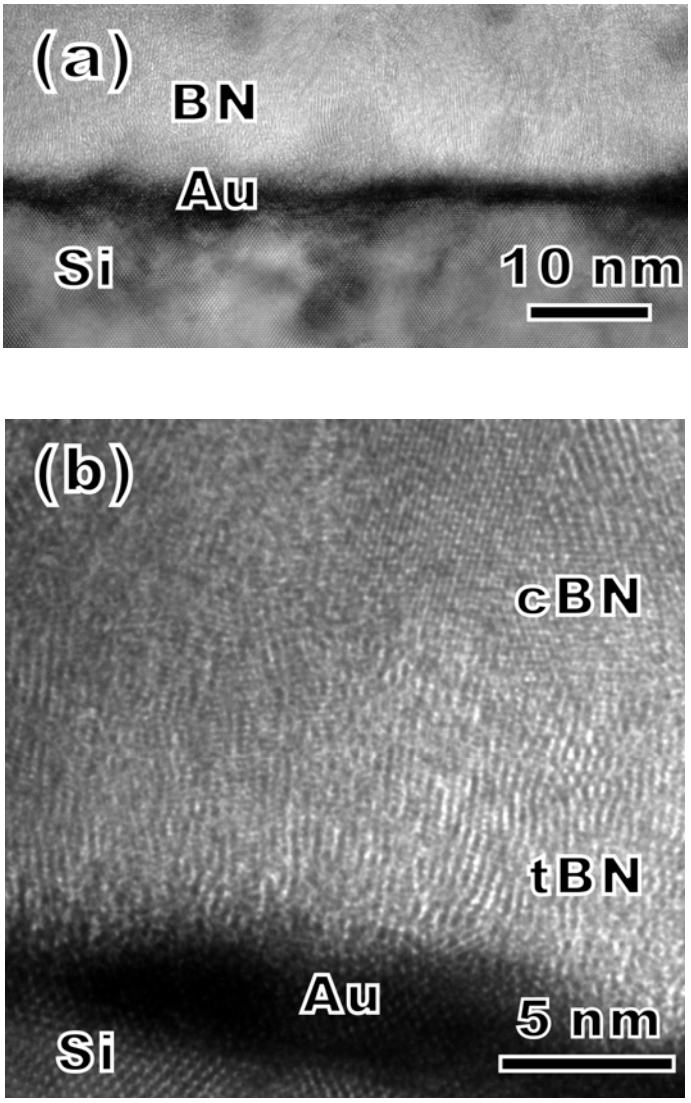

Fig. 8-2. Cross-sectional TEM images showing the structural interfaces of PVD deposited cBN films: (a) low magnification bright field TEM image and (b) high resolution TEM image.

8.3. Study of the turbostratic and cubic boron nitride interface by high resolution transmission electron microscopy

Although experimental studies on cBN nucleation and growth progressed fundamental understanding of elementary processes is inadequate. Difficulties are in nanocrystalline nature of cBN currently available and identification of possible nuclei using well-resolved two-dimensional surface analysis. This would be useful to

determine the orientation of nuclei with respect to the growth surface and their potential realignment in further growth process due to stress forces imposed by the structural difference. The experimental should involve deposition and in situ surface analysis. Fig. 8-3 illustrates several cBN nucleation sites on the tBN layer. The possible orientations of cBN (111) planes are designated by the orange lines. The exposed edges of the sp^2-bonded planes serve as nucleation sites for the cubic phase. Most of the identified cBN crystals as reported in the literature are preferentially oriented with their (111) planes parallel to the sp^2-bonded (0002) planes in the tBN layer. The lattice match following from the tBN (0002) and cBN (111) interplanar spacing (Fig. 8-3b) is 2:3 ($tBN_{(0002)}$:$cBN_{(111)}$). The overall distance of three cBN (111) consecutive atomic planes (~6.3Å) is approximately equivalent to two tBN (0002) adjacent atomic planes (~6.6 to 7.2 Å). Deviation and discrepancy in spacing matching may be induced because of turbostratic nature of tBN and interfacial stress evolved. The direction and spacing of the tBN (0002) are highly related to the cBN nucleation. As shown in Fig. 8-3, the tBN layer next to cBN layer is well aligned and closely packed which is necessary to nucleate cBN. Similarly, Iwamoto *et al* [138] found that near the interface between the amorphous layer and the tBN layer, the orientation of the basal plane is random, and gradually changes and becomes nearly aligned with the surface normal with increasing the distance from the substrate interface. Simultaneously the spacing of tBN (0002) planes reduce their interplanar spacing from 3.6 to 3.3 Å [139]. These changes are obtained by inserting additional tBN planes. In our cBN deposition, it is speculated that the growth front of tBN just before cBN nucleation are capped by forming nanoarches, which is highly reactive and it can facilitate the formation of cBN. When the graphitic BN planes bend at the region of a nanoarch, the B-N bonds bend too and locally the bonding changes its character from sp^2 to sp^3. The transformation is consequence of mechanical forces exerted on adjacent atoms in the bend regions. Nistor *et al* [140] found that the largest nucleation rates for cBN were observed for hBN powder with a large density of nanoarches at their edges under their HPHT experiment. It is believed that these nanoarches constitute nucleation center for cBN and might also be formed

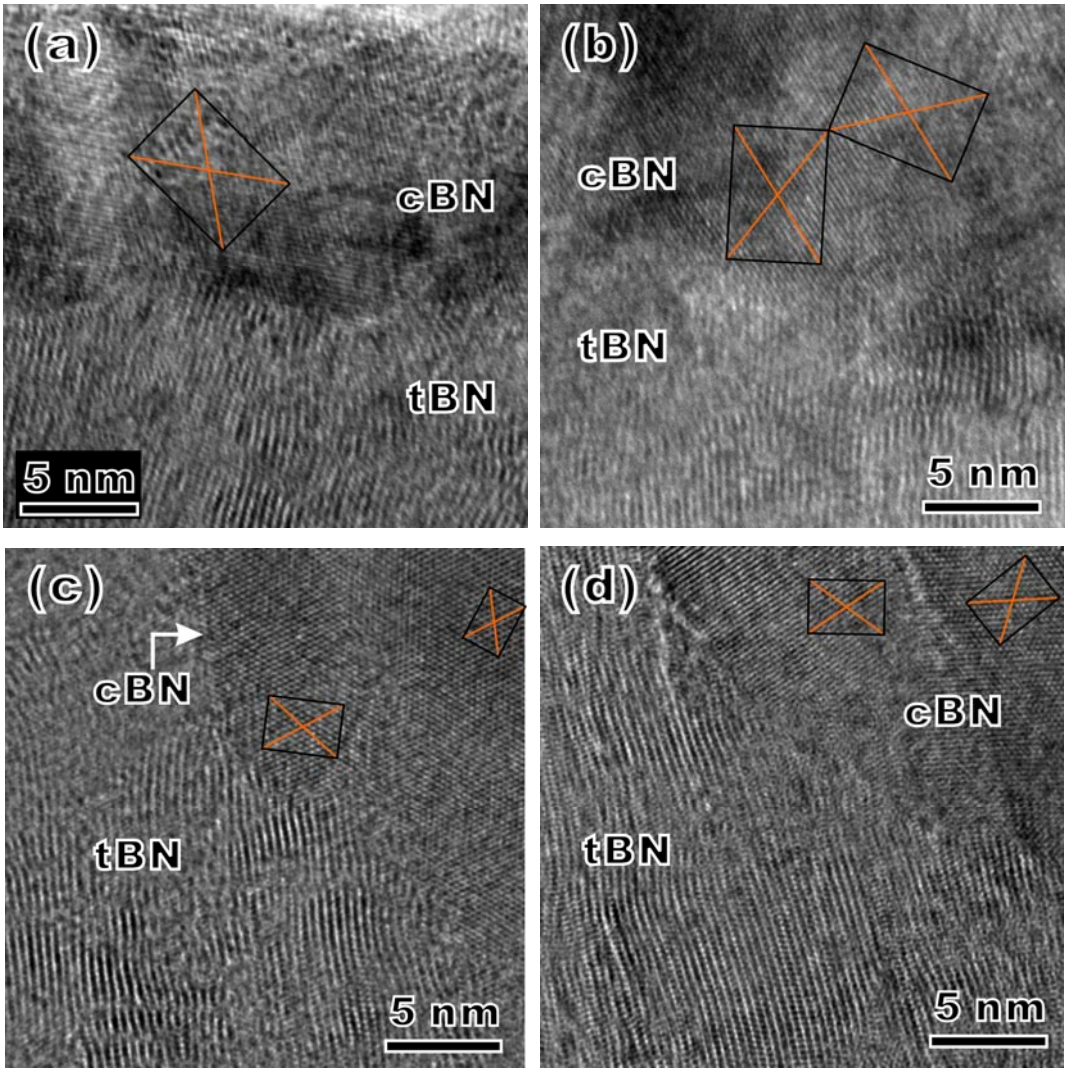

Fig. 8-3. Growth sequence of cBN – tBN-cBN interface: (a), (b), (c) and (d) showing different orientation relationships.

under energetic ion impact during the BN deposition. According to recent experiment by Collazo-Davila *et al* [141] who studied the ballistic atomic displacement of hBN powder using MeV TEM. The energy imparted on B and N atoms can be as high as 431 and 307 eV, respectively, in direct knock-on collisions with the atomic nuclei. The curling and formation of nanoarches under intense electron bombardment were observed.

Evidently, there are at least two orientation possibilities of cBN crystals nucleated

on tBN. The first one is a cBN crystal with (111) planes aligned parallel to the tBN (0002) direction which is roughly perpendicular to the substrate as shown in the lattice-resolved TEM image in Figs. 8-3a and 8-3b. This orientation is in fact the growth in (111) crystallographic direction. The second possibility when the cBN (111) – tBN (0002) does not satisfy the 2:3 matching the growth is the [001] crystallographic direction as depicted in Figs. 8-3c and 8-3d. Since a limited number of HRTEM images were obtained from the tBN-cBN interface region, it is difficult to make conclusion which orientation will give a greater nucleation rate. Some studies on growing nitrides and diamond films under bombardment report the (100) textured growth. This is attributed to the larger spacing of (100) planes than those of (111) planes. The larger spacing of (100) planes enables greater ion channeling effect which also implies that these planes more likely survive under energetic ion bombardment [142]. Jiang *et al* [143] had studied the effect of ion bombardment on the orientation of diamond growth using MW plasma starting with (111) oriented diamond surface. They revealed a number of tiny (100) faceted diamond crystals grown on top of (111) oriented diamond. Jiang *et al* [144] also found the cBN with a preferential alignment of [001] grain axes approximately perpendicular to the film surface. Thus, ion bombardment is another factor which determines the orientation of the crystals initially formed.

8.4. Analysis of cubic boron nitride layer by high resolution transmission electron microscopy

As observed by HRTEM, the grain size of cBN prepared by PVD technique is extremely small (≤ 20 nm) [145]. The tBN phases with 1–2 nm in thickness were found at the boundaries of cBN grains [146]. Although Keunecke *et al* [147] synthesized cBN films with thickness of 2 μm the size of cBN grains size did not change significantly across the film thickness. The small nanocrystallites with practically constant size across the film thickness hints the deposition of PVD cBN to be dominated by secondary nucleation due to the imposing of high bias voltage on the Si substrates

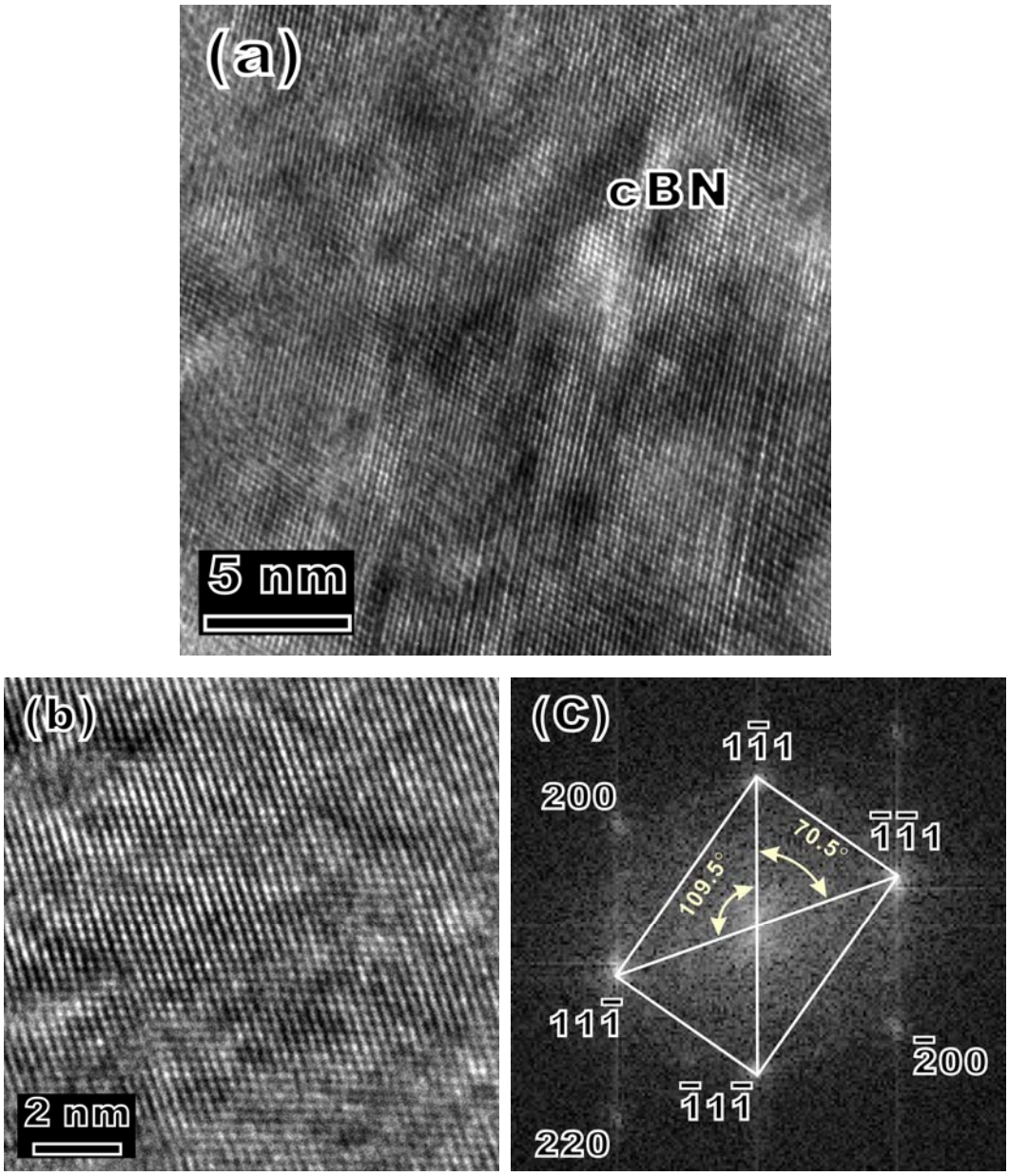

Fig. 8-4. HRTEM images showing a large cBN grain and its FT image.

(–200 V). Cubic BN films grown by PVD process is assisted by highly energetic ions. The energy of ions however dissipates as ions penetrate into deeper regions of the inter-grain boundaries. The lower energy between the neighboring crystallites at their lateral growth expansion then favors deposition of non-cubic phases. Since in this process no chemically reactive species effectively etching the non-cubic phases are involved, the non-cubic phases cannot be removed. Both chemical etching and

sputtering are ineffective in the inter-grain boundary regions. The deposition of the non-cubic phase may then continue until the close of gaps among neighboring grains or expanding non-cubic phase to size supporting cBN nucleation. The increase of ion energy could reduce non-cubic phase enclosed in inter-grain boundaries but simultaneously secondary cBN nucleation sites might be promoted and growth process might be far from the standard deposition conditions yielding BN films with high content of cubic phase. The speculative analysis above also elucidates the reasons why there are no reports on PVD cBN films yielding characteristic Raman phonon peak though high substrate temperature and atomically-flat single crystalline diamond substrates were employed [134]. The HRTEM images, in Figs. 8-4a and 8-4b (b – enlarged image), show (111) crystallographic planes and demonstrates the cBN grain is approximately 30 nm in diameter, whereas all the spots in the corresponding FT image (Fig. 8-1c) are indexed to cBN crystalline phase.

8.5. Investigation of cubic boron nitride surfaces by high resolution transmission electron microscopy

It is surprising that only a few articles report analysis on growth surface [148,149] using HRTEM. The lack of these informations is probably caused by difficulties of separating the surface graphitic BN and polymeric binder materials used in preparation of TEM samples. Yang *et al* [148] employed an ion-milled Si and use it as a substrate to deposit cBN films. Since the as-deposited BN was sufficiently thin for cross-sectional HRTEM, the post-deposition thinning process was omitted. Otherwise, some surface analytical techniques such as XPS and XANES have been used. Park *et al.* [108] found a surface hBN layer (~1.2±0.2 nm) on a cBN thin film using in-situ angle-resolved XPS. The cBN film was prepared by dual ion beam sputtering employing optimized growth conditions (60 mA/cm^2, 350 eV and 460 °C). The presence of surface graphitic BN is probably due to the lack of a selective etching agent during the synthesis and unique deposition mechanism. The observed discrepancies between the CVD of diamond and

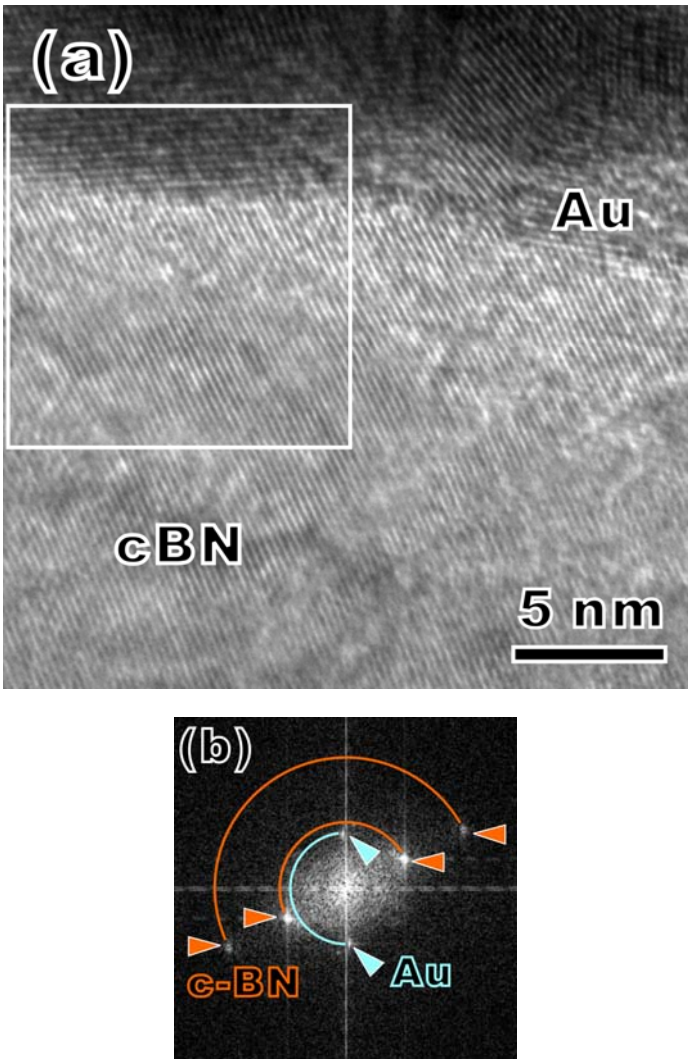

Fig. 8-5. Cross-sectional HRTEM image of the surface region of the film deposited by ECR-MWCVD. A gold coating on the cBN surface protects and marks the surface region.

cBN are in part attributed to the fact that in synthesis of diamond, graphite is easily etched by atomic hydrogen, thereby kinetically hindering its growth under conditions of large super-saturations of atomic hydrogen. In contrast, hBN is not selectively etched by atomic hydrogen with respect to cBN. An alternative mean is therefore necessity to destabilize the hexagonal phase and to create an environment that favors cBN growth. Indeed, Kalss *et al* [81] used hBN and cBN powders with grit size about ~1 μm and performed the reactive plasma etching containing BF_3 and had demonstrated that hBN can be etched away 6-times faster than cBN. The absence of tBN or aBN on the film

surface as reveal by HRTEM (Fig. 8-5) could be attributed to the preferential etching of non-cubic phases. Fig. 8-5 displays cross-sectional TEM overviews of PECVD deposited cBN using fluorine chemistry (Fig 8-5a) and its corresponding Fourier transform image (Fig. 8-5b). A clear interface between the cBN film and the gold layer is seen. The cBN and gold lattices are in direct contact each other. No amorphous layer separating the two crystalline regions is observed. Since gold has larger interplanar spacings (d_{111}) than cBN, their spots are located at the innermost region. The diffraction spots of two different materials (BN and Au) at nearly equivalent angular displacement are the indicative of textural growth as deduced from the particular cBN crystallite whiles other angular displacements of diffraction spots are not revealed by HRTEM. On the other hand cBN films prepared by radiofrequency magnetron sputtering (PVD process) show much more defective nanocrystalline cBN structure with aBN and tBN

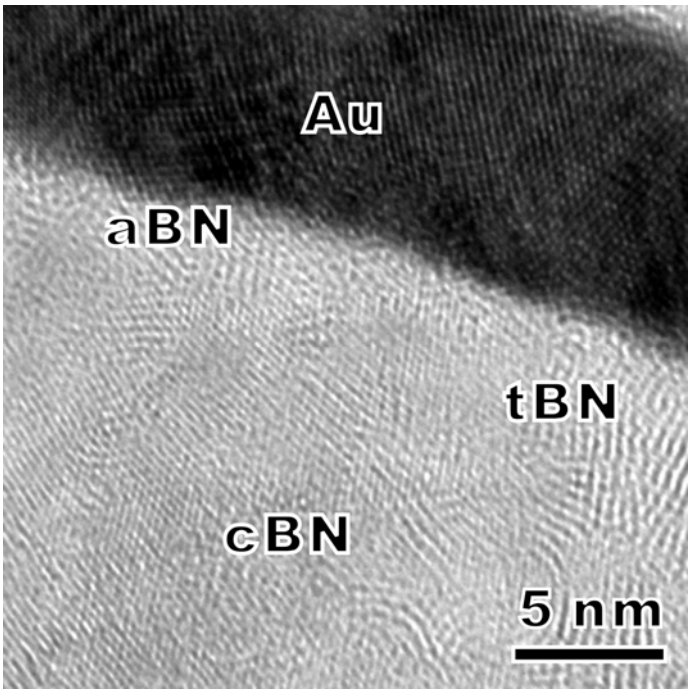

Fig. 8-6. Cross-sectional HRTEM image of the surface region of the film deposited by RF-MS. A gold coating on the cBN surface protects and marks the surface region. The cBN films were deposited at 500 °C and –180 V using pure N_2 gas.

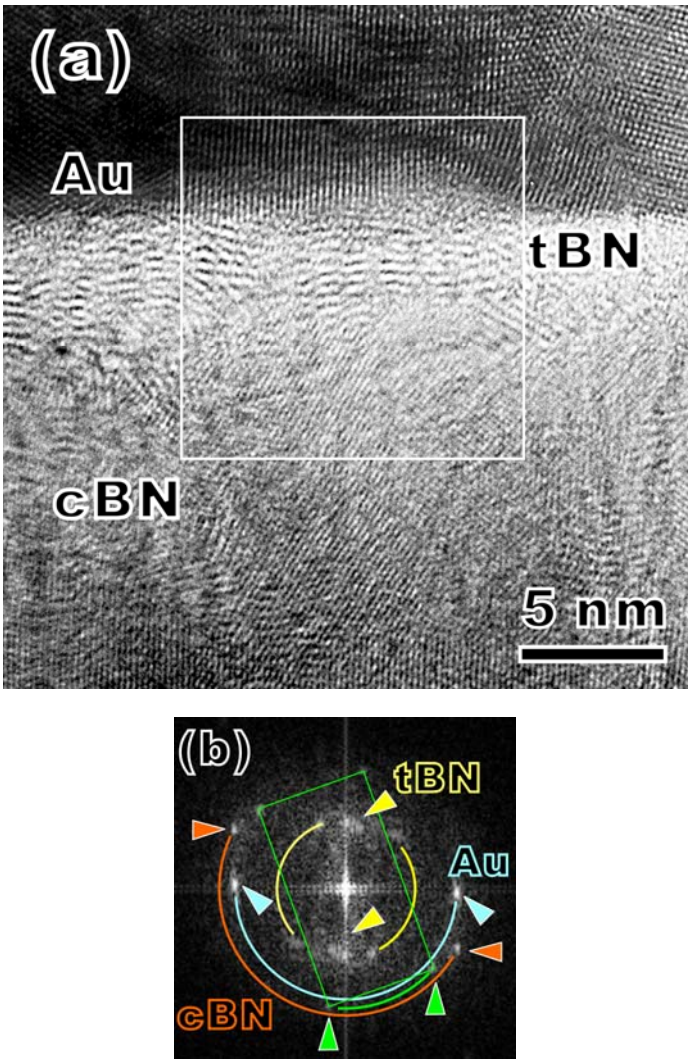

Fig. 8-7. Cross-sectional HRTEM image of the surface region of the film deposited by RF-MS. A gold coating on the cBN surface protects and marks the surface region. The cBN films were deposited at 900 °C and −90 V using Ar/N_2 gas mixtures.

impurities, and a thin aBN top layer as seen in Fig. 8-6. The non-cubic phase with thickness of about 3 atomic layers clearly covers the cBN film. The increase of the substrate temperature to 900 °C and the reduction of substrate bias voltage to −90 V and using an Ar/N_2 (2:1) mixture enable growing larger cBN crystallites but the growth characteristic changes as shown in Fig. 8-7. The surface layer becomes thicker and ordered. The structural transformation might be induced by the enhanced mobility of the

subplanted species at high substrate temperature, which have a great probability to diffuse towards surface. The presence of the tBN with its graphitic basal planes parallel to the substrate could be caused by the lack of stress at the surface region because of the relaxation of stress at higher temperatures. Fourier transformed image collected from the region indicated by a white rectangle illustrates elongated tBN diffraction spots displaced with respect to the gold diffraction spots. It seems that the tBN bends towards the (111) direction of the cBN planes, which is classified as the preferred nucleation sites. The presence of surface tBN might come from insufficient selective etching in the PVD (RF-MS) deposition process. It is interesting is that the interplanar spacing calculated from the diffraction spots denoted by the green rectangle in Fig. 8-7 does not match the spacing being typical for Au, tBN and cBN, but they correlate with interplanar spacing of wBN well. The wBN polytype is often produced by HPHT methods. The reason of its appearance in our films is not known yet. The wBN structure was also reported at cBN film synthesis by others [129] using in PVD technique. The presence of wBN might be related to the puckering of hBN under compressive stress. If the temperature is not high enough to mobilize the atoms sufficiently during deposition, wBN cannot transform to cBN.

The absence of the aBN layer on top of the CVD grown cBN film and its occurrence on the PVD film provides evidence on natural dissimilarity of the growth mechanisms in the two deposition schemes: (i) a surface growth process associated with surface etching for PECVD in contrast to (ii) a subsurface growth leading to the typical aBN overlayer for PVD deposition. The HRTEM data thus substantiates the conclusion that the goal of growing cBN via chemical pathways was indeed achieved using the approach of the fluorine chemistry.

8.6. Growth species involved in cBN growth

Optical emission spectroscopy of the plasma used for cBN growth is expected to reveal the reactive gas species and give insight into the growth mechanism. The small

amounts of BF_3 and H_2 employed in comparison to abundant Ar, He and N_2 inhibit the observation of most reactant species in the actual plasma used for cBN growth. We have therefore chosen to study the composition of the BF_3+H_2 plasma with different H_2/BF_3 ratios (0-5) instead. The study was performed using a substrate holder made of hBN enabling the observation of hBN etching by a BF_3+H_2 plasma. OES of a pure BF_3 plasma (Fig. 8-8a) indicates the formation of fluorine, BF, hydrogen, and nitrogen clusters. Fluorine and BF clusters are expected in the BF_3 plasma. The small amount of hydrogen which decreased with time is most likely due to desorption of hydrogen from the chamber components including the hBN substrate holder. The nitrogen signal was time independent when no nitrogen was supplied to the system. The source nitrogen was hBN holder which was probably etched off during the plasma exposure. The emission intensity of both nitrogen and fluorine decreased with introduction of hydrogen. The intensity is continuously reduced with increasing the flow rate of

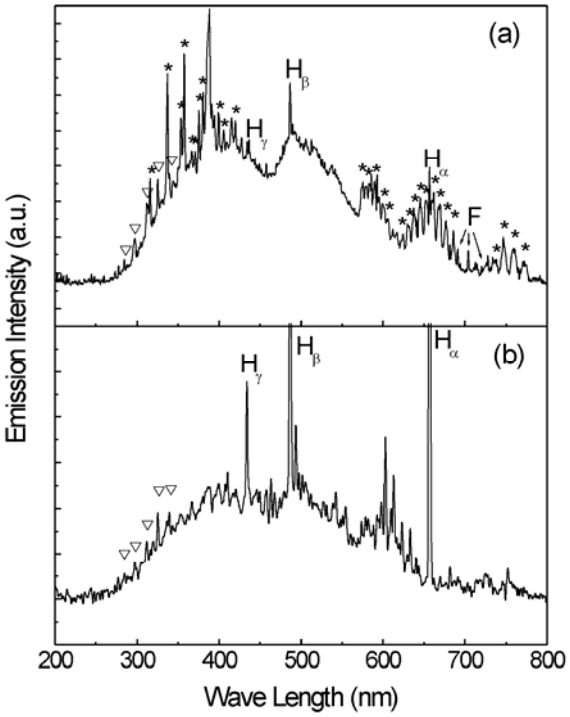

Fig. 8-8. OES spectra of the plasma (impinging on an hBN holder) with a gas flow of (a) 5 sccm BF_3, and (b) 5 sccm BF_3 and10 sccm H_2, respectively. * indicates the emissions from N_2 and ∇ from BF.

hydrogen and vanishes (Fig. 8-8b) at a flow rate of 5 sccm BF_3 and 10 sccm H_2. The nitrogen signal induced by a periodic reducing and increasing the H_2 flow rate was studied. The nitrogen signal was observed only at small hydrogen flow rates. This rules out the residual nitrogen in the system as the nitrogen source. The only possible source is then hBN substrate holder which is etched by fluorine formed in pure or low hydrogen concentration BF_3 plasma. The atomic fluorine concentration decreases with the introduction of hydrogen due to the formation, and HF formed does not seem to react with hBN. The etching of hBN therefore stops when fluorine is effectively compensated at sufficiently high hydrogen concentration as deduced from the nitrogen signal. The etching of hBN is possible only at low H_2/BF_3 ratios. The H_2/BF_3 ratio has to be optimized for cBN deposition. The cBN deposition conditions are met only within a narrow window. On other hand at higher H_2/BF_3 ratios hBN films only evolve. The hydrogen flow rate controls the solid BN production rate from the gas phase, and the ratio of hydrogen to fluorine controls the equilibrium between the film formation and etching.

The last observation made in the presented OES study is the nearly constant emission intensity of the BF_x cluster with increasing hydrogen flow rate, while no signals of BH_x clusters could be detected. This suggests that the growth species are BF_x rather than BH_x clusters. This OES finding is consistent with the stronger chemical bond of B-F (757 kJ/mol) compared to B-H (340 kJ/mol). Quantum mechanical calculations [150] indicate that B-F termination stabilizes the B surface of cBN. The F-terminated B surface was however found resistant to abstraction and adsorption of N containing growth species for further cBN growth. B-F bond breaking followed by surface abstraction and adsorption of nitrogen containing species may be facilitated by the low energy ion bombardment which is still needed for cBN growth from fluorine chemistry.

Angular-resolved X-ray photoelectron spectroscopy (XPS, VG, EscaLab 220i-XL, Al K_α radiation) of cBN films grown by the ECR-PECVD method was finally used to

provide further insight into the cBN growth process. The spectra were collected at take off angles of 10 and 90°, respectively, to evaluate the elemental depth distributions since the probing depth at 90° (~5 nm) is much larger than at 10° (~1 nm). Table 8-1 summarizes the elemental composition of the film in atomic percents. The film is mainly composed of B and N and small amounts of F, C and O. The B/N ratio is smaller than 1 and is reduced from 0.92 to 0.83 for take off angles of 90° and 10°, respectively, indicating B deficient surfaces rather than the bulk B/F ratio of 1. The low fluorine concentration (0.7 and 1.0% for 90° and 10°, respectively) indicates that only a small portion of the surface is terminated by F. These results are in accord with the feeding gas composition of the plasma (BF_3:N_2 = 1.5:50). The high N_2 concentration in the gas phase leads to a high probability of N termination. This point was further verified by exposing the film to a BF_3+Ar+He plasma leading to a significant increase of both the B/N (to >1) and the F concentration (to ~6%). Further exposure to N_2+H_2 plasma decreased the magnitudes of B/N and F to their initial values. Finally, minor carbon and oxygen (revealed by the angle resolved XPS analysis) are adventitious surface constituents adsorbed at air exposure after the film deposition.

Before discussing our proposed cBN growth sequence, we note that N_2 molecules fed to the plasma will decompose to N atoms and then combine with hydrogen or fluorine atoms. The bonding energy of N-H (~340 kJ/mol) and N-F (343 kJ/mol) are

Table 8-1. Compositional analysis as determined by the XPS spectra recorded at take off angles of 10° and 90°, respectively.

	Elemental concentration (at %)	
Take off angle	90°	10°
B	43.7	39.4
N	47.6	47.7
C	5.7	8.7
O	2.3	3.2
F	0.7	1.0

similar [150], so both NH_x and NF_x clusters may exist. The low fluorine concentration in our present XPS data (~1%) however rules out the possibility of N-F termination of the cBN surface, while secondary ion mass spectrometry (SIMS) of a cBN film suggested that nitrogen atoms are partly bonded to hydrogen [144]. It is thus most likely that only NH_x clusters contribute to the surface processes leading to the cBN growth. In addition we note that the absorption energy of NH_x clusters on F-terminated B surfaces is larger (416 kJ/mol) than that of NF_x clusters (17 kJ/mol) [150]. N-H bonds are also found much more effective in abstraction of incoming B-containing gaseous species and in stabilizing and maintaining the sp^3 surface atoms than N-F bonds.

8.7. Growth mechanism of cubic boron nitride films by plasma enhanced chemical vapor deposition using fluorine chemistry

Our experimental findings lead to the following conclusions regarding the cBN growth via fluorine chemistry: (1) the cBN growth is a surface process (HRTEM data), (2) etching of hBN constituents is performed by F atoms in the plasma (OES data), (3) BF_x and the NH_x are the most probable species leading to cBN growth (OES and XPS data), (4) the cBN film surface is B deficient and the termination of dangling bonds by F is minor (XPS data). Based on these conclusions we now offer the following sequence of cBN growth from fluorine chemistry schematically shown in Fig. 8-9:

The excited plasma contains reactive species H, F, BF_x, NH_x responsible for etching of hBN (mainly F) and cBN crystal growth (BF_x and NH_x) (Fig. 8-9a). The cBN surface at any stage contains a large number of N atoms terminated by H and a very small number of B atoms terminated by F.

The cBN crystal surface is activated by surface abstraction due to impingement of plasma species providing free unsaturated sites for further growth (Fig. 8-9b). B-F bond

breaking is most likely assisted by the energetic particle bombardment (bias of ~20V) while N-H bond breaking is easier.

B is added to N activated sites by incorporation of BF_x species, N is added to B activated sites by incorporation of NH_x species (Fig. 8-9c).

Each B surface site is deposited by a NH_x in a much higher rate than the deposition of BF_x on N surface sites (the BF_3/N_2 flow rate feeding the plasma is 1.5/50) leading to a B deficient surface at any stage (sequence step 1) (Fig. 8-9d).

A layer by layer growth of a cBN crystal requires deposition of B on a N surface, then deposition of N on the B surface which means (on a macroscopic scale) that the surface atomic concentration of B and N is equal. The surface of our ECR films is boron deficient due to the plasma composition needed for cBN growth (BF_3/N_2 flow rate=1.5/50). As stated above our experimental findings support the suggestion that N surface atoms are terminated by H while B surface atoms are terminated by F. The N-H bonds of N-H terminated surface sites were found energetically effective in abstraction and adsorption of incoming B-containing species [150]. The H atom terminating a N surface atom will be abstracted by plasma fluorine atoms forming HF and leaving room for BF_x adsorption. The chemical bond strength of B-F is large, making it resistant to abstraction and adsorption of NH_x. In our study the breaking of B-F bonds and formation of a dangling bond needed for NH_2 adsorption and further cBN growth is most likely facilitated by the low kinetic energy ion bombardment of the growing surface (Fig. 8-9b).

The high abundance of N-containing clusters in the plasma (compared to B-containing clusters) dictates that the coverage rate of each B surface atom (fluorine terminated) by nitrogen will be much larger than the coverage rate of nitrogen surface atoms (hydrogen terminated) by boron atoms. This excludes the possibility of a layer-by-layer growth and leaves island formation of cBN with a major surface coverage

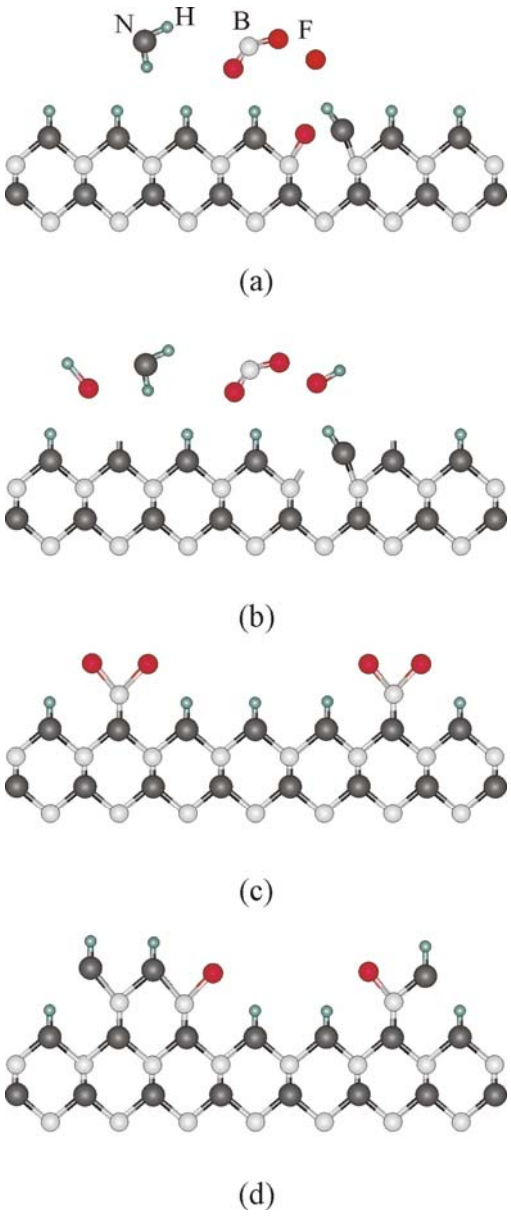

Fig. 8-9. A proposed cBN growth sequence in fluorine based ECR PECVD. The growth is illustrated on a (100) surface.

of hydrogen terminated N atoms as the dominant growth mechanism (Fig. 8-9d). The hydrogen constituent of the plasma determines: (1) the concentration of NH_x species (needed for growth, increases with H concentration), (2) the fluorine atom concentration (needed for activation of H terminated N surface atoms and for etching of non cubic BN constituents, decreases with H concentration) This way the hydrogen to fluorine ratio

controls the deposition rate and phase purity resulting in an optimal window of the H_2/BF_3 ratio for cBN growth [114].

8.8. Summary to the growth mechanism of cubic boron nitride films synthesized by plasma enhanced chemical vapor deposition using fluorine chemistry

HRTEM, OES and XPS studies revealed discrepancies between the PECVD and PVD growth of cBN. The surfaces of cBN films prepared by PECVD are unique and characteristic with certain proportions of surface constituents. The abundance of surface constituents are determined by the composition of used $He(Ar)/N_2/BF_3/H_2$ gas mixture and gas phase and surface reactions. The surface reactions are aided by ions. The detail analysis of new acquired data enables the cBN surface growth sequence as follows: (1) Formation H, F, BF_x and NH_x in the plasma so that the amount of F and NH_x is balanced by the feeding hydrogen concentration, (2) abstraction of hydrogen and activation of N sites by F, (3) abstraction of fluorine and activation of B sites by energetic particle bombardment, (4) growth by adsorption of BF_x (boron source) on N and NH_x (N source) on B, (5) etching of non cubic BN constituents by F. The possibility to grow cBN via surface reactions without the significant damage introduced by high energy ion assisted methods promises that the growth of electronic grade cBN single crystalline wafers (similar to single crystalline electronic grade diamond wafers grown by CVD) is feasible.

Chapter 9. Parametric study of cubic boron nitride deposited by physical vapor deposition

This chapter studies the quality of grown cBN films in relationship with a fundamental deposition parameter, ion beam energy, and substrate property, surface roughness. The precise control of the deposition parameters to reveal the BN nucleation and growth was achieved by employing a mass selected ion beam deposition (MSIBD) techniques. Graded surface roughness was obtained by scratching silicon surfaces using diamond powders with different grain sizes. The root-mean-square roughness of silicon surfaces varied from 0.2 to 170 nm. The analyses of grown BN films show the interfacial tBN thickness increased and nucleation threshold for cBN shifted towards higher ion energy with the increase in substrate roughness, and the orientation relationship of tBN with Si was more random as evident from SAD pattern. The differences in cBN volume fraction however became less obvious at higher ion energy (500 eV). The resulting featureless film morphology at high ion energy is probably associated with the preferred subsurface growth process. On the contrary low ion energy led to a surface-like growth process which predominantly yielded granular morphology.

9.1. Benchmarks in cubic boron nitride synthesis

Alike diamond, cBN exhibits distinctive optical, chemical, electrical and mechanical properties. Some cBN properties are superior to diamond. In particular, cBN has higher thermal stability, higher oxidation resistance, and it is extremely inert to the molten ferrous metals. Therefore considerable efforts have been made to synthesize cBN films and understand their nucleation and growth mechanisms. The primary goals have been enlargement of crystallites, crystal perfection and adherence of cBN films to the substrates *via* lowering the internal film stress and elimination of interfacial non-cubic layers. Up to now, most of the works [71,151] reported the cBN deposition on Si because Si can be used at relatively high temperature, is transparent in infrared and available in device quality.

Although the first syntheses of cBN and diamond are dated to the same period (~50 years ago), the diamond deposition is more advanced. Polycrystalline diamond can be grown with high quality on many substrates. Single crystal diamond films can be synthesized by heteroepitaxial [152] or homoepitaxial [153] growth. On the other hand, cBN grows with poor quality and limited film thickness though diamond and cBN are similar in their structure and properties. Because of correspondence in physical properties technology similar to that of diamond, it might be presumed that diamond deposition conditions could be effective for cBN growth. Recent lowering the particle energy in cBN deposition closer to the thermal energy supports such speculation. For example, surface pretreatment with diamond powders improves the nucleation density of diamond [154]. The selection of proper substrate affects the diamond quality (silicon, iridium, diamond) and would have positive effect on the cBN formation. Using various substrates [155,156] however did not show improvement in cBN quality when compared to Si, and films mostly grow in a conventional sequence of aBN/tBN/cBN layered structures. It was observed that the cBN content in BN films reduces with decreasing the substrate micro-hardness [156]. For instead, the reported content of cubic phase in BN films grown on copper is the lowest among all investigated substrates though the lattice parameters of copper and cBN are close each other. However, for harder substrates like Si [157,158] and diamond [133], the cBN contents can substantially vary with altering the surface roughness. Pascallon *et al.* [133] found that the cBN content drastically reduced when RMS roughness of diamond increased from 16 to 200 nm. Geometric shadowing was thought to cause the cBN reduction. Similar effect was reported by Zhang *et al.* [134] who polished diamond substrate in order to obtain epitaxial relationship between cBN and diamond CVD substrate using their ion beam assisted deposition (IBAD) at ~900 °C. Planarized diamond substrates with an initial RMS roughness of ~1 nm were required to obtain cBN film void of interfacial graphitic layers. However, the reason for using the smooth diamond substrates was not reported. Barely very limited studies [133,157,158] referring to the effect of substrate surface roughness on the cBN nucleation and growth of cBN were conducted, and most of them are only based on infrared

spectroscopic data. In this chapter, systematic investigation of the surface roughness effect on the cBN nucleation on Si substrates as well as the seeding effects are reported. Diamond and alumina powders with different grit sizes were used to abrade the substrate and prepare surfaces with different roughness. The cBN data obtained by AFM, FTIR and TEM are mutually correlated.

9.2. Infrared spectral analysis of boron nitride grown on scratched silicon substrates

Early studies [109,123] report that for the cBN formation the nucleation threshold is at the ion energy of 125 eV and minimal substrate temperature of 150 °C. The subsequent growth can then be maintained at 75 eV and room temperature. This discrepancy between the nucleation and growth condition is probably related to the stability of cBN system at growth conditions and the dissimilarity in surface energy and lattice parameter playing crucial roles in cBN nucleation and growth. Roughening the device quality Si substrates with diamond powders enlarges the real surface area and introduces diamond seeds into the surface. This pretreatment then changes the surface condition and consequently nucleation is affected when compared to the pristine mirror-polished Si substrate.

Fig. 9-1 shows FTIR spectra of BN films prepared on Si surfaces with different surface roughness (RMS – 0.2, 10, 50 and 170 nm) and ion beam energies of 75, 125, 150 and 500 eV. The FTIR spectra are denoted with the RMS values of 10, 50 and 150 nm as induced by diamond powders with grit sizes of 0.25, 1.0, and 3.0 μm, respectively. Each set of spectra of given energy is referred to the spectra obtained from BN films prepared on pristine mirror-polished Si substrates. Obviously the cBN content, deduced from IR spectra, diminishes with the increase in surface roughness. The rougher surface, the smaller cBN and larger hBN contents are obtained and vice versa.

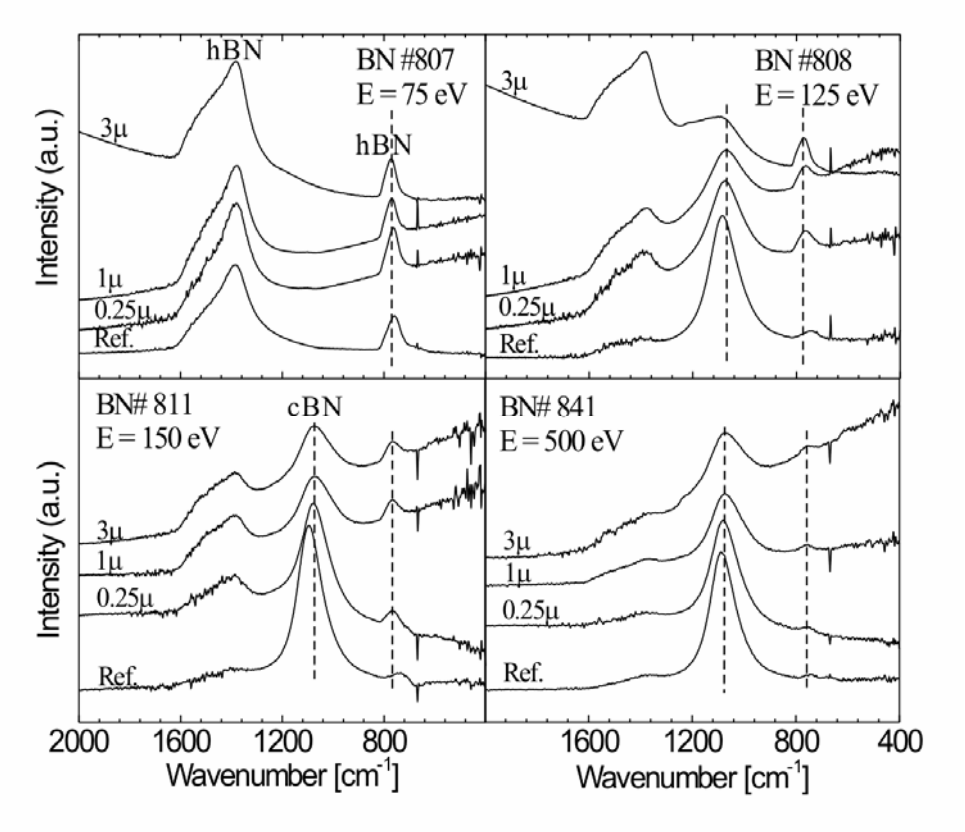

Fig. 9-1. FTIR spectra of BN films prepared on Si substrate with different surface roughness with reference to the films grown on device quality Si surfaces: (ref: 0.2 nm, induced 0.25 μm – 10 nm, 1μm – 50 nm and 3 m – 175 nm in RMS) at ion energies of 75, 125, 150 and 500 eV.

Hexagonal BN is an anisotropic material with characteristic in-plane stretching (1380 cm^{-1}) and out-of-plane bending (780 cm^{-1}) active vibration modes induced in IR absorption spectra. However, their interpretation in terms of the orientation and crystallinity of hBN has not been mastered yet. Shifting the out-of-plane bending, that designates hBN, towards the lower wavenumbers has been used to denote increasing the content of amorphous-like structure [159]. On the other hand the intensity ratio of in-plane stretching to out-of-plane bending ($\delta_{ip/op}$) was related to the orientation of hBN layers. This intensity ratio is at its minimum when hBN basal planes are perpendicular to substrate [160]. Likewise in our cBN films prepared by MSIBD, the out-of-plane bending of hBN

peak shifted towards the lower wavenumbers and simultaneously the aBN phase in the interfacial region expanded with decreasing the surface roughness. The earlier establishment of well aligned tBN, with a smaller value of $\delta_{ip/op}$ accelerates the cBN nucleation, reduces the interfacial tBN and thus increases the overall cBN content. On the contrary poorly aligned tBN with a larger value of $\delta_{ip/op}$ delays the cBN nucleation or prolongs incubation time.

When cBN is formed, the cBN reststrahlen band at ~1094 cm^{-1} shifts towards the higher wavenumbers with decreasing the surface roughness. This blue-shift of the cBN reststrahlen band is normally associated with the accumulation of compressive film. In other words, cBN films grown on rougher substrates tend to have lower internal stress under the same deposition conditions and exhibit smaller blue-shift. The abstracted cBN volume fractions *vs*. the substrate surface roughness at different ion energies, in Fig. 9-2, indicate that at ion energy of 500 eV, the effect of surface roughness on the cBN content is only moderate.

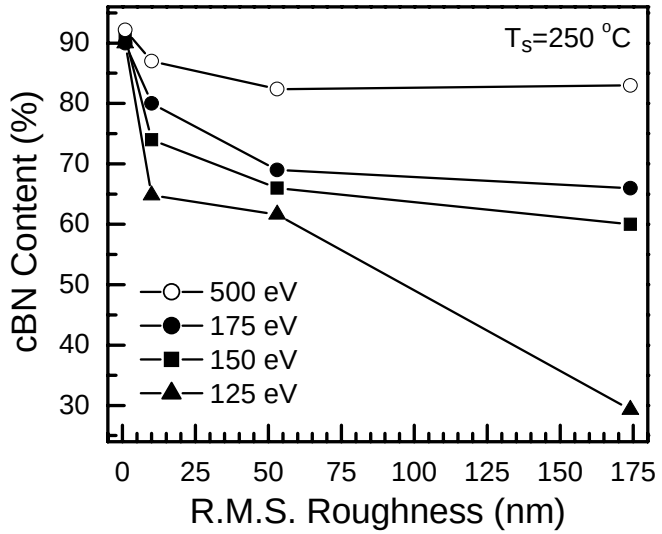

Fig. 9-2. Plots showing the effect of surface roughness on the cBN volume fraction at different ion energies.

9.3. Morphological study of boron nitride films grown on scratched silicon surfaces

Further insight to the structural evolution gives studying the surface morphologies upon the substrate surface roughness and ion energy as illustrated by AFM images in Figs. 9-3 and 9-4. At 75 eV, hBN with granular morphology is obtained. Since the ion ranges in hBN at 75 eV are very shallow (~0.8 nm both for B^+ and N^+ at normal incidence), the BN growth is rather a surface process. The subplanted B and N species in shallower depth then may diffuse to the surface of the growing structure with greater probability and may participate in the formation of a granular microstructure, more likely hBN. The increase in ion energy leads to diminishing the granular structure and the surface becomes featureless at 150 eV and above. This difference arises from the ions subplanted into deeper regions at high ion energies (>150 eV) and their thermal motion which is rather restricted to the interaction volume. The subplanted particles in deeper regions have smaller probability of diffusion to the surface. The higher ion energy also induces more displaced atoms, which is counterproductive in evolution of larger grain sizes. Therefore, BN films somewhat conform their morphology to the substrate. Alike smooth device quality Si substrates, the roughened substrates (Fig. 9-4) show similar course in evolution of granular structures upon the ion energy but with the threshold shifted towards the higher ion energy. Hence rough surface is more favorable to the growth of BN with hexagonal phase and may prolong the cBN incubation time.

Shifting the nucleation thresholds towards the higher ion energy for rougher surfaces is more likely caused by surface geometrical effects. The real area of a rough surface is larger than geometrical. The surface confines many micro-surface environments altering the surface migration and diffusion of particle and even surface energy. These parameters are likely responsible for the dissimilarity in BN topographic structure and threshold for the grain formation. They are associated with ion energies because mobility and thus migration of surface particles also depends on the ion impact energy in addition to thermal

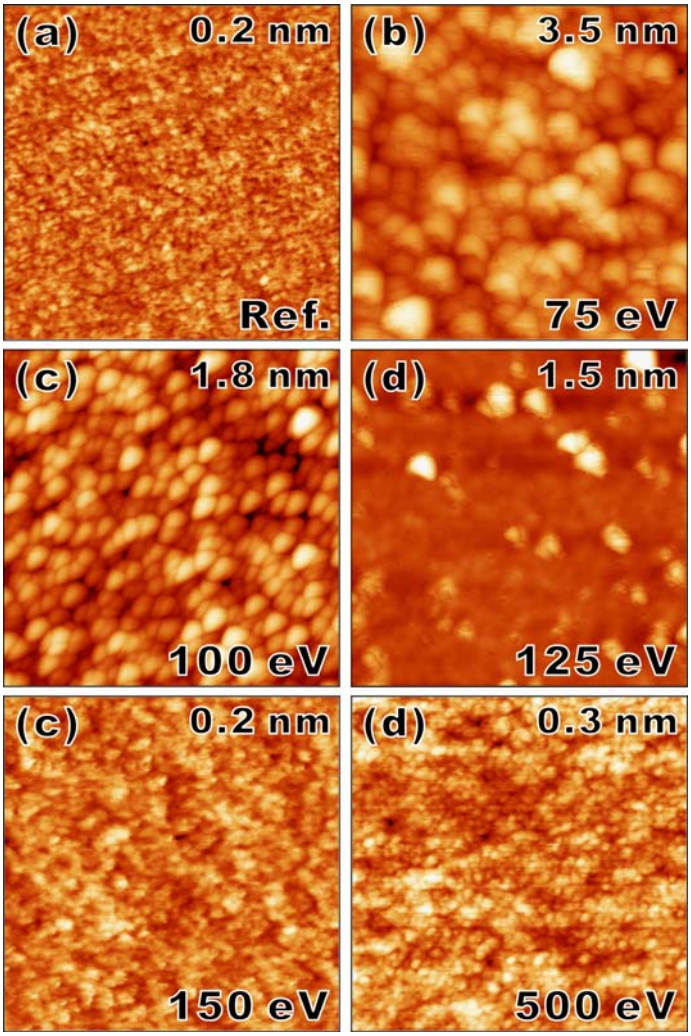

Fig. 9-3. AFM topographical images showing the micro-structural evolution of BN films prepared on mirror-polished Si at different ion energies. The corresponding RMS roughness is shown in each image.

particle energy. Geometrical shadowing was reported to be the cause of the "grain threshold phenomenon" at using IBAD technique [133] with ion beam incident angles of 30-45°. Since our ion beam is paraxial and impinges the geometrical surface at the normal angle, the shadowing effect is implausible. However, taking into account of surface submicro-relief, the ion beam impact angle varies with localized surface features. The localized submicro-relief features are then primarily responsible for areal altering the sticking coefficient and self-sputtering which might also be linked to the evolution of grain structures at different thresholds of ion energy in accord with the surface roughness.

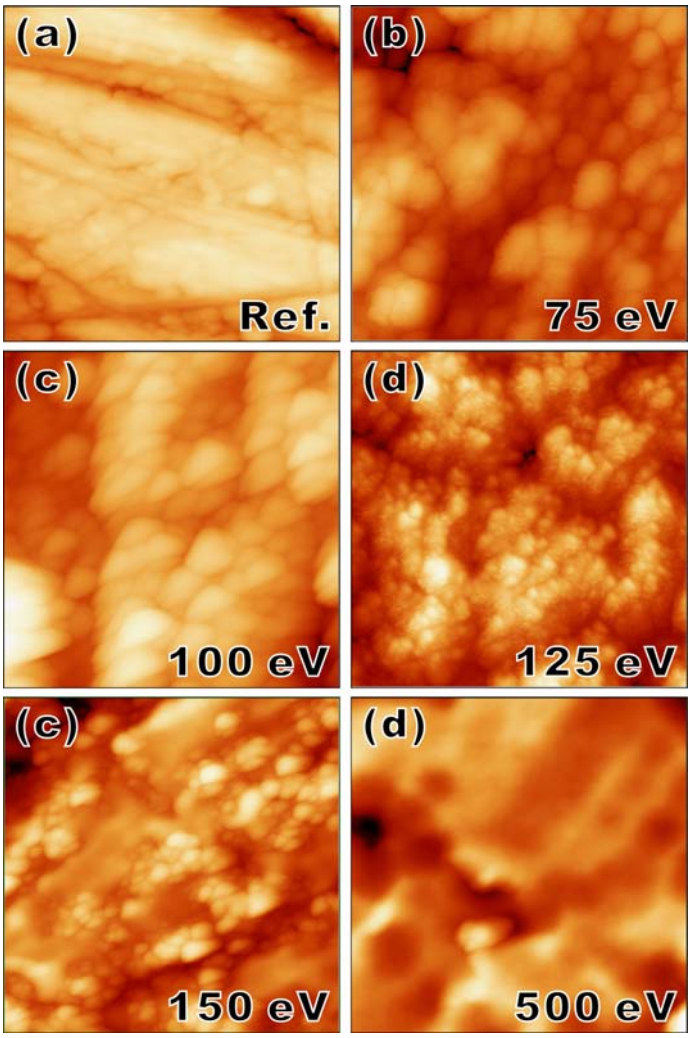

Fig. 9-4. AFM topographical images illustrating the micro-structural evolution of BN films prepared on Si substrate with RMS roughness of 10 nm at different ion energies.

9.4. Microstructural investigation of boron nitride on scratched silicon surfaces

TEM analysis gives further insight into the reasons of discrepancy in BN formation on the substrates with different roughness. One of the examples is in Fig. 9-5, which shows a low magnification bright field TEM image collected from BN films grown on a silicon substrate with RMS of 50 nm and at energy of 500 eV. The BN film is relatively thicker in the region of valleys, which is due to redeposition of sputtered BN

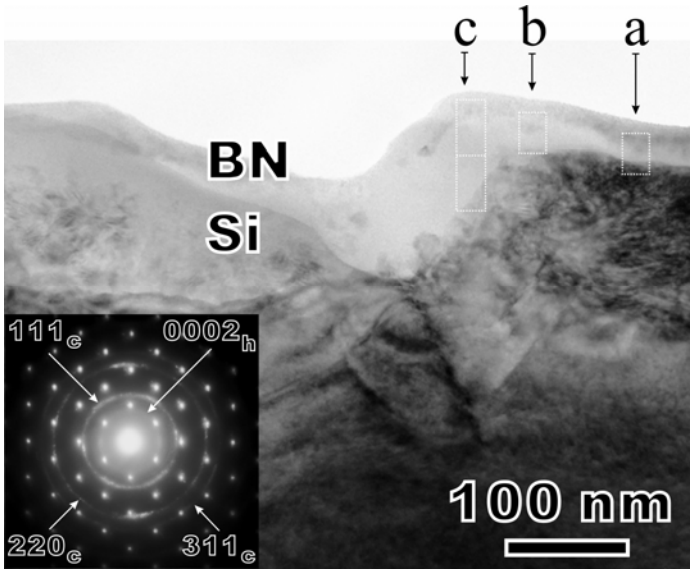

Fig. 9-5. Low magnification bright-field TEM image revealing a BN film prepared on Si surface with RMS roughness of 50 nm at an ion beam energy of 500 eV. The inset is the corresponding selective area diffraction pattern.

material. A similar observation is reported for BN deposition on a rough AlN surface [129]. For a flat film, B and N ions are incident perpendicular to the surface and at 500 eV the total sputter yield is about 0.5-0.6. The situation is different for a locally inclined microsurface. Since the ions are continuously decelerated when approaching the film surface, they are deflected from an inclined microsurface. For a groove-type microstructure the ions are therefore deposited at the opposite inclined microsurface with nearly perpendicular angle of incidence. Compared to a flat surface, the local sputtering yield is therefore not significantly increased. According to TRIM [161] the angular distribution of sputtered atoms is symmetric with respect to the surface normal and is not correlated to the ion angle of incidence. Therefore, material sputtered from this region is partially redeposited inside the groove, and thus reducing the effective sputtering yield significantly. Due to the low energies of resputtered particles on the order of electron-volts a hexagonal BN phase emerges within the groove. As consequence, the BN growth rate inside the groove is increased and ultimately the originally rough surface is planarized. The cBN nucleation then takes place by usual way on a textured tBN layer.

The logical solution to promote or enhance the cBN phase on an initially rough surface is to further increase the average energy of particles participating on the BN formation in the valleys and that is only possible with the increase of ion beam energy.

Detail analysis of the SAD pattern taken from the same sample (RMS = 50 nm; 500 eV), in Fig. 9-5 as inset, shows the most inner continuous electron diffraction pattern with interplanar spacing of 0.315 nm corresponding to the diffraction from the tBN (0002) basal planes. The continuity of this ring suggests the structure with (0002) basal planes rather randomly oriented. It can easily be demonstrated that oriented tBN on rough surfaces can evolve but its thickness has to expand and serve as cBN nucleation sites. The cBN incubation time then is prolonged correspondingly. The tBN (0002) ring then may reveal angular increase in intensity or intensive elongated diffraction spots or discontinuous diffraction features indicating preferential tBN orientations. The remaining rings in the SAD pattern originate in electron diffraction from (111), (220) and (331) cBN planes whereas the array of diffraction spots comes from the Si substrate. In further extent, three representative high-resolution TEM images are presented in Fig.9-6. They are collected from the sample regions denoted a, b, and c as illustrated in Fig. 9-5. All the regions are characteristic with tBN (0002) planes that tend to be perpendicular to the substrate in vicinity of the tBN–cBN transition region. This phenomenological observation illustrates the importance of oriented (0002) tBN planes to serve as cBN nucleation sites [118]. In the flat regions, as seen in (Fig. 9-6a), the tBN nucleates instantly on the Si substrate with a minute amount of amorphous BN material. The amorphous layer however increases with the slope towards the valley as observed in Fig. 9-6b, while the valley region in its topper parts, in Fig. 9-6c-I, confines a smaller cBN crystallite randomly oriented. Below the cBN crystallite–tBN region there is an extensive aBN layer as Fig. 9-6c-II exemplifies. The presence of the these phases in the described location and their extent then explain the broadening of the peaks in the FTIR spectra acquired from the cBN films grown on rough substrate surfaces.

Similar results were obtained also on Si substrates polished by alumina powders.

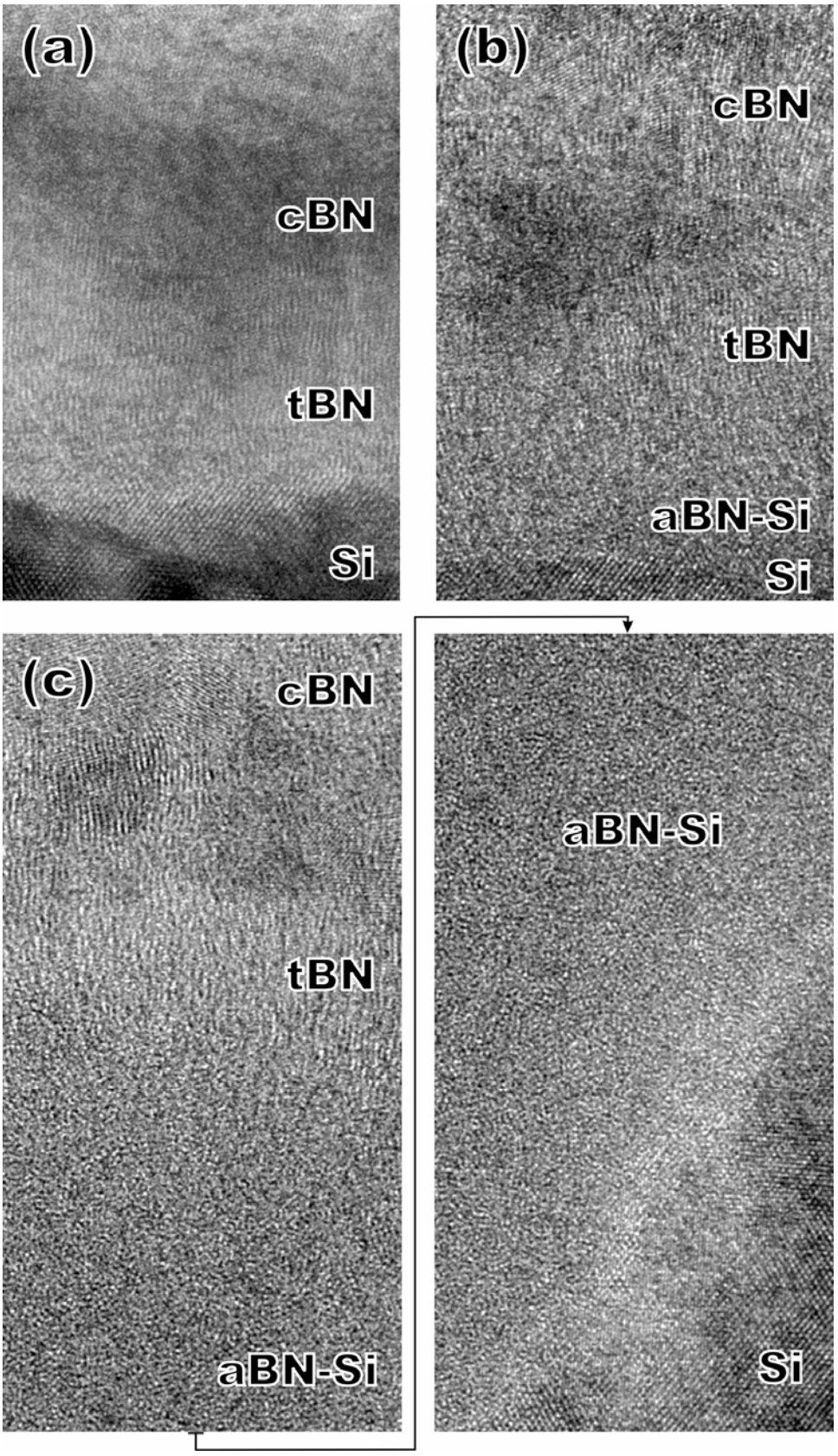

Fig. 9-6. High resolution TEM images collected from the sample regions denoted a, b, and c in Fig. 9-5.

This suggests that the diamond seeding does not have notable effect on the cBN nucleation at the given conditions. The embedded diamond seeds, like the silicon, are amorphized when subjected to ion bombardment at low substrate temperature (250 °C) [129] and fast etched off during the early stage of ion beam exposure. The lattice information cannot thus be replicated to the growing cBN and therefore the surface roughness of substrate is more important in this case. Better evaluation of seeding effects requires temperatures in the neighborhood of 900 °C. Such high temperature might produce false counting of ion charges due to thermionic emission particularly in our MSIBD where the stoichiometry (B:N = 1:1) of cBN films is ensured by current integration in each ion beam cycle.

9.5. X-ray absorption near edge spectroscopic analysis of boron nitride films synthesized on scratched silicon substrates

Prior to detail XANES studies, cBN samples deposited on Si surfaces with different surface roughness (RMS=0.2, 10, 50 and 175 nm) at 150 eV and commercial HPHT (high pressure high temperature) cBN powder were studied by XRD. The obtained XRD spectra (Fig. 9-7) reveal a broadened cBN 111 peak and their position shifts to a higher 2θ value when compared to the cBN powder. For those scratched samples, the cBN 111 peaks are located at almost the same position indicating that they undergo the same lattice contraction of 3.3%, while the sample A_1 with the untreated substrate exhibits larger lattice contraction of 5.3%. In accord with the IR absorption spectroscopic analysis the sample A_1 (1094 cm^{-1}) displays the largest blue-shift of the cBN restrahlen band as compared to those of the scratched samples (1076 cm^{-1}). The larger the blue shift, the greater the inherent compressive stress built inside the film. This will lead to a greater lattice contraction of cBN film. The broadening of the diffraction peaks is associated with smaller grain size and poor crystallinity of cBN crystallites. This is consistent with the TEM results, in which the cBN films synthesized by PVD assisted with energetic species are composed of cBN nanocrystallites. The

anisotropic

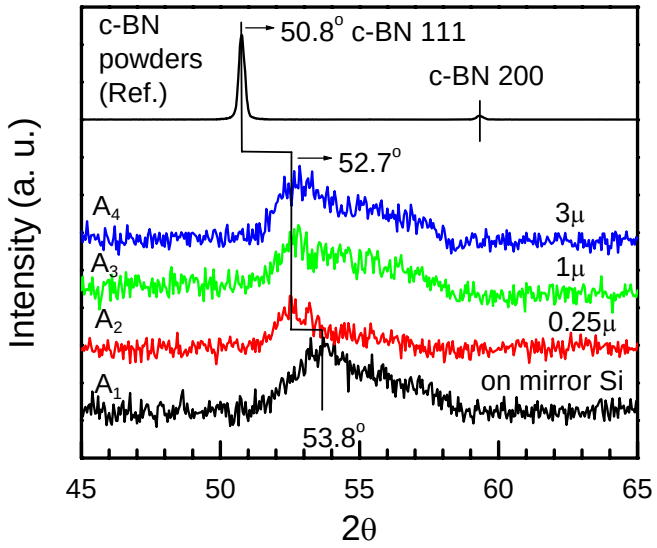

Fig. 9-7. XRD spectra of sample A_1, A_2, A_3, and A_4 prepared by MSIBD at 150 eV. (Rigaku, Co K_α radiation, λ= 0.1792 nm)

broadening of the diffraction peak is probably due to the overlap of some unknown small features at larger 2θ side of the main cBN 111 diffraction peak.

The boron (B) K-edge XANES of the cBN films deposited onto Si substrates with different surface roughness (RMS=0.2, 10, 50 and 175 nm) at 150 eV and commercial cBN and hBN powders recorded in both TEY and FY when the incident X-ray is normal to the sample surface are given in Figs. 9-8a and 9-8b, respectively. A strong and narrow peak at 192 eV (peak 1) corresponds to the excitation of the 1s core-level electron to π^* unoccupied states of sp^2-bonded hBN phase. That peak is characteristic to the commercial hBN powder sample, while it is not present in the spectrum acquired from the commercial cBN powder sample because π^* states are absent in the cBN electronic structure. Besides peak 1, the peaks at 198.1 eV (peak 4), 199.5 eV (peak 5), 204.4 eV (peak 6) and 215.4 eV (peak 8) corresponding to the excitation of the core-level electron to σ^* states of sp^2-boned hBN appear in electronic structure of the commercial hBN powder sample, while the peaks at 194.6 eV (peak 2), 197.7 eV (peak 3) and 214.8 eV

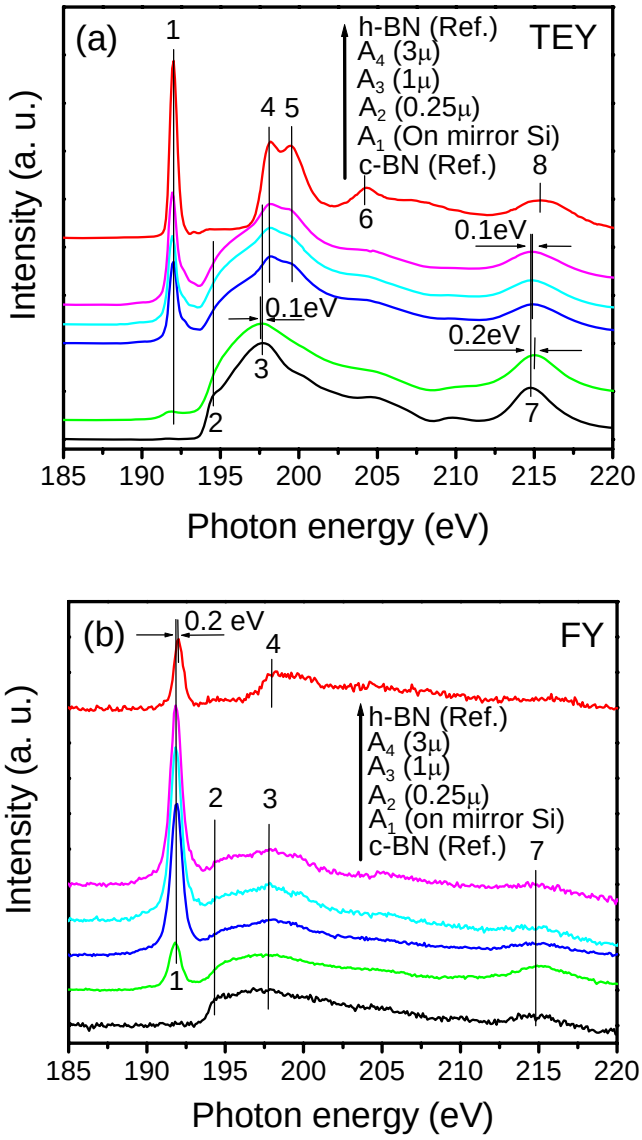

Fig. 9-8. Normal incidence B K-edge XANES recorded in TEY (a) and FY (b) of the thin film sample A_1-A_4 and commercial cBN and hBN powder samples.

(peak 7) related to the excitation of the core-level electron to σ^* states of sp^3-bonded cBN phase appear in the electronic structure of the commercial cBN powder sample. From the XANES in TEY shown in Fig. 9-8a, peak 1, 2, 3 and 7 appear for all four thin film samples, whereas two small features at the position of peaks 4 and 5 appear for three thin film samples with scratched substrate (sample A_2-A_4). This means that all the four thin film samples in the surface region consist of both the sp^3-bonded cBN phase

and the sp^2-bonded hBN phase. The coexistence of hBN peak (peak 1) and cBN peak (peak 2, 3 and 7) in the XANES in FY shown in Fig. 9-8b also confirms that all the four thin film samples are mixtures of cBN and hBN. It is apparent that the intensity of peak 1 in both TEY (Fig. 9-8a) and FY (Fig. 9-8b) of sample A (relative to edge jump), the untreated substrate with a mirror-polished surface, is much weaker than in the other three. In addition, the relative intensities of the sp^2-bonded hBN peak at 192 eV recorded in FY (Fig. 9-8b) of all the four samples is much stronger than those recorded in TEY (Fig. 9-8a). This analysis demonstrates that the ratio of cBN to hBN phase in upper parts of the films is significantly higher than the average of the entire films as TEY is a surface sensitive technique (~5 nm for boron K-edge Anger electrons), while FY is more bulk sensitive (~ hundreds of nm for boron in attenuation length of fluorescent X-ray). This result is consistent with the TEM observations revealing a layer of sp^2-bonded aBN/tBN at the interface between Si substrate and the top cBN films synthesized using PVD assisted by energetic species [69,71]. Therefore, sample A_1 contains less hBN phase at both the film growth surface and film-substrate interface. In other words, the rougher substrate results in higher hBN quantity and impedes the formation of cBN films. Close observation of the XANES in TEY (Fig. 9-8a) reveals that the B K-absorption edge (threshold E_o) of cBN for all the four thin film samples remains the same as that of the reference cBN powder sample (cBN particles size: 4-8 μm). This means that the bottom of the cBN conduction band does not shift and no quantum effect on the optical gap is observed [162]. However, the sample with a smoother substrate (sample A_1) exhibits a 0.1 eV red shift for peak 3 and 0.2 eV blue shift for peak 7, while the samples with scratched substrate (sample A_2-A_4) exhibit a 0.1 eV blue shift for peak 7 in respect to the commercial cBN powder sample. It is hard to determine the position of the peak 3 of sample A_2-A_4 due to overlaying the peak 3 of cBN phase and the peak 4 of hBN phase as larger hBN amount exists at the film surface, when referred to sample A_1. From the XANES in FY (Fig. 9-8b), all four thin film samples exhibit a 0.2 eV red shift for peak 1, relative to commercial microcrystalline hBN powder sample, while the peak 1 in Fig. 9-8a of all the four thin film samples is located at almost the same position as the hBN powder sample. The

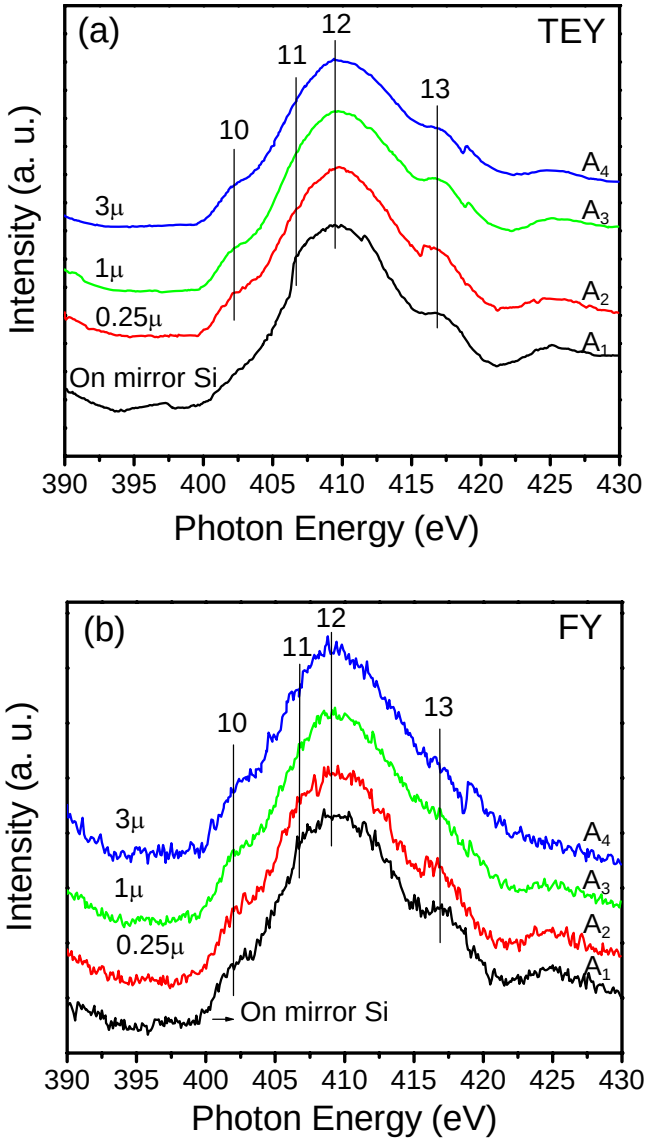

Fig. 9-9. Normal incidence N K-edge XANES recorded in TEY (a) and FY (b) of the thin film sample A_1-A_4.

peak shifts imply a change of energy band structure of the cBN and hBN phases in the thin films, compared with the microcrystalline cBN and hBN. TEY (Fig. 9-9a) and FY (Fig. 9-9b) of the nitrogen (N) K-edge with incident X-ray normal to the sample surface also shows the typical cBN XANES spectra though the differences in resonance features due to the disparity in sp^3 and sp^2 bonding are not so distinct as in B K- edge spectra since some broad σ^* features centered at 406 eV (peak 11), 409 eV (peak 12) and 417 eV (peak 13) always overlap each other [163]. A small shoulder located at 402 eV (peak

10) referring to π^* resonance can be observed from the TEY of samples A_2-A_4 and FY of all four samples. This feature is expected to be significantly weaker than that observed at the B K-edge in sp^2-bonding and negligible in sp^3-bonding, since N is more electronegative than B, the unoccupied densities of states of π^* character are concentrated at the B site. The N K-edge XANES confirms the results obtained from the B K-edge in that all the films are a mixture of cBN and hBN and the ratio of hBN to cBN in the films increases with substrate roughness.

The intensity I (π^*) of peak 1 in TEY for sample A_1 (Fig. 9-10a) increases with decreasing the angle of incidence (α, $\alpha = 90°$ for normal incidence) and can be fitted according to Eq. 9.1, while for sample A_2-A_4 (Figs. 9-10b, 9-10c and 9-10d), it decreases with decreasing α and can be fitted to Eq. 9.2

$$I(\pi^*) = I_{order}\cos^2(\alpha) + I_{disorder} \quad (9.1)$$

$$I(\pi^*) = I_{order}\sin^2(\alpha) + I_{disorder} \quad (9.2)$$

When the probing angle changes from 90 to 20°, the intensity change of peak 1 relatively to the σ* in all the samples is not obvious as compared to the results reported by Rosenberg *et al.* [164]. This may be attributed to two orientation possibilities of the sp^2-bonded BN found near film growth surface. Firstly, supposed the majority is the short-range graphitic BN with a small amount of amorphous BN, some of the graphitic BN is aligned with its basal plane along a certain direction and the other is randomly aligned. If the ratio of the randomly aligned graphitic BN is large, the intensity of peak 1 relative to σ* just changes slightly. Secondly, if the majority is amorphous BN with a small amount of short-range ordered graphitic BN, regardless the plane alignment the relative intensity ratio is dominated by the signal from amorphous BN. The hBN basal planes at the top film surface as a whole have a greater tendency to align in the parallel direction to the film surface for sample A_1 (the spectrum is predominantly cBN likestructure), but preferably in the normal direction to the film surface for samples A_2-A_4 [165]. From samples A_2-A_4, we also observe additional features (peaks 9 in Fig. 9-10, appearing as shoulders of the peaks 1) being attributable to the excitation of the

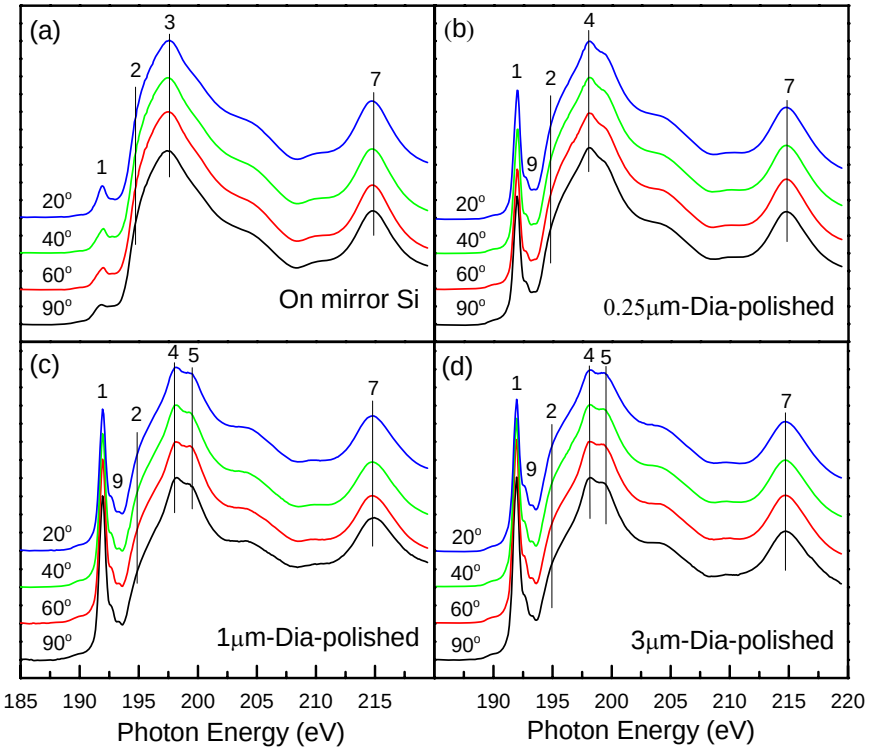

Fig. 9-10. Angular dependence of the B K-edge XANES recorded in TEY of samples A_1 (a), A_2 (b), A_3 (c) and A_4 (d).

core-level electron defect (nitrogen vacancies near boron atoms) energy levels [166]. However, these small features are not noticeable in the FY (Fig. 9-10), indicating that the defect density in the depth of the films is much lower than that of the near film surface. This observation indicates that defects were initially produced near the film surface and then diminished during the further direct bombardment by energetic ions once cBN was formed.

9.6. Nucleation and growth mechanism induced by surface roughness

The energy of ions is one of the key parameters for the formation of cBN films. If the energy of ions is lower than the critical value (energy threshold), only sp^2-BN can be obtained [71,123]. The energy threshold for the nucleation is generally higher than that for the growth of cBN. However, the energy threshold is also affected by the substrate

materials and the deposition technique used. Experimentally, the energy threshold for nucleation and growth was found, on mirror-polished Si substrates using MSIBD [109,123], to be 125 and 75 eV, respectively. Here, we schematically illustrate, in Fig. 9-11a, the effect of the surface roughness on the cBN content at given ion energy. For the ion energy E_1 (150 eV) which is only somewhat higher than the threshold, E_0 (125 eV) and the cBN nucleation on a mirror-polished Si by MSIBD, we can expect that cBN films with very low sp^2-bonded BN phase could be prepared (Fig. 9-8a) as the electrical field near the substrate surface is uniform and the energy distribution of the energetic ions arriving the substrate is narrow, as shown in Fig. 9-11a. For a rough substrate (sample A_4), the distribution of ion energy near the substrate surface is broadened (plot b in Fig. 9-11) and some of the ions have their energies lower than the nucleation threshold (Area 1). As a result, the sp^2-BN content increases in the film. When the ion energy E_2 (500 eV) is significantly higher than the nucleation threshold, nearly all ions have the energy higher than the threshold E_0 even when the ion energy distribution is broadened by the rough substrate surface (plot c in Fig. 9-11).

Therefore, the hBN content should be lower for the sample prepared at higher ion energy if the roughness of the substrate is the same. Experimentally it is found in XANES measurements, as shown in Fig. 9-8, that the hBN content in the BN sample prepared on mirror-polished Si (sample A_1) is lower than that on scratched Si (sample A_4) when they are deposited at the same ion energy (150 eV), and the hBN content in the sample grown at higher ion energy (500 eV, sample A_5) is lower than that deposited at lower ion energy (150 eV, sample A_4) when they are deposited on the substrates with the same surface roughness (Fig. 9-12). Moreover, the hBN phase in sample A_5, is a little higher than that in sample A_1, which may be due to the re-deposition of the species sputtered from the deposited materials of the rough growing surface as discussed above.

The results on the sp^2-BN content in the cBN films deposited by MS (magnetron sputtering) on diamond films with dissimilar thickness giving different surface roughness also support this conclusion. The AFM analyses indicate that the cBN film

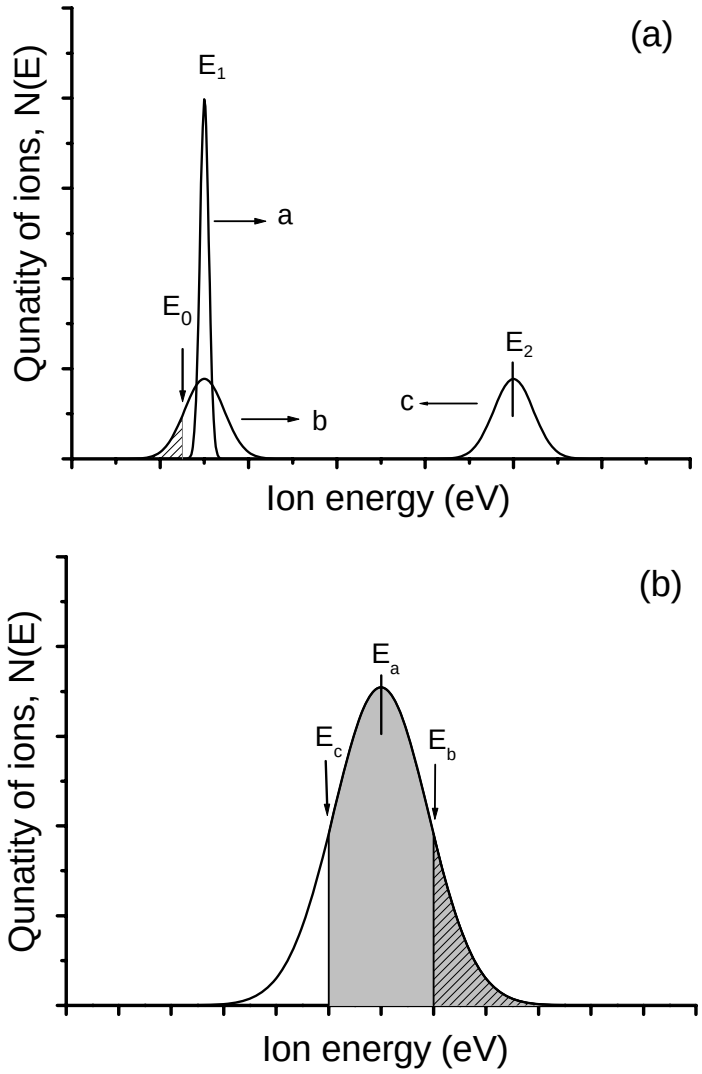

Fig. 9-11. Schematic of the distribution of ions bombarding the mirror-polished and diamond-scratched Si (a) and the energy threshold for the formation of cBN on Si and diamond-coated Si substrate.

surface on the thicker diamond film is much rougher than that on the thinner one (Table 5-4), and the sp^2-BN content in the sample deposited on thicker diamond film is higher both at the surface and over the whole volume of the film. Apart from this, the re-deposition of species sputtered from the deposited materials by the incident energetic ions bombarded on the inclined micro-surfaces of the rough substrate should be another concern. Since the energy of the species sputtered is far less than the incident energetic

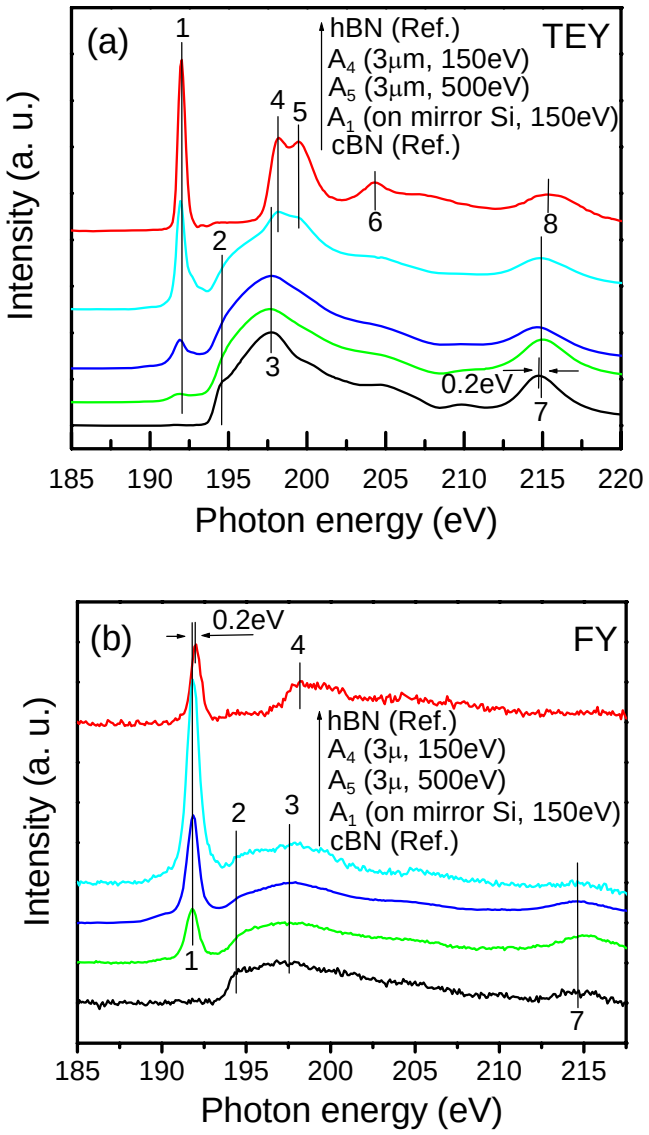

Fig. 9.12. Normal incidence B K-edge XANES recorded in TEY (a) and FY (b) of the thin film samples (A_1, A_4 and $A_{5)}$ prepared by MSIBD technique and reference cBN and hBN samples.

species, the hBN content in the film will increase. Here we extend the above discussion further to the MS technique. The energy distribution of ion in MS system is generally much broader than that in MSIBD system, and the maximum of the distribution is normally at about several tens of eV, as E_a in Fig. 9-11b shows, which is decided by the experimental parameters such as substrate bias and working pressure *etc*. Tsuda *et al* reported that in the case of RF plasmas, ions bombarding the substrate present a wide

energy distribution and the ion energy can spread over a range of some tens of eV [167]. From the measurements and discussion above, we can assume that E_a is smaller than the threshold E_b for the cBN nucleation on Si, but larger than the threshold E_c maintaining the cBN growth. As a result, cBN can be nucleated on Si (sample B_1) but the sp^2-BN content is high because only a small ion fraction exceeds the threshold energy E_b (Area 2 in Fig. 9-11b). In the case of deposition on the diamond-coated substrates (sample B_2 and B_3), the nucleation of cBN is no longer needed and the growth starts directly without precursor layers [134]. Most of the ions has the energy higher than the growth threshold (E_c) which leads to remarkable reduction of sp^2-BN content.

The growth mechanism of cBN film by plasma enhanced CVD (PECVD) substantially differs from the mechanism characteristic for PVD. In the PECVD, cBN is formed from the activated gas phase and surface reactions meditated by reactive additives like, fluorine. The highly reactive species formed allows lowering the nucleation and growth thresholds. Eventually, the deposited sp^2-BN phase content is lowered or removed *via* enhanced etching reactions. These reactions combine both physical and chemical etching effects leading to greater etching selectivity. Thus, mediating fluorine environment plays important role in preferential removing hBN phase, formation of cBN abundant structure and stabilization cBN phase. Hence the discrepancy in hBN phase distribution observed in the samples prepared by PECVD (samples C_1 and C_2) and the sample grown by PVD techniques could be understood. The sp^2-BN content at the film surface is higher than the average value in the depth of the film grown on Si substrates (sample C_1). This is certainly evidence that most of the sp^2-BN phase formed at the growing surface is etched off during the consequent growth process. In PECVD the cBN deposition is carried out *via* the surface chemical reactions which diminish broadening the distribution of the ion energy caused by the increased surface roughness and does not increase the sp^2-BN content in the films. Moreover, the samples are deposited at a considerably lower bias voltage which reduces ion energy well below the value of BN atomic displacement energy. As a result the re-deposition of

sputtered species is likely not probable. A minute amount of sp^2-BN phase detected across the film thickness of the sample deposited on diamond (sample C_2) further confirms the previous TEM observations that cBN nucleates directly on diamond without sp^2-BN precursor interlayers (discussed in Chapter 7).

A model for nanodiamond growth induced by prolonged bias-enhanced nucleation (BEN) and growth was proposed. The model elucidates diamond nucleation on both diamond particles and amorphous carbon phase, and the competition between the diamond re-nucleation and growth determines the diamond grain size. We also believe that cBN nucleates on both cBN particles and sp^2-bonded hBN. However, only the tBN with its basal plane normal or nearly normal to the film surface is generally believed to be the preferable cBN nucleation site [71,118]. For sample A_1 (150 eV, mirror-polished), cBN crystallites are continuously formed in subsurface regions dominated by secondary nucleation process. This process might be the reason of comparatively smaller amount of sp^2-bonded BN phase present on the growth surface. The sp^2-bonded BN coverage, as evidenced from XANES, mainly comprises amorphous sp^2-bonded BN with trace amount of poorly crystallized hBN having their basal planes parallel to the growing surface. However, this orientation does not represent the preferable cBN nucleation sites. It is believed that the cBN growth is dominated by the re-nucleation on cBN crystallites in this case. The growth rate of cBN particles and their re-nucleation rate during the MSIBD process determine the cBN grain size and the film morphology. Thus, the cBN film grown on a mirror-polished Si substrate is very smooth (Fig. 9-3c). The samples denoted A_2, A_3 and A_4 represent cBN grown on surfaces with RMS roughness of 10, 50 and 175 nm, respectively. Cubic BN should mainly nucleate on top of oriented hBN particularly when basal planes are nearly parallel to the surface normal because this orientation is present in the samples and is favorable for cBN nucleation and growth. Therefore, the size of cBN crystallites in the films on scratched Si substrate is determined by the growth rate of cBN crystallite, nucleation rate of cBN on top of sp^2-bonded hBN and the growth rate of sp^2-bonded hBN. Thus, the cBN crystallites are dispersed among the sp^2-bonded hBN as they grow.

This prevents them from their further growth. Larger particles (Figs. 9-6d, and 9-6e) with a structure of an sp^2-bonded hBN matrix containing a large amount of cBN nanocrystallites of ~ nm grain size are buried in this matrix on the scratched Si substrate during the MSIBD process, which is similar to the structure of nanodiamond film prepared by prolonged BEN process [168]. In fact, each particle observed from AFM images contains a large amount of cBN nanocrystallites. It is reasonable to believe that the difference of grain size, morphology and stress results from the nucleation and growth environment during the MSIBD process.

Small grain size on the order of nanometers certainly affect the cBN properties including quantum and surface size effects. The shifts of the cBN XANES resonance shown in Fig. 9-8a indicate the modification in distribution of the density of states in conduction band though no broadering of optical bandgap is not suggested by XANES analysis when the cBN grain size changes. Raty *et al*. [169] reported that the increase of optical bandgap of the structure made of diamond nanoparticles cannot be observed until the grains are reduced to at least 2 nm. Since diamond and cBN resemble each other in their structures and properties the speculative conclusions on grain sizes and properties could be applicable to both the material systems. In this particular case, the cBN crystallites (5-10 nm) are still too large to winder the optical bandgap as expected from quantum phenomenon.

The main reason inducing the XANES peak shift is the large stress built in the films during cBN growth. Compared to the commercial microcrystalline cBN powder, the film samples display larger lattice contraction (the sample A_1 exhibits 5.3% while the samples A_2-A_4 show 3.3% contraction) due to the larger compressive stress which affects the electronic energy band. The shift of hBN XANES peak shown in Fig. 9-8b demonstrates that the change of electronic structure of hBN phase in the depth of the films (underlayer) or at the film-substrate interface is remarkable, while that at the film surface this shift is not noticeable (Fig. 9-8a), relative to the microcrystalline hBN powder sample. This is probably because the compressive stress acting on hBN in the

film depth is much larger than that on the topmost hBN.

9.7. Summary to the surface roughness affecting cBN quality

Substrate surface roughness considerably affects the cBN nucleation. The rougher surface contributes to the random orientation of tBN (0002) basal planes, prolongs the cBN incubation time, and expands amorphous and tBN interfacial layers. The tBN (0002) basal planes serve as cBN nucleation sites. The thickness of BN films varies with local features and is thicker in surface valleys of the roughed surface due to sputtering on inclined micro-surface and recoiled ions hammering BN species into the valleys being planarized in this process. Therefore rougher surfaces shift the cBN nucleation threshold towards the higher ion energies as evident from FTIR and XANES analyses. The large transition non-cubic region at the rough substrate can be reduced by the increase of ion beam energy. Hence, the surface roughness has to be considered as one of nucleation and growth parameters.

Chapter 10. Mechanical characterization of cubic boron nitride films

While previous chapters are focused on fundamental understanding of the parameters affecting the cBN nucleation and growth, this chapter describes the evaluation of the mechanical properties of high quality thick cBN films. The cBN films were prepared by DC jet chemical vapor deposition employing fluorine chemistry. The mechanical properties were investigated particularly by nanoindentation measurements in both cross-sectional and plan-view directions in conjunction with the SEM, TEM and micro-Raman scattering characterization. Such experimental designs enabled to explore the effects of the crystallinity and crystal size/grain boundaries on mechanical properties. The cBN films were also smoothed with fine diamond powders to rule out the error caused by the high surface roughness of the as-deposited samples.

10.1. Accounting problems at mechanical applications

Cubic BN is the second hardest material next to diamond, but its chemical inertness particularly with respect to ferrous materials at high temperature, resistance against oxidation and thermal stability make it superior to diamond and very desirable material in mechanical applications. Performance of many mechanical components in tribology or tools can be improved by coating their coating by cBN films, but the film thickness is important prerequisite in these applications. For example, the film thickness in cutting tools applications should be from 1 to 4 micrometers. However, cBN films commonly prepared by PVD have been too thin and poorly adherent to the substrates. The cBN films thickness was limited to hundreds of nanometers due to the high internal stress induced by ion bombardment during the film growth. The restricted film thickness and poor adhesion of cBN films also made the mechanical characterization, including the hardness measurement, complex and very challenging.

Hardness of bulk materials is routinely measured by several techniques, all established on the measurement of the imprint of an indent probe. Vickers and Knoop indentation were previously adopted to measure the micro-hardness of cBN films [170]. The loads in the range from tens to hundreds milli-netwons (mN) were used for measurements. However, the indent depth was comparable to or even larger than the film thickness. Such deep indents cause the large errors in hardness measurement due to substrate effect. In addition, the static micro-indentation technique applied in the Vickers and Knoop hardness measurements only involved the assessment of residual imprint, which also led to the difficulties in obtaining reliable hardness of cBN films of high elasticity.

Nanoindentation technique with capacity of controlling the loadings as small as tens of micro-newtons (μN), was also used to measure the hardness and elastic modulus of cBN films prepared by CVD and PVD techniques [171,172]. Even such small loadings induced, the indent depth being still comparable to the film thickness for most of PVD films thinner than 200 nm. Mirkarimi et al. [172] deposited 700 nm thick cBN films by a two-step PVD process (reducing the substrate bias after cBN nucleation and performing the growth at a high substrate temperature), and employed nanoindentation measurements using indent depths of ~100 nm. They measured a hardness of about 60–70 GPa and also demonstrated that the substrate effects could become substantial for indention deeper than 12% of the film thickness. Since these films were prepared by sputtering of a B_4C target, the film contained 5% (atomic) of carbon. Therefore, their hardness was probably affected by B–N–C bonded composite and graphitic inclusions.

10.2. Nanoindentation measurement performed on cubic boron nitride films

The deposition of cBN films was performed in a DC plasma jet CVD reactor by using a gas mixture of $Ar–N_2–BF_3–H_2$. Pre-scratched Si wafers of (100) orientation were used as substrates. The deposition process was divided into two steps. In the first step,

cBN films were deposited under a high substrate bias voltage (–85 V) and a low substrate temperature (1000–1040 °C). In the second step, the substrate bias was decreased to –70 V, and the substrate temperature was increased to 1150 °C. The reactant pressure was maintained at 50 Torr, and the total deposition time was 1 hour. The experimental setup and other experimental details are described elsewhere [112,173]. The cBN films prepared by this two-step process were 5 μm thick with confined crystallites of a large size as evidenced by TEM and Raman analysis [173]. To prepare the samples for nanoindentation measurements in the cross-sectional direction, we cut the cBN films into small rectangles, glued the film faces with other Si pieces of the same size, and then mechanically smoothed both top and bottom cross-sectional sides using fine diamond lapping paper with an average crystallite size of 100 nm. The smoothed sample thickness was about 1 mm. A series of indentations was made across the Si substrate *via* cBN film and adhesive in sequence. Indentation lines with an azimuthal angle of 18° to the film-substrate interface were used to increase the sampling points and resolve the cross-sectional hardness of cBN. A step of 2 μm was preset for indentation points to minimize the interaction of the plastic zone induced by adjacent indentations while maintaining a sufficient number of the indentation points across the cBN layer. The nanoindentation measurements were carried out using a MTS Nanoindenter XP equipped with a Berkovich diamond probe. The instrument was calibrated by using a standard fused silica sample prior to measuring the mechanical properties of cBN films. The drift rate was preset to ≤ 0.05 nm/s prior to the beginning of each indentation. All the load-displacement (P–δ) curves used to determine the hardness (H) and elastic modulus were corrected for thermal drift. Indentation modes of constant depth, constant loading and continuous stiffness measurement (CSM) were used in this study. The measured P–δ curve and the formula 8.1 [174]:

$$E_{eff} = \frac{1}{\beta}\frac{\sqrt{\pi}}{2}\frac{S}{\sqrt{A}} \tag{10.1}$$

$$\frac{1}{E_{eff}} = \frac{1-\upsilon_s^2}{E_s} + \frac{1-\upsilon_i^2}{E_i} \tag{10.2}$$

were used to determine the elastic modulus E_s of the samples. E_{eff} is the effective elastic

modulus (the composite elastic modulus of the specimen and the indenter); υ_S is the Poisson ratio of the sample; and E_i and υ_i are parameters of indenter (single crystalline diamond). The effective elastic modulus was calculated from the equation 8.2, where β is a constant of 1.034 for Berkovich tip; S and A are the unloading stiffness and projected contact area obtained in the measurements.

10.3. Plain-view hardness and elastic modulus of cubic boron nitride films

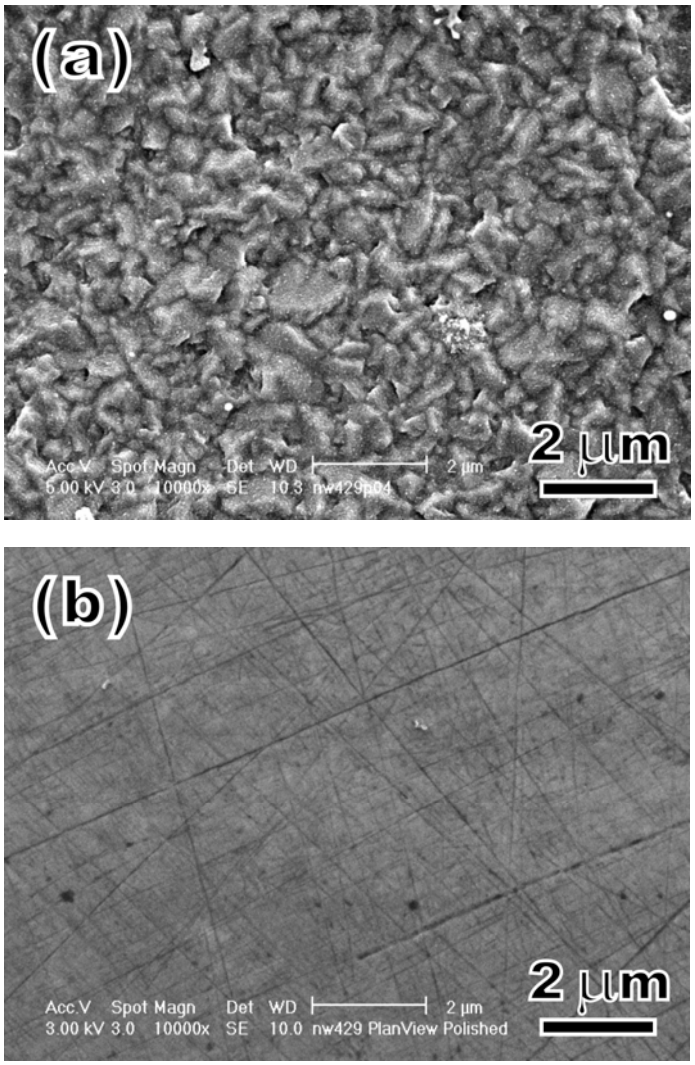

Fig. 10-1. SEM Surface morphologies of (a) as-deposited and (b) polished cBN films.

Fig. 10-1a is an SEM image showing the rough surface morphology of an as-deposited cBN film which has been subjected to hardness test measurements. The hardness testing of the sample with such surface is very difficult. The hardness values, obtained from nanoindentation measurements, were scattered over a range of 40–60 GPa. The data spread over a large interval is primarily caused by the rough, uneven surfaces that result in irregularities of the indentation imprints and faulty determination of the actual projected areas in nanoindentation system. After smoothing the films with fine

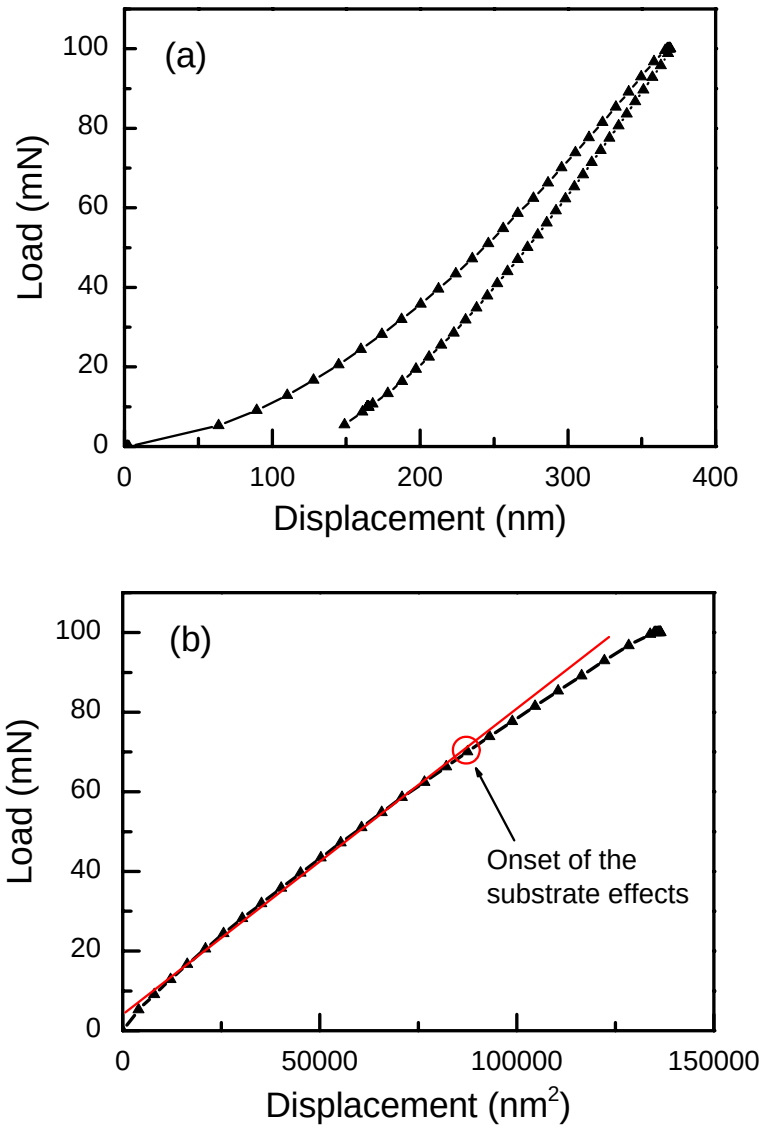

Fig. 10-2. (a) Loading/unloading and (b) loading-displacement square curves of cBN film obtained at a loading of 100 mN.

diamond paper, the obtained surface morphology, as shown in Fig. 10-1b, improved the repeatability of the hardness measurements considerably. An example of loading/unloading curves is shown in Fig. 10-2a. No pop-in and discontinuity are observed in the curve, indicating that cracking did not occur during the measurements. In the case of thin hard films on soft substrates, it is known that the substrate effects cannot be neglected when the ratio of indent depth and film thickness exceeds a certain value. The substrate effect in nanoindentation was estimated from load/unload characteristics following the method proposed by Hainsworth et al. [175]. The load *vs*. the displacement-squared curve of the loading part of the loading/unloading curve (Fig. 10-2a) is shown in Fig. 10-2b). The point where the curve deviates from linearity (displacement of about 300 nm as marked in the figure) indicates the onset of the substrate effects (elastic deformation of the substrate). Therefore, the hardness measured at the displacement below 300 nm can be thought from the cBN film only. Since in indentation measurements of a film on a substrate, the film first elastically deforms as the indenter is displaced into the material, and then plastically deforms [172], the larger displacements are preferred to take the deformation beyond the elastic regime. They also diminish the indentation size effect [176] generally being significant for the superhard materials with small loadings. Considering both the substrate and indentation size effects, we used a high loading (large displacement) for the increase of the accuracy in hardness values, which is feasible only on our thick cBN films so far. The elastic modulus of the cBN film was determined directly from the stiffness obtained from the unloading curve and projected area; the Poisson ratio of cBN was fixed to 0.15 as previously reported for micro-crystalline cBN [177].

The hardness and elastic modulus of the polished cBN film measured at varying displacements were depicted in Fig. 10-3. The results were quite repeatable at different sampling regions. For hardness measurements, a plateau of hardness values over a wide range of displacements ranging from 100 to 300 nm was observed. Beyond this region the hardness decreased. This observation agrees well with the fact, shown in Fig. 10-2b, that the substrate effects begin to play a role in nanoindentation measurements when the

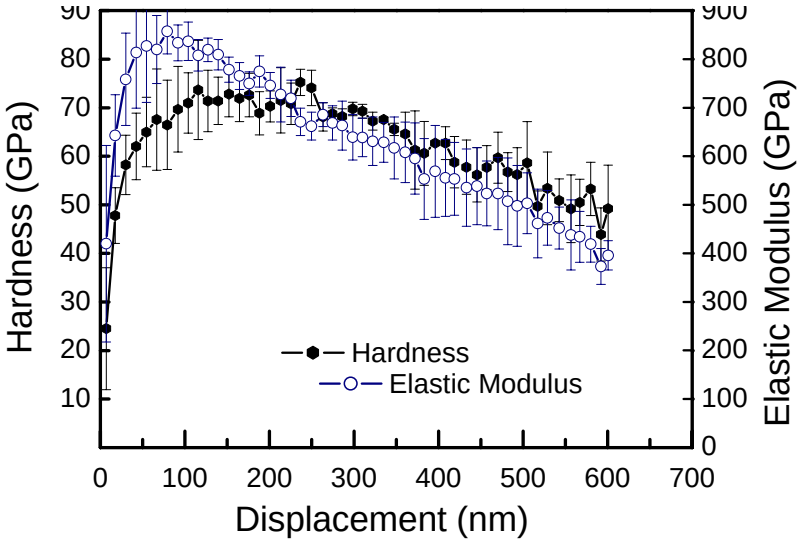

Fig. 10-3. Hardness and elastic modulus of a polished cBN film obtained from a nanoindentation testing in the plan-view direction using continuos stiffness measurement technique.

displacement is larger than 300 nm. From this plateau, a hardness of about 70 GPa was acquired, which is the highest value ever obtained on cBN films deposited by either PVD or PECVD methods. The high hardness measured on these cBN films is believed to result from the high crystallinity and large crystal size, as evidenced by Raman spectroscopy and TEM in our previous report [173]. In addition, because the cBN films measured in this work have the lowest residual stress (~1 GPa) [178], the influence of the high compressive stress normally observed in the films deposited by PVD methods on the hardness measurements [179] was effectively diminished, which can also contribute to the accuracy of measurements. A slight difference in peak positions of the hardness and elastic modulus is observed in the figure, which is due to the different dependence on the projected contact area ($H \propto A^{-1}$ while $E_{eff} \propto A^{-0.5}$) [180]. In the case of the displacements from 100 to 300 nm, the elastic modulus of the cBN film distributed from 680 to 800 GPa. The hardness and elastic modulus measured here are reliable and reasonable as compared to those reported for the bulk cBN [71,177]

10.4. Cross-sectional hardness and elastic modulus of cubic boron nitride films

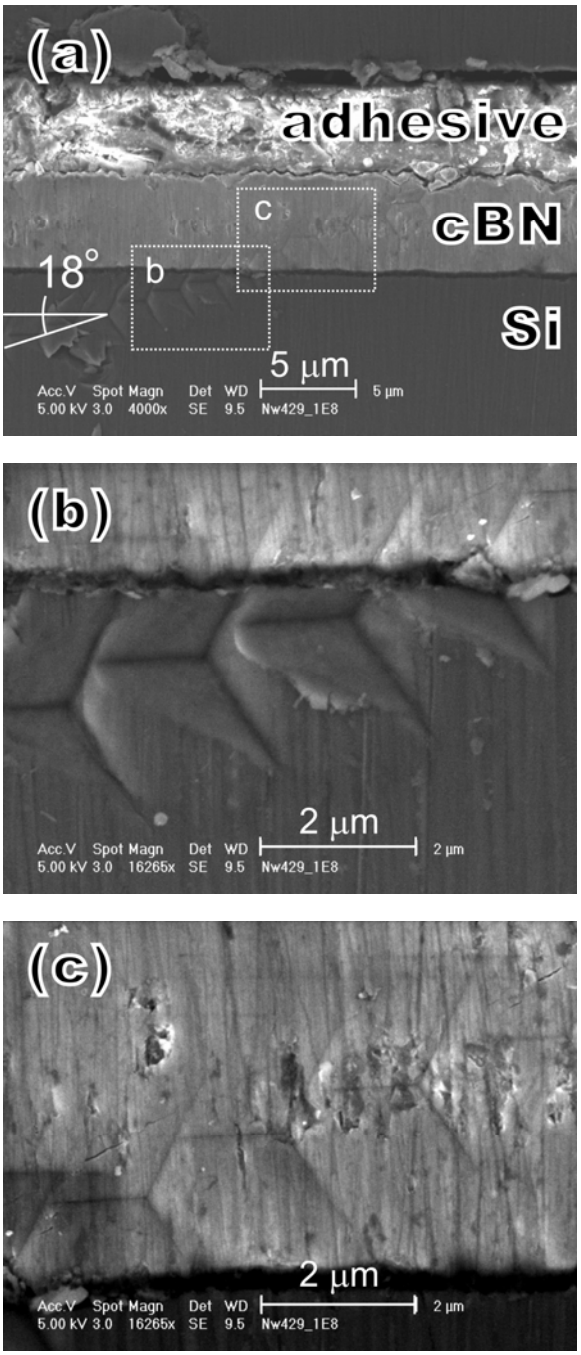

Fig. 10-4. Cross-sectional SEM micrograph showing the residual indentations after unloadings. (a) An overall view at low magnification, and (b) and (c) enlarged views corresponding to the indentation zones as designated in image (a)

The hardness of the cBN film was also measured in its cross-sectional direction across the film thickness. During measurements, the sample was set on a flat stainless holder. Since cBN is much stiffer than Si substrate, a loading for inducing a suitable displacement on cBN may possibly result in enormous cracking and fractures near the indent of Si. Therefore, a constant depth mode was used in our cross-sectional nanoindentation measurements. The contact depth for all indents was preset to 500 nm. This value is believed to be deep enough to probe the cBN hardness in a realistic sense while the substrate (stainless steel holder) effect could be neglected due to the much larger sample thickness. Fig. 10-4 shows three SEM images of the residual indents after the nanoindentation in the direction from the Si substrate to the cBN film surface. No cracking was revealed even for the indentations in the vicinity of interfacial regions. This observation implies that the cBN films are well adherent to the substrates. Indeed such a technique has been employed to evaluate the interfacial adhesion of thin film [181].

Fig. 10-5 illustrates the variation of the nanoindentation hardness measured in the cross-sectional direction of the sample. The measurement was repeated several times. The results are very consistent, as demonstrated by the overlapping of two independent measurements in Fig. 10-5. Corresponding to Fig. 10-5, the initially flat region with a

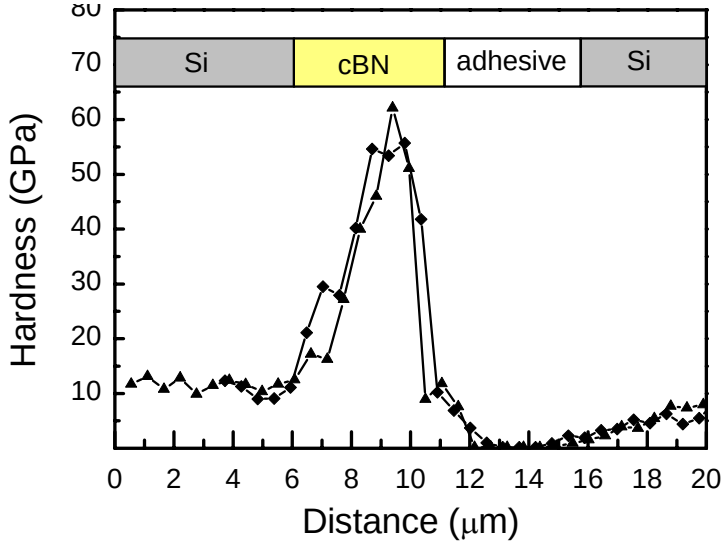

Fig. 10-5. Variation of cross-sectional nanoindentation hardness across the thickness of cBN layer.

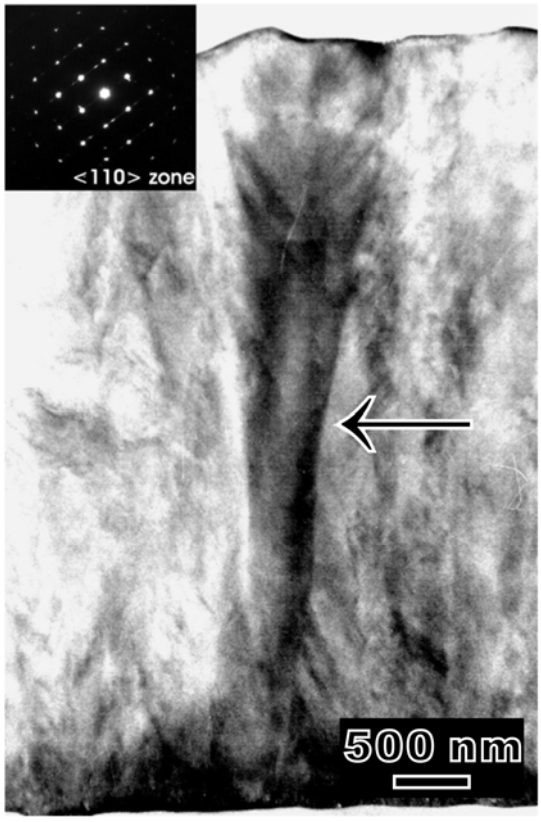

Fig. 10-6. Cross-sectional bright field TEM images of the films deposited by the two-step process. The arrow indicates the position where the process switched to the second step. The corresponding electron diffraction pattern inserted indicates the single crystalline nature of the columns.

hardness of 12 GPa arose from the Si substrate, which agrees well with the value reported for bulk silicon. As soon as the indention entered from the silicon into the cBN zone in the vicinity of the silicon–cBN interface the hardness increased dramatically. The hardness continued to increase steeply as the indentation progressed further from the cBN–substrate interface and reached a maximum of 65 GPa at a depth of about 1–2 μm from the cBN surface–adhesive interface. After crossing the cBN–adhesive interface, a very small hardness of about 0.2 GPa was obtained. The drops in hardness near the surface and interface regions are associated with the soft interfacing substrate and adhesive environments. However, it is interesting to note that the maximum hardness was measured in the cBN zone close to the cBN–adhesive interface, though the

adhesive is incomparably softer than the silicon substrate at the other interface. To understand the asymmetric distribution of hardness across the cBN film cross-section requires looking at the deposition procedure and film microstructure evolved. The films grown by the two-step process induced a columnar growth as observed by both SEM and TEM. Each column was confirmed to be a single crystal with a vertical length almost equal to film thickness (in this case nearly 5 μm) [173]. TEM cross-sectional image of the film deposited by the two-step processes was shown in Fig. 10-6. A strong increase of the columnar lateral size (over 1 μm at the film surface) was observed from the height of about 3 μm of the column (as indicated by the arrow) where the process was switched to the second step [173]. From this point the columns increasingly coalesced, grain boundaries reduced, and crystal size expanded laterally. According to the film microstructure observed, it can be speculated that increasing the crystal size expanding the cBN columns with simultaneous reducing the grain boundaries) from the substrate interface towards the surface is responsible for shifting the hardness maximum towards the surface–adhesive interface. Similar deduction could be obtained from the cross-sectional visible micro-Raman spectra of the corresponding cBN film as depicted in Fig. 10-7. The nearby sampling point is about ~2 μm apart. Inset is the optical micrograph of the sampling region. It is observed that as the sampling area was moved across the whole cBN layer starting from Si towards the adhesive, the corresponding Raman scattering intensity of Si 2nd order peak centered at around 950 cm^{-1} decreased gradually, and eventually vanished. At the same time, the peaks located at about 1052 cm^{-1} and 1302 cm^{-1}, assigned to the vibration modes of cBN, TO and LO phonon modes respectively, were increased accordingly. This implies that the cBN grain sizes are expanding starting from the interface towards the surface which is an evidence of grain coalescence. Moreover, the cross-sectional TEM image shown in Fig. 10-6 demonstratesthat the crystal size in the film lateral direction (columnar lateral size, 1 μm at film surface) is much small than that in the film growth direction (columnar height, nearly 5 μm). The columnar nature of the cBN films may also be the reason for the difference between the hardness measured in the cross-sectional and plan views (65 *vs*. 70 GPa).

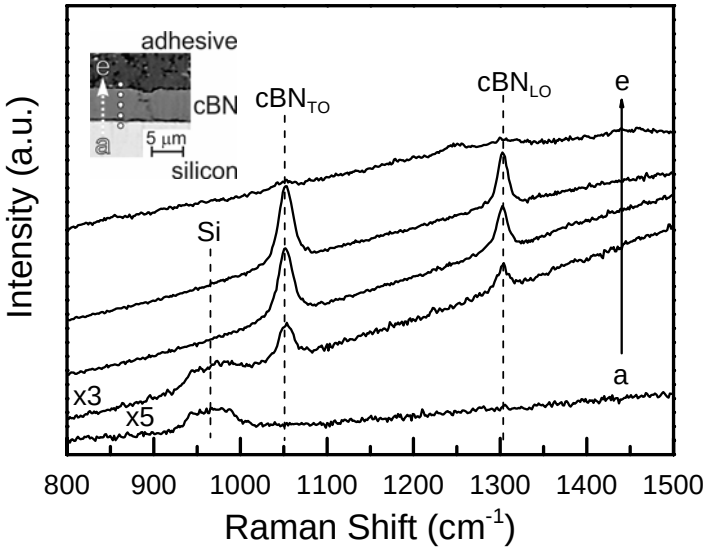

Fig. 10-7. Cross-sectional visible micro-Raman scattering spectra of a 5-μm-thick cBN film. Inset showing the sampling region starting from Si towards adhesive as indicated by the direction from '**a'** to '**e'**.

10.5. Final remarks to hardness measurement

This chapter presents the mechanical characterization of 5-μm-thick, high quality cBN films using nanoindentation measurements in both cross-sectional and plan view directions. It was found that the hardness measured depended strongly on the crystallinity and crystal size/grain boundaries of the cBN films. The consistent and repeatable hardness of 70 GPa and elastic modulus of 800 GPa were obtained on smoothed cBN films, which are the highest values ever obtained on cBN films deposited by either PVD or CVD methods so far. These values are comparable to that reported for cBN crystals synthesized by high-pressure, high-temperature methods.

Chapter 11. Applications of cubic boron nitride /diamond composite in cuttings tools

ECR-plasma coupled with fluorine chemistry evidently provides high quality and low stress cBN films and therefore can be exploited in industrial projects. However, selection of substrate materials is also important. Particularly, the combination of cBN and diamond layers, denoted cBND bilayer composite, has unique mechanical properties above all suitable for machining ferrous materials including tool steels. The cBN film in the cBND composite can be 3-4 μm thick which is the thickness often used in coating tools. The film thickness of different coatings on cutting tools ranges from 1 to 4 μm. The significance of our fluorine assisted deposition is in capacity of growing cBN on rough surfaces because the deposition also involves reactive etching, abstraction, and surface incorporation of specific species. Otherwise rough surfaces deteriorate cBN nucleation as discussed previously. The natural extrapolation of the work described is then deposition of cBND on cutting tools employing ECR-PECVD assisted by fluorine chemistry, testing coated tools and discussion of the coating properties. In this particular case, cobalt cemented tungsten carbide (WC) cutting inserts were selected for their coating by cBND composite bilayers.

11.1. Incentive behind the cubic boron nitride coating of cutting tools

The selection of a substrate or/and buffer layer is vital for cBN deposition since mismatching in physical properties of the substrate, buffer layer and cBN may lead to undesirable aBN/tBN interfacial layers, large film stress, poor adhesion, and prevention of epitaxial growth. Since it was difficult to eliminate the interfacial aBN/tBN layers and films experienced large stress and tended to delaminate very limited studies have been published particularly on special cutting tool materials like cemented tungsten carbide. The inception of BN film depositions often induced by mismatching the material properties is one of the major reasons for poor quality cBN films.

Since diamond chemical reactivity does not allow using diamond coated tools and in many other applications particularly those involving ferrous materials, cBN is much needed. There is enormous demand for cBN tools on the tool market. All the cBN tools are however made of cBN powders prepared by HPHT methods [97] and cemented by metal binders. No tools using cBN coating are industrially available because properties of cBN films have not met required quality. No tools using cBN coating are industrially available because properties of cBN films have been poor. A prime advantage of cBN as a cutting tool material is its stability in contact with steel at high temperatures, while diamond, under these conditions, tends to be dissolved and converted to graphite which is induced by catalyst effects of metals. Alike diamond, cBN is very hard to sinter owing to its strong covalent bonding and its stability at high pressures and high temperatures. Therefore, the direct coating of tools with cBN from the gas phase has received much attention.

Early studies of BN-coated WC substrates were thin in thickness and the film adhesion strength deposited by these methods was generally poor and showed extensive flaking. The first cBN deposition on WC substrate could be dated back to 1990s. Ikeda *et al* [157] synthesized BN films with cubic phase contents of 50% at 400 °C and a substrate power of 100 W using an ion plating technique. Later on, deposition of 150 nm thick cBN films on mirror-polished WC substrates had been reported by Okamoto [182] via a thin boron buffer layer and using diborane precursor in an ECR-PECVD system. Tentative deposition of cBN films on WC at 400 °C via a similar interlayer was also reported by Kumagai [183] employing an IBAD technique. The issue of high substrate surface roughness (promote the formation of graphitic BN at the interface as discussed in Chapter 10) and thin buffer layer thickness (inability to redistribute the built in compressive stress of the BN film) may be the reasons limiting the ultimate cBN thickness on cemented carbide substrates. Until late 1990s, enhancement of substrate adhesion by intentionally increasing the buffer layer thickness up micrometer and by forming an effective intermixing layer at the interface, Setsuhara *et al* [184] were able to deposit cBN coatings as thick as 0.7 μm on WC substrates at 400 °C using an IBAD

method. Adherent cBN films with a thickness up to 0.8 μm on WC substrates were also prepared by reactive RF sputtering in Ar/N discharge through a Ti adhesive layer (0.5 μm), B_4C layer (1.7 μm) and BCN graded layer [147]. In addition to ion plating, IBAD, RF sputtering and ECR-PECVD preparation techniques, Weissmantel *et al* [105] reported that using pulsed laser ablation of hBN layers, cBN films (0.3 μm) with good adhesion could be prepared on WC substrates at high deposition rates (3 μm/h). In practical coating applications, in addition to adhesion and tooling lifetime issue, the deposition rate is another economic concern. The reasonable deposition rate offered by our large-area deposition system using ECR-plasma is a way towards the production of cBND coated cutting tools.

11.2 Deposition and performance of cBND coated cutting tools

Cubic BN–diamond (cBND) composite bilayers seem to be an excellent choice for mechanical and tribological applications. They can be prepared in the form of single or periodic multi-layers and may be adapted on any substrates suitable for diamond deposition. Apart from the exceptional adherence of cBN on diamond, this combination provides outstanding chemical and thermal stability due to the top cBN layer being also the second hardest materials, while the underlying diamond, the hardest material, maintains the best mechanical supporting capacity possible (Fig. 11-1). As shown in Fig. 11-2 the cBND also provides the most effective heat dissipation owing to the highest and second highest thermal conductivities of diamond and cBN [185]. Thus, the cBND coating may effectively lower the temperature of a cutting tool in its contact area with a workpiece so that the machining speed could be increased considerably. In addition, the fluid that used in conventional grinding method can be eliminated as such fluid contains chlorine, sulfur and phosphorus which aggravates the working environment and increases costs for fluid replacement and disposal [186]. Reducing the use of cooling lubricants by minimal quantity lubrication or dry machining will reduce production costs and simultaneously have beneficial environmental impacts [97]. Co is the conventional binder material for cemented WC since it has good wetting abilities for

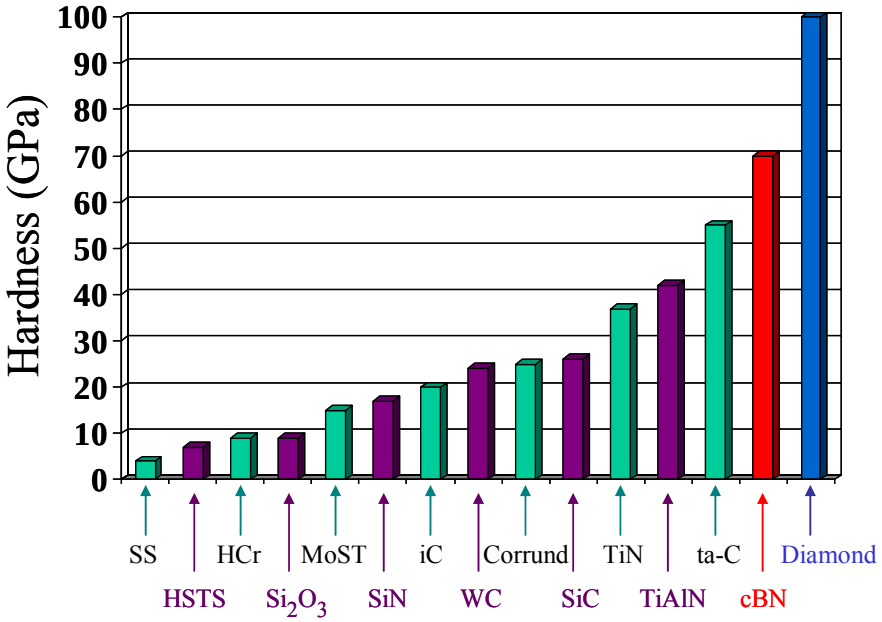

Fig. 11-1. Hardness of the common bulk materials and hard coatings as compared to cBN coatings.

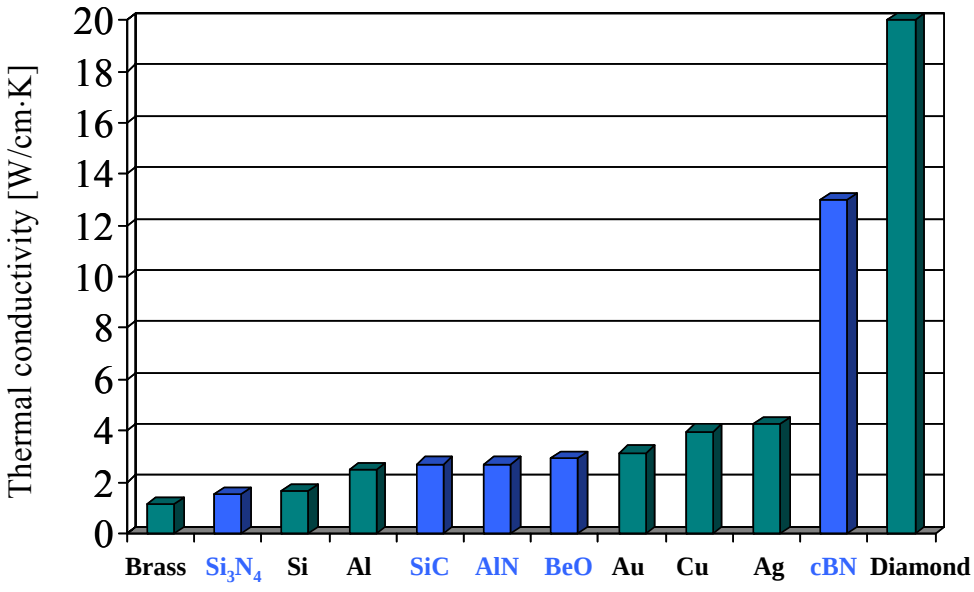

Fig. 11-2. Room-temperature thermal conductivity of cBN and diamond compared to common metallic and ceramic materials.

grains and assists densification during sintering. High concentration of Co in the WC tools can enhance the fracture toughness and shock resistance of the resulting sintered WC ceramics [187]. In general, WC tool life can be prolonged by protective coatings like diamond or cBND. Haubner *et al* [188] reported that direction deposition of diamond on cobalt encounters the problems of high carbon dissolution and high vapor pressure of cobalt at high temperature deposition of diamond (800 °C), which leads to the formation of amorphous carbon. In case of using cBN as a buffer layer for growth of diamond on WC, Cappelli *et al* [187] found that the thin BN layers were not able to prevent Co migration from the tool surface to the growing nuclei and also through the diamond grain boundaries towards the diamond surface. If WC substrates were not chemically etched prior to deposition of PVD cBN at –400 V and 550 °C, the whole coating system would experience strong instability and would lead to a fast delamination of the coating. Yu *et al* [189] attempted to deposit cBN on WC substrate using a high density DC plasma jet deposition system. Similarly, their results show that the presence of Co or the formation of cobalt nitrides at the surface/interface interrupts or suppresses the growth of cBN whereas hBN grows. After the Co depletion by nitric acids treatment, the Co concentration decreases greatly, and thus cBN film synthesis can be obtained on the chemically etched substrate at 1050 °C. Since Co is detrimental to both diamond and cBN growth, the growth surface has to be depleted in Co prior to cBND deposition. Following this scheme the surface of cemented WC was depleted in cobalt by chemical etching (Fig. 11-3a). Subsequently 6-μm-thick CVD diamond films were deposited (Fig. 11-3b), and then 1 μm thick cBN films were grown using the ECR PECVD process, described in Chapter 5, and at ~800 °C (Fig. 11-3c). The Co depleted WC surface results in a rough surface morphology comprising microcrystalline grains of WC. The deposited CVD diamond films are randomly oriented with microcrystalline grains. The lower temperature (800 °C) was used, when compared to cBN growth on silicon (1000 °C), in order to limit the diffusion of cobalt from the bulk of cemented WC to thediamond interface. The grain size of the cBN is very small and cannot be distinguished. The highly-insulating nature and drastic change of surface morphology imply the deposition of cBN films. This result can be further validated by reflectance

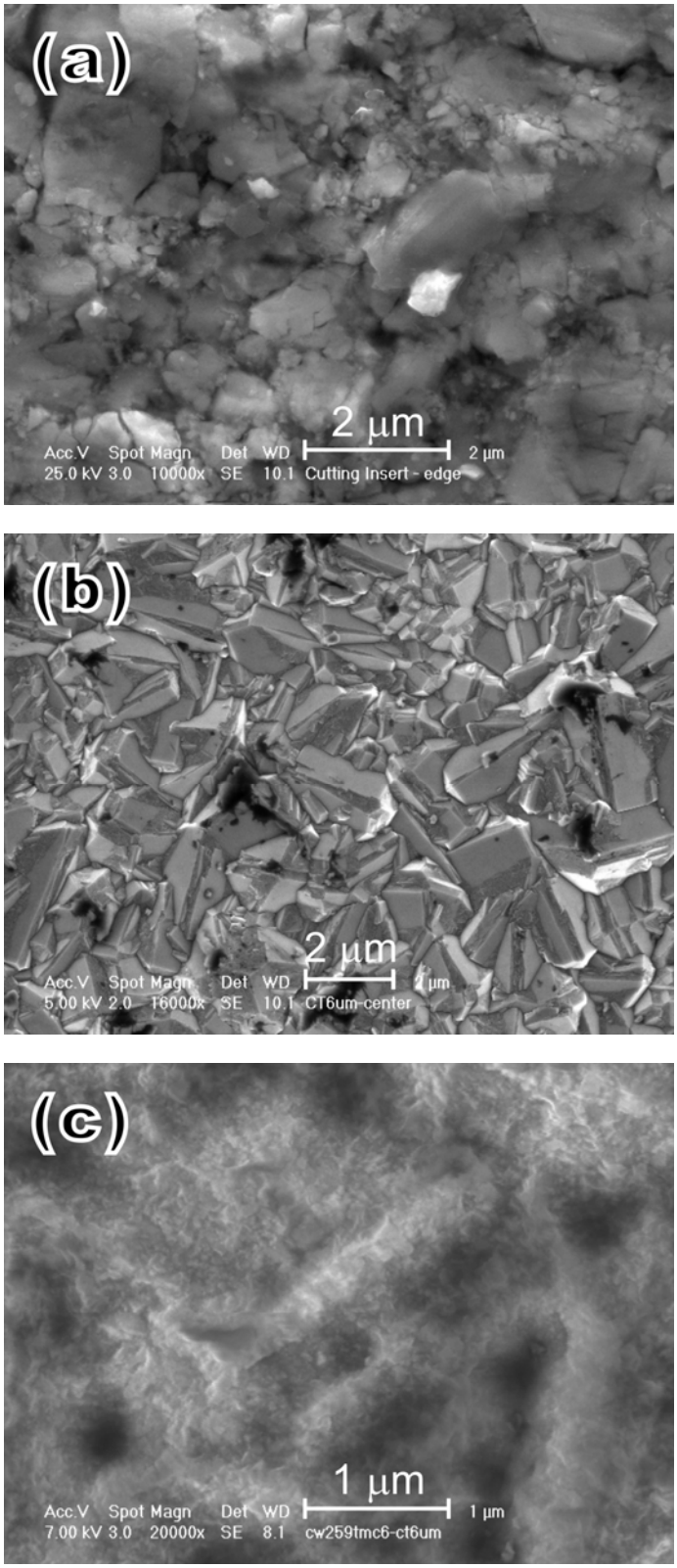

Fig. 11-3. Plain-view SEM micrographs of (a) cobalt-depleted, (b) 6 μm thick CVD diamond coated and (c) cBND coated WC cutting inserts.

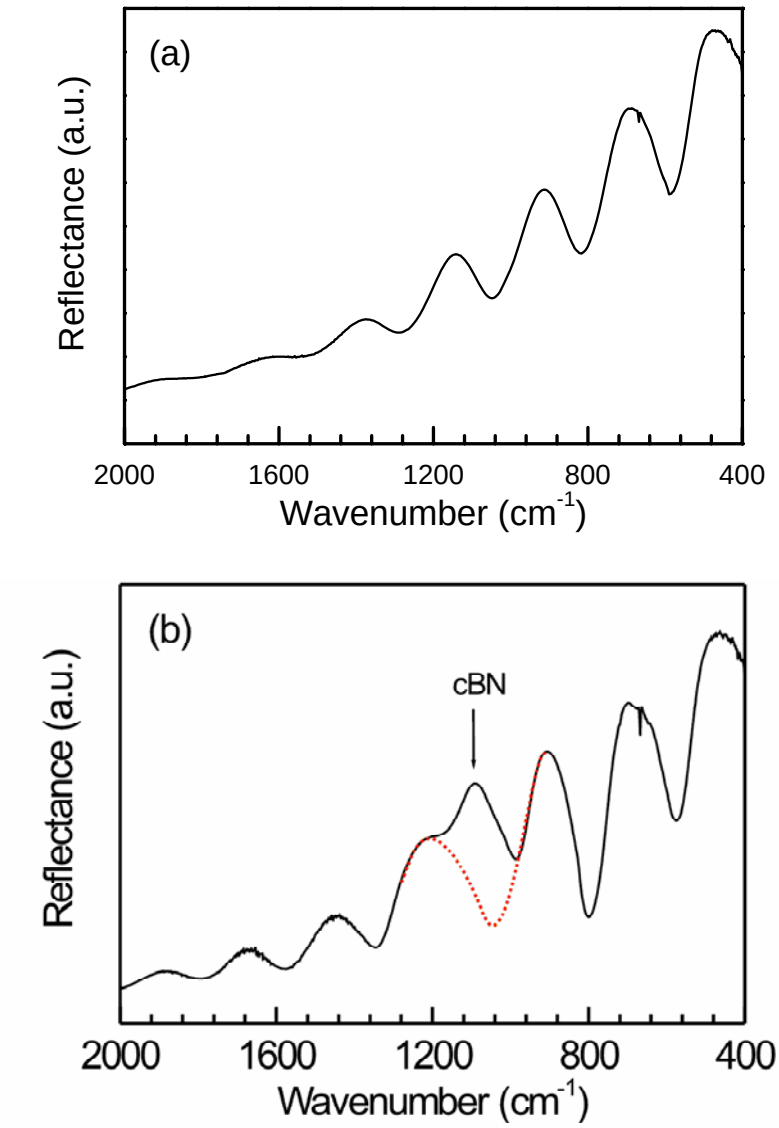

Fig. 11-4. FTIR reflectance spectra of (a) 6 μm thick CVD diamond coated and (c) cBND coated WC cutting inserts. The periodic oscillation is attributed to the interference of IR signal with micrometer thick coatings.

spectra of FTIR as shown in Fig. 11-4. CVD diamond film is infrared transparent. The presence of periodic oscillation pattern is attributed to the thickness interference with IR signal. The comparison between Figs. 11-4a and 11-4b immediately reveals the presence of cBN peak. Due to the thickness variation of CVD diamond at the center and edge of the cutting insert, the oscillation pattern is a little different, but the cBN peak position

practically remains the same which ensures that this peak originates from the sp^3-bonded BN. The cBND coated cutting inserts were tested by milling of mold steel M238 (Hardness Brinell ~250 HB). In severe milling operation the cBND coated and uncoated reference inserts were mounted on a machining head with a diameter of 5 cm.

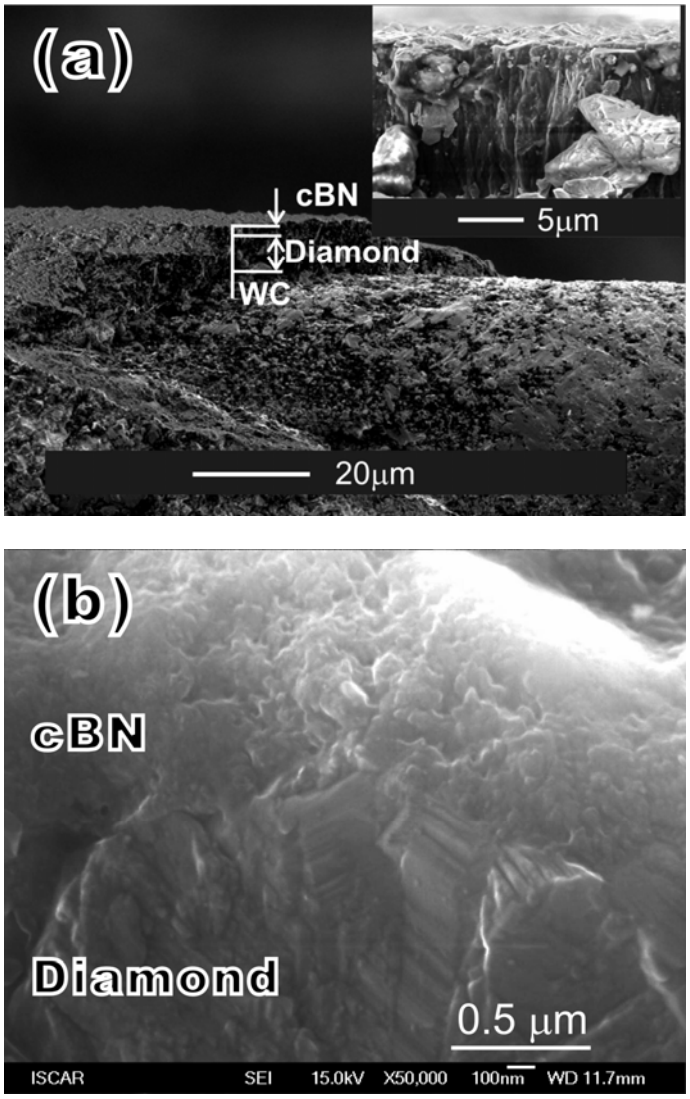

Fig. 11-5. A tungsten cutting insert coated with cBND after a milling test. (a) the WC tool substrate chipped off while the cBND remained intact in surrounding areas; (b) cross-sectional SEM showing the interface between cBN and diamond.

During machining, the inserts periodically impacted on the 30 mm thick plate with length of 30 cm at a peripheral speed of 10.2 m/s. The cutting depth was 0.3 mm. Both

the coated and uncoated inserts failed under these cutting conditions as seen in Fig. 11-5. The WC tool substrate edges chipped off. The cBN and diamond films as well as the tungsten carbide however remained intact in surrounding areas. This is the first demonstration of cBND coated WC cutting insert in the milling test. Instead of using diamond as a universal buffer layer, Bewilogua *et al*. reported that the adhesion and cBN film thickness could be increased with introduction of a buffer layer on both Si and cemented carbide for cutting tool applications [190]. Silicon was first coated with boron carbide (B_4C) at a bias of –100 V, which was followed by a B–C–N gradient layer with increasing nitrogen content at a bias of –200 V. The N_2 component of the Ar/N_2 gas mixture used for sputtering was gradually enriched. Cubic BN was nucleated when only a pure N_2 gas was used (i.e., the Ar supply was disconnected). The nucleation step was then switched to cBN growth process at reduced bias (–130 to 170 V) and elevated temperature (600 °C). Cemented carbide cutting inserts were first coated with titanium and then by a similar sequence of layers as previously described for Si. The cBN films thus deposited on Si and cemented carbide were thicker than 2 and 1 μm, respectively. The films were stable and those deposited on cemented carbide were tested in different turning operations and performed well. Up to now, the cBN coated cutting inserts are still not as good as PcBN inserts prepared by HPHT and cementation methods.

10.3. Summary to cubic boron nitride /diamond coating of cutting tools

Cubic boron nitride/diamond (cBND) composite bilayers were deposited on cemented WC cutting inserts. The surfaces of cutting inserts were depleted in cobalt and deposition was carried out at lower temperature to limit the diffusion of cobalt binder. The cBND coating represents combination of two materials with extreme properties providing high performance of cutting inserts tools though in given test cutting inserts failed The failure however was caused in unsuitable experiment designed in which cutting inserts periodically hammered the narrow a hard steel plate. As a result, all edges

of cutting inserts including referenced uncoated WC inserts chipped off, however the cBN–diamond and diamond–WC remained in tact. No cracks were observed. The chipping occurred in deeper region of WC body. Thus cBND coating due to their performance and mechanical and thermal properties are on the threshold of their implementation into practice, particularly in cutting tools and tribological applications.

Chapter 12. Conclusions

Energetic ion bombardment in N_2 and Ar plasmas conventionally applied to cBN deposition restricts the size of cBN crystallites and induces high internal stress levels limiting the obtainable non-delaminating film thickness (to ~200 nm). This research work however presents the preparation of thick cBN films (>1 μm) with low stress on silicon substrates. One of the important reasons for this considerable qualitative improvement is introducing fluorine chemistry which is provided by a complex He-Ar-N_2-BF_3-H_2 plasma produced in an ECR system. Investigating the effect of ion bombardment, gas composition, substrate temperature and growth time led to growing cBN films at a substrate temperature of 900 °C and very low substrate bias of –30 V. Fourier-transform infrared spectroscopy shows that the films are composed of >80% cBN. Detailed analysis of BN film structures employing HRTEM and transmission EELS indicates that a pure cBN layer is formed on top of an initial turbostratic BN layer which accounts for the small hBN signal in FTIR spectra. The appearance of characteristic TO and LO phonon modes of cBN in visible Raman spectra demonstrates the larger crystalline size (~100 nm – also confirmed by HRTEM) in contrast to the films reported previously.

The PECVD method aided by fluorine chemistry as described in this work is capable of growing cBN directly on diamond with hardly notable conventional nucleation stage. The cBN nucleation on diamond is supported by the extremely low bias voltage –10 V which is considerably lower than the –30 V bias necessary for inducing cBN nuclei on silicon substrates. The direct growth of cBN on diamond is driven by the similarity in the diamond and cBN lattices as well as other physical properties. Despite this resemblance deviation from true epitaxial growth and evolution of twinning crystallites are observed between cBN and diamond. The small-angle grain boundaries are formed at the regions of the interface due the slight lattice mismatch. Therefore, slightly higher bias voltage (ion bombardment with higher kinetic energy) is

suggested to apply at the initial growth stage for building up a little stress to eliminate small-angle grain boundaries and obtain “seamless” epitaxy.

Substrate surface roughness considerably affects the cBN nucleation. The rougher surface contributes to the random orientation of tBN (0002) basal planes, prolongs the cBN incubation time, and expands amorphous and tBN interfacial layers. The tBN (0002) basal planes serve as cBN nucleation sites. The thickness of BN films varies with local features and is thicker in surface valleys of the roughed surface due to sputtering on inclined micro-surface and recoiled ions hammering BN species into the valleys. The surface is planarized in this process. Therefore rougher surfaces shift the cBN nucleation threshold towards the higher ion energies as evident from FTIR and XANES analyses. The large transition non-cubic region at the rough substrate can be reduced by the increase of ion beam energy. Hence, the surface roughness has to be considered as one of the nucleation and growth parameters.

Since the CVD nature of cBN growth using ECR with fluorine chemistry is very different from PVD growth employing harsh ion bombardment, further studies based on HRTEM, OES and XPS studies were established to reveal the cBN surface growth sequence. This includes: (1) Formation H, F, BF_x and NH_x in the plasma so that the amount of F and NH_x is balanced by the feeding hydrogen concentration (2) abstraction of hydrogen and activation of N sites by F, (3) abstraction of fluorine and activation of B sites by energetic particle bombardment, (4) growth by adsorption of BF_x (boron source) on N and NH_x (N source) or B sites and (5) etching of non-cubic BN constituents by F. The possibility of preparing cBN via surface reactions without the significant damage introduced by ion bombardment at reduced ion energies (close to thermal energies) implies that the growth of electronic grade cBN single crystalline wafers (similar to single crystalline electronic grade diamond wafers grown by CVD) is feasible.

Parametric and mechanistic studies piloted the deposition of micrometer thick

cBN films which in return enable their mechanical evaluation. It was found that the hardness measured depended strongly on the crystallinity and crystal size/grain boundaries of the cBN films. The consistent and repeatable hardness of 70 GPa and elastic modulus of 800 GPa were obtained on smoothed cBN films, which are the highest values ever obtained on cBN films deposited by either PVD or CVD methods so far. These values are comparable to that reported for cBN crystals synthesized by high-pressure, high-temperature methods. Finally, demonstration of cBND composite coatings on common tungsten carbide tools was achieved through the chemical depletion of cobalt binder followed by deposition of diamond and cBN in sequence. The resulting coatings were subjected to cutting performance tests by milling the mold steels. The rough substrate surface does not harm the cBN deposition using the developed deposition technique which contrasts the cases of PVD deposition. Instead additional adhesion strength is provided by the enhanced mechanical interlocking between diamond and cBN. The failure of cutting insert at diamond/WC interface suggests that mechanical test was not properly designed as the ceramic inserts periodically encountered with the hard steel plate. The present study however demonstrates the possibility of cBND coatings for practical applications like turning and grinding.

References:

1 F. R. Corrigan, F. P. Bundy, J. Chem. Phys. **63**, 3812 (1975).

2 V. L. Solozhenko, V. A. Mukhanov, N. V. Novikov, Doklady Akademii Nauk Sssr **308**, 131 (1989).

3 B. P. Singh, V. L. Solozhenko, G. Will, Diam. Relat. Mat. **4**, 1193 (1995).

4 V. F. Britun, A. V. Kurdyumov, I. A. Petrusha, Mater. Lett. **41**, 83 (1999).

5 T. A. Friedmann, P. B. Mirkarimi, D. L. Medlin, K. F. McCarty, E. J. Klaus, D. R. Boehme, H. A. Johnsen, M. J. Mills, D. K. Ottesen, J. C. Barbour, J. Appl. Phys. **76**, 3088 (1994).

6 R. Geick, C. H. Perry, G. Rupprecht, Physical Review **146**, 543 (1966).

7 M. I. Eremets, K. Takemura, H. Yusa, D. Golberg, Y. Bando, V. D. Blank, Y. Sato, K. Watanabe, Phys. Rev. B **57**, 5655 (1998).

8 L. Vel, G. Demazeau, J. Etourneau, Mater. Sci. Eng. B-Solid State Mater. Adv. Technol. **10**, 149 (1991).

9 M. C. Polo, M. BenelMekki, J. L. Andujar, N. Mestres, J. Pascual, Diam. Relat. Mat. **6**, 1550 (1997).

10 T. A. Friedmann, K. F. McCarty, E. J. Klaus, D. Boehme, W. M. Clift, H. A. Johnsen, M. J. Mills, D. K. Ottesen, Appl. Phys. Lett. **61**, 2406 (1992).

11 S. Reich, A. C. Ferrari, R. Arenal, A. Loiseau, I. Bello, J. Robertson, Physical Review B (Condensed Matter and Materials Physics) **71**, 205201 (2005).

12 J. A. Sanjurjo, E. Lopezcruz, P. Vogl, M. Cardona, Phys. Rev. B **28**, 4579 (1983).

13 S. Fahy, C. A. Taylor, R. Clarke, Phys. Rev. B **56**, 12573 (1997).

14 D. M. Hoffman, G. L. Doll, P. C. Eklund, Phys. Rev. B **30**, 6051 (1984).

15 M. I. Eremets, M. Gauthier, A. Polian, J. C. Chervin, J. M. Besson, G. A. Dubitskii, Y. Y. Semenova, Phys. Rev. B **52**, 8854 (1995).

16 A. R. Phani, J. Mater. Res. **14**, 829 (1999).

17 S. Komatsu, K. Okada, Y. Shimizu, Y. Moriyoshi, J. Phys. Chem. B **103**, 3289 (1999).

18 C. Schaffnit, H. DelPuppo, R. Hugon, L. Thomas, P. Moretto, F. Rossi, Y. Pauleau, Surf. Coat. Technol. **80**, 13 (1996).

19 Z. L. Akkerman, M. L. Kosinova, N. I. Fainer, Y. M. Rumjantsev, N. P. Sysoeva, Thin Solid Films **260**, 156 (1995).

20 P. Wang, S. Orimo, H. Fujii, Appl. Phys. A-Mater. Sci. Process. **78**, 1235 (2004).

21 C. GomezAleixandre, A. Essafti, M. Fernandez, J. L. G. Fierro, J. M. Albella, J. Phys. Chem. **100**, 2148 (1996).

22 A. Essafti, C. GomezAleixandre, J. L. G. Fierro, M. Fernandez, J. M. Albella, J. Mater. Res. **11**, 2565 (1996).

23 A. Essafti, C. GomezAleixandre, J. M. Albella, Diam. Relat. Mat. **5**, 580 (1996).

24 J. C. Philips, Review of Modern Physics **42**, 317 (1970).

25 K. Watanabe, T. Taniguchi, H. Kanda, Phys. Status Solidi A-Appl. Res. **201**, 2561 (2004); N. Miyata, K. Moriki, O. Mishima, M. Fujisawa, T. Hattori, Phys. Rev. B **40**, 12028 (1989).

[26] T. Taniguchi, T. Teraji, S. Koizumi, K. Watanabe, S. Yamaoka, Jpn. J. Appl. Phys. Part 2 - Lett. **41**, L109 (2002).

[27] A. R. Phani, S. Manorama, V. J. Rao, Semicond. Sci. Technol. **10**, 1520 (1995).

[28] M. Lu, A. Bousetta, A. Bensaoula, K. Waters, J. A. Schultz, Appl. Phys. Lett. **68**, 622 (1996).

[29] D. Litvinov, C. A. Taylor, R. Clarke, Diam. Relat. Mat. **7**, 360 (1998).

[30] K. Nose, K. Tachibana, T. Yoshida, Appl. Phys. Lett. **83**, 943 (2003).

[31] R. H. Wentorf, Jr., The Journal of Chemical Physics **36**, 1990 (1962).

[32] T. Taniguchi, K. Watanabe, S. Koizumi, Phys. Status Solidi A-Appl. Res. **201**, 2573 (2004).

[33] J. L. P. Castineira, J. R. Leite, L. M. R. Scolfaro, R. Enderlein, J. L. A. Alves, H. W. L. Alves, Mater. Sci. Eng. B-Solid State Mater. Adv. Technol. **51**, 53 (1998).

[34] V. A. Gubanov, E. A. Pentaleri, C. Y. Fong, B. M. Klein, Phys. Rev. B **56**, 13077 (1997).

[35] C. Ronning, A. D. Banks, B. L. McCarson, R. Schlesser, Z. Sitar, R. F. Davis, B. L. Ward, R. J. Nemanich, J. Appl. Phys. **84**, 5046 (1998); C. W. Ong, X. A. Zhao, Y. M. Ng, K. F. Chan, T. C. Tsang, C. L. Choy, P. W. Chan, Appl. Phys. Lett. **69**, 3501 (1996).

[36] C. X. Wang, G. W. Yang, T. C. Zhang, H. W. Liu, Y. H. Han, J. F. Luo, C. X. Gao, G. T. Zou, Appl. Phys. Lett. **83**, 4854 (2003).

[37] O. Mishima, K. Era, J. Tanaka, S. Yamaoka, Appl. Phys. Lett. **53**, 962 (1988).

[38] T. Taniguchi, S. Koizumi, K. Watanabe, I. Sakaguchi, T. Sekiguchi, S. Yamaoka, Diam. Relat. Mat. **12**, 1098 (2003).

[39] T. Taniguchi, J. Tanaka, O. Mishima, T. Ohsawa, S. Yamaoka, Appl. Phys. Lett. **62**, 576 (1993).

[40] H. Tomokage, N. Nomura, T. Taniguchi, T. Ando, Diam. Relat. Mat. **9**, 605 (2000).

[41] K. J. Liao, W. L. Wang, C. Y. Kong, Surf. Coat. Technol. **141**, 216 (2001).

[42] L. Duclaux, B. Nysten, J. P. Issi, A. W. Moore, Phys. Rev. B **46**, 3362 (1992).

[43] N. V. Novikov, A. P. Podoba, V. M. Perevertailo, S. V. Shmegera, A. Witek, Diam. Relat. Mat. **9**, 629 (2000).

[44] R. W. Pryor, K. R. Padmanabhan, K. Chawla, Diam. Relat. Mat. **4**, 128 (1995).

[45] D. T. Morelli, J. P. Heremans, G. A. Slack, Physical Review B (Condensed Matter and Materials Physics) **66**, 195304 (2002).

[46] K. Oda, K. Aoki, S. Inada, M. Nagae, T. Yoshio, J. Ceram. Soc. Jpn. **111**, 81 (2003).

[47] K. Oda, T. Yoshio, J. Mater. Sci. **28**, 6562 (1993).

[48] T. Komatsu, Y. Kakudate, S. Fujiwara, J. Chem. Soc.-Faraday Trans. **92**, 5067 (1996).

[49] S. Komatsu, Y. Moriyoshi, M. Kasamatsu, K. Yamada, J. Appl. Phys. **70**, 7078 (1991).

[50] R. H. Wentorf, Jr., The Journal of Chemical Physics **26**, 956 (1957).

[51] F.P. Bundy, R.H. Wentorf, Jr, The Journal of Chemical Physics **38**, 1144 (1963).

[52] O. Mishima, J. Tanaka, S. Yamaoka, O. Fukunaga, Science **238**, 181 (1987).

[53] V. L. Solozhenko, Doklady Akademii Nauk Sssr **301**, 147 (1988).

[54] V. L. Solozhenko, V. Z. Turkevich, W. B. Holzapfel, J. Phys. Chem. B **103**, 2903 (1999).

[55] S. Nakano, O. Fukunaga, Diam. Relat. Mat. **2**, 1409 (1993).

[56] M. Wakatsuki, K. Ichinose, Rev. Phys. Chem, Jpn., 441 (1975).

[57] M. Ueno, K. Hasegawa, R. Oshima, A. Onodera, O. Shimomura, K. Takemura, H. Nakae, T. Matsuda, T. Hirai, Phys. Rev. B **45**, 10226 (1992).

[58] N. V. Novikov, I. A. Petrusha, L. K. Shvedov, S. B. Polotnyak, S. N. Dub, S. A. Shevchenko, Diam. Relat. Mat. **8**, 361 (1999).

[59] H. Lorenz, I. Orgzall, Acta Mater. **52**, 1909 (2004).

[60] H. Sumiya, T. Iseki, A. Onodera, Mater. Res. Bull. **18**, 1203 (1983).

[61] I. A. Petrusha, Diam. Relat. Mat. **9**, 1487 (2000).

[62] J. Y. Huang, Y. T. Zhu, Chem. Mat. **14**, 1873 (2002).

[63] Toshio Kobayashi, The Journal of Chemical Physics **70**, 5898 (1979).

[64] O. Fukunaga, S. Nakano, T. Taniguchi, Diam. Relat. Mat. **13**, 1709 (2004).

[65] V. L. Solozhenko, Y. Le Godec, S. Klotz, M. Mezouar, V. Z. Turkevich, J. M. Besson, Phys. Chem. Chem. Phys. **4**, 5386 (2002).

[66] E. Vlodarchik, R. Trebinski, Shock Waves **7**, 231 (1997).

[67] N. I. Borimchuk, A. V. Kurdyumov, V. V. Yarosh, Khimicheskaya Fizika **9**, 1686 (1990).

[68] D. J. Kester, R. Messier, J. Appl. Phys. **72**, 504 (1992).

[69] H. Hofsäss, C. Ronning, U. Griesmeier, M. Gross, S. Reinke, M. Kuhr, Appl. Phys. Lett. **67**, 46 (1995).

[70] J. Hahn, M. Friedrich, R. Pintaske, M. Schaller, N. Kahl, D. R. T. Zahn, F. Richter, Diam. Relat. Mat. **5**, 1103 (1996); S. Ulrich, J. Scherer, J. Schwan, I. Barzen, K. Jung, M. Scheib, H. Ehrhardt, Appl. Phys. Lett. **68**, 909 (1996).

[71] P. B. Mirkarimi, K. F. McCarty, D. L. Medlin, Mater. Sci. Eng. R-Rep. **21**, 47 (1997).

[72] T. Yoshida, Diam. Relat. Mat. **5**, 501 (1996).

[73] H. Saitoh, W. A. Yarbrough, Appl. Phys. Lett. **58**, 2228 (1991); J. Szmidt, A. Werbowy, A. Michalski, A. Olszyna, A. Sokolowska, S. Mitura, Diam. Relat. Mat. **4**, 1131 (1995).

[74] I. Konyashin, V. Khvostov, V. Babaev, M. Guseva, J. Bill, F. Aldinger, Diam. Relat. Mat. **8**, 2053 (1999).

[75] A. Bartl, S. Bohr, R. Haubner, B. Lux, Int. J. Refract. Met. Hard Mat. **14**, 145 (1996).

[76] K. B. Kim, S. H. Kim, J. Vac. Sci. Technol. A-Vac. Surf. Films **18**, 900 (2000).

[77] R. Freudenstein, S. Reinke, W. Kulisch, Diam. Relat. Mat. **6**, 584 (1997).

[78] W. Dworschak, K. Jung, H. Ehrhardt, Thin Solid Films **254**, 65 (1995).

[79] M. Kuhr, R. Freudenstein, S. Reinke, W. Kulisch, G. Dollinger, A. Bergmaier, Diam. Relat. Mat. **5**, 984 (1996).

[80] D. H. Berns, M. A. Cappelli, Appl. Phys. Lett. **68**, 2711 (1996).

[81] W. Kalss, R. Haubner, B. Lux, Diam. Relat. Mat. **7**, 369 (1998).

[82] T. Ichiki, T. Momose, T. Yoshida, J. Appl. Phys. **75**, 1330 (1994).

[83] B. Deb, R. K. Roy, A. K. Pal, Phys. Status Solidi A-Appl. Res. **198**, 111 (2003).

[84] I. H. Kim, K. S. Kim, S. H. Kim, S. R. Lee, Thin Solid Films **291**, 120 (1996).

[85] A. Soltani, P. Thevenin, A. Bath, Diam. Relat. Mat. **10**, 1369 (2001); A. Soltani, P. Thevenin, A. Bath, Mater. Sci. Eng. B-Solid State Mater. Adv. Technol. **82**, 170 (2001).

[86] D. R. McKenzie, W. D. McFall, W. G. Sainty, C. A. Davis, R. E. Collins, Diam. Relat. Mat. **2**, 970 (1993).

[87] H. Hofsäss, H. Feldermann, R. Merk, M. Sebastian, C. Ronning, Appl. Phys. A-Mater. Sci. Process. **66**, 153 (1998).

[88] S. Reinke, M. Kuhr, W. Kulisch, R. Kassing, Diam. Relat. Mat. **4**, 272 (1995).

[89] Y. Lifshitz, S. R. Kasi, J. W. Rabalais, W. Eckstein, Phys. Rev. B **41**, 10468 (1990).

[90] G. Demazeau, V. Gonnet, V. Solozhenko, B. Tanguy, H. Montigaud, Comptes Rendus De L Academie Des Sciences Serie Ii **320**, 419 (1995).

[91] V. L. Solozhenko, Diam. Relat. Mat. **4**, 1 (1994).

[92] G. Will, G. Nover, J. von der Gonna, J. Solid State Chem. **154**, 280 (2000).

[93] G. Kern, G. Kresse, J. Hafner, Phys. Rev. B **59**, 8551 (1999).

[94] H. Sachdev, R. Haubner, H. Noth, B. Lux, Diam. Relat. Mat. **6**, 286 (1997).

[95] K. Albe, Phys. Rev. B **55**, 6203 (1997).

[96] S. Bohr, R. Haubner, B. Lux, Diam. Relat. Mat. **4**, 714 (1995).

[97] C. P. Klages, M. Fryda, T. Matthee, L. Schafer, H. Dimigen, Int. J. Refract. Met. Hard Mat. **16**, 171 (1998).

[98] V. L. Solozhenko, V. Z. Turkevich, W. B. Holzapfel, J. Phys. Chem. B **103**, 8137 (1999).

[99] C. S. Yoo, J. Akella, H. Cynn, M. Nicol, Phys. Rev. B **56**, 140 (1997).

[100] A. Janotti, S. H. Wei, D. J. Singh, Phys. Rev. B **6417** (2001).

[101] C. X. Wang, Q. X. Liu, G. W. Yang, Chem. Vapor Depos. **10**, 280 (2004); C. X. Wang, Y. H. Yang, Q. X. Liu, G. W. Yang, J. Phys. Chem. B **108**, 728 (2004).

[102] V. L. Solozhenko, D. Hausermann, M. Mezouar, M. Kunz, Appl. Phys. Lett. **72**, 1691 (1998).

[103] I. Bello, C. Y. Chan, W. J. Zhang, Y. M. Chong, K. M. Leung, S. T. Lee, Y. Lifshitz, Diamond and Related Materials **14**, 1154 (2005).

[104] S. Ilias, V. Stambouli, D. Bouchier, G. Nouet, Diam. Relat. Mat. **9**, 1867 (2000).

[105] S. Weissmantel, G. Reisse, Diam. Relat. Mat. **10**, 1973 (2001).

[106] A. Lousa, S. Gimeno, Diam. Relat. Mat. **10**, 1347 (2001).

[107] D. Litvinov, R. Clarke, Appl. Phys. Lett. **71**, 1969 (1997).

[108] K. S. Park, D. Y. Lee, K. J. Kim, D. W. Moon, Appl. Phys. Lett. **70**, 315 (1997).

[109] H. Feldermann, R. Merk, H. Hofsass, C. Ronning, T. Zheleva, Appl. Phys. Lett. **74**, 1552 (1999).

[110] M. Ye, M. P. Delplancke-Ogletree, Diam. Relat. Mat. **9**, 1336 (2000).

[111] D. H. Berns, M. A. Cappelli, J. Mater. Res. **12**, 2014 (1997).

[112] S. Matsumoto, W. J. Zhang, Jpn. J. Appl. Phys. Part 2 - Lett. **39**, L442 (2000).

[113] S. Matsumoto, W. J. Zhang, Jpn. J. Appl. Phys. Part 2 - Lett. **40**, L570 (2001).

[114] W. J. Zhang, S. Matsumoto, Chem. Phys. Lett. **330**, 243 (2000).

[115] A. Sherman, in: (Ed.), Chemical Vapor Deposition for Microelectronics, Noyes Publications, Park Ridge, NJ, 1987.

[116] S. Y. Shapoval, V. T. Petrashov, O. A. Popov, A. O. Westner, M. D. Yoder, C. K. C. Lok, Appl. Phys. Lett. **57**, 1885 (1990).

[117] H.V. Boenig, in: (Ed.), Plasma Science and Technology, Cornell University Press, Ithaca, p.88, 1982.

[118] D. V. Shtansky, O. Tsuda, Y. Ikuhara, T. Yoshida, Acta Mater. **48**, 3745 (2000).

[119] S. Weissmantel, G. Reisse, Thin Solid Films **356**, 256 (1999); Q. Li, L. D. Marks, Y. Lifshitz, S. T. Lee, I. Bello, Phys. Rev. B **65**, 45415 (2002).

[120] W. J. Zhang, S. Matsumoto, K. Kurashima, Y. Bando, Diam. Relat. Mat. **10**, 1881 (2001).

[121] A. Klett, R. Freudenstein, M. F. Plass, W. Kulisch, Surf. Coat. Technol. **119**, 86 (1999).

[122] T. Werninghaus, J. Hahn, F. Richter, D. R. T. Zahn, Appl. Phys. Lett. **70**, 958 (1997); R. M. Erasmus, J. D. Comins, M. L. Fish, Diam. Relat. Mat. **9**, 600 (2000).

[123] H. Hofsäss, H. Feldermann, M. Sebastian, C. Ronning, Phys. Rev. B **55**, 13230 (1997).

[124] D. M. Gruen, I. Buckley-Golder, MRS Bull. **23**, 16 (1998).

[125] C. Wild, N. Herres, P. Koidl, J. Appl. Phys. **68**, 973 (1990).

[126] W. J. Zhang, I. Bello, Y. Lifshitz, S. T. Lee, MRS Bull. **28**, 184 (2003).

[127] W. J. Zhang, S. Matsumoto, Appl. Phys. A-Mater. Sci. Process. **71**, 469 (2000).

[128] N. M. Hwang, J. H. Hahn, D. Y. Yoon, J. Cryst. Growth **160**, 87 (1996).

[129] H. Feldermann, C. Ronning, H. Hofsass, Y. L. Huang, M. Seibt, J. Appl. Phys. **90**, 3248 (2001).

[130] M. Okamoto, Y. Utsumi, Y. Osaka, Jpn. J. Appl. Phys. Part 2 - Lett. **29**, L1004 (1990).

[131] K. M. Chan, MPhil, City University of Hong Kong, 2004.

[132] C. Sun, W. J. Zhang, N. Wang, C. Y. Chan, I. Bello, C. S. Lee, S. T. Lee, J. Appl. Phys. **88**, 3354 (2000).

[133] J. Pascallon, V. Stambouli, S. Ilias, D. Bouchier, G. Nouet, F. Silva, A. Gicquel, Diam. Relat. Mat. **8**, 325 (1999); J. Pascallon, V. Stambouli, S. Ilias, D. Bouchier, G. Nouet, F. Silva, A. Gicquel, Mater. Sci. Eng. B-Solid State Mater. Adv. Technol. **59**, 239 (1999).

[134] X. W. Zhang, H. G. Boyen, N. Deyneka, P. Ziemann, F. Banhart, M. Schreck, Nat. Mater. **2**, 312 (2003).

[135] R. A. Zuhr, S. J. Pennycook, T. S. Noggle, N. Herbots, T. E. Haynes, B. R. Appleton, Nucl. Instrum. Methods Phys. Res. Sect. B-Beam Interact. Mater. Atoms **37-8**, 16 (1989); J. W. Rabalais, A. H. Albayati, K. J. Boyd, D. Marton, J. Kulik, Z. Zhang, W. K. Chu, Phys. Rev. B **53**, 10781 (1996); T. A. Wagner, L. Oberbeck, R. B. Bergmann, Mater. Sci. Eng. B-Solid State Mater. Adv. Technol. **89**, 319 (2002).

[136] W. J. Zhang, X. Jiang, S. Matsumoto, Appl. Phys. Lett. **79**, 4530 (2001).

[137] Y. Lifshitz, T. Kohler, T. Frauenheim, I. Guzmann, A. Hoffman, R. Q. Zhang, X. T. Zhou, S. T. Lee, Science **297**, 1531 (2002).

[138] C. Iwamoto, H. S. Yang, T. Yoshida, Diam. Relat. Mat. **11**, 1854 (2002).

[139] H. S. Yang, C. Iwamoto, T. Yoshida, J. Appl. Phys. **91**, 6695 (2002).

[140] L. Nistor, V. Teodorescu, C. Ghica, J. Van Landyut, G. Dinca, P. Georgeoni, Diam. Relat. Mat. **10**, 1352 (2001).

[141] C. Collazo-Davila, E. Bengu, C. Leslie, L. D. Marks, Appl. Phys. Lett. **72**, 314 (1998); C. Collazo-Davila, E. Bengu, L. D. Marks, M. Kirk, Diam. Relat. Mat. **8**, 1091 (1999).

[142] C. H. Ma, J. H. Huang, H. D. Chen, Thin Solid Films **446**, 184 (2004).

[143] X. Jiang, W. J. Zhang, C. P. Klages, Phys. Rev. B **58**, 7064 (1998).

[144] X. Jiang, K. Helming, W. J. Zhang, S. Matsumoto, Chem. Vapor Depos. **8**, 262 (2002).

[145] S. Watanabe, S. Miyake, W. L. Zhou, Y. Ikuhara, T. Suzuki, M. Murakawa, Appl. Phys. Lett. **66**, 1478 (1995); H. Luthje, K. Bewilogua, S. Daaud, M. Johansson, L. Hultman, Thin Solid Films **257**, 40 (1995).

[146] W. L. Zhou, Y. I. Ikuhara, T. Suzuki, Appl. Phys. Lett. **67**, 3551 (1995).

[147] M. Keunecke, K. Yamamoto, K. Bewilogua, Thin Solid Films **398**, 142 (2001).

[148] H. S. Yang, C. Iwamoto, T. Yoshida, J. Appl. Phys. **95**, 2337 (2004).

[149] H. Hofsäss, H. Feldermann, S. Eyhusen, C. Ronning, Phys. Rev. B **65** (2002).

[150] K. Larsson, J. O. Carlsson, J. Phys. Chem. B **103**, 6533 (1999); B. Marlid, K. Larsson, J. O. Carlsson, Phys. Rev. B **60**, 16065 (1999).

[151] H. Hofsäss, S. Eyhusen, C. Ronning, Diam. Relat. Mat. **13**, 1103 (2004).

[152] Z. Dai, C. Bednarski-Meinke, R. Loloee, B. Golding, Appl. Phys. Lett. **82**, 3847 (2003); M. Schreck, H. Roll, B. Stritzker, Appl. Phys. Lett. **74**, 650 (1999).

[153] J. Isberg, J. Hammersberg, E. Johansson, T. Wikstrom, D. J. Twitchen, A. J. Whitehead, S. E. Coe, G. A. Scarsbrook, Science **297**, 1670 (2002).

[154] S. T. Lee, Z. D. Lin, X. Jiang, Mater. Sci. Eng. R-Rep. **25**, 123 (1999).

[155] P. B. Mirkarimi, K. F. McCarty, G. F. Cardinale, D. L. Medlin, D. K. Ottesen, H. A. Johnsen, J. Vac. Sci. Technol. A-Vac. Surf. Films **14**, 251 (1996).

[156] P. Masri, V. Mortet, M. R. Laridjani, M. Averous, Comput. Mater. Sci. **17**, 520 (2000).

[157] T. Ikeda, Y. Kawate, Y. Hirai, J. Vac. Sci. Technol. A-Vac. Surf. Films **8**, 3168 (1990).

[158] W. Kulisch, R. Freudenstein, A. Klett, M. F. Plass, Thin Solid Films **377-8**, 170 (2000).

[159] A. S. Rozenberg, Y. A. Sinenko, N. V. Chukanov, J. Mater. Sci. **28**, 5675 (1993).

[160] M. Kuhr, S. Reinke, W. Kulisch, Diam. Relat. Mat. **4**, 375 (1995).

[161] J. F. Ziegeler, J. P. Biersack, U. Littmark, in: (Ed.), The stopping and range of ions in solids, Pergamon, New York, 1985.

[162] C. Bostedt, T. van Buuren, T. M. Willey, N. Franco, L. J. Terminello, C. Heske, T. Moller, Appl. Phys. Lett. **84**, 4056 (2004); T. van Buuren, L. N. Dinh, L. L. Chase, W. J. Siekhaus, L. J. Terminello, Phys. Rev. Lett. **80**, 3803 (1998).

[163] D. H. Berns, M. A. Cappelli, D. K. Shuh, Diam. Relat. Mat. **6**, 1883 (1997).

[164] R. A. Rosenberg, P. J. Love, V. Rehn, Phys. Rev. B **33**, 4034 (1986).

[165] A. Chaiken, L. J. Terminello, J. Wong, G. L. Doll, C. A. Taylor, Appl. Phys. Lett. **63**, 2112 (1993).

[166] I. Jimenez, A. F. Jankowski, L. J. Terminello, D. G. J. Sutherland, J. A. Carlisle, G. L. Doll, W. M. Tong, D. K. Shuh, F. J. Himpsel, Phys. Rev. B **55**, 12025 (1997).

[167] O. Tsuda, Y. Tatebayashi, Y. YamadaTakamura, T. Yoshida, J. Vac. Sci. Technol. A-Vac. Surf. Films **15**, 2859 (1997); P. Y. Jouan, G. Lemperiere, Vacuum **45**, 89 (1994).

[168] X. T. Zhou, Q. Li, F. Y. Meng, I. Bello, C. S. Lee, S. T. Lee, Y. Lifshitz, Appl. Phys. Lett. **80**, 3307 (2002).

[169] J. Y. Raty, G. Galli, C. Bostedt, T. W. van Buuren, L. J. Terminello, Phys. Rev. Lett. **90** (2003).

[170] M. Murakawa, S. Watanabe, Surf. Coat. Technol. **43-4**, 128 (1990); T. Wada, N. Yamashita, J. Vac. Sci. Technol. A-Vac. Surf. Films **10**, 515 (1992); S. Nishiyama, N. Kuratani, A. Ebe, K. Ogata, Nucl. Instrum. Methods Phys. Res. Sect. B-Beam Interact. Mater. Atoms **80-1**, 1485 (1993).

[171] D. R. McKenzie, J. Vac. Sci. Technol. B **11**, 1928 (1993); W. Dworschak, K. Jung, H. Ehrhardt, Diam. Relat. Mat. **3**, 337 (1994); Y. Yamada, O. Tsuda, T. Yoshida, Thin Solid Films **316**, 35 (1998).

[172] P. B. Mirkarimi, D. L. Medlin, K. F. McCarty, D. C. Dibble, W. M. Clift, J. A. Knapp, J. C. Barbour, J. Appl. Phys. **82**, 1617 (1997).

[173] W. J. Zhang, S. Matsumoto, Q. Li, I. Bello, S. T. Lee, Adv. Funct. Mater. **12**, 250 (2002).

[174] T. Y. Tsui, G. M. Pharr, J. Mater. Res. **14**, 292 (1999).

[175] S.V. Hainsworth, T.F. Page, in: W.W. Gerberich, H. Gao, J.E. Sundgren, and S.P. Baker (Eds.) Materials Research Society Symposium Proceedings,Vol. **436**, Materials Research Society, Pittsburgh, p.171, (1997).

[176] C.A. Brookes, in: J.E. Field (Ed.), The Properties of Natural and Synthetic Diamond, Academic Press, London, p.515, 1992.

[177] M. P. D'Evelyn, T. Taniguchi, Diam. Relat. Mat. **8**, 1522 (1999).

[178] W. J. Zhang, S. Matsumoto, Phys. Rev. B **63**, 73201 (2001).

[179] S. Veprek, A. S. Argon, Surf. Coat. Technol. **146**, 175 (2001).

[180] E. Martínez, J. L. Andújar, M. C. Polo, J. Esteve, J. Robertson, W. I. Milne, Diam. Relat. Mat. **10**, 145 (2001).

[181] J. M. Sánchez, S. El-Mansy, B. Sun, T. Scherban, N. Fang, D. Pantuso, W. Ford, M. R. Elizalde, J. M. Martínez-Esnaola, A. Martín-Meizoso, J. Gil-Sevillano, M. Fuentes, J. Maiz, Acta Mater. **47**, 4405 (1999).

[182] M. Okamoto, Y. Utsumi, Y. Osaka, Jpn. J. Appl. Phys. Part 1 - Regul. Pap. Short Notes Rev. Pap. **31**, 3455 (1992).

[183] M. Kumagai, M. Suzuki, T. Suzuki, Y. Tanaka, Y. Setsuhara, S. Miyake, K. Ogata, M. Kohata, K. Higeta, T. Einishi, Y. Suzuki, Y. Shimoitani, Y. Motonami, Nucl. Instrum. Methods Phys. Res. Sect. B-Beam Interact. Mater. Atoms **127**, 977 (1997).

[184] Y. Setsuhara, M. Kumagai, M. Suzuki, T. Suzuki, S. Miyake, Surf. Coat. Technol. **119**, 100 (1999).
[185] K. Watari, S. L. Shinde, MRS Bull. **26**, 440 (2001).
[186] M. Yokogawa, K. Yokogawa, H. Honma, Int. J. Jpn. Soc. Precis. Eng. **31**, 187 (1997).
[187] E. Cappelli, S. Orlando, G. Mattei, A. Armigliato, Surf. Coat. Technol. **180-81**, 184 (2004).
[188] R. Haubner, A. Lindlbauer, B. Lux, Diam. Relat. Mat. **2**, 1505 (1993).
[189] J. Yu, S. Matsumoto, J. Mater. Res. **19**, 1408 (2004).
[190] K. Yamamoto, M. Keunecke, K. Bewilogua, Thin Solid Films **377**, 331 (2000); K. Bewilogua, M. Keunecke, K. Weigel, E. Wiemann, Thin Solid Films **469-70**, 86 (2004).

List of publications

I. Papers in international referred journals

1. K.M Leung, **C.Y. Chan**, Y.M. Chong, Y. Yao, K.L. Ma, I. Bello, W.J Zhang & S.T Lee, *Studying the growth of cubic boron nitride on amorphous tetrahedral carbon interlayers*, Journal of Physical Chemistry (2005), in Press.

2. Y.M. Chong, K.L. Ma, K.M. Leung, **C.Y. Chan**, I. Bello, W.J. Zhang, and S.T. Lee, *The synthesis and mechanical properties of cubic boron nitride /nanodiamond composite films,* Chemical Vapor Deposition (2005), Submitted.

3. I.Bello, Y.M. Chong, K.M. Leung, **C.Y. Chan**, K.L. Ma, W.J. Zhang, S.T. Lee, A. Layyous, *Cubic boron nitride films for industrial applications*, Diamond Related Materials (2005), Submitted.

4. X.T. Zhou, T.K. Sham, W.J. Zhang, **C.Y. Chan**, I. Bello, S.T. Lee & Hofsäss, *Cubic phase content and structure of BN films from an X-ray absorption study,* in Preparation.

5. X.T. Zhou, T.K. Sham, W.J. Zhang, **C.Y. Chan**, I. Bello, S.T. Lee & Hofsäss, *X-ray absorption studies on cubic boron nitride thin films*, Physical Review B (2005), Submitted.

6. X.T. Zhou, T.K. Sham, **C.Y. Chan**, W.J. Zhang, I. Bello, S.T. Lee & Hofsäss, *Effect of substrate surface on the structure and electronic properties of cubic boron nitride films*, Journal of Applied Physics (2005), Submitted.

7. W.J. Zhang, **C.Y. Chan**, K.M. Chan, X.M. Meng, Y. Wu, I. Bello & S.T. Lee, *An interface study on the cubic boron nitride films deposited on diamond*, Journal of Physical Chemistry B (2005), in Press.

8. W.J. Zhang, **C.Y. Chan**, X.M. Meng, M.K. Fung, I. Bello, Y. Lifshitz, S.T. Lee & X. Jiang, *The mechanism of chemical vapor deposition of cubic boron nitride films from fluorine-containing species*, Angewandte Chemie International Edition (2005), in Press.

9. **C.Y. Chan**, S. Eyhusen, X.M. Meng, I. Bello S.T. Lee, C. Ronning & H. Hofsäss, *The effect of surface roughness on phase purity of cubic boron nitride films*, Diamond and Relation Materials (2005), in Press.

10. I. Bello, **C.Y. Chan**, W.J. Zhang, Y.M. Chong, K.M. Leung, S.T. Lee & Y. Lifshitz,

Deposition of thick cubic boron nitride films: The route to practical applications, Diamond and Related Materials **14**, 1154 (2005)

11. W.J. Zhang, Y. Wu, **C.Y. Chan**, W.K. Wong, X.M. Meng, I. Bello, Y. Lifshitz & S.T. Lee, *Structuring single- and nano-crystalline diamond cones*, Diamond and Related Materials **13**, 1037 (2004).

12. P.W. Shum, Z.F. Zhou, K.Y. Li & **C.Y. Chan**, *Mechanical and tribological properties of amorphous carbon films deposited on implanted steel substrates*, Thin Solid Film **458**, 203 (2004).

13. W.J. Zhang, I. Bello, Y. Lifshitz, K.M. Chan, Y. Wu, **C.Y. Chan**, X.M. Meng & S.T. Lee, *Thick and adherent cubic boron nitride films grown on diamond interlayers by fluorine-assisted chemical vapour deposition,* Applied Physics Letters **85,** 1344 (2004).

14. W.J. Zhang, I. Bello, Y. Lifshitz, K.M. Chan, X.M. Meng, Y. Wu, **C.Y. Chan** & S.T. Lee, *Epitaxy on diamond by CVD, The route to high-quality cBN for electronic applications*, Advanced Materials **16**, 1405 (2004).

15. **C.Y. Chan**, W.J. Zhang, S. Matsumoto, I. Bello & S.T. Lee, *A nanoindentation study of thick cBN films prepared by chemical vapor deposition*, Journal of Crystal Growth **247**, 438 (2003).

16. **C.Y. Chan**, W.J. Zhang, X.M. Meng, K.M. Chan, I. Bello, Y. Lifshitz & S.T. Lee, *The growth of thick cBN films employing fluorine chemistry and ECR deposition*, Diamond and Related Materials **12**, 1162 (2003).

17. **C.Y. Chan**, W.J. Zhang, K.M. Chan, I. Bello & S.T. Lee, *Synthesis of boron nitride films using electron cyclotron resonance microwave plasma and an H_2-BF_3-N_2-Ar-He gas system*, Chemical Vapor deposition **9**, 181 (2003).

18. W.J. Zhang, **C.Y. Chan**, K.M. Chan, I. Bello, Y. Lifshitz & S.T. Lee, *Deposition of large-area, high quality cubic boron nitride by ECR-enhanced microwave CVD*, Applied Physics A: Materials Science and Processing **76**, 953 (2003).

19. K.W. Lee, Y.W. Chung, **C.Y. Chan**, I. Bello, S. T. Lee, A. Karimi, J. Patscheider, M.P. Delplancke-Olgetree, D. Yang, B. Boyce & T. Buchheit, *An international round-robin experiment to evaluate the consistency of nanoindentation hardness measurement of thin films*, Surface and Coatings Technology **57**, 168 (2003).

20. W.J. Zhang, X.M. Meng, **C.Y. Chan**, Y. Wu, I. Bello & S.T. Lee, *Oriented single crystal diamond cones and their arrays*, Applied Physics Letters **82**, 2622 (2003)

21. W.J. Zhang, Y. Wu, W.K. Wong, X.M. Meng, **C.Y. Chan**, I. Bello, Y. Lifshitz & S.T. Lee, *Structuring nano-diamond cone arrays for improved field emission*, Applied Physics Letters **83**, 3365 (2003).

22. I. Bello, W. J. Zhang, K.M. Chan, **C.Y. Chan**, Y. Wu, F. Meng, C.W. Lam, L. Liu, W. Y. Luk, *Diamond and cubic boron nitride: synthesis and electronic applications*, Proceed. Internat. Conf. Semiconductor Devices and Microsystems, Eds. J. Breza and D. Donoval, Smolenice, Slovakia 1992 pp 1-11, ISBN 0-7803-7276-X.

23. **C.Y. Chan**, K.H. Lai, M.K. Fung, W.K. Wong, I. Bello, R.F. Huang, C.S. Lee, S.T. Lee & S.P. Wong, *Deposition and properties of tetrahedral carbons prepared on magnetic hard disks,* Journal of Vacuum Science and Technology A **19(4)**, 1606 (2001).

24. K.H. Lai, **C.Y. Chan**, M.K. Fung, I. Bello, C.S. Lee & S.T. Lee, *Mechanical Properties of DLC Films Prepared in Acetylene and Methane Plasma using Electron Cyclotron Resonance Microwave Plasma Chemical Vapor Deposition,* Diamond and Related Materials **10**, 1862 (2001).

25. J. Qi, **C.Y. Chan**, I. Bello, C.S. Lee, S.T. Lee, J.B. Luo & S.Z. Wen, *Film thickness effects on mechanical and tribological properties of nitrogenated diamond-like carbon films*, Surface and Coatings Technology **145**, 38 (2001).

26. R.F. Huang, **C.Y. Chan**, C.H. Lee, J. Gong, K.H. Lai, C.S. Lee, K.Y. Li, L.S. Wen & C. Sun, *Wear-resistant multilayered diamond-like carbon coating prepared by pulse biased arc ion plating,* Diamond and Related Materials **10**, 1850 (2001).

27. K.Y. Li Z.F. Zhou, **C.Y. Chan**, I. Bello, C.S. Lee & S.T. Lee, *Mechanical and tribological properties of diamond-like carbon films prepared on steel by ECR-CVD process*, Diamond and Related Materials **10**, 1855 (2001).

28. N.G. Shang, C.H. Lee, X.T. Zhou, F.Y. Meng, **C.Y. Chan**, S.T. Lee & I. Bello, *Investigation of diamond film deposition on steel without and with ion beam nitriding pretreatment*, Journal of Vacuum Science and Technology A **19(6)**, 2969 (2001).

29. M.K. Fung K.H. Lai, **C.Y. Chan**, I. Bello, C.S. Lee, S.T. Lee, D.S. Mao & X. Wang, *Mechanical properties and corrosion studies of amorphous carbon on magnetic disks prepared by ECR plasma technique*, Thin Solid Films **368**, 198 (2000).

30. M.K. Fung, K.H. Lai, H.L. Lai, **C.Y. Chan**, N.B. Wong, I. Bello, C.S. Lee & S.T. Lee, *Diamond-like carbon coatings applied to hard disks,* Diamond and Related Materials **9**, 815 (2000).

31. C. Sun, W.J. Zhang, N. Wang, **C.Y. Chan**, I. Bello, C.S. Lee & S.T. Lee, *Crystal morphology and phase purity of diamond crystallites during bias enhanced nucleation and initial growth stages,* Journal of Applied Physics **8**, 3355 (2000).

II. Patents

1. S.T. Lee, I. Bello, W.J. Zhang & **C.Y. Chan**, *Fabrication of single crystal diamond tips and their arrays,* United States – Patent Application Publication, US2004 0079280, (2004).

III. Conference papers

1. I. Bello, Y.M. Chong, K.M. Leung, **C.Y. Chan**, K.L. Ma, W.J. Zhang, S.T. Lee & A. Layyous, *Cubic boron nitride films for industrial applications*, The 10th international conference on new diamond science and technology, 11-14 May, 2005, Tsukuba, Japan.

2. A.C. Ferrari, S. Reich, C. Casiraghi, R. Arenal de la Concha, A. Loiseau, R. Gago, B. Abendroth, W.J. Zhang, **C.Y. Chan**, I. Bello & J. Robertson, *UV Raman spectroscopy of boron nitrides,* 15th European conference on diamond, diamond-like carbon material and carbon nanotubes, nitrides & carbide, 12-17 September, 2004, Italy.

3. I. Bello, W.J.Zhang, **C.Y. Chan**, Y. Lifshitz & S.T. Lee, *Deposition of thick cubic boron nitride films: Route to practical applications,* 15th European conference on diamond, diamond-like carbon material and carbon nanotubes, nitrides & carbide, 12-17 September, 2004, Italy. (Invited)

4. W.J. Zhang, **C.Y. Chan**, I. Bello & S.T. Lee, *Deposition and characterization of thick cBN films prepared by CVD methods,* International conference on Metallurgical coatings and thin films, 19-23 April 2004, Boston, USA.

5. I. Bello, W.J. Zhang, K.M. Chan, Y. Wu, **C.Y. Chan**, Y. Lifshitz & S.T. Lee, *Synthesis of adherent cubic boron nitride-diamond composite films*, 14th European conference on diamond, diamond-like materials, carbon nanotubes, nitrides & silicon carbide, 7-12 September, Salzburg, Austria.

6. W.J. Zhang, Y. Wu, **C.Y. Chan**, X.M. Meng, W.K. Wong, I. Bello, Y. Lifshitz & S.T. Lee, *The synthesis of single crystalline and nano-diamond cones,* 14th European

conference on diamond, diamond-like materials, carbon nanotubes, nitrides & silicon carbide, 7-12 September, Salzburg, Austria.

7. W.J. Zhang, **C.Y. Chan**, S. Matsumoto I. Bello & S.T. Lee, *A nano-indentation of thick cubic boron nitride films prepared by chemical vapor deposition,* 14th European conference on diamond, diamond-like materials, carbon nanotubes, nitrides & silicon carbide, 7-12 September, Salzburg, Austria.

8. Y. Wu, W.J. Zhang, **C.Y. Chan**, X.M. Meng, W.K. Wong, I. Bello, Y. Lifshitz & S.T. Lee, *Novel diamond cone arrays: single crystalline and nanocrystalline,* Applied diamond conference and Frontier carbon technology joint conference 2003, 18-21 August, Tsukuba, Japan.

9. **C.Y. Chan**, W.J. Zhang, K.M. Chan, S. Matsumoto, I. Bello, & S.T. Lee, *A nano-indentation study of thick cBN films prepared by chemical vapor deposition,* Applied diamond conference and Frontier carbon technology joint conference 2003, 18-21 August, Tsukuba, Japan.

10. W.J. Zhang, **C.Y. Chan**, X.Meng, I. Bello, Y. Lifshitz & S.T. Lee, *The growth species in synthesis of cBN films by ECR-enhanced microwave plasma CVD in a He(Ar)/N_2/BF_3/H_2 gas system,* 8th International conference on new diamond science and technology, 21-26 July 2002, The University of Melbourne, Australia.

11. **C.Y. Chan**, W.J. Zhang, X.M. Meng, K.M. Chan, Y. Lifshitz, S.T. Lee, I. Bello, *Fluorine chemistry applied to form thick (>1μm) cBN films by ECR*, 8th International conference on new diamond science and technology, 21-26 July 2002, The University of Melbourne, Australia.

12. K. M. Chan, **C.Y. Chan**, W.J. Zhang, Y. Lifshitz, S.T. Lee & I. Bello, *Reducing the stress of cBN films in magnetron sputtering deposition*, Diamond 2002 – 13th European conference on diamond, diamond-like materials, carbon nanotubes, nitrides, & silicon carbide, 8-13 September 2002, Granada, Spain.

13. I. Bello, W.J. Zhang, K.M. Chan, **C.Y. Chan**, Y. Wu, F. Meng, C.W. Lam, W.Y. Luk, *Diamond and cubic boron nitride synthesis and electronic applications*, The 4th international conference on advanced semiconductor devices and Microsystems, 14-16 October 2002, Smolenice Castle, Slovakia.

14. W.J. Zhang, **C.Y. Chan** & S.T. Lee, *The synthesis of cubic boron nitride films by ECR-enhanced microwave plasma CVD: a chemical or a physical method,* The 9th international symposium on advanced materials (ISAM2002), 3-7 March, 2002, Tsukuba, Japan.

15. **C.Y. Chan**, K.H. Lai, M.K. Fung, C.S. Lee, S.T. Lee & I. Bello, *Investigation of tetrahedral amorphous carbons prepared on magnetic hard disks,* International conference on Materials for Advanced Technologies, 1-6 July, 2001, Singapore.

16. N.G. Shang, F.Y. Meng, **C.Y. Chan**, Q. Li, C.S. Lee, S.T. Lee & I. Bello, *Diamond grown on steel via in-situ formed interlayers,* International conference on Materials for Advanced Technologies, 1-6 July, 2001, Singapore.

17. **C.Y. Chan**, K.H. Lai, M.K. Fung, W.K. Wong, I. Bello, R.F. Huang, C.S. Lee, S.T. Lee & S.P. Wong, *Deposition and Properties of Tetrahedral Carbon Films Prepared on Magnetic Hard Disks,* American Vacuum Society 47th International Symposium, 2-6 October 2000, USA.

18. K.H. Lai, **C.Y. Chan**, M.K. Fung, I. Bello, C.S. Lee & S.T. Lee, *Mechanical Properties of DLC Films Prepared in Acetylene and Methane Plasma using Electron Cyclotron Resonance Microwave Plasma Chemical Vapor Deposition* The 7th International Conference of New Diamond Science and Technology (ICNDST-7), 23-28 July 2000, Hong Kong.

19. R.F. Huang, **C.Y. Chan**, K.H. Lai, K.Y. Li, I. Bello, C.S. Lee, S.T. Lee & L.S. Wen, *Diamond-like carbon coatings on aluminium alloy substrates*¸ The 7th International Conference of New Diamond Science and Technology (ICNDST-7), 23-28 July 2000, Hong Kong.

20. R.F. Huang, **C.Y. Chan**, Z.F. Zhou, K.Y. Li, I. Bello, C.S. Lee & S.T. Lee, *Large-scale fabrication of wear resistant TiN coatings on polymers by pulsed arc ion plating,* The 7th International Conference of New Diamond Science and Technology (ICNDST-7), 23-28 July 2000, Hong Kong.

21. K.Y. Li, R.F. Huang, J. Gong, **C.Y. Chan**, Z.F. Zhou, I. Bello, C.S. Lee, S.T. Lee, L.S. Wen & C. Sun, *Microstructure and tribological properties of CNx/DLC composite coatings,* The 7th International Conference of New Diamond Science and Technology (ICNDST-7), 23-28 July 2000, Hong Kong.

22. K.Y. Li, R.F. Huang, J. Gong, **C.Y. Chan**, Z.F. Zhou, Bello, C.S Lee, S.T. Lee, L.S. Wen, and C. Sun, *Wear- and oxidation-resistant (Ti,Al)N coatings prepared by pulse biased vacuum arc ion plating,* The 7th International Conference of New Diamond Science and Technology (ICNDST-7), 23-28 July 2000, Hong Kong.

23. **C.Y. Chan**, K. H Lai, M.K. Fung, J. Gun, I. Bello, C.S. Lee & S.T. Lee, S.P. Wong, *Properties of tetrahedral carbon prepared on magnetic hard disks,* The 7th International Conference of New Diamond Science and Technology (ICNDST-7), 23-28 July 2000, Hong Kong.

Studying the growth of cubic boron nitride on amorphous tetrahedral carbon interlayers

K.M. Leung, **C.Y Chan**, Y.M. Chong, Y. Yao, K.L. Ma, I. Bello, W.J Zhang, S.T. Lee

Center Of Super-Diamond and Advanced Films (COSDAF), Department of Physics and Materials Science, City University of Hong Kong, Hong Kong SAR, PR China

Abstract

The growth of cubic boron nitride (cBN) films on bare silicon and amorphous tetrahedral carbon (ta-C) layers prepared on silicon substrates was studied. The cBN films were prepared by radio-frequency magnetron sputter-deposition at ~870 °C. The original ta-C interlayers were graphitized and restructured under high temperature and possibly ion bombardment during BN deposition. The majority of graphitic basal planes were nearly perpendicular to the surface of silicon substrates. The BN films grown on these restructured carbon layers were deposited with higher content of cubic phase and did not show delamination signs. Turbostratic BN (tBN) basal planes extended carbon basal planes and their edges served as cBN nucleation sites. The cBN films grown on textured ta-C interlayers were insensitive to the ambient environment. The residual sp^3-bonded carbon phase confined in the interlayers probably acts as a diffusion barrier preventing the oxidation of dangling bonds near BN interface and thus precludes weakening the interface as a result of volume expansion. The carbon interlayers also improve the crystallinity of the oriented tBN because they are continuation of carbon graphitic basal planes so that the volume fraction of nitrogen-void (N-void) defects in the sp^2-bonded BN intermediate layers is reduced. The strong sp^3-bonded carbon matrix could thereto withstand large compressive stress and facilitates deposition of thicker cBN films.

The synthesis and mechanical properties of cubic boron nitride /nanodiamond composite films

Y.M. Chong, K.L. Ma, K.M. Leung, C.Y. Chan, I. Bello, W.J. Zhang, and S.T. Lee

Center Of Super-Diamond and Advanced Films (COSDAF), Department of Physics and Materials Science, City University of Hong Kong, Hong Kong SAR, PR China

Abstract

Large-area cubic boron nitride (cBN)/nanodiamond (ND) composite films were deposited on silicon substrates using two plasma processes: (i) the ND layer with thickness of 3 μm were prepared by conventional plasma enhanced chemical vapour deposition (PECVD) and (ii) the top cBN layer with thickness of 3.6 μm was grown using electron cyclotron resonance (ECR) MPCVD assisted with fluorine chemistry and low kinetic energy of ions induced at a substrate bias of –30 V. These thick films are smooth and well adherent to the silicon substrate. Although cBN grew on ND layer the cBN crystallites are enlarged when compared to those of cBN structure and cBN films yield sharp and well resolved Raman peaks when spectral acquisition is in the cross-sectional direction. Because of the strengthen adhesion and mechanical properties by layer structure and their smooth surface the film could be used in mechanical and some device applications.

Cubic boron nitride films for industrial applications

I.Bello[a], Y.M. Chong[a], K.M. Leung[a], **C.Y. Chan**[a], K.L. Ma[a], W.J. Zhang[a], S.T. Lee[a], A. Layyous[b]

[a] *Center Of Super-Diamond and Advanced Films (COSDAF), Department of Physics and Materials Science, City University of Hong Kong, Hong Kong SAR, PR China*

[b] *R&D Materials, ISCAR Ltd, Tefen, Israel.*

Abstract

The effects of kinetic energy, chemical nature of substrates and temperature on the synthesis of cBN films are explored to obtain cBN films with industrial quality. Carbon including amorphous carbon, nanocrystalline and polycrystalline diamond enables deposition of stable, thick and adherent cBN films characteristic with cBN Raman peaks. Although temperature has been designated as unimportant parameter the higher cBN quality is obtained at higher temperature. Cutting WC inserts were deposited via polycrystalline diamond at 800 °C by plasma enhanced chemical vapor deposition (PECVD). The quality of cBN films grown by PECVD is considerably better than the films prepared by physical vapor deposition (PVD) being caused by the lower kinetic energies of particles used in PECVD. As a result, growth mechanism is surface process which differs from the growth models previously proposed.

Cubic phase content and structure of BN films from an X-ray absorption study

X.T. Zhou[a], T.K. Sham[a], W.J. Zhang[b], C.Y. Chan[b], I. Bello[b], S.T. Lee[b], H. Hofsäss[c]

[a]*Department of Chemistry, University of Western Ontario, London, ON Canada N6A 5B7*

[b] *Center Of Super-Diamond and Advanced Films (COSDAF), Department of Physics and Materials Science, City University of Hong Kong, Hong Kong SAR, PR China*

[c] *II. Institute of Physics, University of Göttingen, Friedrich-Hund-Platz 1, D-37077, Göttingen, Germany*

Abstract

From the X-ray absorption near-edge spectroscopies (XANES) both in total electron yield (TEY) and in fluorescence yield (FY) at the B and N K-edge of the mixtures consisting of hexagonal boron nitride (hBN) powders and cubic boron nitride (cBN) powders with various phase ratios, the relationship between the shape of XANES, e.g. the relative intensity of some specific peaks corresponding to hBN and cBN respectively, and the phase content ratio has been established experimentally. Based on the above calibration results, the cubic phase content in some boron nitride (BN) thin films prepared by various physical vapor deposition (PVD) or plasma enhanced chemical vapor deposition (PECVD) both at the film surface and in the whole film has been determined quantitatively and the structure of the thin films deduced. Compared to their values estimated by Fourier transform infrared spectroscopy (FTIR) technique, we suggest that the cubic phase content in BN thin films by FTIR technique is overestimated significantly.

X-ray absorption studies on cubic boron nitride thin films

X.T. Zhou[a], T.K. Sham[a], W.J. Zhang[b], C.Y. Chan[b], I. Bello[b], S.T. Lee[b], H. Hofsäss[c]

[a]*Department of Chemistry, University of Western Ontario, London, ON Canada N6A 5B7*

[b] *Center Of Super-Diamond and Advanced Films (COSDAF), Department of Physics and Materials Science, City University of Hong Kong, Hong Kong SAR, PR China*

[c] *II. Institute of Physics, University of Göttingen, Friedrich-Hund-Platz 1, D-37077, Göttingen, Germany*

Abstract

Cubic boron nitride (cBN) films synthesized by various energetic species assisted physical vapor deposition (PVD) and chemical vapor deposition (CVD) techniques on Si and diamond-coated Si substrates have been investigated by boron K-edge angle-resolved X-ray absorption near-edge spectroscopy (XANES) in both total electron yield (TEY) and fluorescence yield (FY) modes. A quantificational method based on X-ray absorption studies has been established to determine the film structure, the quantity and distribution of the partially-ordered turbostratic (tBN) and amorphous (aBN) sp^2-hybridized BN phases, and the tBN/aBN ratios. The preferable direction of the tBN basal planes at the interface between cBN and substrate is dependent on the nature of the substrates. For Si substrates, a layered structure of aBN/tBN/cBN is revealed, and the tBN is well aligned with their (0002) basal planes normal to the substrate surface. On the contrary, for diamond-coated Si substrates, an aBN layer is absent and the tBN planes inclined to the substrate surface by about 60°. The content of the sp^2-bonded BN in the cBN films deposited on diamond-coated Si substrates reduces remarkably due to a much lower threshold of the ion energy for the formation of cBN than that on Si substrates. Rougher substrate surfaces are harmful to the formation of cBN films with high phase purity because of the broadening of ion energy distribution and the re-deposition of sputtered species. The change of the electronic structure of the PVD cBN films with respect to buck cBN has been investigated and the crystallinity of cBN films has also been evaluated from the XANES plots.

Effect of substrate surface on the structure and electronic properties of cubic boron nitride films

X.T. Zhou[a], T.K. Sham[a], C.Y. Chan[b], W. J. Zhang[b], I. Bello[b], S.T. Lee[b], H. Hofsäss[c]

[a]*Department of Chemistry, University of Western Ontario, London, ON Canada N6A 5B7*

[b] *Center Of Super-Diamond and Advanced Films (COSDAF), Department of Physics and Materials Science, City University of Hong Kong, Hong Kong SAR, PR China*

[c] *II. Institute of Physics, University of Göttingen, Friedrich-Hund-Platz 1, D-37077, Göttingen, Germany*

Abstract

Cubic boron nitride (cBN) films were prepared by mass-selected ion beam deposition (MSIBD) technique. The effects of substrate surface roughness were investigated by boron and nitrogen K-edge X-ray absorption near-edge spectroscopy (XANES), X-ray diffraction (XRD) and atomic force microscopy (AFM). All the films are a mixture of nanocrystalline cubic BN (cBN) and hexagonal BN (hBN) phases. The ratio of cBN in the films decreases with increasing substrate surface roughness. A significant large lattice contraction of the cBN crystallites in the films, relative to the bulk, is observed. It is also found that the electronic structure of nanocrystalline cBN films by MSIBD technique is somewhat different from that of microcrystalline cBN. We attribute the effect of the nature of the substrate on the morphology and structure of the cBN films to the orientation of hBN basal plane on the top surface of the films during their growth, and the lattice contraction and energy band structure change of cBN films to the large compressive stress, respectively.

An interface study on the cubic boron nitride films deposited on diamond

W.J. Zhang, C.Y. Chan, K.M. Chan, X.M. Meng, Y. Wu, I. Bello, and S.T. Lee

Center Of Super-Diamond and Advanced Films (COSDAF), Department of Physics and Materials Science, City University of Hong Kong, Hong Kong SAR, PR China

Abstract

The nucleation and growth of cubic boron nitride (cBN) films deposited on silicon and diamond coated silicon substrates utilizing fluorine chemistry-assisted chemical vapor deposition (CVD) were studied comparatively. The incubation layer, amorphous/turbostratic BN, essential for the nucleation of cBN on silicon substrate was not observed, indicating that the nucleation step of cBN on diamond was skipped. An intensively reduced critical bias voltage (down to −10 V) to maintain the cBN growth was revealed. Twinning crystal orientation relation and small angle grain boundaries were observed between cBN and underlying diamond crystallites due to a slight lattice mismatch between cBN and diamond (cBN larger by 1.34%). The seamless epitaxy of cBN on diamond was found being associated with the stress formation at the interface region. A higher bias voltage at the initial growth stage is recommended to eliminate the small angle grain boundaries.

The mechanism of chemical vapor deposition of cubic boron nitride films from fluorine-containing species

W.J. Zhang[a], C.Y. Chan[a], X.M. Meng[a], M.K. Fung[a], I. Bello[a], Y. Lifshitz[a,b], S.T. Lee[a], X. Jiang[c]

[a] *Center Of Super-Diamond and Advanced Films (COSDAF), Department of Physics and Materials Science, City University of Hong Kong, Hong Kong SAR, PR China*

[b] *Department of Materials Engineering, Technion Israel Institute of Technology, Haifa 32000, Israel.*

[c] *Institute of Materials Engineering, University of Siegen, Paul-Bonatz-Strasse 9-11, 57076 Siegen, Germany*

The unique properties of cubic boron nitride (cBN) make it an excellent material for mechanical and electronic applications. Powders of cBN were synthesized by usinga highpressure, high-temperature method and films of cBN were deposited by energetic ion-assisted physical vapor deposition (PVD). The latter technique involves two distinct stages: nucleation and growth. The nucleation of cBN is preceded by a soft incubation interlayer of, first, amorphous BN (aBN) and, second, turbostratic BN (tBN). cBN nucleates on the edges of the basal planes of tBN. Energetic particle bombardment is crucial to cBN nucleation but results in highly stressed, nanocrystalline cBN films with poor adhesion and a limited thickness, thus hinderingboth mechanical and electronic applications. Deposition through energetic particle bombardment is a shallow implantation ("subplantation") process, that is, nucleation and growth occur at several atomic layers below the surface. This process is the origin of the sp^2-bonded aBN/tBN top surface layer that covers the cBN crystallites in PVD cBN films.

The effect of surface roughness on the phase purity of cubic boron nitride films

C.Y. Chan[a], S. Eyhusen[b], X.M. Meng[a] I. Bello[a], S.T. Lee[a], C. Ronning[b], H. Hofsäss[b]

[a] *Center Of Super-Diamond and Advanced Films (COSDAF), Department of Physics and Materials Science, City University of Hong Kong, Hong Kong SAR, PR China*

[b] *II. Institute of Physics, University of Göttingen, Friedrich-Hund-Platz 1, D-37077, Göttingen, Germany*

Abstract

Boron nitride (BN) films have been deposited on silicon (Si) substrates with various root-mean-square surface roughness (0.2 to 170 nm) using mass-selected ion beam deposition (MSIBD). Mechanical scratching by either diamond or alumina powders with different powder sizes was used for substrate pretreatment. The effects of substrate surface roughness and seeding for the subsequent growth of BN films at different ion energies (75 – 500 eV) were investigated by Fourier-transform infrared spectroscopy (FTIR), atomic force microscopy (AFM) and high resolution transmission electron microscopy (HRTEM). The analyses show the interfacial turbostratic BN (tBN) thickness increased and nucleation threshold for cubic BN (cBN) shifted towards higher ion energy with the increase in substrate roughness. The orientation relationship of tBN with Si was more random as evident from selected area diffraction (SAD) pattern. However, the differences in cBN volume fraction became less obvious at higher ion energy (500 eV). Resulting featureless film morphology at high ion energy is probably associated with the preferred subsurface growth process. On the contrary low ion energy induced surface-like growth process which yields dominating granular morphology.

Deposition of thick cubic boron nitride films: The route to practical applications

Bello[a], C.Y. Chan[a], W.J. Zhang[a], Y.M. Chong[a], K.M. Leung[a], S.T. Lee[a], Y. Lifshitz[a,b]

[a] *Center of Super-Diamond and Advanced Films (COSDAF) and Department of Physics and Materials Science, City University of Hong Kong, Hong Kong SAR, PR China*

[b] *Department of Materials Engineering, Technion, Israel Institute of Technology, Haifa 32000, Israel*

Abstract

Physical and chemical vapor deposition approaches of growing thick cubic boron nitride (cBN) films needed for practical applications are reviewed. The interfacial soft hexagonal/amorphous boron nitride (hBN/aBN) layers and large stress associated with cBN deposition are suppressed through: (1) reduction of ion energy, (2) deposition at elevated temperatures, (3) post-deposition treatment, (4) use of buffer layers and (5) introduction of halogen chemistry. The most striking recent application of fluorine chemistry on diamond interlayers in our laboratory yielded thick, epitaxial cBN films with well-resolved Raman cBN spectra. This opens the road for growing adherent and thick large area poly- and single crystalline cBN with no soft interlayer and the quality sufficient for mechanical and electronic applications.

Structuring single- and nano-crystalline diamond cones

W.J.Zhang, Y.Wu, C.Y.Chan, W.K.W ong, X.M.Meng, I.Bello, Y.Lifshitz, S.T.Lee

Center of Super-Diamond and Advanced Films (COSDAF), and Department of Physics and Materials Science, City University of Hong Kong, Hong Kong SAR, PR China

Abstract

A novel method of nanostructuring diamond films into cone arrays through bias assisted reactive ion etching (RIE) is reported. It can be applied for both micro-crystalline diamond, forming single-crystalline cones and for nanodiamond films, forming nanodiamond cones.The density and the geometry of the cones are controlled by the initial texture of the diamond films and by the RIE conditions.Pyramidal (001)-textured films yield very sharp single-crystalline cones with the [001] axis perpendicular to the substrate surface, an apical angle of approximately 28° and a tip radius as small as 2 nm.Cones made of nanodiamonds with a similar apical angle of 28° and a variety of densities and sizes can be structured from nanodiamond films.A possible application is field electron emission (FEE), which is significantly improved in nanostructured cone arrays of all types of diamond films.The FEE of nanodiamond cone arrays is better than that of single-crystalline cone arrays of diamond with a similar density and geometry.

Diamond and Cubic Boron Nitride: Synthesis and Electronic Applications

I.Bello, W.J. Zhang, K.M. Chan, C.Y. Chan, Y. Wu, F.Y, Meng, C.W. Lam, J. Liu, and W.Y. Luk

Center of Super-Diamond and Advanced Films (COSDAF), and Department of Physics and Materials Science, City University of Hong Kong, Hong Kong SAR, PR China

Abstract

This paper reviews recent progress in deposition of diamond and cubic boron nitride (cBN) films. It aims at the effort of preparing smooth surfaces, improving crystallinity and enhancing adhesion of diamond and cBN films. The properties of these materials, multi-stage growth process and difference in synthesis of diamond and cBN films are discussed. Resolving the nucleation and growth stages, deposition at different temperatures, post deposition treatment, possible chemistry, and mechanism behind are introduced as well. We report the most striking results achieved in our laboratories including the deposition of thin smooth oriented diamond film with coalescent diamond crystals and the deposition of thick cubic boron nitride films yielding well-resolved Raman spectra. The difference between the syntheses of polycrystalline and nano-crystalline diamond films are shown to be in gas phase environments. While the CH_3 radicals are responsible for the growth of polycrystalline films the CVD environment with abundant C_2 dimers results in the deposition of nanocrystalline diamond. Special attention deserves manufacturing single crystal diamond nano-tips and their arrays. These single crystal diamond nano-tips have a very high aspect ratio, an apical angle of 28^o and a radius of 5 nm. Finally, we present review of potential and current applications of diamond in electronic areas.

Epitaxy on diamond by chemical vapor deposition: A route to high quality cubic boron nitride for electronic applications

W.J. Zhang, I. Bello, Y. Lifshitz, K.M. Chan, X.M. Meng, Y. Wu, C.Y. Chan, S.T. Lee

Center of Super-Diamond and Advanced Films (COSDAF), and Department of Physics and Materials Science, City University of Hong Kong, Hong Kong SAR, PR China

Abstract

Cubic BN (cBN. an analogue material to diamond) has a set of extreme properties similar to diamond, including high hardness, wide bandgap (>6 eV). high transparency up to the deep ultraviolet spectral region, excellent thermal conductivity, chemical inertness, and high dielectric strength, making it a unique material for many applications. Cubic BN is potentially a superior semiconductor material to diamond because n-type cBN doping is easier to achieve. Nevertheless, the advance of the science and technology of cBN has been severely hampered by the poor quality of the material available. High-pressure, high-temperature techniques produce only powders of cBN crystallites. Ion-assisted physical vapor deposition (PVD) techniques typically lead to randomly oriented, thin **(**<200 nm**)** cBN films of poor crystalline quality and adhesion with substrates due to an interlayer of non-cubic BN phases. The existing methods cannot provide cBN films of the quality required for electronic applications. Here we describe the epitaxial growth of thick, adherent. cBN films on as-deposited diamond substrates utilizing fluorine-assisted chemical vapor deposition (CVD). Diamond films have been deposited on a host of materials with good adhesion and crystalline quality. The present work implies that diamond can be used as a universal interlayer to grow pure (i.e., without non-cubic BN forms), adherent cBN films on all of these materials. The crystalline quality and the morphology of the cBN film are expected to follow those of the diamond interlayer. This achievement offers a logical path for producing large-area, single-crystal cBN films, and opens exciting possibilities for the electronic applications of cBN.

Mechanical and tribological properties of amorphous carbon films deposited on implanted steel substrates

P.W. Shum[a], Z.F. Zhou[a] , K.Y. Li[a], C.Y. Chan[b]

[a] *Department of Manufacturing Engineering and Engineering Management (MEEM), City University of Hong Kong, Hong Kong SAR, PR China*

[b] *Centre Of Super Diamond and Advanced Films (CSODAF) and Department of Physics and Materials Science, City University of Hong Kong, Hong Kong SAR, PR China*

Abstract

Hydrogen-free amorphous carbon (a-C) films were deposited using unbalanced magnetron sputtering technique from graphite targets on AISI 440C steel substrates implanted with (1) carbon (C), (2) titanium (Ti), and (3) titanium followed by carbon (Ti+C), respectively. After deposition, the adhesion strength of the films was examined by scratch test and Rockwell-C indentation test. The tribological performance of the films was evaluated by a typical ball-on-disk tribometer and a reciprocating wear tester. A dynamic impact tester was also carried out to study the fatigue strength of the films. In order to study the effect of the pre-treatment of steel substrates by means of ion implantation on the actual performance of a-C films, the implanted substrates were investigated by using X-ray photoelectron spectroscopy and nano-indentation, from which the composition depth profile as well as the hardness (H) and elastic modulus (E) depth profiles could be accurately obtained. As a result, due to higher contents of carbide bonds appeared at the outmost surface of the C and Ti+C implanted substrates, a critical load over 65 N was obtained, indicating good scratch resistance of the films. The combination of high interfacial strength and high plastic deformation resistance (H^3/E^2) of the Ti+C implanted substrates led to a higher load-carrying capacity and longer duration lifetime in the sliding wear test. In the dynamic impact test, the good adhesion strength and high toughness of C and Ti+C implanted substrates improved the impact resistance of the films.

Thick and adherent cubic boron nitride films grown on diamond interlayersby fluorine-assisted chemical vapor deposition

W.J. Zhang, I. Bello, Y. Lifshitz, K.M. Chan, Y. Wu, C.Y. Chan, X.M. Meng, S.T. Lee

Center of Super-Diamond and Advanced Films (COSDAF) and Department of Physics and Materials Science, City University of Hong Kong, Hong Kong SAR, PR China.

Abstract

Using plasma-enhanced chemical vapor deposition (PECVD) based on fluorine chemistry, the limitations hindering the practical use of cubic boron nitride (cBN) films in mechanical applications have been overcome. The CVD method presented is characteristic with (a) the direct cBN growth on diamond without soft, noncubic BN interface layers, (b) the synthesis of cBN films with extraordinary adhesion to the substrates and high mechanical properties, and (c) the scalable process providing thick, large-area cBN films at high deposition rate even on rough and untreated surfaces. These prime technological properties open the route to the mechanical exploitation of cBN films, particularly in tribological and tool applications. The reduction of the bias voltage in the PECVD process presented to a value of −20 V not only provides high-quality films, but also gives physical insight into the cBN growth mechanism.

A nanoindentation study of thick cBNfilms prepared by chemical vapor deposition

C.Y. Chan[a], W.J. Zhang[a], S. Matsumoto[b], I. Bello[a], S.T. Lee[a]

[a] *Center Of Super Diamond and Advanced Films (COSDAF) and Department of Physics and Materials Science, City University of Hong Kong, Hong Kong SAR, PR China.*

[b] *Advanced Materials Laboratory, National Institute for Materials Science, 1-1 Namiki, Tsukuba, Ibaraki 305-0044, Japan*

Abstract

The mechanical properties of high-quality cubic boron nitride (cBN) films were systematically investigated by nanoindentation measurements performed in both cross-sectional and plan-view directions. The large film thickness (B5 mm) allows the effective ruling out of both substrate and indenter size effects. The hardness and elastic modulus values were found to be 70 and 800 GPa, respectively, which are the highest values ever obtained on cBNfilms deposited by either PVD or CVD methods so far (comparable to those reported for cBNcrystals synthesized by high-pressure high-temperature methods). The variation of hardness across the cBNfilm thickness was investigated. In conjunction with the transmission electron microscopic observations, the relationship of the hardness measured with the crystallinity and crystal size/grain boundaries was discussed.

The growth of thick cBN films employing fluorine chemistry and ECR deposition

C.Y. Chan, W.J. Zhang, X.M. Meng, K.M. Chan, I. Bello, Y. Lifshitz, S.T. Lee

Center of Super Diamond and Advanced Films (*COSDAF*), *Department of Physics and Materials Science, City University of Hong Kong, Hong Kong SAR, PR China.*

Abstract

Energetic ion bombardment in N and Ar plasmas conventionally applied to cubic boron nitride (cBN) deposition restricts the size of cBN crystallites and induces high internal stress levels, limiting the non-delaminating film thickness obtainable (to ~100 nm). The introduction of fluorine chemistry via a complex He-A-N_2-BF_3-H_2 plasma produced in an electron cyclotron resonance (ECR) system overcomes such limitations and enables the preparation of thick cBN films (>1 μm) with low stress. The films were deposited using a low substrate bias (–40 V) and high substrate temperature (900 °C). Fourier-transform infrared (FTIR) spectroscopy shows that the films are composed of >80% cBN. Detailed analysis of BN film structures employing highresolution transmission electron microscopy (HRTEM) and transmission electron energy loss spectroscopy (EELS) shows that a cBN layer with high phase purity is formed on top of an initial turbostratic BN (tBN) layer, which accounts for the small hexagonal BN (hBN) signal in FTIR spectra. The appearance of characteristic transverse optical (TO) phonon and longitudinal phonon (LO) modes of cBN in visible Raman spectra demonstrates the larger crystalline size (~100 nm, also confirmed by HRTEM) in contrast to the films reported previously. The ion bombardment, gas composition, substrate temperature and growth time significantly affect the phase purity and crystallinity of the cBN films formed, as further elucidated in this paper.

Synthesis of boron nitride films using electron-cyclotron resonance microwave plasma and an H_2-BF_3-N_2-Ar-He gas system

C.Y. Chan, W.J. Zhang, K.M. Chan, I. Bello, S.T. Lee

Center of Super Diamond and Advanced Films (*COSDAF*), *Department of Physics and Materials Science, City University of Hong Kong, Hong Kong SAR, PR China.*

Abstract

Boron nitride (BN) films with high crystallinity and phase purity (>80 %) in the cubic phase were synthesized over large areas using fluorine chemistry and electron-cyclotron resonance (ECR) microwave plasma. Plasma-enhanced fluorine chemistry was provided by a complex H_2-BF_3-N_2-Ar-He gas mixture. Each component of the mixture was optimized in accordance with its function. Such a procedure allowed the preparation of thick cBN films at a bias voltage as low as −30 V. Micrometer-thick cBN films exhibiting columnar growth were obtained. However, ion bombardment was still indispensable for the cBN growth. The effects of deposition lime and ion bombardment on the phase purity and crystallinity of the cBN films were investigated.

Deposition of large-area, high-qualitycubic boron nitride films by ECR-enhanced microwave-plasma CVD

W.J. Zhang, C.Y. Chan, K.M. Chan, I. Bello, Y. Lifshitz, S.T. Lee

Center of Super Diamond and Advanced Films (*COSDAF*), *Department of Physics and Materials Science, City University of Hong Kong, Hong Kong SAR, PR China.*

Abstract

Large-area, 1-μm-thick cubic boron nitride (cBN) films were deposited on (001) silicon substrates by electron-cyclotron-resonance-enhanced microwave-plasma chemical vapor deposition (ECR-MP CVD) in a mixture of He-Ar-N_2-BF_3-H_2 gases. With the assistance of fluorine chemistry in the gas phase and substrate reactions, the phase purity of the sp^3-configuration was improved to over 85% at a reduced substrate bias voltage of −40 V. The grown films show clear Raman transversal optical (TO) and longitudinal optical (LO) phonon vibration modes, characteristic of cBN. Such Raman spectral characteristics are the first ever observed in cBN films prepared under ECR-MP CVD conditions.

An international round-robin experiment to evaluate the consistency of nanoindentation hardness measurements of thin films

K.W. Lee[a], Y.W. Chung[a], C.Y. Chan[b], I. Bello[b], S.T. Lee[b], A. Karimi[c], J. Patscheider[d], M.P. Delplancke-Ogletree[e], D. Yang[f], B. Boyce[g], T. Buchheit[g]

[a]*Department of Materials Science and Engineering, Northwestern University, Evanston, IL 60208, USA*

[b] *Center Of Super Diamond and Advanced Films* (*COSDAF*) *and Department of Physics and Materials Science, City University of Hong Kong, Hong Kong SAR, PR China*

[c] *Department of Physics, Swiss Federal Institute of Technology* (*EPFL*), *CH-1015 Lausanne, Switzerland*

[d] *Department of Surface and Joining Technology, Swiss Federal Laboratory for Materials Testing and Research, Ueberlandstr. 129, CH-8600 Duebendorf, Switzerland*

[e] *Industrial Chemistry CP 165y63, Universite Libre de Bruxelles, 50 Av F.D. Roosevelt, 1050 Brussels, Belgium*

[f] *Hysitron Inc., 5251 West 73rd Street, Minneapolis, MN 55439, USA*

[g] *Department 1835yMS 0889, Sandia National Laboratories, 1515 Eubank Blvd. SE, Albuquerque, NM 87185, USA*

Abstract

We conducted an international round-robin experiment to determine the consistency of nanoindentation hardness measurements of thin films among six different laboratories, using three different samples. These samples were chosen to present a challenge of indenting at small loads (mN range). They were: 250-nm-thick TiN_x, 700-nm-thick TiC, and 500-nm-thick TiB_2/TiC multilayer coatings (each layer being 3-nm thick), prepared at Northwestern University using magnetron sputtering on silicon (001) substrates. Each research team was free to use whatever nanoindenter and analysis methods at its disposal. This round-robin experiment demonstrates that for the hardness range of interest (15–35 GPa) and using well-documented procedures and analysis methods, the

reported results from all laboratories are essentially the same, allowing for a statistical spread of approximately (14). For consistent hardness measurements, four precautions must be observed: (i) proper tip-area function calibration, (ii) using sharp indenters, (iii) performing nanoindentation measurements with minimal thermal drift and with drift correction, (iv) using smooth samples, and (v) measuring the full hardness–maximum penetration curve.

Oriented single-crystal diamond cones and their arrays

W.J. Zhang, X.M. Meng, C.Y. Chan, Y. Wu, I. Bello, and S.T. Lee

Center Of Super-Diamond and Advanced Films (COSDAF) and Department of Physics and Materials Science, City University of Hong Kong, Hong Kong SAR, PR China

Abstract

One of the major problems in material science has been the difficulty in modification of the most endurable material, diamond, due to its extreme hardness and chemical inertness. Here, we report the development of a conical structure of diamond by performing bias-assisted reactive ion etching in hydrogen plasma. The diamond cones produced by this method are uniformly distributed over large areas on silicon substrates. Each cone was identified to be a single crystal with an apical angle as small as 28° and a very sharp tip (tip radii ~2 nm). Their [001] axes are perpendicular to the substrate surface and parallel to each other. Such striking structures of individual single-crystal diamond cones and their arrays, in addition to their scientific value, may lead to a breakthrough in the design of high-performance mechanical and electronic devices.

Structuring nanodiamond cone arrays for improved field emission

W.J. Zhang, Y. Wu, W.K. Wong, X.M. Meng, C.Y. Chan, I. Bello, Y. Lifshitz, S.T. Lee

Center Of Super-Diamond and Advanced Films (COSDAF) and Department of Physics and Materials Science, City University of Hong Kong, Hong Kong SAR, PR China

Abstract

A structuring method capable of producing uniform, large-area cone arrays of diamond films was developed. The technique employs bias-assisted reactive ion etching and is applicable to any structure of diamond films ranging from microcrystalline to nanocrystalline. Variation of the etching conditions enables control of the cone density, geometry, and height. Surface nanostructuring of cone arrays significantly improves the field emission properties of diamond films of all kinds. The turn on field is reduced to 6 and 10 V/μm for nanodiamond and microdiamond films, respectively, (compared to 25 V/μm for as deposited surfaces). Lower cone density yields better field electron emission (lower turn-on electrical field) due to the screening in high-density cone arrays. The field emission properties are determined by both the enhancement factor of the cone array and the emitting properties of the material. The field electron emission properties of nanodiamond arrays are better than cone arrays of single crystalline diamond with a similar cone density and cone geometry.

Deposition and properties of tetrahedral amorphous carbon films prepared on magnetic hard disks

C.Y. Chan[a], K.H. Lai[a], M.K. Fung[a], W.K. Wong[a], I. Bello[a], R.F. Huang[a], C.S. Lee[a], S.T. Lee[a], S.P. Wong[b]

[a] *Center Of Super Diamond and Advanced Films* (*COSDAF*) *and Department of Physics and Materials Science, City University of Hong Kong, Hong Kong SAR, PR China*

[b]*Department of Electronic Engineering, Chinese University of Hong Kong, Hong Kong SAR, PR China*

Abstract

The areal density of information stored on the hard disk has doubled every two years. This substantial increase in disk storage has resulted from the application of giant magnetoresistance heads, new thin film media, and better electronic recording channels. However, such an increase cannot be easily attained without reducing the separation between the magnetic read-write head and magnetic recording medium surfaces. Thiscan be achieved by using a thinner protective overcoat. In this study, ultrathin tetrahedral amorphous carbon (*ta*-C) films were deposited on magnetic hard disks (CoCrTa/Cr/NiP/Al–Mg) by a magnetic filtered cathodic arc deposition under different substrate bias voltages. The obtained films exhibited smoother surfaces than the uncoated disks as indicated by the atomic force microscopic measurement. The Raman spectra acquired showed a single asymmetric Lorentzian curve shape. Tetrahedral amorphous carbon coatings were subjected to an accelerated corrosion test in vapors of concentrated hydrochloric acid for 24 h. The corrosion test demonstrated a reduced density of corrosion sites when compared to conventional diamond-like carbon films. Similarly, the scratch resistance of the *ta*-C coated disks, investigated by a nanoindenter, showed significant improvement in comparison to uncoated disks.

Mechanical properties of DLC films prepared in acetylene and methane plasmas using electron cyclotron resonance microwave plasma chemical vapor deposition

K.H. Lai, C.Y. Chan, M.K. Fung, I. Bello, C.S. Lee, S.T. Lee

Center Of Super Diamond and Advanced Films (*COSDAF*) *and Department of Physics and Materials Science, City University of Hong Kong, Hong Kong SAR, PR China*

Abstract

Diamond-like carbon (DLC) films were deposited on silicon using methane and acetylene plasma induced by electron cyclotron resonance microwave plasma chemical vapor deposition (ECR-MPCVD). The mechanical properties of DLC films were characterized by micro-Raman system, atomic force microscope, tribometer, nanoindenter used for both hardness and nano-scratch test measurements. The mechanical properties of both DLC films, prepared in methane and acetylene plasmas, respectively, strongly depended on the kinetic energy of impinging particles. The deposition at −120 V substrate bias gave rise to DLC films with the best mechanical properties for both methane and acetylene plasmas. The hardness measurements with variable indentation depth showed the characteristic changes in hardness values implying elastic deformations of supporting substrates. The maximum hardness value of DLCM films was 20 GPa while that of DLCA films was 28 GPa. However, the hardness dropped when DLC films were prepared at substrate biases more negative than −120 V due to the thermal graphitization. The improvement in DLC properties usually provided the films with smaller hydrogen content and higher density of sp^3 bondings. These parameters were engineered through controlling the deposition parameters. Particularly, the bombardment of growing DLC films by energetic ions showed to be extremely important to yield films with lower internal stress.

Film thickness effects on mechanical and tribological properties of nitrogenated diamond-like carbon films

J. Qi[a], C.Y. Chan[a], I. Bello[a], C.S. Lee[a], S.T. Lee[a], J.B. Luo[b], S.Z. Wen[b]

[a] *Center Of Super Diamond and Advanced Films* (*COSDAF*) *and Department of Physics and Materials Science, City University of Hong Kong, Hong Kong SAR, PR China*

[b] *State Key Laboratory of Tribology, Tsinghua University, Beijing 100084, PR China*

Abstract

Nanoindentation, nanoscratch and ball-on-disk tests were used to determine the film thickness effect on the mechanical and tribological properties of nitrogenated diamondlike carbon CN films, which were deposited on Si 100 substrates by an electron cyclotron resonance microwave plasma chemical vapor deposition (ECR-MPCVD) system. Except for the film with a thickness of 20 nm, there existed peak values of hardness for all films thicker than 44 nm. When the thickness ranged from 44 to 235 nm, the peak values of hardness and the corresponding indentation depth increased along with increasing film thickness. The results of scratch resistance tests showed that the critical loads of the fracture were independent of thickness for thinner films, however, they increased rapidly with increasing thickness for thicker films. Ball-on-disk sliding tests indicated that the friction coefficient decreased with increasing thickness for thinner films, while there was no obvious thickness dependence of the friction coefficient for relatively thicker films. The formation of transferred layer and graphitization of the films during sliding resulted in the decrease of friction coefficients at early stages of sliding.

Wear-resistant multilayered diamond-like carbon coating prepared by pulse biased arc ion plating

R.F. Huang[a], C.Y. Chan[a], C.H. Lee[a], J. Gong[a], K.H. Lai[a], C.S. Lee[a], K.Y. Li[b], L.S. Wen[c], C. Sun[c]

[a] *Center Of Super Diamond and Advanced Films* (*COSDAF*) *and Department of Physics and Materials Science, City University of Hong Kong, Hong Kong SAR, PR China*

[b] *Department of Manufacturing Engineering and Engineering Management (MEEM), City University of Hong Kong, Hong Kong SAR, PR China*

[c] *Institute of Metal Research, Academia Sinica, Shenyang, PR China*

Abstract

Diamond-like carbon coatings have been deposited by a pulse biased arc ion plating. In order to improve their adherence to metal substrate, two systems of graded transition layers, namely Ti/TiN/TiC and Ti/TiCN/TiC, have been applied. The structure and composition of the diamond-like carbon/transition composite coatings were studied by scanning electron microscopy, Raman spectroscopy and energy dispersive X-ray spectroscopy. The total thickness of the coatings was within a range of 1.0 - 2.0 μm. Such multi-layer coatings showed excellent properties including high hardness, low friction coefficient and long wear-resistant lifetime. Diamond like carbon coatings as well as their wear tracks developed by sliding steel balls have been investigated by scanning electron microscopy. The results of the analysis, particularly that of the tribological study showed that the wear resistance and film-to-substrate adherence of diamond like carbon coatings with stainless steel surface were dramatically improved by using a graded transition layer and pulse biased arc ion plating.

Mechanical and tribological properties of diamond-like carbon films prepared on steel by ECR-CVD process

K.Y. Li[a], Z.F. Zhou[b], C.Y. Chan[b], I. Bello[b], C.S. Lee[b], S.T. Lee[b]

[a] *Department of Manufacturing Engineering and Engineering Management (MEEM), City University of Hong Kong, Hong Kong SAR, PR China*

[b] *Center Of Super Diamond and Advanced Films* (*COSDAF*) *and Department of Physics and Materials Science, City University of Hong Kong, Hong Kong SAR, PR China*

Abstract

Diamond-like carbon DLC films were prepared on AISI 440C steel substrates at room temperature by the electron cyclotron resonance chemical vapor deposition (ECR-CVD) process in C2H2-Ar plasma under different conditions. In order to prevent the interdiffusion of carbon and improve the adhesion strength of DLC films, functionally gradient Ti/TiN/TiCN/TiC supporting underlayers were deposited on the steel substrates in advance. Using the designed interfacial transition layers, relatively thick DLC films 1-2 μm were successfully prepared on the steel substrates without delamination. By optimizing the deposition parameters, DLC films with hardness up to 28 GPa and friction coefficients lower than 0.15 against the 100Cr6 steel ball were obtained. In addition, the specific wear rates of the films were found to be extremely low (~10 m^3/Nm). The friction-induced graphitization mechanism of DLC was confirmed by micro-Raman analysis.

Investigation of diamond film deposition on steel without and with ion beam nitriding pretreatment

N.G. Shang. C.H. Lee, X.T. Zhou, F.Y. Meng, C.Y. Chan, S.T. Lee, I. Bello

Center Of Super Diamond and Advanced Films (*COSDAF*) *and Department of Physics and Materials Science, City University of Hong Kong, Hong Kong SAR, PR China*

Abstract

The surface morphology, film quality, interface structure, growth rate and adhesion of diamond films prepared by hot filament chemical vapor deposition on commercial steel substrates with and without ion beam nitriding pretreatment were investigated by scanning electron microscopy, X-ray diffraction, scanning Auger spectroscopy, a Vickers micro-indenter, and micro-Raman spectroscopy. Apart from quite different surface morphologies, both the quality and growth rate of diamond films deposited on the ion beam nitrided steel substrates were higher than those on the unnitrided steel substrates. Similar diamond/steel interface structures were observed on both the nitrided and unnitrided steel. Diamond films were grown on steel substrates via carbide interlayers formed *in situ* during the diamond deposition rather than via a graphitic soot interlayer. Ion beam nitriding appeared to enhance the diamond growth through thickening of the carbide interlayer. The adhesion of diamond films on the nitrided steel was tested by a Vickers micro-indenter.

Mechanical properties and corrosion studies of amorphous carbon on magnetic disks prepared by ECR plasma technique

M.K. Fung[a], K.H. Lai[a], C.Y. Chan[a], I. Bello[a], C.S. Lee[a], S.T. Lee[a], D.S. Mao[b], X. Wang[b]

[a] *Center Of Super Diamond and Advanced Films* (*COSDAF*) *and Department of Physics and Materials Science, City University of Hong Kong, Hong Kong SAR, PR China*

[b] *Ion Beam Laboratory, Shanghai Institute of Metallurgy, Chinese Academy of Sciences, Shanghai 200050, People's Republic of China*

Abstract

Diamond-like carbon (DLC) were prepared on magnetic disk surfaces using an electron cyclotron resonance assisted microwave plasma chemical vapor deposition (ECR-MPCVD) system with variable radio-frequency (r.f.) substrate bias. Surface roughness of DLC deposited on hard disks was investigated by atomic force microscopy (AFM), which revealed that the DLC coated surfaces are smoother than those of the uncoated disks. Nitrogen incorporation into the (*a*-C:N) further reduced the root-mean-square (RMS) roughness to 2.5 Å for films prepared at a substrate bias of −120 V. Scratch resistance was improved when the DLC coatings were deposited at bias voltages greater than −90 V. However, the nitrogen introduction into the films deteriorated their scratch resistance. When the DLC films were subjected to an accelerated corrosive environment, pinhole density remarkably varied with the deposition conditions. The DLC films deposited with lower substrate biases and nitrogen incorporation resulted in poorer corrosion resistance. Internal stress, hydrogen content and graphitic cluster size of these films were correlated with data acquired by Raman analysis.

Diamond-like carbon coatings applied to hard disks

M.K. Fung, K.H. Lai, H.L. Lai, C.Y. Chan, N.B. Wong, I. Bello, C.S. Lee, S.T. Lee

Center Of Super Diamond and Advanced Films (*COSDAF*) *and Department of Physics and Materials Science, City University of Hong Kong, Hong Kong SAR, PR China*

Abstract

Amorphous carbon (*a*-C:H) films were prepared on the surface of magnetic disks using an electron cyclotron resonance assisted microwave plasma chemical vapor deposition (ECR-MPCVD) system with variable radio-frequency substrate bias voltage. As indicated by the atomic force microscopy measurements, the surfaces of the hard disks coated with 10 nm thick films were smoother than those of the uncoated disks. The scratch resistance of coated disks increased at biases greater than −90 V. Corrosion resistances of the coatings was also studied by exposure to vapor of hydrochloric acid (HCl) for 24 h. The analysis showed that the radio-frequency bias voltage was a critical parameter affecting the chemical compositions, mechanical properties and corrosion resistance of the films.

Crystal morphology and phase purity of diamond crystallites during bias enhanced nucleation and initial growth stages

C. Sun, W.J. Zhang, N. Wang, C.Y. Chan, I. Bello, C.S. Lee, and S.T. Lee

Center Of Super Diamond and Advanced Films (*COSDAF*) *and Department of Physics and Materials Science, City University of Hong Kong, Hong Kong SAR, PR China*

Abstract

The crystal morphologies and phase composition of diamond crystallites during bias enhanced nucleation and initial growth stages in microwave plasma chemical vapor deposition were investigated. Diamond nuclei were first formed in the central regions of substrates and then propagated to the sample edges. During the course of bias nucleation, excessive ion bombardment induced secondary nucleation sites on the already formed nuclei. The secondary nucleation deteriorated the overall alignment of the growing crystals. Hence, the elimination of secondary nucleation and homogeneous nucleation over substrates are fundamental requirements for the deposition of large-area uniformly oriented diamond films. Decreasing reactant pressure was found to be effective for improving plasma homogeneity and consequently nucleation uniformity. The results of bias enhanced nucleation within a pressure range from 8 to 20 Torr showed that the lower pressure of reactants enlarged the area of oriented diamond films. However, the optimum bias and duration of nucleation was found to be specific for each pressure.

US 20040079280A1

(19) **United States**

(12) **Patent Application Publication** (10) **Pub. No.: US 2004/0079280 A1**

Lee et al. (43) **Pub. Date: Apr. 29, 2004**

(54) **FABRICATION OF SINGLE CRYSTAL DIAMOND TIPS AND THEIR ARRAYS**

(76) Inventors: **Shuit-Tong Lee**, Hong Kong (HK); **Igor Bello**, Hong Kong (HK); **Wenjun Zhang**, Hong Kong (HK); **Chit Yiu Chan**, Hong Kong (HK)

Correspondence Address:
Intellectual Property Group
Bose McKinney & Evans LLP
2700 First Indiana Plaza
135 North Pennsylvania Street
Indianapolis, IN 46204 (US)

(21) Appl. No.: **10/282,779**

(22) Filed: **Oct. 29, 2002**

Publication Classification

(51) **Int. Cl.**[7] **C30B 23/00**; C30B 25/00; C30B 28/12; C30B 28/14

(52) **U.S. Cl.** **117/89**

(57) **ABSTRACT**

The present invention deals with the generation of sharp single crystal diamond tips and the arrays of these tips, and their fabrication technology. The invention combines the deposition of synthetic diamond films with reactive etching processes. Upon the diamond orientation prepared and reactive etching environment with considerable directivity of ions, single crystal diamond tips with different apical angles can be fabricated. Very sharp diamond tips with an apical angle of no more than about 28° and a tip radius smaller than 50 nm are fabricated on pyramidal-shaped [001]-textured diamond films by subsequent reactive etching., The technology is based on selective etching of sp^2- and sp^3-hybridized carbons by the activated constituents of an etching environment, in particular based on atomic hydrogen, in a way similar to ion bombardment, which contributes to overall etching and local conversion of diamond to graphitic phase promoting further etching with chemically activated species. This novel method is capable of forming diamond tip arrays over large areas with great uniformity and high reproducibility. The diamond tips prepared are single diamond crystals with their [001] axes parallel each other and normal to the substrate surface. The invented technology enables the control of the apical angle, radius and density of the diamond tips.